KTH Industrial Engineering and Management

Simulation of turbocharged SI-engines - with focus on the turbine

Fredrik Westin

Doctoral thesis
KTH School of Industrial Engineering and Management
Royal Institute of Technology
SE-100 44 Stockholm

TRITA – MMK 2005:05
ISSN 1400-1179
ISRN/KTH/MMK/R-05/05-SE

TRITA – MMK 2005:05
ISSN 1400-1179
ISRN/KTH/MMK/R-05/05-SE

Simulation of turbocharged SI-engines – with focus on the turbine

Fredrik Westin

Doctoral thesis

Academic thesis, which with the approval of Kungliga Tekniska Högskolan, will be presented for public review in fulfilment of the requirements for a Doctorate of Engineering in Machine Design. The public review is held at KTH - The Royal Institute of Technology, room M3, Brinellvägen 64 Stockholm, on 31 May 2005, 14.00.

”On and on we're charging to the place so many seek
In perfect synchronicity of which so many speak
We feel so close to heaven in this roaring heavy load
And then in sheer abandonment, we shatter and explode.
I'm your turbo lover
Tell me there's no other”
Judas Priest

Introduction

The research objective

This PhD-thesis is the outcome of a project initiated by Saab Powertrain AB and started by Prof. Hans-Erik Ångström at KTH in 2000. The initial objective was to investigate a wide range of boosting systems in order to sort out the system most suitable for boosting downsized SI-engines. Since downsizing is a well-known method for reduction of the fuel consumption of SI-engines it is of all engine manufacturer's interest to investigate the technology. Saab had at the start of the project developed the third development step of its heavily downsized engine concept SVC, Saab Variable Compression. The engine had half the displacement of its competitors and subsequently it needed approximately twice the normal boost pressure. These high levels of boosting, together with the small displacement, set very high demands on the boosting system in terms of transient response and efficiency. One single turbocharger was not enough for the task and the question was with what to replace it.

The investigation should be done with 1D engine simulations. Unfortunately it was very soon detected that the current state of the simulation software was not good enough to fulfil the task with sufficient precision. The decision was made by both Saab Powertrain and KTH to change the objective to an investigation of the accuracy of the simulations instead, and that is what the main part of this thesis deals with.

Turbocharging can both increase the power density of an engine as well as decrease the fuel consumption of a vehicle. However, to fully explore the potential, some problems must be overcome during the development of the engines. For low engine speeds, turbocharged engines often have less torque than N/A-engines with comparable peak torque and speed. For the highest speeds, the turbine inlet temperature limits the maximum power of the engine. In addition, especially for low engine speeds, the turbocharged engine has slower transient response than a N/A-engine. All of these issues are related to the gas exchange process of the engine and selection of turbocharger components. To optimise this process, virtually all engine manufacturers use 1D engine simulation codes. Unfortunately these simulation codes, for certain engine modes, have problems in accurately predicting the performance of the engine.

For the mid-speed region, where the wastegate is open, the codes have reasonable prediction accuracy. The simulation controls the wastegate to the set boost-pressure, just as the real controller on the engine. Very seldom do measurement data of the wastegate massflow fraction, to correlate with the

simulation results, exist. However, for the low speed region, where the wastegate is closed, the simulation is much more sensitive to an error in predicted turbine power. The reason is that there is no control mechanism to adjust the turbine power. Therefore this region, up to where the wastegate is opened on the engine, normally cannot be simulated accurately without calibrating the simulation model against measurement data for the particular engine in question. The same also holds for transients, since the wastegate is closed up to when the desired boost pressure is reached.
Thus, the most useful tool for removing two of the turbocharged engine's largest drawbacks has drawbacks in itself exactly where it can be of largest use.

The process

For this project there existed funding for one full-time employed PhD-student to work both in a test-cell and with computer simulations in a commercial simulation code. At the start of the project there was little activity around 1D simulations both at KTH and at Saab. In addition a brand new test cell needed instrumentation and installation of the engine. To fulfil the task both the measurement technique needed further investigation and proper use of the simulation tool had to be learned.

The thesis

The thesis text describes the work done within the project. The aim is to share experience gained when simulating (and doing measurements on) the turbocharged SI-engine as well as describing the limits of current state of the technology. In addition an overview of current boosting systems is provided.
The target readers of this text are engineers employed in the engine industry as well as academia who will get in contact, or is experienced, with 1D engine performance simulation and/or boosting systems. Therefore the text requires general knowledge about engines.

The papers included in the thesis are, in reverse chronological order:

[8] SAE 2005-XX-XXX ***Calculation accuracy of pulsating flow through the turbine of SI-engine turbochargers - Part 2 Measurements, simulation correlations and conclusions*** Westin & Ångström
To be submitted to the 2005 SAE Powertrain and Fluid Systems Conference in San Antonio

[7] SAE 2005-01-2113 ***Optimization of Turbocharged Engines' Transient Response with Application on a Formula SAE / Student engine*** Westin & Ångström
Approved for publication at the 2005 SAE Spring Fuels and Lubricants Meeting in Rio de Janeiro

[6] SAE 2005-01-0222 ***Calculation accuracy of pulsating flow through the turbine of SI-engine turbochargers - Part 1 Calculations for choice of turbines with different flow characteristics*** Westin & Ångström
Published at the 2005 SAE World Congress in Detroit April 11-14, 2005

[5] SAE 2004-01-0996 ***Heat Losses from the Turbine of a Turbocharged SI-Engine – Measurements and Simulation*** Westin, Rosenqvist & Ångström
Presented at the 2004 SAE World Congress in Detroit March 8-11, 2004

[4] SAE 2003-01-3124 ***Simulation of a turbocharged SI-engine with two software and comparison with measured data*** Westin & Ångström
Presented at the 2003 SAE Powertrain and Fluid Systems Conference in Pittsburgh

[3] SIA C06 ***Correlation between engine simulations and measured data - experiences gained with 1D-simulations of turbocharged SI-engines*** Westin, Elmqvist & Ångström
Presented at the SIA International Congress SIMULATION, as essential tool for risk management in industrial product development in Poissy, Paris September 17-18 2003

[2] IMechE C602/029/2002 ***A method of investigating the on-engine turbine efficiency combining experiments and modelling*** Westin & Ångström
Presented at the 7th International Conference on Turbochargers and Turbocharging in London 14-15 May, 2002

[1] SAE 2000-01-2840 ***The Influence of Residual Gases on Knock in Turbocharged SI-Engines*** Westin, Grandin & Ångström
Presented at the SAE International Fall Fuels and Lubricants Meeting in Baltimore October 16-19, 2000

The first step in the investigation about the simulation accuracy was to model the engine as accurately as possible and to correlate it against as accurate

measurements as possible. That work is covered in the chapters 3 and 5 and in paper no. 3 in the list above. The scientific contribution here is to isolate the main inaccuracy to the simulation of turbine efficiency.

In order to have anything to compare the simulated turbine efficiency against, a method was developed that enables calculation of the CA-resolved on-engine turbine efficiency from measured data, with a little support from a few simulated properties. That work was published in papers 2 and 8 and is the main scope of chapter 6 in the thesis. The scientific contributions here are several:

- The application on a running SI-engine is a first
- It was proven that CA-resolution is absolutely necessary in order to have a physically and mathematically valid expression for the turbine efficiency. A new definition of the time-varying efficiency is developed.
- It tests an approach to cover possible mass accumulation in the turbine housing
- It reveals that the common method for incorporating bearing losses, a constant mechanical efficiency, is too crude.

The next step was to investigate if different commercial codes differ in the results, even though they use equal theoretical foundation. That work is presented in chapter 4, which corresponds to paper 4. This work has given useful input to the industry in the process of choosing simulation tools.

The next theory to test was if heat losses were a major reason for the simulation accuracy. The scientific contribution in this part of the work was a model for the heat transport within the turbocharger that was developed, calibrated and incorporated in the simulations. It was concluded that heat losses only contributed to a minor part of the inaccuracy, but that is was a major reason for a common simulation error of the turbine outlet temperature, which is very important when trying to simulate catalyst light off. This work was published in paper 5 and is covered in chapter 7.

Chapter 8, and papers 6 and 8, covers the last investigation of this work. It is a broad study where the impact of design changes of both manifold at turbines on both simulation accuracy as well as engine performance. The scientific contribution here is that the common theory that the simulation inaccuracy is proportional to the pulsation amplitude of the flow is non-valid. It was shown that the reaction was of minor importance for the efficiency of the turbine in the pulsating engine environment. Furthermore it presents a method to

calculate internal flow properties in the turbine, by use of a steady-flow design software in a quasi-steady procedure. Of more direct use for the industry is important information of how to design the manifolds as well as it sheds more light on how the turbine works under unsteady flow, for instance that the throat area is the single most important property of the turbine and that the system has a far larger sensitivity to this parameter than to any other design parameters of the turbine. Furthermore it was proven that the variation among individual turbines is of minor importance, and that the simulation error was of similar magnitude for different turbine manufacturers.

Paper 7, and chapter 9, cover a simulation exercise where the transient performance of turbocharged engines is optimised with help from factorials. It sorts out the relative importance of several design parameters of turbocharged engines and gives the industry important information of where to put the majority of the work in order to maximize the efficiency in the optimisation process.

Overall, the work presented in this thesis has established a method for calibration of models to measured data in a sequence that makes the process efficient and accurate. It has been shown that use of controllers in this process can save time and effort tenfold or more.

When designing turbocharged engines the residual gas is a very important factor. It affects both knock sensitivity and the volumetric efficiency. The flow in the cylinder is in its nature of more dimensions than one and is therefore not physically modelled in 1D codes. It is modelled through models of perfect mixing or perfect displacement, or at a certain mix between them. Before the actual project started, the amount of residual gases in an engine was measured and it's influence on knock was established and quantified. This was the scope of paper 1. This information has been useful when interpreting the model results throughout the entire work.

Fredrik Westin
Stockholm, March 2005

Acknowledgements

The author is indebted to many people for being able to perform the work presented in this thesis.

First, Professor Hans-Erik Ångström, the man who has literally built the Division of Internal Combustion Engines at KTH.

The Swedish Energy Agency for providing all the funding for the project.

Per-Inge Larsson, Technology Leader for boosting systems within Fiat-GM-Powertrain, for providing support, encouragement and introducing me to many knowledgeable persons within the business.

To my great friends, Emil Åberg, Marcus Larsson, Gustav Berggren and Fredrik Jansson, for all the discussions we have had exploring the fantastic world of engines.

All the colleagues at the div. of Internal Combustion Engines for making the time there very pleasant. Henrik Nilsson for the never-ending stream of stories during the coffee-breaks, Fredrik Agrell for introducing me to the fantastic world of naturally aspirated in-line sixes, and to all the rest of you colleagues.

Dr Raymond Reinmann, Eric Olofsson and several others at Saab Powertrain, mainly for support and interesting discussions during the beginning of the project.

Dr Bill Connor at Garrett Engine Boosting systems for providing hardware and testing time for the work presented in Chapter 8.

Lars Almqvist, the Saab librarian, for his world-class service delivering the papers referred to in this thesis.

Table of contents

Chapter 1

Boosting downsized SI-engines – a literature review of potential fast responding, wide range boosting systems[1]

1.1 Introduction

Downsizing is an efficient method for reduction of the fuel consumption of SI-engines. However, when the engine's displacement is reduced it will be very dependent on it's boosting system. Since the engine needs a high boost pressure to produce enough power it is necessary for the acceleration behaviour of the engine that the charging system has a fast transient response. In this literature review the results of previous work in this field of boosting systems for high boost pressure and fast response is presented.

No literature review can cover everything published within a specific field. In this work the scope has been to review enough literature to give an insight into every kind of boosting system that might be considered for use on a downsized SI-engine.

It turned out that no scientific work could be found in the specific field of boosting systems for a boost level of about pressure ratio π=3 for SI-engines of passenger car size together with fast response. Very little scientific work is

[1] The chapter was written in 2002 and only slightly updated. Hence the lack of papers from 2002 and onwards.

published on SI-engine pressure charging. For truck- and larger sized diesels however there are more publications. In this report interesting information is presented regardless of if the work is done on SI- or Diesel engines. The problems faced by the designer are the same for both engines, however the SI-engine tends to be more challenging due to the larger speed range with subsequently wider flow range, which also is further increased due to throttling at part load. In addition, SI-engines demand more controllability due to the knock problem. Together this encourages the entire gas exchange process to be regarded as a complete air management system instead of just looking at the boosting system itself.

1.2 Mechanical supercharging

1.2.1 Screw and Roots types

Mechanical supercharging is probably the oldest way of boosting the IC engine, Ansdale [1.1]. A supercharger is simple to install and in most cases it doesn't need any complicated control.

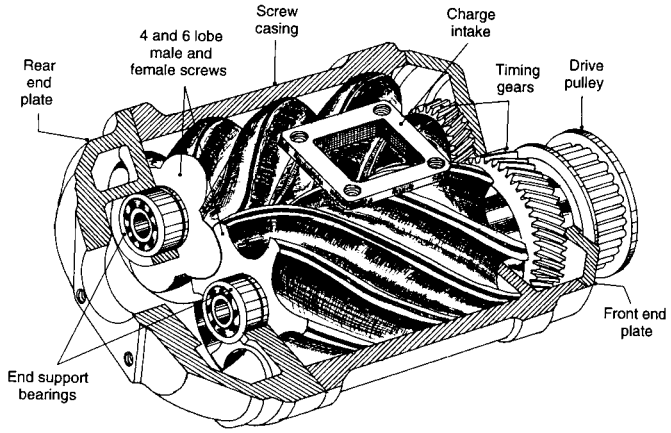

Figure 1.1. Cut-away view of the Lysholm screw supercharger. It has two rotors, a male and a female, forming a set of chambers between themselves and the housing. The chamber's volume is changing during the rotation and thus compresses the air internally. Picture from Heisler [1.2].

Since the power needed to drive the supercharger is taken directly from the crankshaft, most development work has been invested to increase the efficiency and to minimize the parasitic losses when the supercharger is not needed (i.e. part load of the engine). The most common types on the supercharger market today are the Lysholm compressor and the Roots blower. Both are displacement pumps and from a first glance they look very similar. They differ

on one big point, the Lysholm screw has internal compression while the Roots hasn't.

The Lysholm Compressor has proven to have the highest adiabatic η_{ad} and total η_{tot} (adiabatic + mechanical) efficiency. Takabe et. al. [1.3] reports η_{tot}=70% for Lysholm and η_{tot}=50% for the Roots blower, this in spite of the Lysholm's higher speed and subsequently expected lower mechanical efficiency due to the higher step up gear ratio. Eaton shows data corresponding to isentropic efficiency in the 55% range for their three-lobe, twisted Roots blower [1.4], that is for pressure ratios well below 2. The three-lobed, twisted rotors are said to be more silent than the straight, two-lobed type. Still Mercedes are forced to use quite bulky silencers in conjunction with the supercharger [1.5].

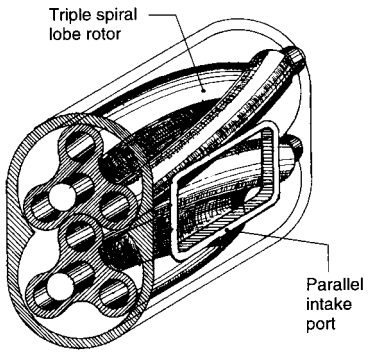

Figure 1.2. Cut away view of the Roots type supercharger. It has two similar rotors forming discrete volumes but with constant volume. Therefore it has no internal compression. The three lobe, twisted type shown here is the most modern type, used by for instance Mercedes and manufactured by Eaton. A more classical Roots blower has only two lobes per rotor and the rotors are straight. Picture from Heisler [1.2].

The Lysholm Compressor works with internal compression. If this internal compression can be done with a minimum of friction losses internally in the air, i.e. turbulence, the compression can be very close to adiabatic. Lehmann et. al. has shown this for a Wankel type compressor [1.6]. Since the Wankel type and the Lysholm compressor both show similar total efficiencies it is fair to assume that the Lysholm also works close to adiabatic conditions. The Roots on the other hand works without internal compression, the compression takes place as the air is discharged from the blower outlet instead of inside the supercharger. This means that the compression takes place at isochoric conditions (i.e. constant volume). This process is known to be more power consuming and heat producing than the adiabatic process, see fig 1.3.

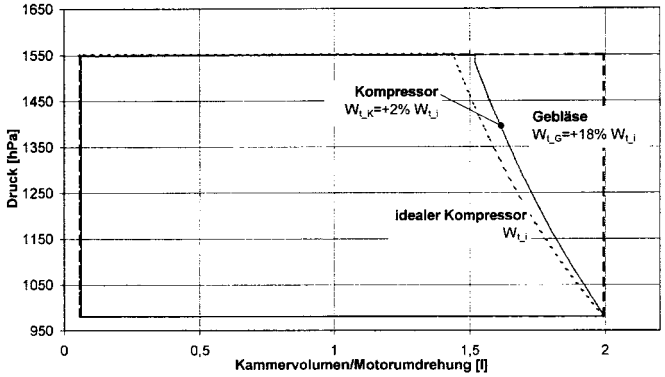

Figure 1.3. Differences in compressor work due to compression processes. Kompressor means compressor with internal compression and Gebläse means blower. Idealer Kompressor stands for ideal adiabatic process. Figure from [1.6].

However, the actual efficiency on the engine is very dependent on the engine conditions. To be able to exploit the high efficiency of a compressor[2] it is necessary to match the internal compression pressure to the engine inlet manifold pressure. If this cannot be done the working process will be a combination of near adiabatic compression inside the compressor and isochoric compression (or expansion, depending on if the charge pressure is higher or lower than the compressor outlet pressure) at the discharge from the compressor outlet. Thus the resulting efficiency will have a value between the near adiabatic and the efficiency of the isochoric process [1.6].
However, it does not seem as if efficiency decreases that very much with a relatively small difference between the charge pressure and the internal compression pressure, judging from fig. 1.4 where driving power for a screw and a roots blower are displayed vs. speed for two pressure ratios. Here it can be seen that the screw performs significantly better than the roots. But in the figure the deviation in compressor internal compression from the charge pressure is very small.

[2] From here and onwards compressor is used for a supercharger with internal compression and blower for the ones without internal compression

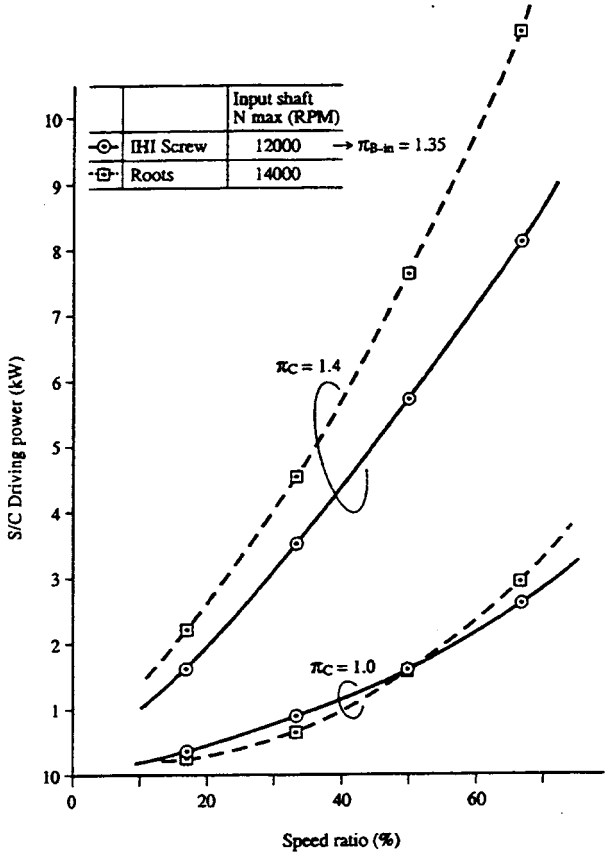

Figure 1.4 Compressor driving power for π=1.4 and π=1.0. π=1.0 is achieved by a simple discharge valve in the middle of the compression phase. Figure from [1.7].

If the compressor was fitted with variable inlet and exhaust port timings the internal compression could be controlled to equal the charge pressure for all engine running conditions (assuming enough variability), this would of course maximize efficiency over the entire range. Lehmann et. al. [1.6] tested such a compressor but with limited variability and only for expansion operation, but the principle of affecting the efficiency by varying inlet and outlet openings is proved.

1.2.2 Centrifugal compressor as a supercharger

The centrifugal compressor has an isentropic efficiency that well can match, and sometimes exceed, the efficiency of a Lysholm screw compressor. As

opposed to screw and roots types it is not a displacement pump. Instead it is a dynamic machine where the rotor increases the internal energy of the air, both through increased density and increased velocity. The velocity is then carefully diffused to recover the kinetic energy as static pressure. Consequently the centrifugal compressor has internal compression.
Unfortunately the flow vs. speed characteristics of the centrifugal compressor is very non-linear, why a fixed gear ratio between the compressor and the crankshaft results in a very peaky boost pressure delivery. Despite this it has been used in cars, for instance in Duesenberg and Studebaker during the 1930s and 1950s, respectively.
Not only the need for a gearbox causes trouble for the designer if using a centrifugal compressor on the engine. It also has a much higher speed, up to 10 times higher than a roots and about 3-5 times the speed of a screw compressor, well above 100000 rpm. High speeds can lead to both sound problems if gears are used and the torque needed for acceleration can be rather high even if the moment of inertia is not particularly high. The expression for acceleration of a specific rotor with a moment of inertia I_{rotor} shows why, see eq. 1.1. If the speed for a centrifugal compressor is, say 5 times higher, than for some conventional screw compressor, and the acceleration times are supposed to be the same for both, then the acceleration (dN/dt) has to be 5 times higher as well. Furthermore, the speed at start of acceleration is also 5 times higher. Therefore the moment of inertia has to be 25 times smaller in order to offset the increased acceleration power for the unit with higher working speed.

$$P_{acc} = \frac{2\pi N_{turbo}}{60}\tau = \left(\frac{2\pi}{60}\right)^2 I_{rotor} N_{turbo} \frac{dN_{turbo}}{dt} \qquad \text{eq. 1.1}$$

Where:
P ..... Power [W]
τ ..... Torque [Nm]
N ..... Speed [rpm]
I_{rotor} ..... Polar moment of inertia of the rotor [kgm^2]

Together this will place very high demands on the gearbox for the compressor.
On the positive side can be mentioned price, since the same compressors can be used as for turbochargers, which have been optimised for cost over decades and also produced in very large volumes why the unit cost for the compressor will be very low. However, the gearbox will probably be expensive.
One example of such a machine is the Rotrex supercharger [1.8, 1.9]. It is belt driven from the crankshaft and has an internal planetary drive with a fixed ratio

of 9,483:1 where the rollers are of friction type, i.e. not gears as on ordinary planetary gearboxes. Unfortunately no good performance data of an engine fitted with this type, or the power consumption of the gearbox have been found.
Though, it seems like the demands of the gearbox as continuously variable, silent, extremely low inertia and low cost are too large problems to be overcome.

1.2.3 Parasitic losses

The largest problem of using a mechanical supercharger on a downsized engine is not the top-end performance, but the parasitic losses on part load. Miyagi et. al. [1.7] showed that for a Lysholm compressor only 20-30% of the parasitic losses come from mechanical losses and the rest from losses in the airflow, i.e. unnecessary pumping. Therefore it is most important to try to minimize the airflow losses.

Clutch

The most obvious way of limiting the parasitic losses is to have a clutch to engage and disengage the compressor. Using a clutch has the advantage of reducing both losses in the air and the mechanical losses, assuming that the clutch is positioned on the crankshaft end of the belt. Since the compressor has a non-negligible inertia and that it rotates with high speed it is necessary to apply large amounts of torque in order to accelerate the compressor to working speeds within reasonable time. These torque impulses will result in comfort problems if the work has to be taken from the crankshaft. This problem has been covered by Kemmler et. al. [1.10]. They show that it can take up to 35 Nm in very short peaks as the compressor is engaged, the total acceleration time was 25 ms and the end (blower) speed was 3775 rpm. This low-end speed indicates that the device was a Roots blower. Takabe et. al. [1.3] have shown that by making the male rotor in the Lysholm compressor hollow the moment of inertia can be reduced by 42%, however the comfort problems still persists. Two further measures to fight this problem have been presented; longer engagement times and using the expansion work to rotate the compressor. Kemmler et. al. [1.10] used a hydraulic clutch to be able to control the engagement times. They were able to reduce the engagement torque from 35 Nm to 15 Nm if the engagement time was extended to 0,5 s. If the engagement time was allowed to be 1,2 s the maximum torque did not exceed the steady state driving torque.
By having the engine inhale the inlet air through the compressor some amount of the expansion work of the air will be input to the compressor shaft, and if the clutch is disengaged this torque will accelerate the compressor speed to a

specific value. This means that the torque at the engagement will decrease due to less need of acceleration.
Kemmler et. al. [1.10] reports that about 30% of steady-state speed can be reached before engagement starts. The same also holds for Miyagi et. al. [1.7] for the Lysholm compressor they tested.
Stubbemann et. al. [1.11] investigated if it was possible to extract work from the expansion of the inlet air at low- and part load conditions. They found that ideally 73% of the expansion work could be used but the practical maximum limit was about 50%. The largest drawback is however the small amount of work available.

Pressure relief valves

If a clutch is not used it is preferable to dump the charge pressure back to the inlet of the supercharger. For a Roots blower this results in a large decrease in driving power. If the outlet is connected to the inlet no compression work is done, the parasitic losses will thus only come from the mechanical losses in the blower and the pressure losses in the flow from outlet to inlet of the blower. This is the way Mercedes have decreased the parasitic losses on the M111 engines (200 and 230 Kompressor). They use an Eaton M45 Roots blower and a by-pass from outlet to the inlet and the blower is always connected to the crankshaft, Fortnagel et. al. [1.12]. Unfortunately they do not present the driving power of the blower during these running conditions.
On a compressor the parasitic losses don't decrease by using recirculation. Since the compression is internal the compressor will do compression work regardless. To decrease the compressor driving power the compression has to be punctuated. Both Lehmann et. al. [1.6] and Miyagi et. al. [1.7] used a relief valve approximately in the middle of the compression process. See figure 1.5 to see the Wankel-type compressor with relief valve used by Lehmann et. al. In fig. 1.4 above the compressor driving power at pressure relief conditions (π_c=1) can be seen. It is obvious that the power for the Roots blower with recirculation is almost reached. For Lehmann's et. al. [1.6] work it is more difficult to see the results from the pressure relief since they at the same time vary the volumetric efficiency of the compressor.

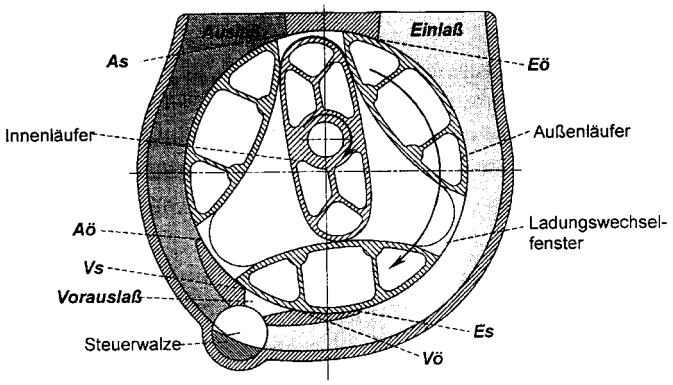

Figure 1.5 The wankel-type compressor with discharge valve investigated by Mercedes. Einlass=Inlet, Auslass=Outlet, Eö=Inlet Open, Es=Inlet close, Vö=discharge valve opens, Vs=discharge valve close, Vorauslass=discharge, Steuerwalze=Control valve, Aö=Outlet opens, As=Outlet close, Aussenläufer=Outer rotor, Innenläufer=Inner rotor. Figure from [1.6].

Both examples above [1.6, 1.7] have punctuated the compression process at one location. It would be preferable to be able to punctuate the compression work during the entire compression process. In this way no internal compression work would occur and it would have the same characteristics at part load as a Roots blower. However, no engine manufacturer has put such a solution in production.
Lehmann et. al. [1.6] were able to control the extent of the punctuation and were thus able to vary the pressure at outlet opening and can thus control the matching between outlet pressure and charge pressure. However, essentially that is a waste of compression work, it would be better to control outlet opening timing in order to only use the compression work needed, or more accurately open the compressor when a set chamber pressure is reached.

Throttle before compressor

By having the throttle before the compressor the pressure ratio would still be the same but the mass flow clearly decreased. Hori et. al. [1.13] showed that the driving power of a compressor is:

$$P = \frac{1}{\eta_{tot}} \dot{m}_{air} \eta_{vol} R T_{01} \frac{\gamma}{\gamma - 1} \left(\left(\frac{P_{02}}{P_{01}} \right)^{\frac{\gamma - 1}{\gamma}} - 1 \right) \qquad \text{eq. 1.2}$$

where:

P ..... driving power of the compressor

$\eta_{tot} = \eta_{ad} \cdot \eta_{mech}$ ..... efficiency as a product of adiabatic and mechanical efficiency

$\dot{m}_{air}$ ..... mass flow of air

η_{vol} ..... volumetric efficiency of the supercharger

R ..... specific gas constant for air (=287 [J*kg/(mol*K*m^3)])

T_{01} ..... total temperature at compressor inlet

$\gamma = \frac{c_p}{c_v}$ ..... ratio of specific heats

P_{02} ..... total pressure at compressor outlet

P_{01} ..... total pressure at compressor inlet

Which implies that the driving power is linearly dependent on mass flow.
Lehmann et. al. [1.6] state that with a throttled inlet the mechanical stresses on the compressor increases. But unfortunately they don't explain why. Oil leakage is expected if the compressor is not built for use under sub-atmospheric conditions.
Takabe et. al. [1.3] found that with 0.2 Bar abs in the compressor inlet the driving power was reduced by 30%. This indicates that it is difficult to achieve substantial savings in driving power with a throttle at the compressor inlet.
Takabe et. al. [1.3] also found that the force on the poly-V belt was higher than expected due to speed fluctuations of the engine. Within one engine cycle the speed fluctuates, which gives a pulsating force on the belt. These pulsating forces were decreased with a rubber damper on the crankshaft pulley.

1.3 Turbocharging

No literature study about turbocharging is complete without covering Turbocharging the Internal Combustion Engine by Watson and Janota [1.14]. In spite of being 20 years old it is still unbeaten on the throne as the true bible in the field. It covers all the fundamentals in a very good way, but it has to be complemented by papers on newer issues such as the latest versions of variable geometry, electric assist and calculation methods.

1.3.1 Single-turbo systems

The transient behaviour of a single-turbo system can of course be improved by turbocharger development. However, optimising the flow through blade angles etc. is a continuous process that has been going on for many years, so no dramatic improvements are to be expected within a small time frame.

A rigid turbine, with or without wastegate, of today's design is not able to supply enough power to the compressor for the boost pressure required for low speed and during transients. In addition, the flow range of a centrifugal compressor is a limiting factor. In fig. 1.6 below, the range of a centrifugal compressor, expressed as difference in mass flow between choke and surge conditions divided by the choking mass flow, is displayed as a function of pressure rise over the stage for an ensemble of built machines and operation points.

It is clear that the range will be narrower as the boost pressure rises. This will cause trouble if the turbine has enough efficiency at the extreme flows to both be able to push the compressor into surge and choke, for instance if electric assist is used for low engine speeds. Moreover, if higher boost pressures are demanded, it will be even more difficult to achieve satisfactory width of the usable range.

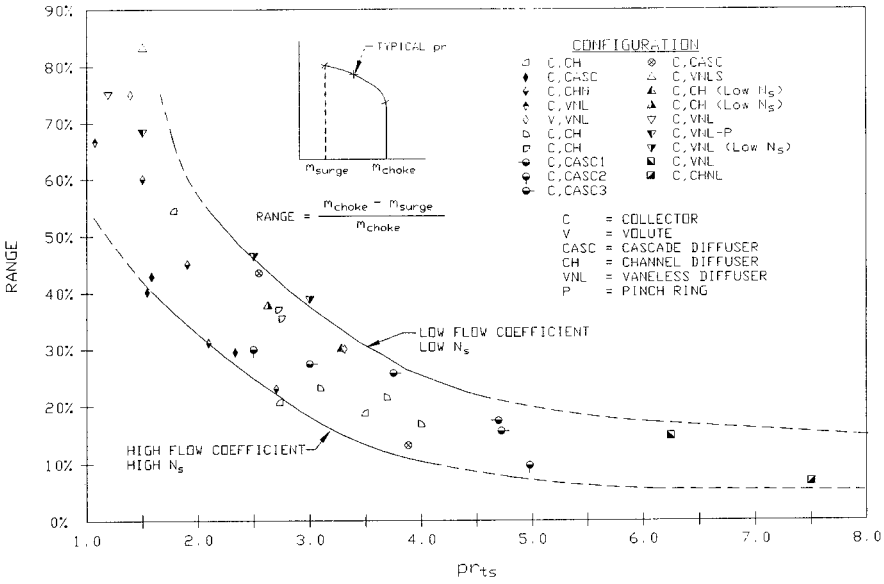

Figure 1.6. The flow range of a single stage centrifugal compressor as a function of pressure rise. The range will decrease substantially if the pressure ratio is increased from for instance 2 to 3. Figure from [1.15].

Porsche did an interesting survey in 1990 [1.16]. For their 4-cyl. 944 engine they tested four different single turbo system layouts. They compared the standard system, which had very long headers and subsequently a large volume manifold, to a system with substantially shortened (21-28% of std) runners and a volume that was only 30-38% of std. To this smaller manifold they connected the std turbo (single inlet wastegated), a twin entry (but single wastegate) unit and a variable geometry turbo (VGT). To evaluate the transient behaviour they ran a test where they simulated a vehicle acceleration in 2nd gear starting at 2000 rpm and 2 Bar BMEP. As measure of transient performance they used Δrpm to 15 Bar BMEP. With the variable geometry the turbo response improved by almost 60%, and for the twin entry 24% and for only reducing the manifold size by almost 22%. The vast improvement for the variable geometry turbine was not only due to the possibility of varying the turbine flow behaviour, but also from s 60% decrease in rotor inertia. The variability allowed the choice of a turbine wheel with a 18% smaller turbine wheel diameter. The other side of the coin of using variable geometry was a decrease in top end efficiency decreasing the maximum power output from the engine. Furthermore they concluded that the overall efficiency of the turbocharger is of the same order of importance as rotor moment of inertia when determining response characteristics.

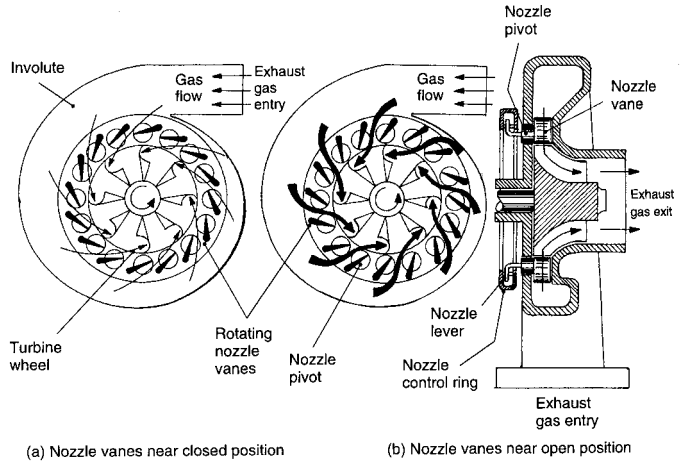

Figure 1.7. VGT turbocharger with variable guide vanes. Figure from Heisler [1.2].

Thus, by using variability the exhaust energy absorbing capabilities of the turbine is increased substantially at off design average mass flows, resulting in vast improvements especially during transients. This is what lies behind the success of passenger car diesels during the last 5-10 years. A lot is published about these variable turbines [1.2, 1.14, 1.17, 1.18, 1.19, 1.20, 1.21, 1.22]. Unfortunately the most efficient technology, VGT (variable guide vane diffuser

turbine) hitherto is not available for SI-engines due to temperature durability. Figure 1.7 shows the very small guide vanes with their delicate control mechanism. The only variable turbine suitable for otto-engine temperatures is the VST from 3K-Warner (figure 1.8), but it is not as efficient as the VGT [1.20, 1.21]. Figure 1.9 shows the spool-up time for 4 different turbine solutions. It has not been put in production on any car yet. A third technology, VNT, varies the width of the turbine diffuser in the same way as showed for a variable compressor in fig. 1.12, but no such turbo have been released for SI-engines yet.

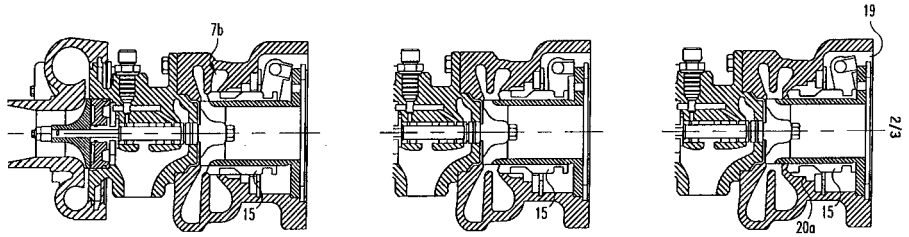

Figure 1.8. VST turbocharger from 3K-Warner. It varies the geometry by connecting/disconnecting a second volute (7b) to the same rotor, by means of a coupling device, no. 15 in the figure. It also has a bypass channel (20a) working as a wastegate. Figure from patent document [1.22].

Kemmler et. al. [1.17] state the VGT will require the use of waste gate on SI-engines but that will not be required for the VST. However, since the VST have internal bypass of the turbine it essentially already has a wastegate. The difference is that it requires only one actuator to both vary the geometry and actuate the wastegate, for the VGT two actuators are required, one for each function.

Willand et. al. [1.21] made a very thorough investigation of means of reducing response time for a single turbocharger. With a SiN (Silicon Nitride) turbine wheel the inertia (of the turbine wheel alone) was decreased with 64% and with TiAl 50% compared to standard inconel wheels, see figure 1.10.

Another means for further improvement of the turbo response is to decrease the bearing friction. Willand et. al. [1.21] states that, at low speeds, the friction power can amount up to a third of all available turbine power. By changing to ball bearings the turbine power to overcome friction can be reduced by 50%. Unfortunately no data shows how much this can reduce transient response. In contrast to Willand the turbocharger manufacturers say that the mechanical efficiency of the turbocharger is 95-100% for all operation points.

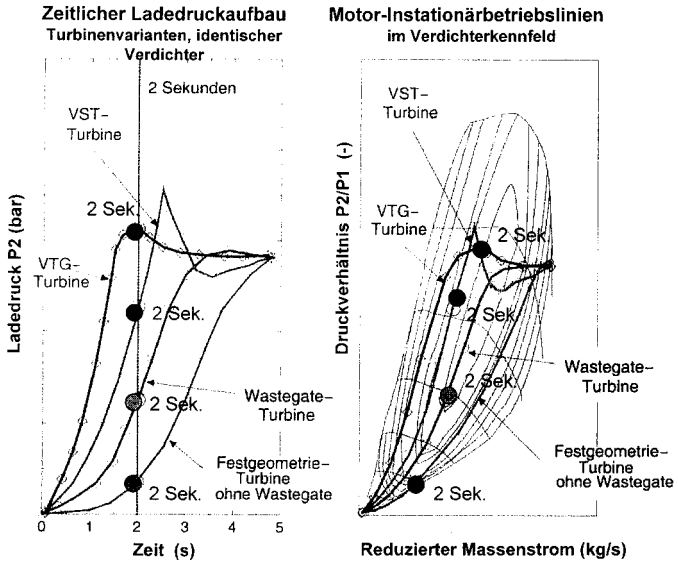

Figure 1.9. Boost pressure after a 2 s transient for 4 different turbine configurations. The inertia for the rotor was the same for all test. Figure from [1.21].

As turbine power is increasing at low speeds, and subsequently on low mass flows, the compressor will eventually run into surge. To avoid surge, the compressor map has to be widened. Means of doing that is ported shroud (or Map Width Enhancer) and variable compressors. Ported shroud enables some portion of the inlet flow to recirculate from slightly after the rotor inlet back to the inlet. At surge conditions the compressor then senses a higher inflow than the actual and thus the surge line is moved a bit to the left in the map. For choke condition the port acts as an increase in inlet area and thus enables some extra inflow. See left portion of fig. 1.11.
According to Concepts NREC [1.23] about 30-50% of the compressor work input is found as kinetic energy at the diffuser inlet. About 45-60% of this kinetic energy is then recovered as static pressure in the diffuser. If the diffuser has guide vanes, like the ones in a VGT turbine diffuser, this pressure recovery efficiency can be 55-75% but in a much narrower flow range. Therefore guide vanes must be variable to be suitable in automotive environments. By making the diffuser (without vanes) narrower, the surge line can be moved to the left in the map, which will reduce surge. Unfortunately this will narrow the entire map, so the diffuser gap has to be variable, as shown in fig. 1.12.

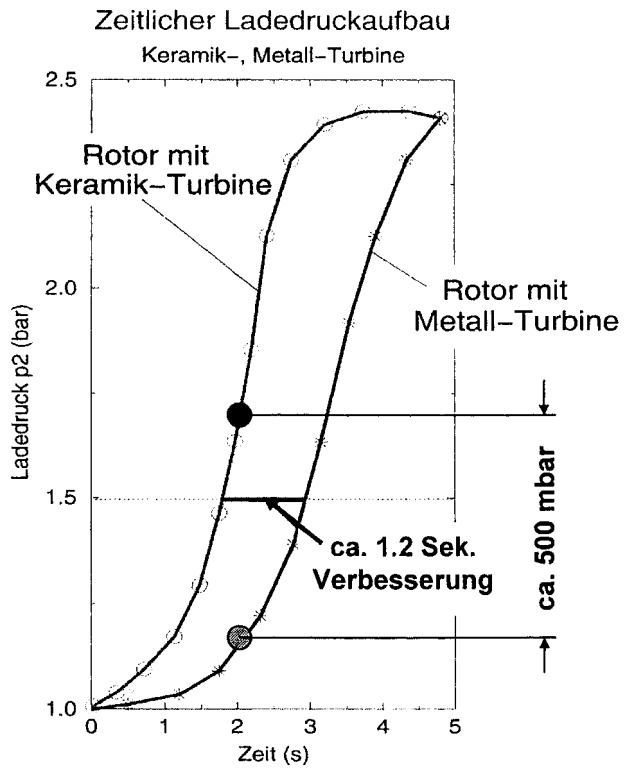

Figure 1.10. Increase in transient response due to decreased moment of inertia of the turbine wheel. Figure from [1.21].

Guide vanes can also be fitted to the compressor inlet. As figure 1.13 shows, with co-swirl on the inlet flow the entire map is moved leftward, enabling higher boost pressure for lower mass flows. If the guide vane generates opposite swirl the map is moved rightwards, moving the choke region towards higher mass flows. Unfortunately also the inlet guide vanes make the map narrower, so the inlet guide vanes have to be variable [1.21].

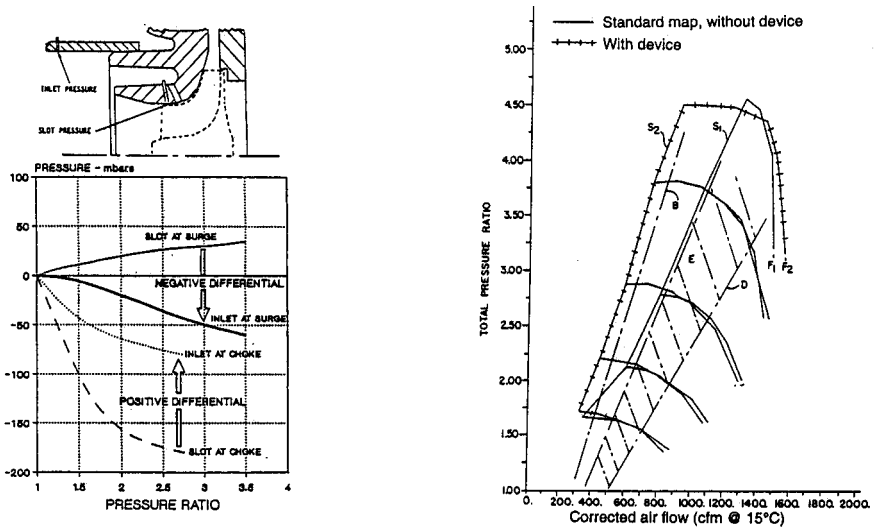

Figure 1.11. During surge the pressure is higher in the slot than in the inlet, therefore air is recirculated from the slot to the inlet. At choke the inlet has higher pressure than the slot and therefore the extra air flows into the compressor from the inlet through the slot. Figure from [1.23].

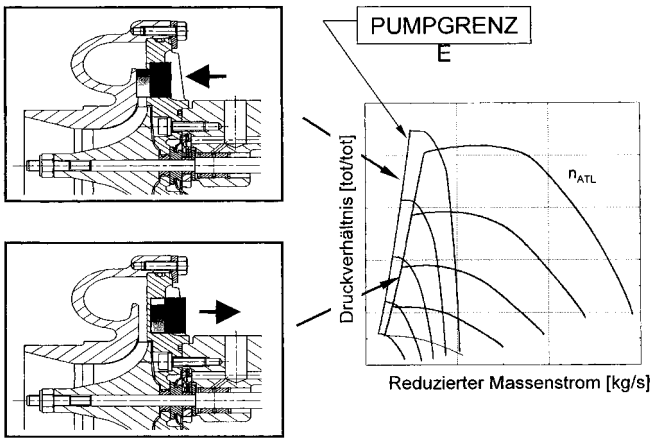

Figure 1.12. By narrowing the diffuser width the map can be moved to the left, unfortunately the map becomes narrower so the diffuser width has to be variable. Figure from [1.21].

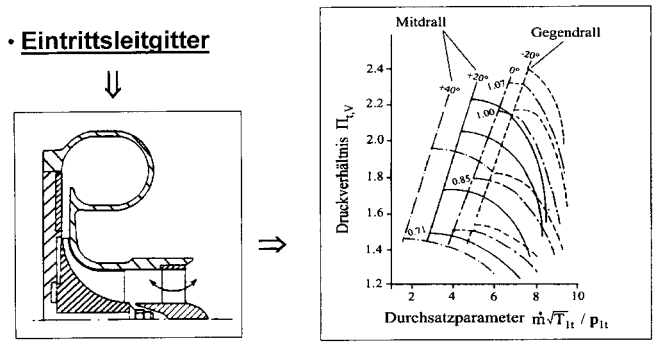

Figure 1.13. Variable guide vanes in the compressor inlet. Mitdrall is co-swirl and Gegendrall opposite swirl. Picture from [1.21].

A third way is to increase the mass flow through the compressor by controlling the opening of the pressure relief valve. This will, for the same mass flow to the engine, increase the mass flow through the compressor. With more mass flow more boost pressure can be used without surge. According to Fieweger et. al. [1.24] such recirculation can be more effective than variable geometry in the compressor. The drawback is of course that more compressor power is needed in order to pump a larger mass flow, and thus a higher turbine power resulting in higher backpressures.
The conclusion that can be drawn from this is that if it was possible to manufacture turbines with high enough efficiency to drive the compressor to the boost pressures required over the entire operating range, the compressor probably must have variable geometry.

1.3.2 Sequential systems

A more extreme case of variable geometry is sequential turbocharging. Instead of varying the geometry of one charger the number of chargers is changed.
The reason for using sequential turbocharging is to widen the flow range for the boost pressure required. Since still only one compressor stage is used it does not necessarily increase the boost pressure.
Volvo tested sequential systems presented in an SAE paper in 1991 [1.26] as a part of a methanol engine program. The engine was a six-cylinder unit and the boost pressure target was as usual, slightly below 2 Bar abs. They state that a parallel turbo system has around 30% lower inertia than a single turbo with the same top end flow characteristics, and thus should have a benefit in terms of response. To further increase the response sequential systems was investigated. They conclude that a series-sequential system was beneficial over a parallel-sequential system. The reason for that was the difficulty of achieving a smooth

transition from one-turbo operation to two-turbo operation for the latter. However, the series-sequential system has a narrower flow range because the entire mass flow has to go through both compressors, on the other hand, the two-stage compression would allow for higher boost pressures with maintained reasonable flow range. Fig. 1.14 shows Volvo's series-sequential turbo-system.

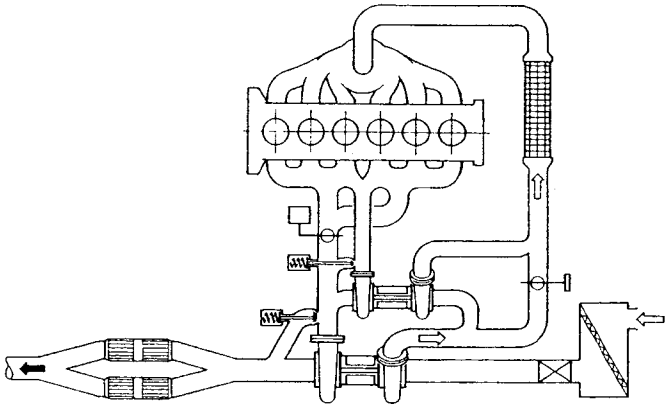

Figure 1.14 The series-sequential systems tested by Volvo. It consists of a LP and HP turbo where the LP turbine can be disconnected by means of a butterfly valve in the exhaust manifold. Another butterfly valve at the compressor side can change from series operation to operation of the HP compressor alone. Figure from [1.26].

Both Porsche and Mazda have used sequential turbocharging on production engines. In a course material from Concepts NREC [1.27] some details of these systems are revealed.
On these systems both turbochargers were probably of the same size, unfortunately this is not very clear in [1.27]. Both systems uses control valves to switch on and off both compressor and turbine on the second turbocharger. When the second turbocharger is switched on, the turbine is fed with exhausts before the compressor outlet is opened, which will result in a faster acceleration of the turbocharger. Running a compressor with closed outlet will eventually result in surge. It would be preferable to have the control valve at the inlet, but then oil leakage problems will occur since most turbochargers oil seals are not built for sub-atmospheric conditions. Mazda solved the surge problems by opening the pressure relief valve during the acceleration process, then no pressure build up will occur but still the rotor is accelerated.

1.3.3 Two-stage systems

No publications have been found covering two-stage turbocharging of Otto-engines. Traditionally it has been used for boost pressures far above 2 Bar abs

[1.27] but 3K have presented a two-stage system for 3 bar abs of boost pressure, but for diesel engines, see Pflüger et. al. [1.28]. Figure 1.15 shows an example of the division of pressure ratio between the HP and LP compressors.
The system consists of two unequal sized turbochargers with wastegate on the HP stage and intercooling after each stage. The system is optimised for a 12-liter diesel engine and the HP and LP stage's sizes are 85% and 112% respectively of the size of a single turbo optimised for the same engine. No transients were tested but in the text it is stated that two-stage is better in transients than a sequential turbo system.
At the low speed end the 2 Bar abs boost pressure point is moved from 1000 rpm for the single turbo system to 700 rpm for the two-stage system.
In 2004 BMW released the new 535d-model equipped with a 3K-developed 2-stage boosting system [1.29]. The system is similar to the truck-sized system with the addition of a wastegate for the LP-stage. On paper the system, and the engine, looks very promising with impressive performance. 3K described the differences in matching between the two systems in a very informative paper at the 9. Aufladetechnische Konferenz in Dresden [1.30]. As a literature on radial compressor design constraints it is very informative reading. They conclude that if both the boost pressure and range should be increased simultaneously with at least maintained efficiency a single stage compressor must be fitted with variable guide vanes probably both at inlet and in the diffuser, or a two-stage system must be employed. Since the two-stage system consists of known technology, they think it is a safer route.
Cantemir [1.31] also describes a twin-turbo, sequential system where the compressors is run in series (two-stage) operation for the low speed range of the engine and switched to parallel mode for the higher speed range. He argues that with turbochargers of equal size the shape of the compressor maps are very suitable for this kind of operation. The turbines are always run in parallel. Unfortunately no performance figures of the system are presented.

1.4 Hybrid systems

It is preferable to use the power in the exhaust gases to drive the charger. But having only one conventional turbocharger will not cover the entire speed/load range of the engine satisfactorily. One solution to this is to have the turbocharger laid out for a fraction of the engine's entire range and to use a mechanical charger as a supporting device where the turbocharger cannot fulfill the targets on its own.

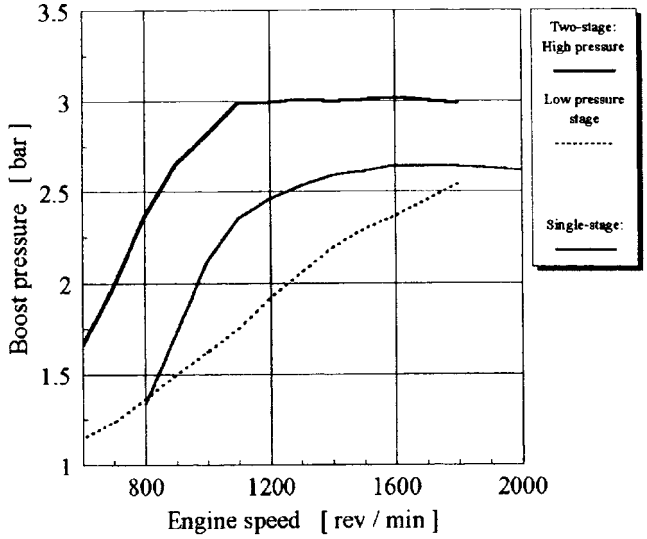

Figure 1.15. Maximum possible stationary boost pressure for the single turbo system and the two-stage system. Figure from [1.27].

A combination of a turbocharger and some other charging device of different kind than a turbo, is called a hybrid system. Several manufacturers have used them in production (ex. Volvo trucks) or in competition (ex. Lancia Delta SP4) vehicles, but surprisingly little is published about these systems.
The most obvious way of combining a turbo and a supercharger is to use the turbo in the high and medium speeds and support it with a supercharger on low speeds and during transients.
Schmitz et. al. [1.32] have used a Wankel-type compressor as a support for a turbo on a 8.8 litre diesel engine. The compressor was positioned upstream the turbocharger due temperature limitations on the compressor inlet temperature. The compressor was connected to the engine via a clutch and the inlet air could be bypassed the compressor over a check valve. The result in transient performance is presented in fig. 1.16. Where it can be seen that the time to maximum charge pressure is reduced by 66% with the hybrid system. However, it can also be seen that the charge pressure is reduced to 70% of maximum as the compressor is disengaged but recovers in a few seconds. On a small displacement SI-engine such a pressure fall is expected to result in comfort problems, or at least very uneven torque characteristics. No comfort problem is however reported by Schmitz. A diesel engine can keep the torque constant by having the fuelling constant, and thus the transient fluctuations in airflow

results in a possible lambda-related smoke-problems rather than a problems with fluctuating torque transient. In addition diesel engine has larger inertia per volume displacement while the compressor has about the same inertia per volume displacement regardless of if it's working with a diesel- or otto-engine. Therefore SI-engines are more prone to exhibit comfort problems with engagement of supporting superchargers. Since the compressor has no variability it is expected that it is not working with optimum efficiency for all running conditions, but no efficiency figures are shown.

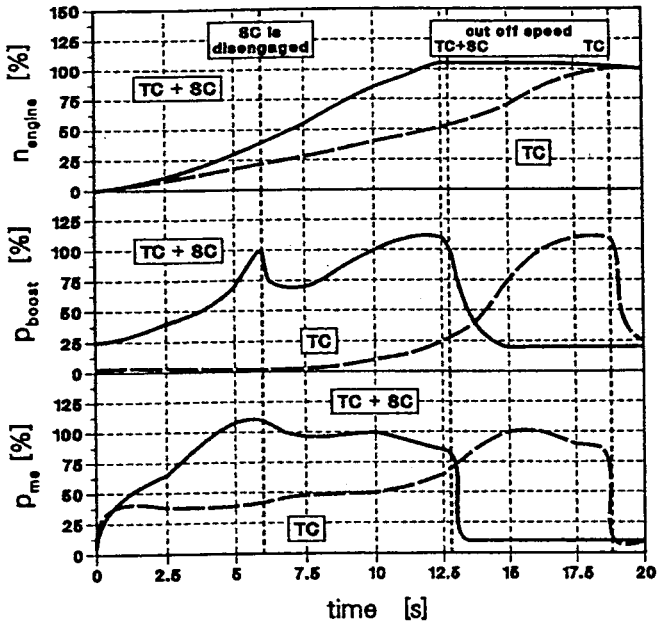

Figure 1.16. Boost pressure characteristics for a turbocharged heavy diesel engine with and without supporting supercharger. Figure from [1.32].

Japanese compressor manufacturer IHI has in two papers [1.13, 1.30] shown their Lysholm compressor in a hybrid system on a 8.8 liter diesel engine. They have in opposition to Schmitz et. al. [1.32] chosen to place the compressor between the turbo and the engine inlet manifold. Neither system has any charge cooling between the two stages, only one cooler after the two stages.
Unfortunately no transient response data is presented [1.13, 1.30], but steady state performance at low speeds is increased. The compressor is connected to the engine over a clutch and no comfort problems are reported. But, Takabe et. al. [1.30] saw a need for decreased inertia anyway due to clutch overload at engagement at high compressor loads.
No figures on compressor efficiency during operation are presented.

1.5 Electrically driven or assisted solutions

A lot of work has been published on electrically driven or assisted chargers [1.20, 1.21, 1.24, 1.34, 1.35, 1.36]. Unfortunately almost all of those are simulation work, probably because electrically assisted turbochargers are so easy to simulate and so difficult to realize.

Electric assist has been used in two ways, either by having an extra electrically driven supercharger supporting the turbo at low loads and during transients or by having the electric motor attached directly on the turbocharger shaft.

Habermann et. al. [1.34] show that during the first two seconds of a transient on a turbocharged engine only very small fractions of 1 kW is available on the turbocharger shaft for acceleration, see figure 1.17.

This opens the possibility for improving the transient behaviour with addition of quite small amounts of electric power. Habermann added 1.8 kW of power and assumed 90% efficiency of the electric motor and 5% extra inertia on the shaft. The results for a 1.4 litre otto-engine fitted with the e-assisted turbo compared to a naturally aspirated 2.0 litre engine are showed in fig. 1.18. The acceleration time of the turbocharger from 2000 rpm to 160000 rpm was 2 sec.

Fieweger et. al. [1.24] simulated a 1.9 litre diesel passenger car engine with e-assisted turbo. The results from a simulated vehicle acceleration as a function of the power added to the turbocharger shaft is shown in fig. 1.19. The simulations were done with GT-Power coupled with Simulink.

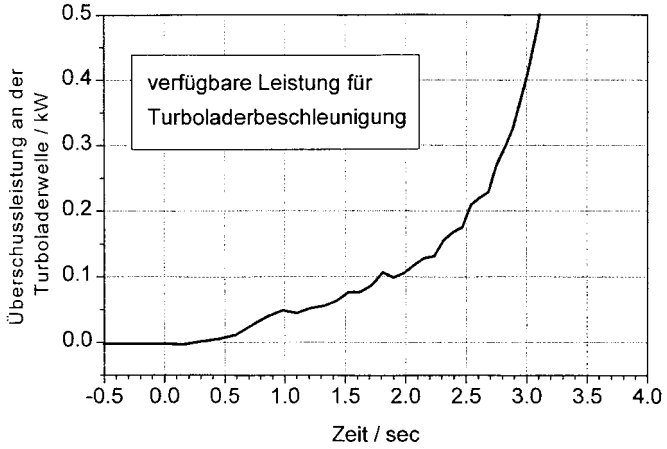

Figure 1.17. The power available for acceleration at the turbocharger shaft for a 1.4-liter, turbocharged engine, as a function of time during a transient. Figure from [1.34].

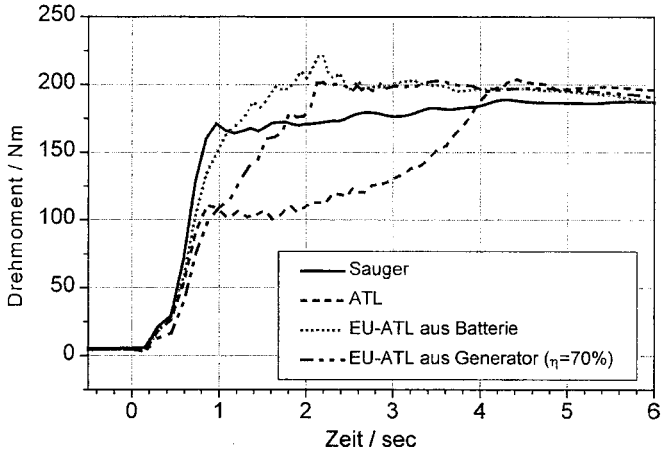

Figure 1.18. Transient performance of an e-assisted turbocharged 1.4 litre otto compared to a 2.0 liter NA-engine. Sauger *means naturally aspirated,* ATL *means turbocharger (with wastegate),* EU-ATL aus Batterie *means e-assisted turbocharger with battery power and* EU-ATL aus Generator *means e-assisted turbocharger with power from the alternator. Figure from [1.34].*

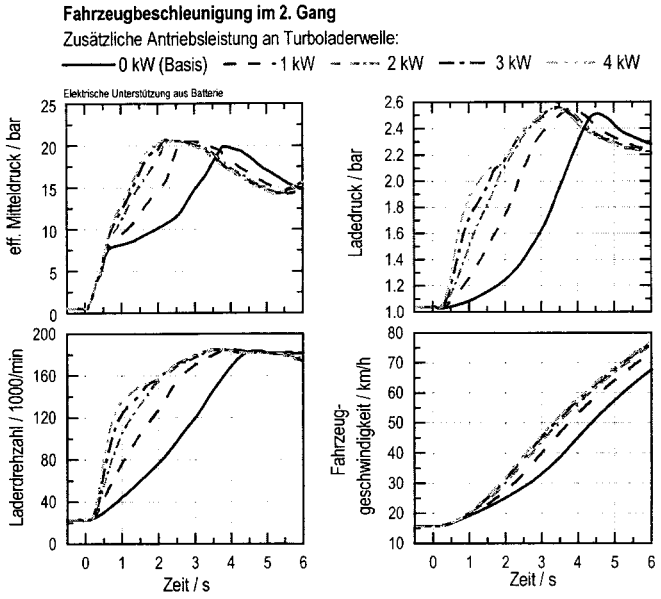

Figure 1.19. Simulated vehicle acceleration in 2nd gear for different power on the turbocharger shaft. Eff. Mitteldruck = *BMEP,* Ladedruck = *Boost pressure,* Laderdrehzahl = *Turbocharger speed,* Fahrzeuggeschwindigkeit = *Vehicle speed,* Zeit = *Time. Figure from [1.24].*

The e-assisted turbo can also be used as a means of increasing the maximum possible boost pressure, at least on low speeds [1.24]. But with only 2 kW of power on the turbocharger shaft the surge line was traversed for 1250 rpm engine speed.
If the electric machine on an electrically assisted turbo is given generating properties the machine can be used as a generator when the available turbine power is higher than what is necessary to drive the compressor [1.37]. Ford did a simulation exercise (mean value model) on such a system where they set out the target that the e-assisted turbo should be able to regenerate its own power. Max power both in power delivery and absorption was limited to 1.5 kW and it allowed for a 15% improvement in takeoff performance for the vehicle tested. Furthermore they concluded that the moment of inertia of the rotor had to increase by 250% in order to offset the acceleration improvement allowed by the electric assist. The assumed efficiencies for the motor and generator were 90% and 70% respectively.
Another way of using electric assist is to have an extra electrically driven supercharger to support the turbocharger at the same running conditions as the e-assisted turbo [1.20, 1.21]. 3K has a electrically driven centrifugal compressor (eBooster) that they market, and Turbodyne [1.36] has had it for some years.
Hoeckner et. al. [1.20] have tested eBooster against an e-assisted turbo and their conclusion is that the eBooster offers a faster response due to the fact that the rotor of the electric motor can have a lower inertia because it is not connected to the turbine wheel. This is shown by Habermann et. al [1.34], but the difference it not very large. The eBooster also offers the possibility of higher boost pressures without variable compressors if it is fitted in series with the regular turbo. A third advantage for the eBooster is that the electric motor doesn't have to stand as high temperature as for the e-assisted turbo.

Table 1.1. Pros and cons for eBoost and e-assisted turbocharger, conclusions drawn from [1.20, 1.21, 1.34].

	EBooster	**e-assisted turbocharger**
Response	+	
Max boost pressure	+	
Temperature sensitivity	+	
Weight		+
Packing		+
Complexity	+	
Technological availability	+	

Willand et. al. [1.21] assumed that a variable compressor is absolutely necessary for the e-assisted turbo and drew the conclusion that eBooster is a better solution than e-assisted turbo. The pros and cons for eBooster and e-assisted turbo are listed in table 1.1.

1.6 Conclusions

In this chapter a wide variety of alternatives to the single turbocharger with wastegate, that offer an increase in work range and/or boost pressure, have been considered. The systems are investigated on a wide variety of engines, ranging from a 1.4-litre SI- to 12-litre CI-engines. Therefore it was difficult to draw any safe conclusions about the systems' pros and cons. The conclusion is thus that an investigation has to be done where all systems are tested on the same engine. Doing such an investigation experimentally would be very expensive. Therefore computer simulations were chosen for the task. However, as will be seen in chapter 3 in this work the predictability of the computer simulations are too poor to allow for an investigation as suggested above. Possible differences between systems could well be hidden behind calculation errors. Therefore the suggested investigation could not be carried out within this work.

In table 1.2 an attempt is made to summarize the properties of the most promising systems. For the mechanical supercharger, with and without clutch must considered separately, and for electric assist one must separate the electrically assisted turbocharger and the e-booster. The most promising system (sum of + and -) is the twin, series sequential system, which is also what BMW has selected for the new 535d model where higher boost pressure and wider range was an important development target [1.29].

Table 1.2. Summary of the properties of the most probable systems. For the mechanical supercharger, with and without clutch must considered separately, and for electric assist one must separate the electrically assisted turbocharger and the e-booster. Thus the double rows.

System type (WG turbo baseline)	**Response**	**Range**	**System efficiency / BSFC**	**Max power**	**Low speed**	**Comp-lexity**
Mechanical Supercharger	w cl. 0 w/o cl. +++	+++ +++	- - - - - -	++ ++	+++ +++	- ++
Twin parallel turbo	+	+	0	+	+	0
Twin, series sequential	++	+++	++	+++	++	-
Twin, parallel sequential	++	++	++	++	++	- - -
VGT	++	+	0	0	++	- - -
Hybrid turbo- and super-charging	++	+++	0	++	+++	- - -
E- assisted booster	ETurbo ++ EBooster ++	0 ++	0 0	0 +	++ ++	- - -

Leisure reading

Among the collection of although interesting and information-packed, but often quite boring, or at least hard to read relaxed, there are some golden eggs. I'm talking about papers written in a tone so relaxed, and about a subject so joyful, that they are more suitable for reading in the hammock (or on the beach) than in the study. The first of these is Hans Mezger's "Turbocharging Engines for Racing and Passenger Cars" [1.38] from 1978. An exposé over the turbocharging adventures within the house of firma Dr. Ing. H.C.F. Porsche Aktiengesellschaft starting at Büchi's patent, through the fire-breathing, 1000hp+, Porsche 917 to the, at the time present, 911 turbo.

Another one is from Daimler-Benz AG "Some Special Features of the Turbocharged Gasoline Engine" from 1979 [1.39]. There it is concluded, from tests on the solid twin-cam, in-line six of the time, that the control of the boost pressure is the weak point of turbocharged gasoline engines, and that the use of a wastegate is not suitable for passenger cars.

1.7 References

1.1 Ansdale, Richard F "A Reconnaissance of Supercharging Technology 1902-1980" SAE Paper 810003
1.2 Heisler Heinz. "Advanced engine technology" SAE International 1995 ISBN 1 56091 734 2
1.3 Takabe et. al. "Second generation Lysholm Compressor" SAE Paper 980774
1.4 www.eaton.com 020820
1.5 Enderle C. et. al. "Neue Vierzylinder-Ottomotoren von Mercedes-Benz mit Kompressoraufladung" MTZ Motortechnische Zeitschrift no. 7-8 2002 pp. 580.
1.6 Lehmann et. al. "Ein neuartiges Regelkonzept für mechanische Lader" 7. Aufladetechnische Konferenz in Dresden 2000 pp. 145-167
1.7 Miyagi et. al. "Experimental study of New Lysholm Supercharger with a Simple Unloading System" SAE Paper 960952
1.8 http://www.roulunds-rotrex.com/rotrex/ , issue 020822
1.9 Kolstrup A, Rasmussen H M. "Supercharging Internal Combustion Engines" HdT Tagung Aufladung von Verbrennungsmotoren, Berlin 000330-000331.
1.10 Kemmler et. al. "Entwicklungstendenzen aufgeladener Ottomotoren" 7. Aufladetechnische Konferenz in Dresden 2000 pp. 28-42
1.11 Stubbemann et. al. "Mechanische Lader im Expansionsbetrieb – lohnt sich der Aufwand?" 7. Aufladetechnische Konferenz in Dresden 2000 pp. 171-187.
1.12 Fortnagel et. al. "Technischer Fortschritt durch Evolution – Neue Vierzylinder-Ottomotoren von Mercedes-Benz auf Basis des erfolgreichen M111" MTZ 61 7/8 2000 pp. 458-464
1.13 Hori et. al. "Examinations of a Lysholm Compressor's performance and the engine performance supercharged by the Lysholm Compressor" IMechE Paper no. C554/019/98 1998.
1.14 Watson N, Janota M S. "Turbocharging the Internal Combustion Engine" MacMillan Press 1982 ISBN 0 333 24290 4
1.15 Japikse D, Baines N C. "Introduction to turbomachinery" Concepts ETI & Oxford University Press 1997. ISBN 0-933283-10-5
1.16 Brüstle C, Wagner J, Tran Van K, Burk K. "Turbocharging techniques for sports car engines" IMechE C405/055 1990.
1.17 Kemmler et. al. "Entwicklungstendenzen aufgeladener Ottomotoren" 7. Aufladetechnische Konferenz in Dresden 2000 pp. 28-42
1.18 Kakernaak et. al. "DAF Rennmotor mit Doppel-VGT-Lader" MTZ no. 11 2000

1.19 Jenny, E. ”Beschleunigungsverhalten von Diesel- und Otto-PKW-Motoren mit Turboladern fixer und variabler Geometrie, mechanischen Ladern und Comprex” VDI-Berichte nr 910, 1991
1.20 Hoeckner et. al. ”Moderne Aufladekonzepte für PKW-dieselmotoren” 7. Aufladetechnische Konferenz in Dresden 2000 pp. 115-133
1.21 Willand et. al. ”Entwicklung innovativer Aufladesysteme” 7. Aufladetechnische Konferenz in Dresden 2000 pp. 369-412
1.22 Borg-Warner Inc. PCT Patent no. WO 00/73630 A1
1.23 Concepts NREC Course material ”Turbocharging the internal combustion engine” Chapter 3 Centrifugal Compressor Technology and Design, Nick Baines 2000
1.24 Fieweger et. al. ”Potential des elektrisch unterstützten Turboladers bei modernen PKW DI-dieselmotoren” 7. Aufladetechnische Konferenz in Dresden 2000 pp. 345-367
1.25 Westin et. al. “The Influence of Residual Gases on Knock in Turbocharged SI-Engines” SAE-Paper 2000-01-2840
1.26 Backlund O, Keen P R, Rydquist J E, Giselmo K, Sundin L “Volvo’s MEP and PCP Engines: Combining Environmental Benefit with High Performance” SAE Paper 910010
1.27 Concepts NREC Course material ”Turbocharging the internal combustion engine” Chapter 5 Turbocharger system development, Nick Baines 2000
1.28 Pflüger K “Regulated two-stage turbocharging – KKK’s new charging system for commercial diesel engines” IMechE C554/035/98 Turbocharging and Turbochargers 1998.
1.32 Schmitz et. al. “Potential of Additional Mechanical Supercharging for Commercial Vehicle Engines” SAE Paper 942268
1.30 Takabe et. al. ”Second generation Lysholm Compressor” SAE Paper 980774
1.29 Stütz W, Staub P, Mayr K & Neuhauser W “Neues 2-stufiges Aufladekonzept für PKW-dieselmotoren” 9. Aufladetechnische Konferenz in Dresden 2004.
1.30 Tomm U & Schmitt F “Optimierung von Hoch- und Nieder-druckverdichter für die zweistufig geregelte Aufladung” 9. Aufladetechnische Konferenz in Dresden 2004.
1.31 Cantemir Codrin-Gruie “Twin turbo strategy operation” SAE Paper no 2001-01-0666
1.34 Habermann et. al. ”Aufladung von Verbrennungsmotoren als Massnahme zur Verbrauchsverbesserung” HdT-Tagung26-27/6/2000 München, Downsizingkonzepte für Otto- und Dieselfahrzeugen
1.35 Zellbeck et. al. “Die elektrisch unterstützte Abgasturboaufladung als neues Aufladekonzept” MTZ 60 (1999) pp. 386 ff.

1.36 http://www.turbodyne.com/ 020820
1.37 Kolmanovsky I, Stefanopoulou A G "Evaluation of Turbocharger Power Assist System Using Optimal Control Techniques" SAE Paper 2000-01-0519
1.38 Mezger Hans, "Turbocharging Engines for Racing and Passenger Cars" SAE Paper 780718
1.39 Hiereth H, Withalm G, "Some Special Features of the Turbocharged Gasoline Engine" SAE Paper 790207

Chapter 2

Literature study on unsteady flow performance of radial turbines

2.1 Problem description

Calculations of the work output from the turbocharger's turbine is a large problem when trying to predict the performance of an engine design.

There doesn't seem to exist any geometrically detailed, physically accurate, parametric model of the turbine, proven to give accurate results. Instead calculations of turbine performance are based on performance maps commonly measured by the turbocharger manufacturer. These maps are measured with steady-flow flow-benches and they show the adiabatic efficiency and speed as functions of mass flow and pressure ratio.

The problem arises when the turbo is used on the engine, where the mass flow and pressure ratio are non-steady. So, how can the steady flow maps be used in that unsteady flow?

Just using time- or energy-averaged quantities does not give good results. Instead the quasi-steady assumption has become the standard method. Watson & Janota [2.1] have a good description of quasi-steadiness in their *Turbocharging the internal combustion engine*; "the turbine behaves at any instant in an identical manner under steady or unsteady flow ('quasi-steady flow')". Thus, in a quasi-steady (QS-) calculation of the turbine performance as in GT-Power, the mass flow rate and efficiency can be read from the maps at any instant since speed

and pressure ratios are calculated from previous cycles and surrounding components.

2.2 Comparisons between measurements in pulsating flow benches and QS-calculations

Due to their simplicity, quasi-steady calculations have become the standard method despite the fact that the results usually deviates from experiments.
Chen and Winterbone [2.2] suggest the usage of the Strouhal number (ratio of two timescales) to determine if a device can be treated quasi-steadily or purely unsteady.

$$Str = \frac{\tau_A}{\tau_B} \qquad \text{eq. 2.1}$$

Where τ_A is the propagation time of a fluid particle and τ_B is the timescale of the unsteady flow. If Str<<1 the problem can be treated quasi-steadily but if Str>>1 unsteady effects dominate. In the intermediate region both effects probably are important. Chen & Winterbone conclude that the volute is unsteady but the rotor, due to it's short flow paths, can be treated quasi-steadily.
Rowland Benson at UMIST [2.3] used a flow bench with a drum-type pulse generator and cold air to investigate possible correlations between pulse shape, frequency and the calculation error using the QS-assumption to calculate mass flow and power output. Unfortunately no clear, useful correlations could be found. The size of the errors encountered for QS-calculations was 10-20% for the mass flow and 20-50% for the pressure ratio (worse for higher pulsation amplitude).
Dale & Watson, at Imperial College, London, [2.4] presented in 1986 results from another pulsating flow-bench test of the turbine performance. They compared unsteady test data with quasi-steady calculations. One of the main points was that with steady flow turbine maps measured with the standard procedure, using a compressor, matched to the turbine as for use on an engine, as a dynamometer, the necessary map range (in terms of pressure ratio) for calculation of an unsteady flow pulse through the turbine could not be covered. The compressor could not absorb enough power for steady flow if the desired pressure ratio was to be achieved on the turbine side. To cover the satisfactory range, they therefore used an eddy-current dynamometer. However, using several different compressors, or elevate the pressure level on the compressor side to increase massflow, could also be a solution to the problem. As will be

shown in Chapter 3 this problem still exists with the maps acquired from the turbocharger manufacturers.
They also showed that the measured instantaneous efficiency could deviate as much as 10% from the efficiency value acquired in a QS-calculation, and that it could be both higher and lower than that value, however the mean unsteady efficiency was a few percentage points below the QS-acquired value. Unfortunately it is not stated whether that average is an energy, mass or time average.
The instantaneous efficiency was acquired through mass flow measurements with hot-wire anemometers positioned right upstream of the pulse generator. It should be noted that the pulse shape and amplitude is quite different from the situation on an SI-engine.
Another important discovery was, that as the blade speed ratio (rotor tip speed divided by the isentropic nozzle outlet speed, U/C_s) decreased at the peak of the pulses, the efficiency decreased substantially, from maximum 70% down to 32% for U/C_s=0.25. They also observed that the blade speed ratio at maximum efficiency could deviate away from the standard value U/C_s=0.707. For an isentropic radial inflow turbine with complete exhaust recovery and 50% reaction the efficiency vs. U/C_s has the shape of a parabola and peak efficiency occurs at U/C_s=0.707 [2.1, 2.5]. In a subsequent publication [2.6] they showed an efficiency vs. U/C_s trajectory for two different pulses that both deviated from the parabolic shape normally stipulated for steady flow.

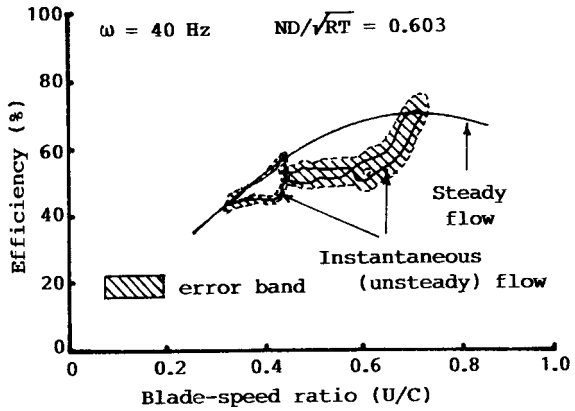

Figure 2.1. Efficiency vs. blade speed ratio for steady and unsteady flow. It is obvious that the unsteady trajectory can deviate from the steady flow trajectory. Figure from [2.6].

A similar investigation was published by Capobianco et. al in 1989 [2.7]. They also used a pulsating cold-flow bench, but with the compressor as a dynamometer.
They measured mass flow rate and turbine power and compared with QS predictions. The result was that the predicted mass flow was 5-10% lower, the predicted power 10-15% lower and predicted efficiency 0-5% lower than measured on the bench.
Baines et. al. [2.8], also at Imperial College, did another investigation on the test bench used by Dale & Watson [2.4, 2.6]. In all these three investigations it was necessary to shift the pressure and mass flow signals versus the torque signal due to a finite propagation time from the pressure and mass flow measurement location down to the turbine wheel. Baines et. al. assumed that this phasing should be done corresponding to the bulk flow speed as opposed to the two previous investigations that assumed correspondence to the velocity of sound. This phasing can have a rather large influence on the calculated instantaneous efficiency. The resulting values should thus always be judged from how they were acquired, and since there exist two different phasing strategies the data sets cannot be compatible. Baines' et. al. motivation for their method is that if the ts-efficiency is plotted vs. pressure ratio, the bulk-flow phasing is the only way to get the trajectories closed.
In contrast to the Baines group, Winterbone et. al. [2.9, 2.10] concluded that the volute is quasi-steady and the rotor is unsteady. The experimental setup used is quite similar to the ones described above, aside from the dynamometer which in this case is hydraulic. The conclusion is based on pressure measurements from several locations inside the volute showing that for every instant the pressure is almost equal for all circumferential locations.
Similar to the Baines group a phase difference between pressure delivery and torque output is observed. It is stated that the torque delivery lag is much longer than the wave propagation time from pressure measurement location. From that it is concluded that some dynamic effects occur in the rotor.
Steady flow measurements with static pressure taps on the volute wall are also presented and they show that the static pressure can vary up to 10% over the circumference. This pressure difference will cause the stator outlet flow angle to vary over the circumference and Winterbone calls this "a major cause of inefficiency in vaneless turbines" [2.9].
In a somewhat later paper Winterbone & Pearson [2.11] showed some data from the same flow bench along with a review of some of the papers mentioned above. The most important point made is that the phase difference between inlet pressure and output torque is due to dead volumes and finite propagation times from measurement location and rotor. It is stated that the phase difference is correlated against the gas propagation time halfway around

the circumference. Subsequently the results from the papers about unsteady efficiency etc. of radial turbines have all been very dependent on setup and phase-adjustment method.
Overall, the paper of Winterbone & Pearson [2.11] is a very good summary and thus a good choice as first reading for someone new to the field.

2.3 On-engine turbine performance and efficiency determination

To be able to determine whether the QS-analysis performs well or not one must have a reasonable idea of how the turbine actually works on the engine. That requires detailed measurement of the turbine performance on the engine.
Not many publications have been found that shows efficiency or even performance data from on-engine measurements.
Ehrlich [2.12] did a vast investigation on a truck-sized diesel engine. The measurement setup was impressive with instantaneous total (single point, Pitot-tube with recessed transducer) and static pressure measurements enabling mass flow measurements. The use of single point total pressure measurement was justified with flow field pictures taken with PIV. The frequency response of the total pressure probe was justified through shock-tube tests. Instantaneous temperatures were measured with thermocouples that normally are too slow but in this case compensated mathematically to acquire satisfactory response characteristics.
Only mean value of turbocharger speed was measured by a magnetized nut at the compressor side.
From the measurements it is observed that the inlet and outlet mass flows are not identical all the time. Therefore mass accumulation must occur in the turbine. From this Ehrlich concludes that a traditional isentropic efficiency cannot be calculated. Therefore only output and input power data is presented, no efficiency figures.
Furthermore it is pointed out that a simple order-of-magnitude heat transfer calculation shows that the heat transfer is not negligible compared to the turbine shaft power. And this even though the engine is a low output diesel with turbine inlet temperatures significantly lower than for those on a high output SI-engine (*author's note*).
Ehrlich also found that significant temperature fluctuations due to combustion led to significant density variations, which in turn led to large mass fluctuation in the turbine, causing an energy storage in the turbine volume.
Unfortunately several of Ehrlich's measurement methods would be very difficult to apply to an SI-engine. The engine he used was an in-line six diesel with quite low output (5.9 liters, peak torque 569 Nm @ 1600 rpm) and the

turbine was a twin entry unit. The low speed and only three cylinders per turbine inlet results in a pulse frequency significantly lower than for a four-cylinder SI-engine. This will make it less probable for the recessed total pressure probes to have satisfactory response characteristics. This in combination with an even more difficult temperature measurement task (higher temperature and higher gas velocities) will make the mass flow determinations very, very difficult, if possible.
Luján et. al. [2.13] tried a somewhat different route towards the determination of an on-engine turbine efficiency. Instead of trying to measure the quantities regarded as very difficult (instantaneous total pressure, mass flow and temperature) they used results from correlated 1D engine simulations. However, they did not calculate an instantaneous, but a cycle-averaged efficiency. Thus the (assumed constant) compressor power was divided by the integral of the instantaneous input power to the turbine. This value was then compared to the manufacturer's steady flow efficiency as well as the efficiency obtained from calculation of averages of pressure, temperatures and mass flow. The result was that the efficiency calculated from average values was 13% lower than the steady flow efficiency and the cycle averages efficiency was 30% lower. It should be pointed out that the friction losses or heat transfer was not included in the analysis, neither was the power used and delivered by the speed fluctuations of the turbo rotor.
Furthermore they defined a pulsation parameter to which they tried to correlate the efficiency difference between the maps and cycle average value from measurements/simulations. No really good correlation was however found.
A similar approach was used by Ogink [2.14]. He measured static pressures, average temperatures and instantaneous turbospeed and calculated an instantaneous efficiency. For the mass flow he used simulated values. Unfortunately the turbo-speed measurements were not correlated in time to the pressure measurements, which made phasing necessary. This phasing together with necessary phasing of mass flow gave too high uncertainty to give reliable results.

2.4 Flow analysis in the turbine

As seen above, a lot of measurements have been done as well as many 1D-calculations. A lot of information has been collected but there always seem to have been some measurement problem that has shadowed the picture. Therefore it would be very beneficial if a full 3D flow analysis of the pulsating flow through the turbine could be done. Many 3D CFD- as well as experimental investigations on steady flow operation have been conducted

[2.15, 2.16] but since the similarities in operation between steady and unsteady flow are unknown this is not looked into in depth here.
To be able to model a phenomenon one must have at least a slight idea about the mechanisms that influence the phenomenon in question. At least it can be expected that the problems occurring when modelling steady flow will probably be carried over to the unsteady flow modelling. Therefore flow analyses made for steady flow are necessary to look at even for unsteady flow work. Modelling often strives to decrease the number of dimensions taken into account to reduce the complexity. This involves neglecting certain phenomena. One of the first assumptions that comes into mind is to assume equal conditions circumferentially around the rotor inlet. Even this assumption has been proved wrong by several investigators, for instance Lymberopoulos et. al. [2.17] and Winterbone et. al. [2.9, 2.10]. An even more close assumption is that the conditions are equal over the axial coordinate at rotor inlet, but even this has been proven wrong by Baines and Yeo [2.18]. Thus, modelling involves significant amounts of averaging and simplifications which will deteriorate the accuracy. The only model that necessarily not has to do all these simplifications is CFD.
Only one paper has been encountered where the authors have succeeded in making a complete 3D CFD calculation of unsteady flow propagation and work transfer in a radial turbocharger turbine, Lam et. al. [2.19].
Within this paper several important points are made. First it is stated that the propagation time from housing inlet to halfway around the circumference is correlated to the acoustic velocity for the mass flow and bulk flow propagation for the temperature. Secondly, it is pointed out that the pulse amplitude is damped quite heavily through the volute and nozzle-vanes.
A comparison is made between efficiencies calculated for a reference calculation with steady flow and unsteady efficiency. For an efficiency defined as the ratio of time averages of input and output work there is a 5.2% discrepancy between the efficiencies for the entire stage but only 0.2% discrepancy if only the rotor is considered.
The conclusion is thus that the rotor works in QS-mode while the stator is unsteady. This is the same conclusion as reached by Chen and Winterbone [2.2] with the Strouhal number method.

2.5 Alternative models

There are several ways to investigate a problem not fully understood. One way is to do observations and from these observations draw conclusions about the phenomenon. That is similar to do direct measurements and conclude from those. Another method, which is very convenient in this case when

observations are very difficult to do, is to make models of the phenomenon and simulate. Then overall results can be compared between measurements and the simulations. This has led to the publication of a few alternative methods to the QS-method described first in this chapter.

Baines et. al. [2.8] suggest that the turbine could be modeled with the volute as a volume where mass can accumulate during the pulse cycle and that the rotor can be treated with the QS-assumption. Unfortunately the results are only shown as graphs of ts-efficiency vs. U/C_s for three mass flows. Therefore it is difficult to get a good numerical value of the accuracy of the simulations, but the trajectories look quite similar to the measured ones.

A slightly higher level of detail is suggested by Chen and Winterbone [2.2]. They still treat the rotor quasi-steadily but the volute is treated as a tapered pipe in which unsteady effects are fully accounted for. The exit of the tapered pipe is a calculated mean station, which approximately can be assumed to be the average distance propagated through the turbine housing for all gas particles entering the housing. The exit area of the tapered pipe is defined through

$$A_2 = \frac{2\pi}{(2\pi - \varphi_2)} A_{2,real} \qquad \text{eq. 2.2}$$

From A_2 and absolute gas velocity the flow angle out from the volute can be derived. Thus the volute model has a length, volume and flow angle associated with it, properties that significantly increase the level of refinement. The model is calibrated against steady flow measurement data with good results and results from unsteady simulations showed. Unfortunately no unsteady measurement results were available to compare with.

With Ehrlich's [2.12] experimental data as a base Hu [2.20] developed a turbine model based on the solutions of governing equations for conservation of mass, energy and momentum for control volumes through the turbine. In the turbine wheel, every blade passage was divided into two control volumes, one purely radial (with centrifugal pressure field) and one purely axial. The volute, nozzle and rotor all share the same governing equations, but they have different source terms. Promising graphs of simulated turbine efficiency, unsteady pressures and massflows was derived. However, Hu was not able to show any correlations between his simulations and Ehrlich's measurements in terms of turbine performance (power and/or efficiency).

At Purdue development continued with King [2.21], who incorporated Hu's model into GT-Power. The model used steady flow maps to calibrate loss coefficients and assumed that the loss mechanisms worked equally under steady and unsteady flow, i.e. are quasi-steady.

King detected very large differences in calculated as well as measured ideal turbine power and the calculated actual turbine power. He pointed out that Ehrlich had referred this to mass accumulation in the turbine but King concluded that it rather would be referred to large torque fluctuations on the shaft. Unfortunately there existed no high-resolution speed measurements to calculate the torque fluctuations on the shaft.
King succeeded in coupling his model with GT-Power. However he did not fine-tune the GT-Power model to the actual engine. Neither did he simulate the compressor and subsequently the speed fluctuations of the shaft. Therefore he could not directly compare the model's result compared to measured data. These are drawbacks that make the judgement of the model's performance very difficult.
Some short additional facts about King's model:

- losses only in the rotor
- big pressure jump from volute to nozzle in steady flow operation – due to lack of pressure gradient in other direction than meanline flow (1D)
- only trendwise agreement of mass storage compared to Ehrlich's data

In all, King's model is a promising start towards having a parameterised model in GT-Power, but it appears to still need significant development before it can be a valuable tool to an engine designer.

2.6 References

2.1 Watson N. & Janota M.S. "Turbocharging the internal combustion engine" 1982 ISBN 0 333 24290 4
2.2 Chen H & Winterbone D "A method to predict performance of vaneless radial turbines under steady and unsteady flow conditions" ImechE Paper C405/008
2.3 Benson Rowland S. "Nonsteady flow in a Turbocharger Nozzleless Radial Gas Turbine" SAE Paper 740739
2.4 Dale A & Watson N "Vaneless radial turbocharger turbine performance" IMechE Paper C110/86
2.5 Baines N.C. & Chen H. "Performance parameters and assessment" Radial turbine, VKI LS 1992-05 (1992)
2.6 Dale A, Watson N & Cole A.C. "The development of a turbocharger turbine test facility" Inst. Engrs. Seminar pp. 75-84 1988
2.7 Capobianco M, Gambarotta A, Cipolla G "Influence of the pulsating flow operation on the turbine characteristics of a small internal combustion engine turbocharger" IMechE paper C372/019 1989

2.8 Baines N.C., Hajilouy-Benisi A., Yeo J.H. "The pulse flow performance and modeling of radial inflow turbines" IMechE paper C484/006/94 1994
2.9 Winterbone D.E., Nikpur B., Frost H. "A contribution to the understanding of turbocharger turbine performance in pulsating flow" IMechE paper C433/011 1991
2.10 Winterbone D.E., Nikpur B., Alexander G. I. "Measurement of the performance of a radial inflow turbine in conditional steady and unsteady flow" ImechE Paper C405/015 1990
2.11 Winterbone D.E. & Pearson R.J. "Turbocharger turbine performance under unsteady flow – a review of experimental results and proposed models" IMechE paper C554/031 1998
2.12 Ehrlich Daniel "Characterization of unsteady on-engine turbocharger turbine performance" Ph.D. Thesis, Purdue Univ. USA 1998
2.13 Luján J.M., Galindo J. & Serrano J.R. "Efficiency Characterization of Centripetal Turbines under Pulsating Flow Conditions" SAE Paper 2001-01-0272
2.14 Ogink, Roy "Determination of the on-engine turbine efficiency of an automotive turbocharger" M. Sc. Thesis no. MMK 2000:49 MFM52 The Royal Institute of Technology (KTH), Dept. of Machine Design. Stockholm
2.15 Japikse D, Baines N C. "Introduction to turbomachinery" Concepts ETI & Oxford University Press 1997. ISBN 0-933283-10-5
2.16 Osako K., Higashimori H. & Mikogami T. "Study on the Internal Flow of Radial Turbine Rotating Blades for Automotive Turbochargers" SAE Paper 2002-01-0856
2.17 Lymberopoulos N, Baines N C and Watson N "Flow in single and twin entry radial turbines" ASME Paper 88-GT-59 1988
2.18 Baines N C and Yeo J H "Flow in a radial turbine under equal and partial admission conditions" ImechE Paper C423/002
2.19 Lam J K-W, Roberts Q D H & McDonnell G T "Flow modeling of a turbocharger turbine under pulsating flow" ImechE Paper C602/025/2002
2.20 Hu Xiao "An advanced turbocharger model for the internal combustion engine" PhD-Thesis Purdue Univ. USA 2000
2.21 King Aaron J "A turbocharger unsteady performance model for the GT-Power internal combustion engine simulation" PhD-Thesis Purdue Univ. USA 2002

Chapter 3

Simulation of turbocharged SI-engines

3.1 Introduction

1D engine simulations are an essential part of the engine development. It is not only a cost- and time effective method; certain information can be very difficult to obtain without performing simulations. Commercial one-dimensional simulation codes facilitate the work and results can be achieved with very little effort, compared to only doing experiments to reach the same goal. This chapter intends to explain possibilities and limitations of this tool, and give advice on it's use.

The work presented in this thesis is carried out on and around a turbocharged, 4-cylinder SI-engine, more detailed data is presented in Table 3.1. The fuel was ordinary pump gasoline (95 RON) and it was port fuel injected.
For the main part of the work the engine maintained it's production version of turbocharger and manifold. The turbocharger was a wastegated, single entry, vaneless turbine, as is standard for SI-engines. The manifold was a cast-iron, compact 4-2-1 design (see figure 5.11 for a picture).
For the last part of the work (see chapter 8) both manifold and turbocharger was changed. The turbocharger was of the same type, but from another manufacturer and with the wastegate welded closed. The manifolds were built up from welded steel tubes and of three different designs, more on that later.

Table 3.1. Engine data.

No. cylinders	4
Valves per cylinder	4 (pent-roof)
Bore x stroke [mm]	90 x 78
Max power [kW]	151
Max torque [Nm]	280
Max inlet pressure, controlled [Bar]	1.8
Valve diameters [mm]	33 (inlet), 29 (exhaust)

3.2 Description of the simulation model

Initially the modelling task was to make predictive simulations of various boosting systems for a downsized, variable compression engine. The work started with validation of the modelling software against measured data on the engine in the table. This showed that the modelling technique has not reached a level of total predictivity; it is not possible to input geometric data for the engine and expect to get the same results as if the same engine was built and tested. A lot of the sub-models within the software need calibration against measured data, some sub-models even need calibration for every single speed and load.

Three sub-models are more troublesome than others: turbocharger, in cylinder process and valve flow. The reason for the difficulty in simulating these phenomena is that they are all clearly 3D-problems and the 1D approach used in the engine simulation codes is not detailed enough. Such problems might be overcome in two ways, either by inserting measured data to aid the calculations or to have a more sophisticated model locally just for the phenomenon in question. This can be done either by coupling GT-Power to a CFD code or to use a parametric model with a high level of detail. It was decided that coupling GT-Power to a CFD code should be avoided due to the heavy work input necessary for performing CFD calculations. This work aimed at exploring the problem associated with the turbocharger. The task thus is to explore how more data could be added or how the model could be made more sophisticated, all in order to increase the accuracy, or predictivity of the simulations.

In order to be able to understand the problem one must be familiar with what the software actually does when simulating the engine. Basically it is a simulation of the gas flow through the engine with 0- or 1-dimensional models of all other aspects such as cylinder, combustion, friction and turbocharger.

3.2.1 Pipe flow

For the pipe flow, the governing equations (continuity, energy, and momentum) are solved simultaneously for mass flow, density and internal energy. From these three variables every other gas property can be calculated [3.1].

The 1D approach means that all pipes are divided into discrete lengths with assumed constant condition over the cross section. The information about the gas state lacks spatial resolution inside every discrete volume. The lengths of the discretisation volumes are recommended to be 40% of the bore diameter for the intake side and 55% of the bore on the exhaust side.

The pressure loss in the pipes is modelled through the wall friction, which is represented by the sand roughness of the wall material in question. For the cast iron exhaust manifold 0.12 mm was used, for the steel tube manifolds 0.03 mm, for the cast aluminium 0.2-0.25 mm depending on the casting quality and for plastic and rubber 0.0025 mm. The heat transfer through the wall was modelled using the wall material properties, surface roughness and wall temperatures. Both imposed wall temperatures and data acquired from the wall temperature solver in GT-Power was used.

It was necessary to adjust both inner and outer wall heat transfer properties to get both gas and wall temperatures equal to measurements. The heat transfer between gas and inner wall was adjusted by multiplying a constant, values between 0.5-1 was commonly used, dependent on both manifold type and operation point. The heat transfer from the manifold wall to the surroundings was adjusted through an external convection coefficient, whose value normally ranged between 40-80 [W/(m²K)], also this value depended on manifold type and operation point.

The heat transfer between the manifold and the cylinder head was modelled by a contact resistance over the flange area, the value 0.5 [K/W] was used throughout the work.

3.2.2 Turbocharger

For simulation of the compressor and turbine of the turbocharger only one sub-model for each exist in GT-Power. This model is based on steady flow flow-bench measurements of the turbine and compressor. Such measurements are compiled into performance maps, one for the compressor and one for the turbine, where the speed and efficiency are plotted against pressure ratio and mass flow. For the compressor side this approach shows good accuracy between measurements and simulations, but for the turbine the results are worse, which will be covered later in this text.

In the simulation model the wastegate was represented by a PI-controller controlling an isentropic nozzle. However, the difficulties of measuring the actual mass flow through the wastegate restrained this investigation to cases where the wastegate is really closed, which for the standard turbocharger meant that max allowed speed was 1950 rpm.

Calculation procedure

The calculation procedure of the turbine and compressor is briefly described in the GT-Power manual [3.1]. The turbospeed and pressure ratio are calculated by the software, and then the efficiencies and mass flows are looked up in the turbine and compressor maps respectively.
The turbine and compressor power are calculated from:

$$P = \dot{m}\left(h_{in} - h_{out}\right) \qquad \text{eq. 3.1}$$

where the inlet enthalpy is calculated from the upstream gas condition and the downstream enthalpies are:

$$h_{out,turbine} = h_{in} - \Delta h_{s,T}\eta_s \qquad \text{eq. 3.2}$$

$$h_{out,compressor} = h_{in} + \frac{\Delta h_{s,C}}{\eta_s} \qquad \text{eq. 3.3}$$

The enthalpy change is calculated from similar formulas for turbine and compressor, which are:

$$\Delta h_{s,C} = c_p T_{0,in}\left(\left(P_{0,out}/P_{0,in}\right)^{(\gamma-1)/\gamma} - 1\right)$$

$$\Delta h_{s,T} = c_p T_{0,in}\left(1 - \left(P_{out}/P_{0,in}\right)^{(\gamma-1)/\gamma}\right) \qquad \text{eq. 3.4}$$

where c_p and $T_{0,in}$ are for the machine inlet conditions
The turbospeed is calculated from the torque (im-)balance between compressor and turbine, as shown in eq. 3.5:

$$\Delta\omega = \frac{\Delta t}{J_{rotor}}\left(\tau_{turbine} - \tau_{compressor} - \tau_{friction}\right) \qquad \text{eq. 3.5}$$

where:
$\Delta\omega$ ..... change in shaft speed per timestep
Δt ..... calculation timestep
J_{rotor} ..... turbo rotor moment of inertia
τ ..... torque

Thus the speed calculations need a start value, however the calculations are not sensitive, just a guess is good enough to set off the calculations in the right direction.
The pressure ratio π is also calculated by the code. However, this procedure is not explained in the manual, but was explained in an e-mail from Brad Tillock at the Gamma Technologies support (see Appendix).
The pressure ratios are determined from the pressure in the adjacent sub-volumes immediately upstream and immediately downstream of the compressor and turbine. The turbine is described as a metering device; pressure ratio and speed is looked up in the maps and then the correct amount of mass flow is applied. This mass then ends up changing the pressure ratio in an indirect manner for the next timestep.

Map treatment

The maps for the turbine and compressor performance, obtained from the manufacturers, contain only discrete points. For the turbo shown below there were 60 points of speed and efficiency as functions of pressure ratio and mass flow for the turbine and 34 for the compressor.
In order to get a continuous distribution of the map data that can be used in the quasi-steady calculations the software has to interpolate the data. In addition, the data in the original map usually does not cover the entire operation range when used on a piston engine with its pulsating flow. To cope with this problem the software also has to extrapolate the data.
For the compressor the main problem usually is that the map is not measured at speeds low enough. In this case the map starts at 80000 rpm, which isn't too large problem for the steady state, full load simulations, but for the transients where the turbocharger starts at around 25000 rpm. For the compressor map, GT-Power extrapolates the mass flow rate from the lowest pressure ratios in the measured map down to pressure ratio π=1. It then corrects the mass flow rate so that it scales linearly with speed. The user can control the process

slightly by entering the minimum efficiency imposed on the extrapolated part of the map.
In fig. 3.1 the interpolated and extrapolated compressor efficiency map is shown along with the original map points from the manufacturer.

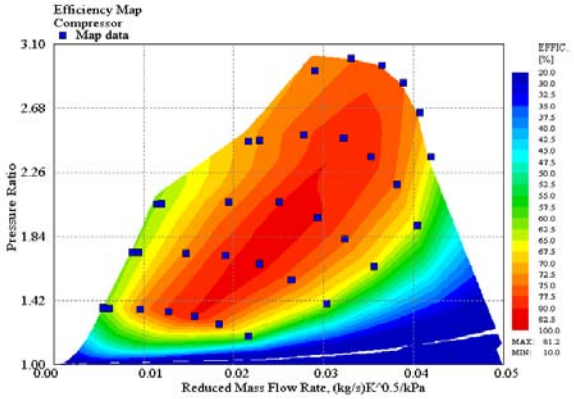

Figure 3.1. Interpolated and extrapolated compressor map as used in GT-Power. Squares are the original map points.

For the turbine side the problem has more to it than just a speed range limit. Due to the pulsating flow into the turbine the pressure- and mass-flow-range that is covered during one engine cycle is very large. Unfortunately the turbocharger manufacturers are not very keen on measuring the maps more extensively. There are several potential reasons for this. One is that it requires expensive flow benches with a dynamometer [3.2, 3.3, 3.4] to cover the entire range, but it could be partly overcome by measuring two or three turbine maps with different compressors, offering different power absorption capabilities. Map measurements with greater range are discussed by Pucher & Nickel [3.5]. Another potential reason is that the efficiencies are lower at the extremes, and the manufacturers only want to show the best sides of their product. In fig. 3.2 below an extrapolated turbine speed map can be seen along with the original map points. In fig. 3.17 an efficiency map with instantaneous operation line is displayed.

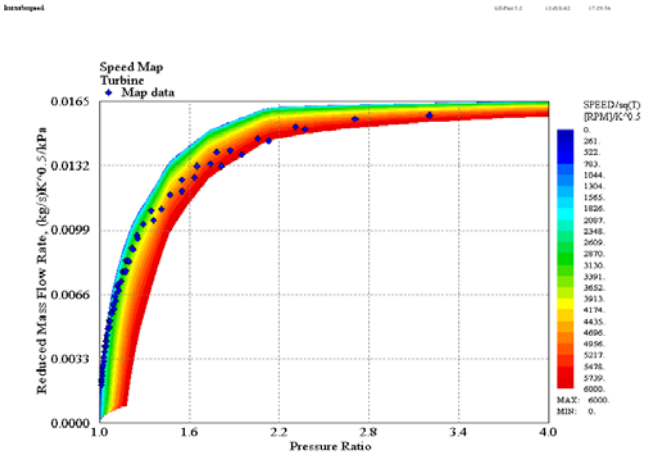

Figure 3.2. The interpolated and extrapolated turbine map. Squares are the original map points. Colour indicates constant speed.

The turbine map from the manufacturer consists of constant speed lines with a handful of different sets of mass flow, pressure ratio and efficiency. GT-Power stipulates that the peak efficiency must be contained within every speed line. Every such speed line is then extrapolated down to a very low pressure ratio and up to choking conditions, as can be seen in fig. 3.2.

Steady flow theory states that if the data in the original map is plotted as efficiency vs. U/Cs all data points would collapse onto a parabolic curve, with a well-defined peak. This peak should be positioned at $U/C_s=0.707$ if the reaction is 50% which seems to be common for vaneless radial turbines. Reaction is the ratio of expansion between rotor and stator (housing), no reaction means that all expansion occurs in the stator, more on that in chapter 8. However, as shown in Ch. 2 this is questionable how the turbine works under unsteady flow.

Though, without an assumption about the U/C_s the extrapolation cannot be done. In figures 3.3 and 3.4 the extrapolation is shown in more detail. Figure 3.4 shows how the individual map points in each speedline is first interpolated (upper quadrant) and then extrapolated (lower quadrant) to enable maps covering the entire range of operation as in figure 3.2. The process is described more in detail in the GT-Power manual [3.1].

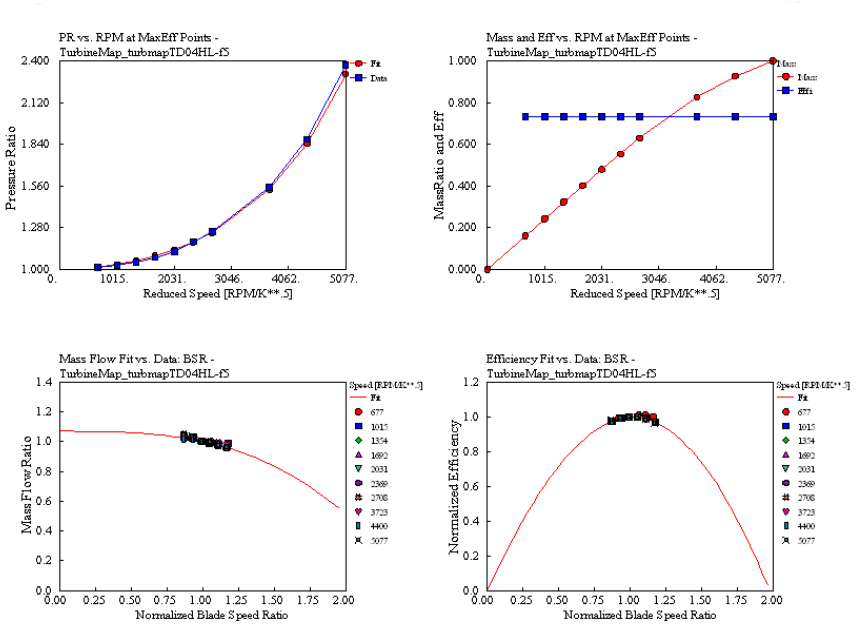

Figure 3.3. Extrapolation of the turbine map. Upper left quadrant shows the interpolated swallowing curve of pressure ratio vs. speed, the swallowing curve consists of the point for maximum efficiency for every speed line. The upper right quadrant shows the corresponding data for mass flow (normalized with max mass flow) vs. speed, the actual efficiency for every point is also shown. The lower left quadrant shows mass flow ratio vs. blade speed ratio (normalized with U/C_s=0.707). The lower right quadrant shows the efficiency vs. the blade speed ratio. The blade speed ratio is normalized with 0.707 because it is proven that the efficiency has its peak here for steady flow and 50% reaction. For the two lower quadrants, the solid line is the extrapolated parabola-shaped curve.

3.2.3 In-cylinder process

For the combustion both the Wiebe-model and burn-rate curves have been used. In the end, the burn-rate method (calculated in GT-Power from cylinder pressure) was preferred due to the increased accuracy having the entire analysis, of pressure to heat-release in both ways, using the same model.

However, due to the inherent cycle-to-cycle variations in an SI-engine, averaging techniques are adopted to give a general estimate of the cylinder pressure. The number of cycles necessary for such statistical evaluation depends on the severity of the cycle variability. Lancaster et. al. [3.6] suggest that at least 300 consecutive cycles need to be collected for acquiring accurate averaging.

Figure 3.5 shows the individual combustion parameters for 500 measured consecutive cycles. The Wiebe curve is in essence a curve fit to the heat release obtained through the cylinder pressure. A different approach is to estimate the laminar and turbulent flame speed. The disadvantage of this method is the extent of model calibration needed and the tuning parameters' dependence on operating condition.
As can be understood by examining figure 3.5, it can be preferable to work with averaged data. The mean combustion parameters can be calculated by using ensemble averaged cylinder pressure or averaging the combustion parameters for individual cycles. Table 3.2 gives the average values for these different calculation approaches.

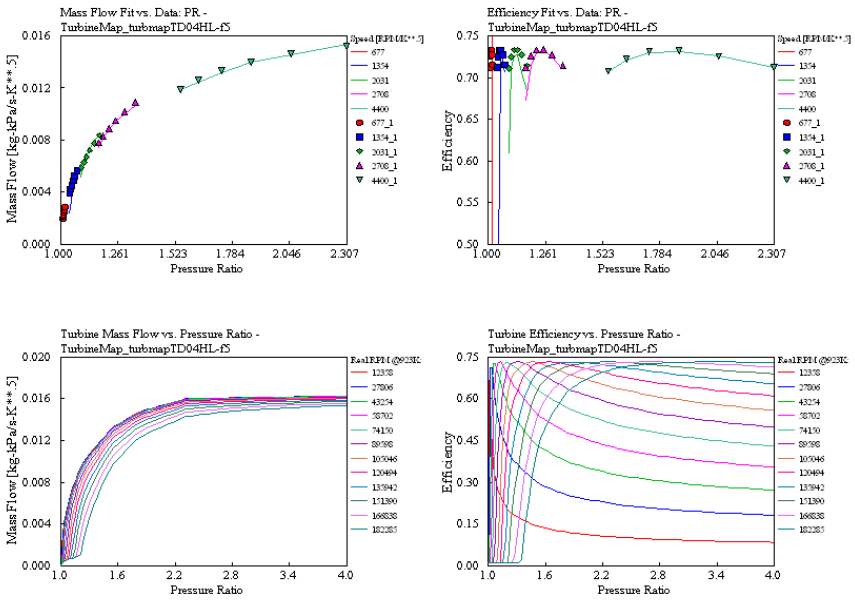

Figure 3.4. Extrapolation of the turbine map The upper two quadrants show the original map points with the interpolation of mass flow vs. pressure ratio (left) and efficiency vs. pressure ratio (right). The lower quadrants show the same curves but after the extrapolation is done.

Table 3.2. Averaged combustion data for the cycles in figure 3.5.

Based on:	50 % burnt	Duration
Average pressure	12	24.25
Individual cycles	12.21	23.33

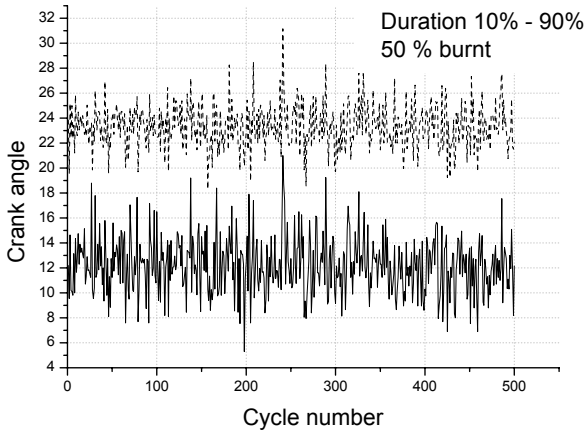

Figure 3.5. Combustion duration (10% - 90%) and the crank angle for 50% burned mass for 500 cycles at 3000 rpm.

The difference between the averaged values might not be considerable, but it is important to realise the reason for these differences and that this will depend on the cycle variability. An averaged pressure will become unphysical due to averaging effects. Furthermore, the heat release analysis is not a linear function of the pressure, in contrast to the calculation of IMEP. Hence using average pressure to obtain average combustion data will aggravate the unphysical behaviour. The preferred way is to calculate the individual combustion parameters for each cycle and then calculate the average of these.
Even though the average is taken over many cycles the combustion parameters will show an abnormal combustion. For most applications this abnormality can be neglected. On the other hand, when studying phenomena like knock, where combustion is fundamental to the problem, it is more suitable to study several individual cycles rather than averaged data.
The in-cylinder heat transfer rate was determined by using a modified version of the Woschni-model [3.1]. The cylinder wall temperatures were chosen as

recommended in the GT-Power manual, but in the upper range of the recommended intervals due to assumed higher internal thermal stresses on turbocharged engines than NA-engines.

3.2.4 Valve flow

In this work the valve flow is modelled with measured valve flow data. No measurement equipment for measurement of valve flow data was available in time at KTH Combustion Engines and the flow data had to be supplied by Saab. The only flow data available at Saab was measurement of the forward flow coefficient for the intake valve. The flow data was measured as volume flow as a function of valve lift for a pressure ratio over the valve of 10" of water (2.5 kPa). Blair [3.7] recommends that the flow coefficients should be measured for much larger pressure ratios, for both forward and backward direction and also for inlet and exhaust valves separately. For this work it was decided to use the data available until it was determined that it was too bad to work with, and this has not been proven yet. The engine's air consumption is predicted within measurement accuracy and the instantaneous inlet and exhaust manifold pressures are modelled correctly. However, for the cylinder pressure trace to fit the measured value for the time around exhaust valve opening the exhaust valve opening timing had to be delayed 4 CAD. This could be caused by inaccurately simulated mass flow through the valve at the very low lift and very high pressure ratio. However, another possible explanation could be that the exhaust valve opening timing is not known with a better accuracy than 4 CAD due to uncertainties in the phasing of the timing chain in volume production, lack of rigidity in the hydraulic valve-lifters etc.; therefore nothing can be said with certainty.

3.2.5 Intercooler

The intercooler on the engine is of air-water type, which differs from the engine's standard air-air intercooler.
It was modelled both with GT-Power's heat-exchanger model and as a bundle of thin pipes. The wall temperature of the intercooler was controlled by a PI-controller to give an inlet manifold gas temperature equal to measured.
An even simpler method, where the wall- and coolant-temperatures were set to the measured intercooler outlet temperature and the heat transfer coefficients were cranked up considerably, was tested. However, it was sensitive to wall temperatures in the rest of the intake system and therefore not used.

3.3 Results

3.3.1 Criteria

When using the 1D simulation to design a new engine it is obvious that output torque or BMEP is a very interesting parameter to look at. However, due to the uncertainty related to the measured mean pressures it is not obvious which is best to compare with, BMEP or IMEP. The simulated BMEP is dependent on the FMEP model in the software through eq. 3.6:

$$BMEP = IMEP(g) + PMEP - FMEP = IMEP(n) - FMEP \quad \text{eq. 3.6}$$

Where IMEP(g) is the gross IMEP, i.e. only for the power and exhaust strokes, while the net, IMEP(n), is for the entire cycle. FMEP can be modeled through the Chen and Flynn friction model [3.8] or through inserted measured FMEP data. A short test of the Chen and Flynn model showed that it would require extensive calibration to give results close to the, however uncertain, measured values. Thus the measured values for FMEP were used directly in the simulation model. But to avoid influence from the uncertain measured FMEP values, IMEP was chosen to be the parameter to compare simulations and measurements with.
To be able to check the results from the turbocharger model, instantaneous pressures before and after both compressor and turbine was necessary. However, for temperatures only average (mass/energy) values were available.
Mass flows of air and fuel were also included as comparison criteria. Unfortunately the ingested air mass is only known with 10% inaccuracy why the fit for air mass flow allows quite large error bars. The fuel flow was measured with quite high accuracy but in the simulations the fuel flow was coupled to the air mass flow via the imposed measured lambda values. Therefore no really good fit could be achieved, and the reason for that is that the measurement data are too uncertain and that the simulations results unfortunately rely on the most inaccurately measured values, the air mass flows.

3.3.2 Speed and load points

There does not seem to exist any satisfying method to measure the mass flow through the integral wastegate. Therefore one is constrained to test cases where the wastegate is closed, otherwise the uncertainty in turbine mass flow would be too large to enable a thorough investigation of the turbine work process.
With the closed WG the engine was only stable below 2000 rpm, depending on which turbocharger that was used.

If cases with open wastegate would have been included, the wastegate opening, and thus it's mass flow, probably always could have been adjusted enough to enable a good match of turbo speed against measured data. However the pressures, especially at the turbine inlet would not be perfect.

3.3.3 Output data

Here follows a presentation of the most interesting simulation outputs compared to measured data.

Averaged data

Simulated IMEP shows reasonable agreement with measured data, as can be seen in fig. 3.6. The difference is about 0.25 Bar for all three cases and well within the expected uncertainty in the measured IMEP, related to cylinder imbalance etc. (see Ch. 5).

Figure 3.7 shows that the PMEP show quite a bad match between measurements and simulations. If the pressure traces during the scavenging period are investigated they show quite a good similarity between measurements and simulations, see figure 3.8. This indicates that the PMEP for cylinder one on the engine, which is the cylinder from which all the input data to the model is taken, might be simulated quite well. Thus, the other three cylinders might show different pressure traces but still be compared to the measurements from cylinder one.

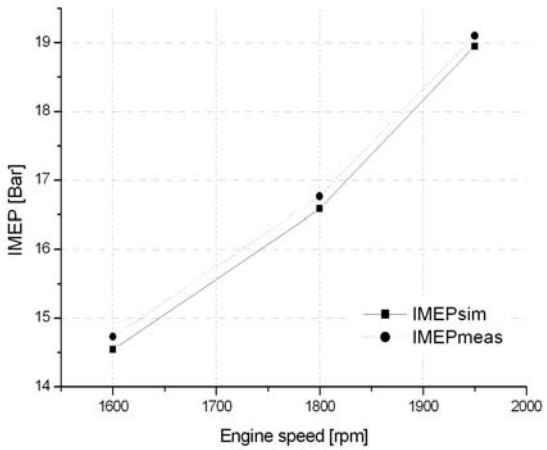

Figure 3.6. Simulated IMEP compared to measured.

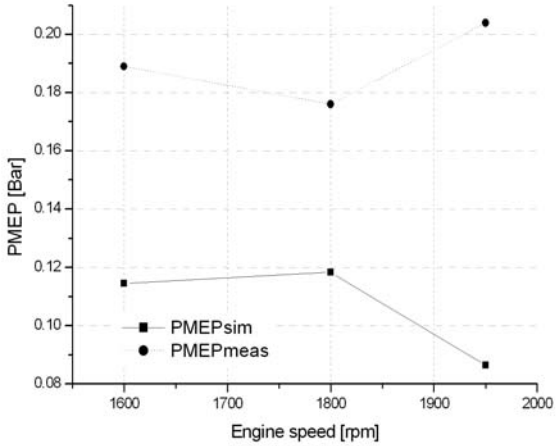

Figure 3.7. Simulated PMEP compared to measured.

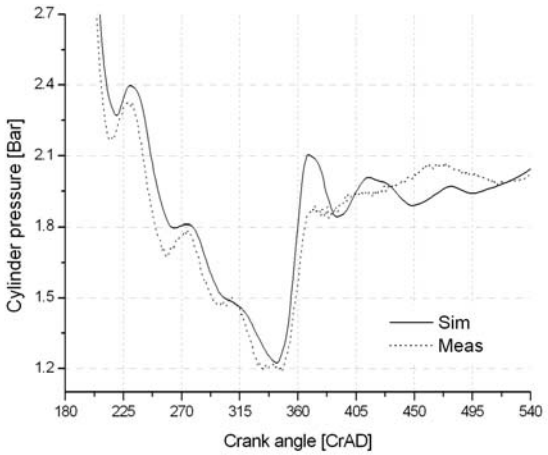

Figure 3.8. Measured and simulated cylinder pressure during the scavenging period, for cylinder one at 1950 rpm, shows fair similarity between the pressure traces.

This further justifies that the cylinder imbalance on the real engine is the reason for the bad match for the entire engine's PMEP and that cylinder pressure measurements for all cylinders are necessary to achieve a high accuracy for the PMEP measurement.
However, since the focus of this work is on the performance of the turbocharger it is the pressure traces and temperatures that are of greatest importance.
Figure 3.9 shows that the average values of the pressure before (P1T) and after (P2T) the turbine are modelled quite accurately. However, this was only enabled through adjustments of the pressure ratio multiplier in the turbine model, which had to be given the value 0.88. This value cannot be case dependent and could thus only be fine tuned for one speed, in this case 1950. This explains the somewhat worse result for P1T at 1800 rpm. In later work the same adjustment was made, now case-dependent using the mass flow multiplier instead, more on that in a later chapter.
Figure 3.10 shows the compressor outlet (P2K) and inlet manifold (Pin) pressures from simulations and measurements. Unfortunately these measurement results are a bit erroneous with a higher pressure in the inlet manifold than after the compressor. One should expect a certain pressure drop over the intercooler.

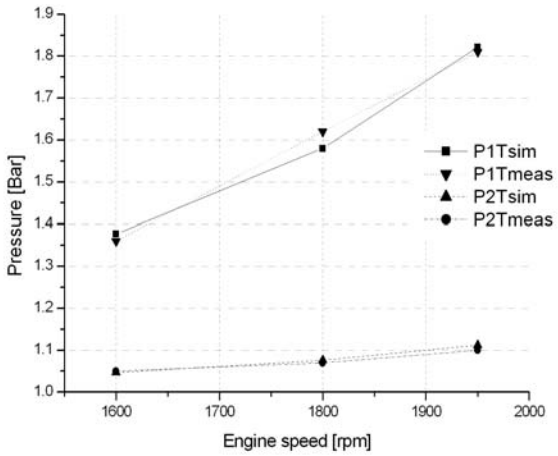

Figure 3.9. Turbine inlet, P1T, and outlet, P2T, pressures from measurement and simulations.

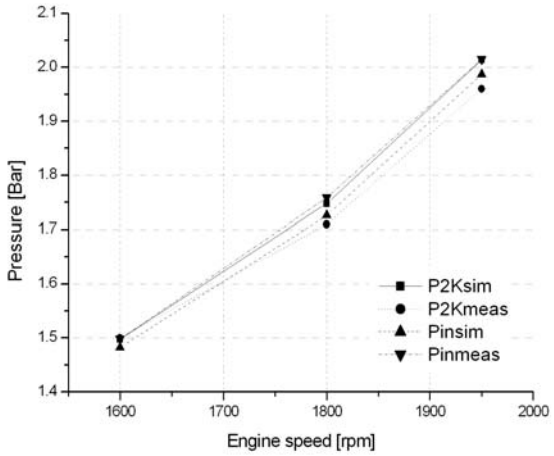

Figure 3.10. Comparison between measured and simulated compressor outlet (P2K) and inlet manifold (Pin) pressures. Unfortunately the measurement data quality is not very good for these points.

The compressor model was not tweaked at all and within (the however rather poor) measurement accuracy the simulation results matched the measured well.
The next important parameter is the turbocharger speed. As fig. 3.11 shows, the simulation results show an astonishingly good similarity between measurements and simulations. Unfortunately this could only be achieved by adjusting the turbine efficiency multiplier for every individual speed point. As will be shown later, without this adjustment the results will not be very good.
The air mass flow is another important parameter to get correct in order to simulate accurately. The comparison between simulation and measurement is shown in fig. 3.12. The match does not seem to be very good. However, the difference is between 5 and 10% and the measurement accuracy of the air mass measurement is not very much below 10%, therefore the match is within the error margin. Just to clarify the difficulty in measuring air mass flows, both the value acquired from the direct air mass measurements and the value calculated from fuel flow and lambda measurements are displayed.

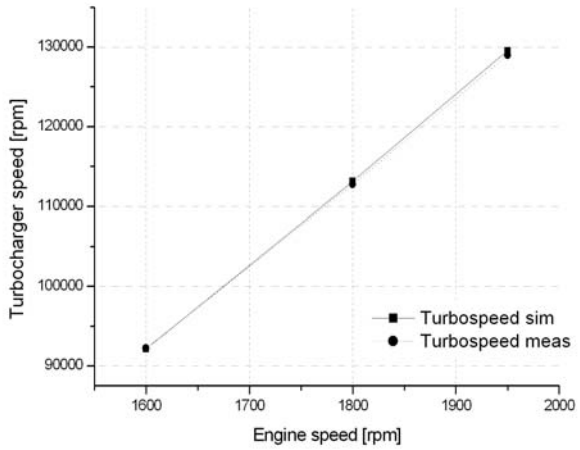

Figure 3.11. Average turbocharger speed from simulations and measurements.

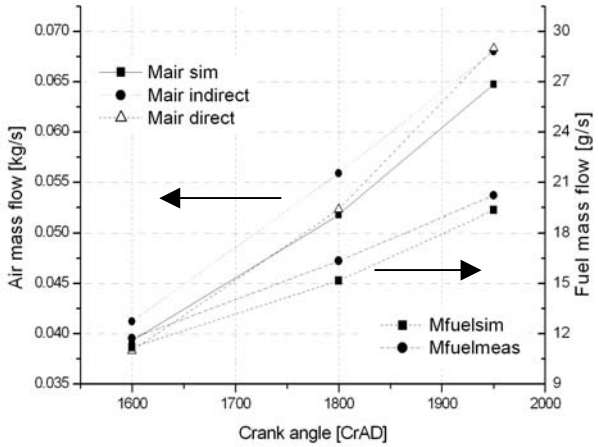

Figure 3.12. Average air and fuel mass flow. The error seems very large, but still within the error margin of the air mass measurement. For clarity both the indirect and direct measurements of air mass flow is enclosed (see Ch. 5 for further details).

In the same graph the simulated and measured fuel flow are displayed. In the simulation model the measured lambda was imposed on the model, therefore the simulated fuel flow entirely depends on the airflow simulations. On the

other hand, the fuel flow measurement is much more accurate, and if the airflow simulations and the fuel flow and lambda measurements are perfect then there would be no difference in the measured and simulated fuel flow values. However, no more effort was put into this since focus of the work is not to perfectly model fuel flow. It is questionable whether the maximum error of the fuel mass flow measurements is smaller than the difference between measured and simulated fuel flow.

Crank angle resolved data

The real test of the performance of a simulation model is to compare crank angle resolved data. To investigate the work transfer in the turbine this data is absolutely necessary. Here only data for 1950 rpm is shown, but there are no general differences in terms of matching quality between simulations and measurements for the other speeds. All measurement data presented here is ensemble averages over 100 consecutive cycles.

The cylinder pressure in fig. 3.13 shows a good match except for a 3% error in the compression pressure at 0 CAD. The reason for this could either be non-perfectly modelled air mass or non-perfectly simulated heat transfer inside the cylinder. The air mass is, as was shown above, simulated within it's measurement accuracy. To see whether the heat transfer inside the cylinder could cause the difference a very simple simulation exercise was done on a single cylinder version of the investigated engine. The cylinder pressure and temperature traces were compared for two cases, one with the wall temperatures and convective heat transfer as for the full engine, and another with a convective heat transfer multiplier of 2 (compared to 1 for the std case) and 10% decreased wall temperatures within the cylinder (increasing the gas/wall temperature gradient causing the heat transfer rate to increase). The difference in compression pressure at TDC (combustion started after TDC) was 3-4% lower for the case with higher heat transfer rate. This difference is as large as the error between compression pressures for simulation and measurements for the entire engine case for 1950 rpm. Subsequently, not enough fine-tuned in-cylinder heat transfer could explain the over-estimated compression pressure for the simulation.

Nevertheless, since the power stroke is fairly well matched as well as the exhaust stroke, the IMEP and the pressure delivery to the exhaust manifold is ok and thus further work on the in-cylinder heat transfer was not considered necessary.

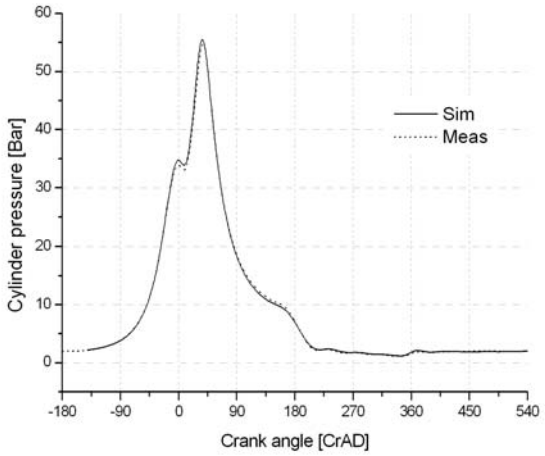

Figure 3.13. Cylinder pressure. The largest discrepancy is seen at TDC where the simulated cylinder pressure is approx. 3% higher than measured.

Since this is a turbocharger study the single most important simulation parameter is the turbine inlet and outlet pressure traces. These are presented in fig. 3.14 below. Both the inlet and outlet pressures show good agreement between measured and simulated values. But it is very important to point out that this is the result of substantial amounts of adjustments.
The measured pressure at turbine inlet for the pulse between 180-270 CAD is substantially higher than both simulated pressure and the rest of the measured peaks. This pulse emanates from cylinder 1. The reason for the high measured pressure is the position of the transducer. It was not possible to mount it absolutely perpendicular to the flow from cylinder one, so it measures a little bit of dynamic pressure as well. For later measurements series the positioning was made with more care and this phenomenon was eliminated.
Nevertheless, the flow from the other cylinders is perpendicular to the transducer so the influence from the little extra dynamic pressure from cylinder 1 was assumed to be negligible.
Moreover, the simulated intake plenum pressure is compared to the measured in fig. 3.15. The large fluctuations show good correlation but the higher frequency ripple was not modelled accurately. But this ripple was assumed to have negligible influence on the performance; hence no work was input to investigate it.

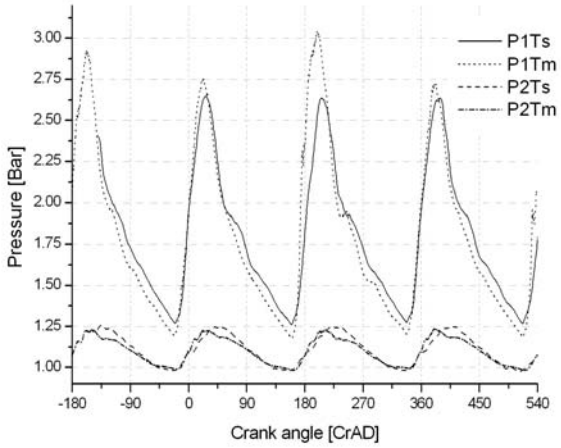

Figure 3.14 Exhaust pressures, where P1T is turbine inlet pressure, P2T outlet, s for simulated and m for measured.

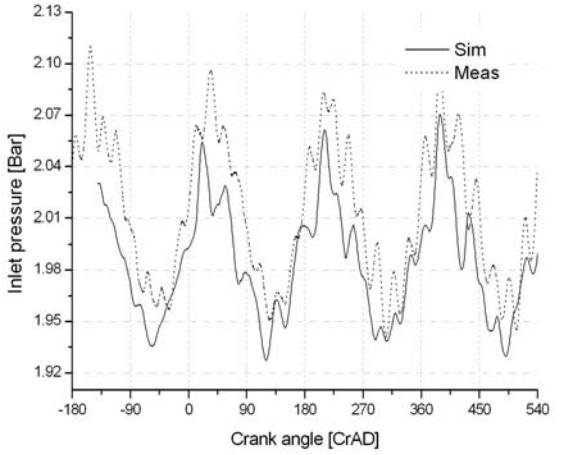

Figure 3.15. Inlet pressure at the inlet manifold plenum.

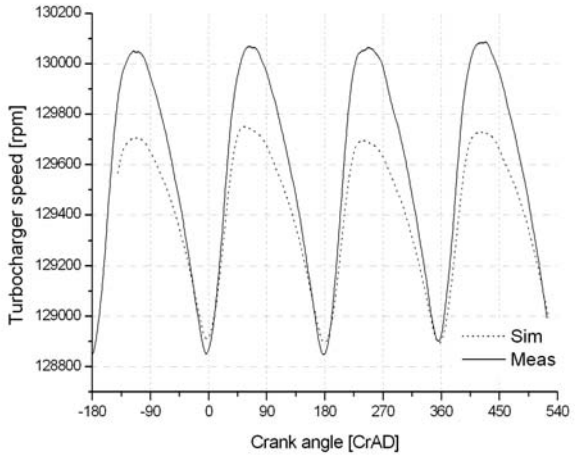

Figure 3.16. Comparison between measured and simulated instantaneous turbospeed, at 1950 rpm engine speed, shows a 25% error in fluctuation amplitude.

Similar fluctuations as for the inlet pressure can be seen in the compressor outlet pressure, despite that there are more than 1 m of piping and an intercooler in between. Therefore these fluctuations were first thought to originate from the speed fluctuations from the compressor. But simulations with an imposed steady compressor speed showed the same fluctuations, hence it was concluded that the fluctuations originate from the filling of the cylinders, having propagated upstream from the intake plenum.

Finally, the most important parameter when simulating turbocharged engines, the instantaneous turbospeed, is displayed in fig. 3.16. As mentioned above, the average turbospeed is tremendously well matched, but only as a result of adjustments. The fluctuation amplitude of the simulated turbospeed is not very well matched to the measured, the error is approx. 25%. The reasons for this can be many: the friction model, turbine power production or compressor power consumption. More on this in a later chapter.

The compressor power consumption probably can be written off most easily since the pressure delivery, outlet temperature etc. from the compressor have good matches for most cases without having to be adjusted. The friction model assumes a friction power loss that is a constant fraction of the turbine output power. A more detailed friction model would divide the friction power loss into at least thrust bearing friction and radial bearing friction. Then one would expect the thrust bearing friction force to depend on pressure differences between compressor and turbine and the radial bearing friction being

dependent mostly on speed. So the friction model might, at least partly, be a source of error here.
However, the most probable source of the fluctuation amplitude error is the treatment of the turbine maps. In fig. 3.17 the turbine map for this particular case is shown. The diamonds are the map data points provided by the turbocharger manufacturer, the circles are the cycle-average operation points (there are several of them since every calculation cycle point is shown, the rightmost one is for the converged calculation cycle), the solid line is the instantaneous operation line for the converged cycle. The coloured field is the extra- and interpolated map used by GT-Power for the calculations.
If only the average operation point is considered it seems like reliable data quite close to the real map points is used. Unfortunately this is incorrect if the instantaneous operation line is considered. Here it can be seen that it is only for a minor portion of time when the turbine is working under conditions covered by the original map. And worse is, the portion of the operation line covered by the map is for lowest mass flow and pressure ratio, that is when the turbine power is at lowest.
Thus, the fact that the fluctuation amplitude is not well modelled could be a hint that the extrapolation is part of the problem.

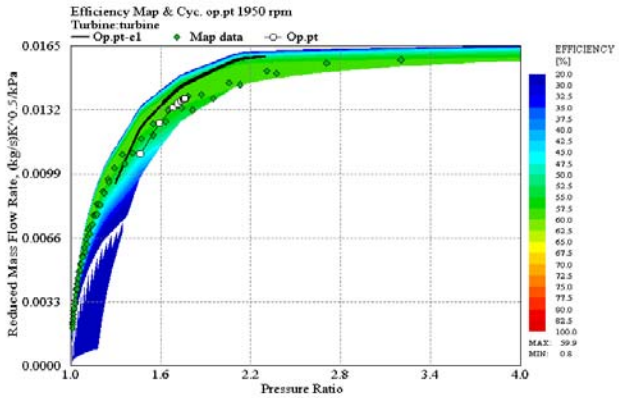

Figure 3.17 Turbine map. Diamonds are the original map points from the turbo manufacturer, the circles are average operation points where the rightmost one is for the converged calculation cycle, the black line is the instantaneous operation line and the field is the extra- and interpolated map data used by GT-Power during the simulations.

3.3.4 Model calibration scheme

For reasons previously mentioned, models of turbocharged SI-engines are very sensitive to their input data, much more than naturally aspirated engines. In addition, several adjustment factors are added together with the turbocharger model. Therefore it is not the best way to try to run the model with a free-floating turbocharger for the first time. Improper input data can make the boost pressure deviate very much from what is expected, and the different boost pressure can make it very difficult to analyse which data is wrong.
Therefore, if measured data for the turbocharger speed is available, it is better to have a PI-controller controlling the turbospeed to measured values. For the range where the wastegate is closed the controller controls the turbine efficiency multiplier, and when the wastegate is open, the opening area of it. Then adjustments are made on other aspects of the model until the results match, thus the model is calibrated. In the end, the resultant values of the turbine efficiency multiplier is read from the simulations and input to the model. Finally the controller on the efficiency multiplier can be removed and the model is validated and can be used for further development.
If measured values for the turbospeed is not available, the controller on the wastegate (that controls the boost pressure) is used over the entire range, and the resulting lowest speed of desired boost pressure will be quite uncertain.
Here follows a description of a sequence of data, which have been found to be very convenient when calibrating a simulation model against measured data. They are in order of importance and each new step increases the level of refinement of the model calibration. Due to the interdependence of certain parameters, reversing the relative order might make calibration work of a previous step useless. Of course different data is important for different purposes, and therefore the model needs to be checked and adjusted differently. The following scheme is for the purpose of general performance determination from a model.

1. Average air mass flow
First the turbocharger is run with controlled speed, here equal to measured, to ensure that the proper compressor working point is achieved. Without accurate air mass flow no engine model can be of any good for gas-exchange related purposes. However, for measurement accuracy reasons it is of little use to try to adjust the engine model so that the discrepancy between measured and simulated values are smaller than the measurement inaccuracy.

2. Air/Fuel ratio or lambda
Important data for both engine power output and for exhaust gas temperature. Commonly the desired (measured) air-fuel ratio is an input value to the model and the match between measured and simulated value for the fuel flow is therefore as good as for the air mass flow.

3. IMEP
Instead of torque the gross IMEP (IMEPg; for the compression and expansion strokes only) [3.9] is preferred as a measure of the model's ability to predict the engine output. If the engine is very symmetric and PMEP is equal for all cylinders, the net IMEP (IMEPn) can also be used (which was the common case in this work). If BMEP, or torque, is used, then the model needs to have an accurate sub-model for FMEP. Such sub-models cannot be created without knowing FMEP thoroughly from measurements, which requires motoring of the engine and/or accurate pressure analysis for every cylinder on the engine to acquire the PMEP and IMEP symmetry.

4. Cylinder pressure trace
Accurate cylinder pressure trace and combustion phasing is crucial for accurate IMEP but also for exhaust temperatures. A correct match for the cylinder pressure trace is also a double-check that the air consumption is accurately modelled and that in-cylinder heat transfer is accurate. A good fit of cylinder and port pressures during the overlap period also ensures well-modelled pressure wave propagation.

5. Turbocharger speed
If measured data is available, and a controller controls the speed to this value, this step is simple. Just check that the turbine efficiency multiplier does not have an unrealistic value (values between 0.7-1.3 have been detected for realistic models) and that the wastegate mass flow fraction is ok (up to 50% of the exhaust gas stream on max power point).
Calibrating a model without having measured the turbocharger speed can be very difficult, if possible to achieve at all with reasonable accuracy.

6. Turbine inlet pressure trace
Good fit for turbine inlet pressure trace is necessary for prediction of the turbine power. The turbine inlet pressure trace is determined by the cylinder pressure at valve opening, the valve flow capabilities, the length and volume of the manifold and the mass flow map of the turbine. The amount of adjustment required to get good fits for this data, for the non-wastegated speeds, depends on the turbine maps. Crank-angle resolved data is essential since it is necessary

to achieve a good fit for the shape of the curve to ensure proper turbine operation.

7. Inlet manifold pressure trace
To check that the pressure pulsations and inlet ramming process is modelled correctly.

8. Inlet manifold average temperature
To check that the engine is fed with air of correct density. This value is governed by the prediction of compressor efficiency, intercooler-model and the wall temperature and heat transfer of the piping from intercooler to the inlet plenum.

9. Average turbine inlet gas temperature
Without accurate turbine inlet gas temperature the turbine model has no chance to predict turbine power accurately. The turbine inlet temperature is governed by the combustion phasing and the in-cylinder, port and manifold heat transfer.

10. Compressor outlet temperature
Shows if the compressor model predicts accurate efficiency. If that is not the case the efficiency must be manipulated, either through an efficiency multiplier or direct manipulation of map data. Accurately modelled compressor outlet temperature and inlet manifold temperature is also a proof of accurately modelled intercooler effectiveness [3.10].

11. Turbine outlet pressure trace
The turbine power output is determined by the pressure ratio over the turbine, therefore the turbine outlet pressure trace is an important parameter. This parameter is largely governed by the exhaust manifold's pressure pulsation behaviour, why it has proven to be necessary to model the entire exhaust system all the way back to the exit of the tailpipe. Cutting the piping in the model and imposing some measured value of the pressure at that location, as a boundary condition, does not give the appropriate pulse reflection behaviour. It has been necessary to fine-tune pipe lengths as well as muffler and catalyst-volumes to get this data reasonably close to measured. The fluctuation amplitude of turbine outlet pressure can be several tenths of the absolute average pressure, thus it is far from constant.

The data presented in the figures in this chapter is a result of adjustment according to this scheme. Every single one of the three cases above has it's own set of adjustment parameters.

Table 3.3. Necessary turbine efficiency multipliers for different speeds.

Engine speed [rpm]	Turbine efficiency multiplier [-]
1600	0.738
1800	0.794
1950	0.826

The way the turbo is adjusted in this work mainly follows these guidelines. The hard work was with the turbine. First the pressure ratio multiplier was adjusted to 0.88 for 1950 rpm and the measured speed imposed in order to get the correct pressure ratio over the turbine (using the mass flow multiplier would give the same result).
Most time had to be spent for adjustment of the turbine efficiency multiplier to accurately model the turbocharger speed. The values necessary for the three cases presented above are shown in Table 3.3. More examples of parameter values and discussion around influencing parameters can be found in Chapter 8.
Not only the turbine model needed adjustment for the turbocharger speed to be accurate. The turbine inlet temperature needed much work to get it to equal the measured value. The exhaust manifold wall temperature was measured both close to the cylinder head and close to the turbine/manifold flange. These values could differ much due to the cooling of the manifold to the cylinder head. For the data shown in this chapter the average value of these two measured values was used and imposed on the entire manifold. In other chapters the wall temperature solver was used and calibrated against these measured data.
If the wall temperature is imposed, the user can only control the heat transfer through the surface roughness of the pipe inner wall (defined as sand-roughness) and through a heat transfer multiplier. Recommended values for the wall surface (sand-) roughness for the cast iron was 0.26 mm and for drawn tubing 0.0015-0.0025 mm. The manifold on this engine is cast heat resistant steel (Inconel) and a bit smoother than ordinary cast iron. Therefore 0.18 mm was chosen. Later measurements showed that it was 0.12 mm, see chapter 7.
To adjust the heat transfer multiplier a target optimisation was run where the software adjusts the multiplier until the measured gas temperature is emulated (a controller was later employed for the same task).
The same procedure was run for the exhaust ports, but here the wall temperature was 550K. This was chosen according to the recommendations of cylinder head temperature in the manual.

Table 3.4. Necessary values for the heat transfer multipliers to achieve measured gas temperatures, the wall temperature was imposed values from measurements.

Engine speed [rpm]	Manifold heat transfer multiplier	Exhaust port heat transfer multiplier
1600	0.373	0.45
1800	0.352	0.45
1950	0.277	0.45

With two adjustable parameters and one wall temperature that is not measured (exhaust ports) there exist more than one solution that end up with the same gas temperature. Therefore it was not considered necessary to adjust the exhaust port heat transfer multiplier individually for all speeds.
The results of the multiplier adjustments are presented in Table 3.4.

Single point adaptation

The previous section showed that with adjustments the software can simulate the performance of a turbocharged engine. The question now is, what if the engine model is adjusted for only one point, in this case 1950 rpm full load, will the model perform reasonably well over a larger range? Unfortunately that is not the case. In fig. 3.18 and 3.19 it can be seen how the turbocharger speed deviates for 1600 and 1800 rpm, and subsequently the IMEP goes way too high.

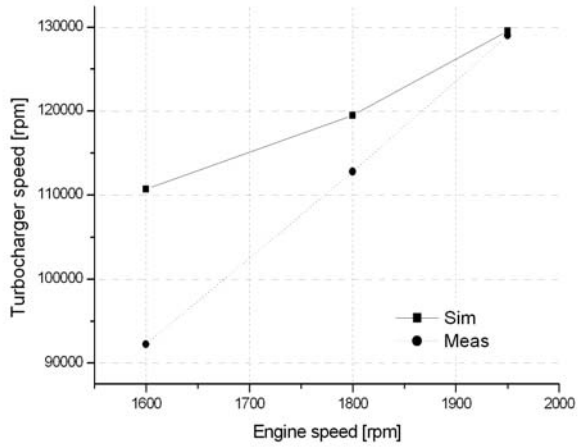

Figure 3.18. Turbocharger speed. Comparison between measured and simulated where the model is only adapted to measured data for 1950 rpm.

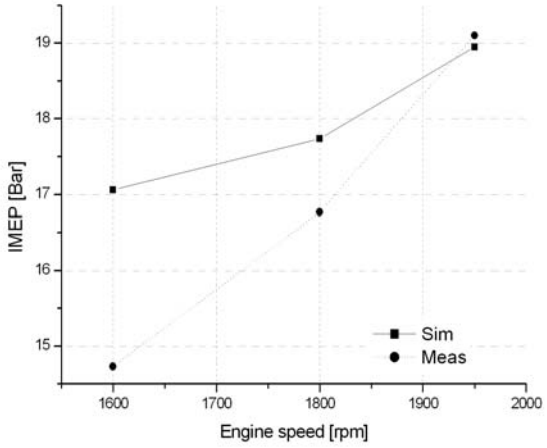

Figure 3.19. Comparison of measured and simulated IMEP if the simulation model is only tweaked for 1950 rpm.

Adjustment methods

In the text above several parameters has been mentioned that needed adjustments. Throughout this work different numbers of parameters have been used as well as several methods to adjust them. The parameters have been turbine efficiency multiplier, turbine mass flow multiplier, wall heat transfer coefficient, convective multiplier, compressor efficiency multiplier as well as wall temperatures. The methods to adjust them have changed from:

- manually adjusting the parameters and rerun the simulation
- using the target optimisation function where GT-Power iterate through several runs until a final value has been reached for the results and parameter in question
- the final method where PI-controllers are utilized

The last method has gained a lot in efficiency compared to the earlier. Instead of running several iterative runs, as for the target optimisation, all adjustments of several parameters can be carried out in a single run. It is done by having a PI-controller actuate the parameter to be adjusted and some measured result are input as target value for the control. With this method several parameters can be adjusted automatically with only marginally increased simulation time than for an ordinary single simulation run. The extra effort required to setup the control is easily retrieved by less time needed for setup and analysis. As an example the turbospeed control is shown. The PI-controller block senses the current turbospeed via a sensor. It actuates the turbine efficiency multiplier via

an actuator. The target value for the control is the measured turbospeed. The P and I factors necessary were 0.0001 and 0.0005 respectively. These factors were scaled for other control purposes with the ratio of common control error and target value for the control in question. The controls used were turbocharger speed (turbine efficiency multiplier), average manifold pressure (turbine mass flow multiplier), turbine inlet temperature (exhaust wall heat transfer multiplier), turbine outlet temperature (heat loss in the turbine), exhaust manifold wall temperature (convective heat transfer of manifold outer wall) and inlet temperature (intercooler wall temperature). At most 6 simultaneous controllers. Problems with oscillations were overcome by making the controllers' speeds different. Generally there were no problems with oscillations.

Predictivity

So, what if one would try to make a truly predictive simulation. Without using any multipliers, at least in terms of the turbocharger, but still using measured data for the valve flow and combustion.

The data presented in figure 3.20 are from a simulation where no multipliers were used for the turbine and compressor. Nevertheless, for the exhaust manifold heat transfer the multipliers are maintained in order to have the same amount of energy delivered to the turbine. The figure shows that the inlet pressure is over-predicted for the speeds below 2000 rpm where the wastegate is closed in the measured case. However, in this simulation model the wastegate had to be opened earlier to avoid over-boost. Figure 3.21 shows the mass fraction of mass flow through the wastegate. For the measurements the mass fraction is zero for 1950 rpm and below but positive and unknown for higher speeds.

These two pictures illustrate a very important point. When the wastegate is closed the simulated turbine power commonly is erroneous. But when the wastegate is open in the real case the mass flow fraction through it is unknown and this enables the model to control the wastegate so that required boost pressure (i.e. measured or target) is reached anyway.

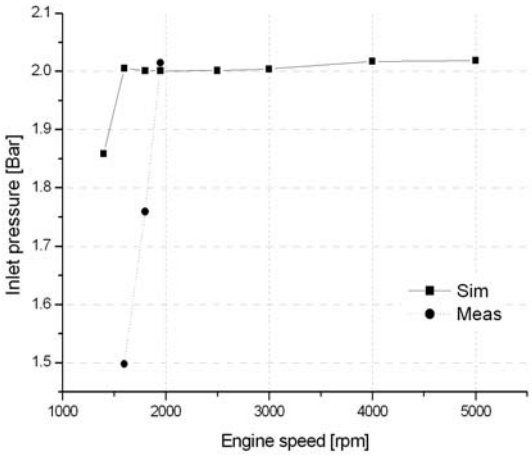

Figure 3.20. Inlet pressure as a function of speed at full load. The simulation over-predicts the boost pressure for the cases where the wastegate was closed in the real case, that is 1950 rpm and below.

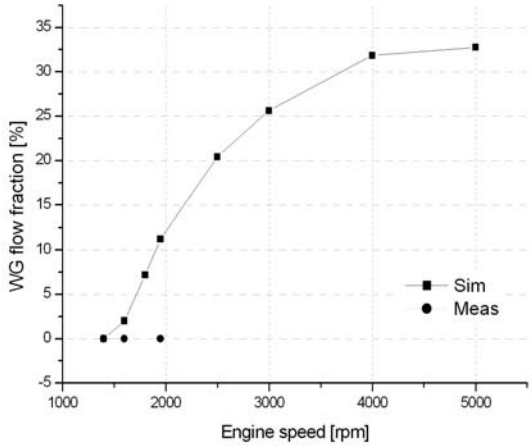

Figure 3.21. The fraction of total exhaust flow that goes through the wastegate. For the measured case the fraction is 0 for 1950 rpm and lower, but positive and unknown for higher speeds.

3.3.5 Reducing the level of detail

The model used in this work had a very high level of detail in the geometry of the piping. It is interesting to study how high level of detail that is necessary to produce data with enough accuracy. Therefore the pipe geometry was simplified, mostly on the intake side. The pipe geometry from the intercooler to the throttle was simplified so that the total lengths and total volumes were maintained but the pipe had the same cross section over the entire length, the major bends were however kept. The intake and exhaust runners were also simplified in the same manner.
This resulted in no significant differences for the overall performance of the engine and neither any particular difference in the exhaust pressure traces.

3.4 Transients

3.4.1 Introduction to transient simulation

Predicting the response characteristics of an engine design using 1D simulations, and optimising the system with regards to throttle response, peak power and efficiency are very important parts of the engine design work. Performing predictive transient simulations could be very useful if they had high accuracy. They are essential for optimisation of volumes in intake- and exhaust systems, for choosing turbines, intercoolers etc. However, the lack of predictivity has limited the usefulness.
Unfortunately, but quite naturally, what is most desirable is also hardest to achieve. If a model cannot predict the performance for discrete steady-state points, then it will not be able to predict transient performance either. So, we first have to learn how to emulate, and improve from there towards predictivity. However, even emulating is difficult task. As shown previously, a steady state case can be emulated/simulated by adjusting some appropriate multipliers to get the desired result. This is not as applicable for transient simulations since a continuous range of data is needed as the engine traverses a speed and/or load range.
The transients covered here are steady speed transients. The reason is to decouple the boosting system's characteristics from the vehicle it is used in. If the speed would be ramped then the particular ramp of choice would both be dependent on the vehicle as well as affect the behaviour of the boosting system. Therefore results from steady speed transients are more general.
Transient simulations are difficult for several reasons:

1. Compressor and turbine maps are normally not available below 80000 rpm. Thus the software has to extrapolate the maps, which might make the turbocharger performance data unreliable.
2. Physically accurate models for inlet and exhaust side wall temperatures are necessary. In particular the thermal behaviour of the intercooler and exhaust manifold and turbine housing are important.
3. A transient model for combustion is needed in order for the simulated combustion to follow how ignition timing and burn duration changes with changing IMEP.

3.4.2 Transient experiment

The transient simulations, as well as the transient measurements, shown here differs somewhat from the steady-state cases described earlier. The biggest difference lies in the measurement of exhaust manifold properties. No long thermocouple existed, only a short 3 mm unit, the pressures were measured with strain-gauge transducers recessed approx. 120 mm from the pressure-tap and no exhaust manifold wall temperature existed. Therefore the measurement data are not as accurate as for the steady cases above, but by no means deficient.

The dynamometer control was upgraded [3.11] to be able to perform transient measurements. The performance of the control is showed in fig 3.22. The measurement frequency was 10Hz for both speed and load.

The particular transient run in this case is 45 Nm to full load for 2000 rpm. The engine had an electronic throttle and no measurement of the throttle position was performed. Thus the throttle opening in the simulation model had to be adjusted so that the pressure-increase up to atmospheric inlet pressure was equal in simulations and measurements.

At the transient tests the turbo was fitted with the standard wastegate actuation and it was at start assumed that the wastegate would stay closed. Unfortunately that was not the case. A linear potentiometer positioned on the wastegate actuator arm indicated slight opening of the wastegate, as can be seen in figure 3.23. The flow area was however not calculated even though it would be possible. The reason is that the flow modelling of the wastegate would be too difficult in the 1D simulations, and therefore no accurate value for the wastegate mass flow would be acquired anyway.

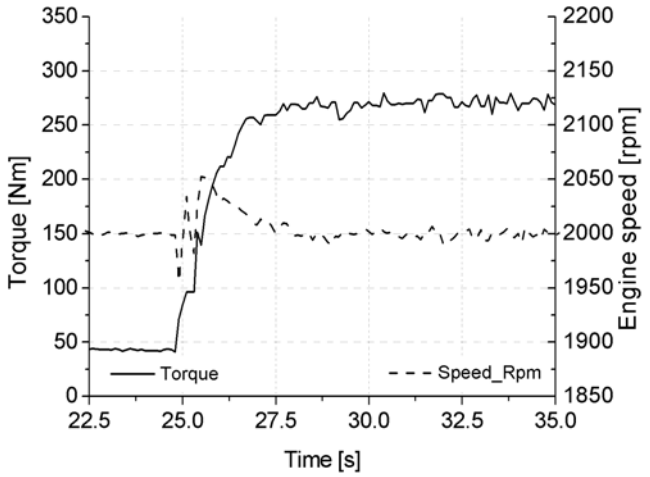

Figure 3.22. Engine speed and torque during a transient showing the control performance of the transient dynamometer.

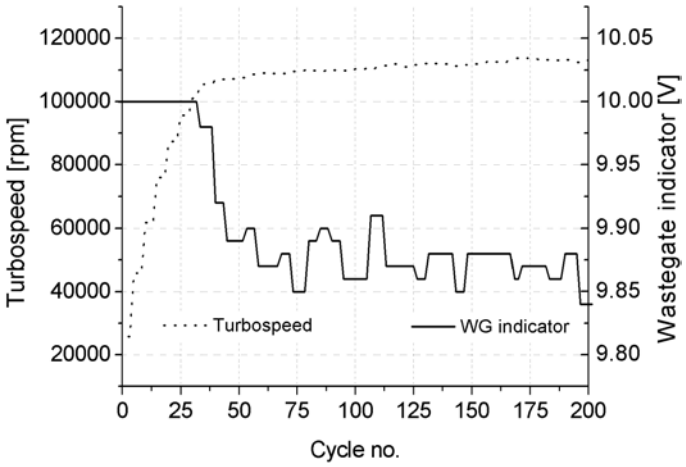

Figure 3.23. Turbospeed vs. cycle number for the transient. The speed trace looks slightly different from other presented curves, and the reason is that this one comes from the slow measurement system while the others are from the fast. The WG indicator is the voltage output from the linear potentiometer on the wastegate actuator arm. Thus a value less than 10V means an open wastegate.

3.4.3 Transient model changes compared to steady state

Some changes had to be made to the steady-state model to be run transient. During the transient measurements the ignition angle change as a result of changing inlet pressure. An ignition information map (i.e. maps of Wiebe parameters) as function of engine load, or inlet pressure, could easily be derived from steady-state measurements and put into the model. However, here an even simpler option was chosen: the points of 50% burned and 10-90% burn duration were calculated for every measured cycle during the transient and input to the model as functions of cycle number in the transient event. The amount of fuel burned follows the simulated airflow and requested lambda. This enables the simulation results to show very realistic cycle-to-cycle variations. However they are not really predicted, the procedure is more like recording and playback.
In addition a ramp function was added to the throttle. It was ramped from 2.3° open to 90° in 61 ms (1 cycle) according to table 3.5.
Different turbine settings were used:
Sim 1 ..... The same adjustment factors as for 1950 rpm steady state, wastegate closed
Sim 2 ..... Same as above but wastegate controlled by a PID-controller in the simulation, boost pressure target set to 1.75 Bar which was the final boost pressure in the measured transient
Sim 3 ..... No adjustments used at all, wastegate same as in Sim2
For all the above cases the wall temp settings were as for 1950 rpm, full load, steady state. It would be more proper to use the wall temps according to the part load conditions before the transient, but the transient simulations were done before wall temp measurements were available.
Finally, the turbine efficiency multiplier was manually adjusted, to give the same turbospeed vs. time in the simulations as in measurements.

Table 3.5. Throttle-opening ramp used in the transient simulation.

Time [s]	Throttle angle [°]
0	2.3
0.959	2.3
0.96	3
0.975	6
0.99	9
1.005	12
1.02	90

3.4.4 Transient results

Since the steady state cases has shown that problems originate from the turbine power, and that the overall results are good as long as the turbospeed is accurately simulated, the focus here is on the turbospeed. In fig. 3.24 the turbospeed for the three first simulation cases (Sim1-Sim3) are shown along with measured data. It is obvious that for the two cases with turbine performance multipliers with values set for 1950 rpm steady state (Sim1 & Sim2) the turbo acceleration is far too slow. Sim1, with closed wastegate, overshoots the measured final turbospeed while Sim2, with controlled wastegate, succeeds in emulating the measured final speed. The simple explanation to that is that the wastegate was actually open in the measurements, as was displayed in fig. 3.23. Note also that most of the measured pressures and turbospeeds appear to be very noisy. However, it is not noise, it is the natural fluctuation of the data since it is crank angle resolved instantaneous data, not cycle averaged.

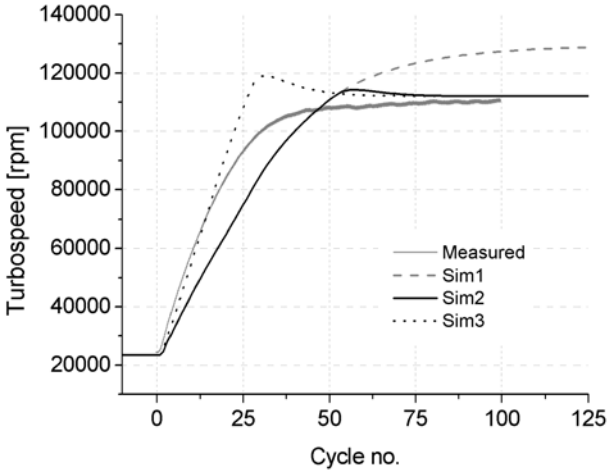

Figure 3.24. Comparison between measured turbospeed and three different simulations. The measured turbospeed appears noisy, but it is the fluctuations due to exhaust pulsation that are seen.

Nevertheless, as fig. 3.23 shows, the wastegate is closed until approximately cycle 30-35. The underestimation of the turbine speed thus shows that the turbine power during this period also is underestimated.
If no factors are used, as in Sim3 in fig 3.24, then the first 10 or so cycles are emulated fairly well, but then the simulated turbospeed overshoots up to the point where the wastegate opens in the simulations.

It is easy to suspect the extrapolated turbine efficiency map to cause these errors, but before anything can be said about the accuracy of the extrapolated turbine map the turbine inlet temperature has to be checked.
Thus, lets go back to fig. 3.24 and consider the Sim3 curve. For the first part of the transient (approx. up to cycle 13) the turbospeed seem to be fairly accurately simulated, however probably with higher inlet energy in the simulations than in the measurements due to transient wall temperatures, as will be shown below. Thus the turbine efficiency must be under-estimated for this part. For the second part, from cycle 13 up to where the wastegate opens at approx. cycle 30, the turbine speed is overestimated, but we cannot know if the reason is too high turbine efficiency or just the over-estimated inlet energy due to too high temperature. For the third part the wastegate is open and we do not know the actual (real, on-engine) flow through the wastegate, so we cannot draw any conclusions from that part of the curve. However, the multipliers needed to emulate the steady state speed in the steady simulations, where the inlet temperatures are not over estimated, clearly show that the map over-estimates the turbine efficiency for this part of the map.
Thus, for the first part of the transient the efficiency is under-estimated and for the latter part of the transient the efficiency is over-estimated.
Here it must be remembered that the turbine map used in the simulation is a combination of measured data and extra- and interpolated regions. Figure 3.25 below shows the turbine efficiency map where the original map points are shown as diamonds, the cycle-average operation points are the circles, the continuous field is the extra- and interpolated map used for the continuous calculations and the solid trajectory is the instantaneous operation line for the last cycle. It is clear that the average operation points are very close to real map data, but unfortunately the instantaneous operation conditions deviate both above and below the row of real map points. Thus the calculations depend heavily on the extrapolated data, and all the possible error connected to the extrapolation.
Further manual adjustment of the turbine efficiency multiplier finally resulted in a good match between simulated and measured turbospeed, as seen in figure 3.26. Note here that the wall temperatures are adjusted somewhat to more accurately emulate the measured case, more on that below (see Table 3.6).

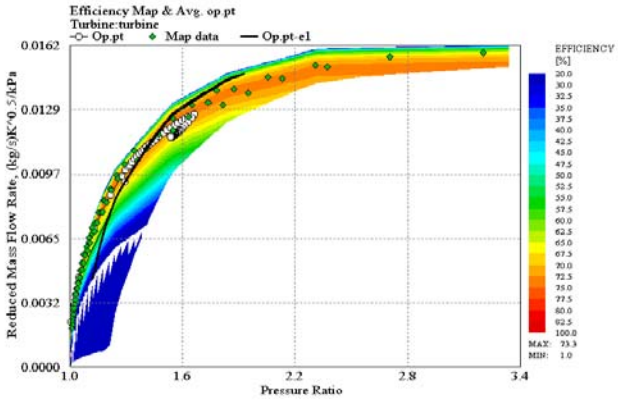

Figure 3.25. Turbine map with original map points as green squares, cycle average operation points as white circles and black trajectory is the instantaneous operation line for the last cycle. The colored field is the extra- and interpolated map used in the simulations.

To achieve the results shown in figure 3.26 the turbine efficiency multiplier was changed from the value 0.758 which was used for the 1950 rpm steady state case. The procedure of adjusting the efficiency multiplier was as follows: first the efficiency multiplier was adjusted for the low-speed point at the beginning of the transient, along with throttle opening in order for the inlet pressure and turbocharger speed to match measured. That resulted in the value 1.42 for the multiplier. Then the multiplier had to be adjusted for the high-speed point after the transient, which resulted is the value 0.693. Throughout the simulation the turbine efficiency multiplier was linearly interpolated between 1.42 for the turbospeed of 0 rpm and 0.693 @105000 rpm. With the turbine efficiency multiplier unchanged from the steady-state simulations the time to a certain boost pressure could be 100% longer than measured.

The necessity for a multiplier as large as 1.42 for the low load case is justified by the fact that, at 25000 rpm and low mass flows, the turbine operates in a regime far away from the measured map, which is the basis for the model. Thus the input data to the turbine work calculations might be very unreliable at this point.

With all these calibration tricks a very good agreement between measurement and simulation for performance can be achieved, as seen in figure 3.27. The agreement between IMEPn also indicates that the air consumption is modelled very accurately.

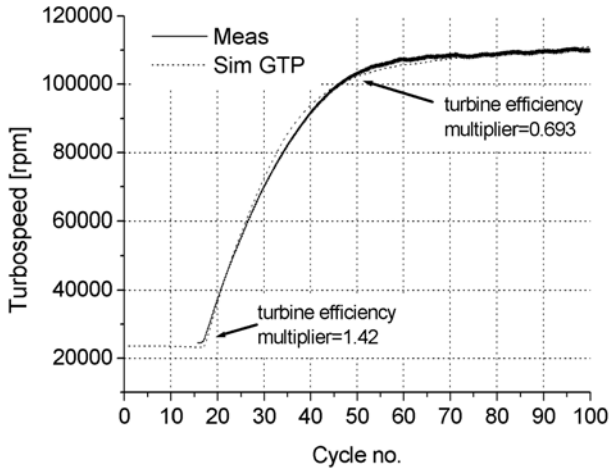

Figure 3.26. Simulated and measured turbospeed, turbine efficiency multiplier linearly interpolated.

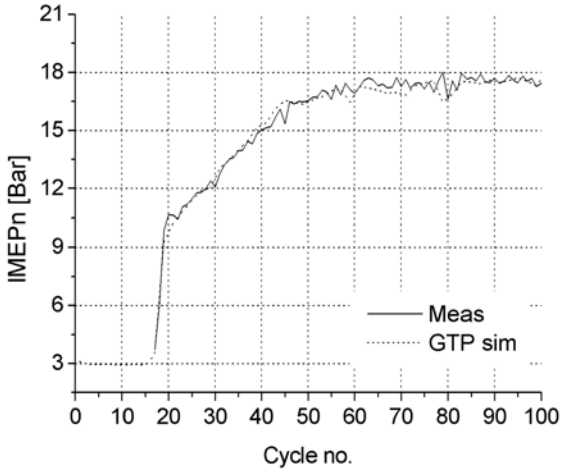

Figure 3.27. The net (720 CAD) IMEP.

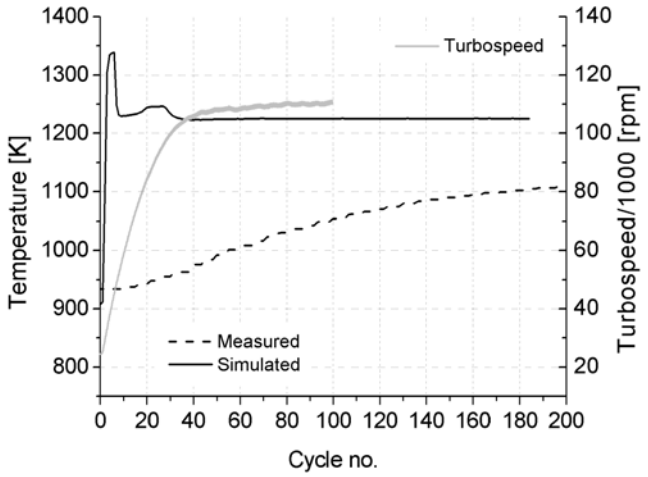

Figure 3.28. Comparison between measured and simulated turbine inlet temperatures. Turbospeed is included to show the timescale of transient.

In fig. 3.28 the turbine inlet temperature is compared between the measurement and the simulation case without adjusted factors (Sim 3). The measured temperature responds very slowly to the increased gas mass flow as the throttle opens. This is due to heating of all the components from inside the cylinder down to the turbine rotor, possibly also including the thermocouple itself. In the simulation this heating is not simulated at all since measured steady state full load wall temperatures are imposed for all parts in the model. Consequently the turbine is probably fed with much higher inlet energy in the simulations than in the real case.

If the wall temperatures are decreased compared to the full load steady state case the results are somewhat different. In addition, a thermocouple model was used to simulate the thermal inertia of the thermocouple. Figure 3.29 shows the simulated exhaust gas temperature along with simulated thermocouple temperature and measured thermocouple temperature. Note here that for this transient simulation the wall temperatures were not fine-tuned enough for the simulated gas temperature at the beginning of the transient to equal the thermocouple-measured, but the error is below 5% which was considered sufficient in this case. The second point to note is that the thermocouples are not fast enough to measure the gas temperature during the transient, which simply is due to thermal inertia. The third point is that the simulated and measured thermocouple temperatures do not rise at the same rate. This is

probably because the thermocouple is modelled as a 3 mm sphere while the thermocouple used in the measurements is a 3 mm shielded thermocouple which is a 3 mm thick rod with the thermocouple bead internal at the end of the rod. Therefore the real, rod-shaped thermocouple is hard to copy in the simulation, since it must be modelled as a sphere that has a different thermal inertia. But this poses no problems for steady state simulations when the thermocouples are given appropriate times for the temperature to converge.
For gas temperatures on the intake side of the engine 1.5 mm thermocouples could be used which proved to be fast enough to measure the transient temperatures, but on the exhaust side 3 mm thermocouples were necessary for durability reasons and they could not be proven to be fast enough to give reliable gas temperature measurements at turbine inlet and exit. During the transient, wall temperatures were not measured, but simply assumed. In Table 3.6 the wall temperatures during steady state at 1950 rpm and for the 2000 rpm transient are presented.

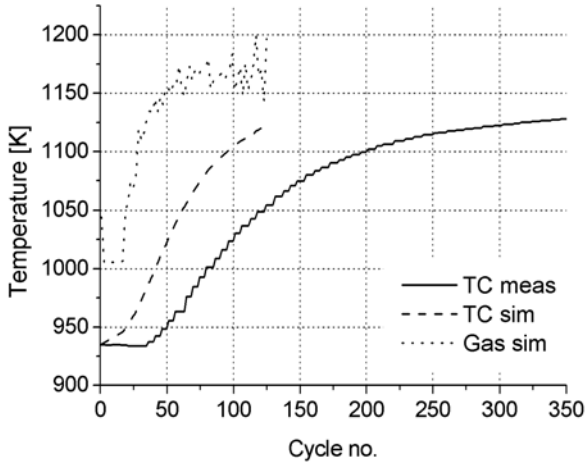

Figure 3.29. Simulated and measured thermocouple temperatures during an engine transient.

Table 3.6. Wall temperatures imposed to the model for 1950 rpm steady state and 2000 rpm transient simulations.

	Steady state [°C]	Transient [°C]
Intercooler water	61	40
Exhaust manifold wall	618	300
Head	327	227
Piston	327	227
Intake wall	50	40

Finally it is just pointed out that the compressor does not seem to cause any big problems. The inlet pressure is displayed in figure 3.30. Apparently the inlet pressure is somewhat over-predicted in the simulation. The IMEP results still indicate that the air mass in the cylinder is correctly simulated. This assumption is justified by the inlet temperature, which is over-predicted by approx. 10K in the simulations. The reasons for this may be different compressor efficiency due to heat transfer in the turbocharger or wall temperature in the intake system leading to different volumetric efficiencies. Thus the density is similar in measurements and simulation because the over-predicted pressure is compensated by an over-predicted temperature.

3.4.5 Discussion on transients

Of course there are a number of points where these simulations can be improved. It is very obvious that transient simulations demand a physically accurate heat transfer and wall temperature model for the exhaust manifold and turbine housing. But the point to be made is; even though the delivered flow power to the turbine is over-predicted the turbine power is under-predicted in one part of the work range, and over predicted in another. Therefore the turbine modelling has to be investigated in more detail and that is much better done with steady state simulations.
A more thorough heat transfer analysis of the turbocharger and piping system is addressed in chapter 7. Unfortunately there was no time to use that thermal model in transient conditions.
Although it has not been possible in this work to perform predictive transient simulations, they are still believed to be able to give proper trends and can therefore be used as tools for optimising the engine-turbo-system in certain aspects. An example of that is presented in the last chapter of this thesis.

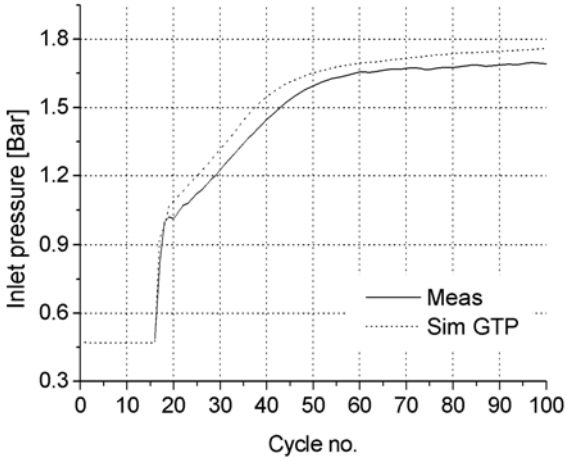

Figure 3.30. Measured and simulated inlet pressure.

3.5 References

3.1 GT-Power User's Manual and Tutorial ver. 6.0 Gamma Technologies
3.2 Dale A, Watson N & Cole A.C. "The development of a turbocharger turbine test facility" Inst. Engrs. Seminar pp. 75-84 1988
3.3 Winterbone D.E., Nikpur B., Frost H. "A contribution to the understanding of turbocharger turbine performance in pulsating flow" IMechE paper C433/011 1991
3.4 Winterbone D.E. & Pearson R.J. "Turbocharger turbine performance under unsteady flow – a review of experimental results and proposed models" IMechE paper C554/031 1998
3.5.Pucher H & Nickel J "Vermessung erweiterter Kennfeldbereiche von Fahrzeugmotoren-turboladern" 8. Aufladetechnische Konferenz 1-2 Oktober 2002, Dresden. Pp. 321-339.
3.6 Lancaster D.R., Krieger R.B., Lienesch J.H. "Measurement and Analysis of Engine Pressure Data", SAE paper no. 750026
3.7 Blair G P "Design and simulation of 4-stroke engines" SAE R-186, ISBN 0-7680-0440-3
3.8 Chen S.K., Flynn P. F. "Development of a single cylinder compression ignition research engine" SAE Paper 650733
3.9 Heywood John B "Internal Combustion Engine Fundamentals" McGraw-Hill New York ISBN 0-07-100499-8
3.10 Watson N, Janota M S "Turbocharging the Internal Combustion Engine" MacMillan Press 1982 ISBN 0 333 24290 4
3.11 Rygran Erik "Transientreglering av motorbroms" Report from Project course in Internal Combustion Engines, KTH Machine Design 2001

3.6 Appendix

Email from Brad Tillock

Subject: RE: Turbo question
Date: Mon, 8 Jul 2002 16:48:00 -03.600
From: Support <Support@gtisoft.com>
To: turbo@kth.se

Dear Fredrik,
The pressure ratios are determined from the pressure in the adjacent sub-volumes immediately upstream and immediately downstream of the compressor or turbine (Pin/Pout). Static or total quantities are specified by the user in the Compressor or Turbine components. The determination of the pressures depend on the entire system. The mathematics of which are 1000s of lines of code.
Whether the user specify the inlet and outlet pressure flags as total or static, it is important that the flow components adjacent to the turbine or compressor have a correctly defined diameter. This is because the velocity used in the calculation is taken just inside the adjacent flow components.
Your turbine nozzle diameter should probably be set to the inlet pipe diameter of the adjacent element downstream. The volume of the flow passages within a turbine or compressor should be added to the adjacent flow components since GT-Power does not assign any volume to turbines and compressors. As you can see the turbine is just an elaborate metering device; we look up pressure ratio and speed and then let the correct amount of mass through. This mass then ends up changing the pressure ratio in an indirect manner for the next timestep.
I am sorry if there is still some confusion on my part. If you still have questions I can ask a developer here to look at your questions.

Best Regards,
Brad

Chapter 4

Comparison of two commercial engine simulation software and measured data

4.1 Introduction

In the previous chapter 1D engine simulations of a turbocharged SI-engine in GT-Power was described briefly. The problems with predictivity encountered in GT-Power, were they general problems or software specific? In this chapter this is checked by comparing results from two different 1D engine simulation software (GT-Power and Virtual Engines) as well as with measured data.

4.2 Investigation setup

The simulation models used for this work were built up in GT-Power v. 5.2 [4.1] and Virtual 4-stroke v. 5 [4.2]. They are quite similar in layout, but differ some in the details. The engine is the same 2-liter unit as in previous chapters.

4.2.1 Simulation model input

For all submodels aside from the turbocharger, the simplest possible options were chosen. The reason is that the main focus is the accuracy of the turbocharger modelling. Another reason is the availability of a large measured dataset, which enables use of simple empirical submodels. Thus, the combustion is modelled with the Wiebe-function adapted to ensemble-averaged heat-release curves derived from measured cylinder-pressure traces. The

intercooler is modelled by inserting the correct volume and length. As wall temperature the measured compressor gas outlet temperature is imposed and the heat transfer coefficient is set to a sufficiently high value. The piping of the engine (in the test cell setup) is modelled from the normal location of the airbox to the tailpipe exit. For the manifolds and the exhaust pipe the model geometry was input as close as possible to the real manifold and piping geometry. For the intake side (from compressor outlet to throttle plate) it was not necessary to model every change in geometry. Preserving total length and volume was sufficient. The engine's twin catalytic converters were modelled with plenum volumes and the pressure loss of the catalyst carriers was modelled with an orifice, which was calibrated at a high-speed, high-load point (5000 rpm, WOT).
The turbocharger was modelled with compressor and turbine maps supplied by the manufacturer of the turbocharger. For the compressor the data was in referred/corrected format [4.3], which seems to be standard and similarly used by both software.
However, for the turbine map data two data formats are common:
corrected / referred:

$$RPM_{ref} = \frac{RPM_{actual}}{\sqrt{\frac{T_{actual}}{T_{reference}}}},\ \dot{m}_{ref} = \dot{m}_{actual}\frac{\sqrt{\frac{T_{actual}}{T_{reference}}}}{\frac{P_{actual}}{P_{reference}}} \qquad \text{eq. 4.1}$$

and reduced:

$$RPM_{red} = \frac{RPM_{actual}}{\sqrt{T_{actual}}},\quad \dot{m}_{red} = \dot{m}_{actual}\frac{\sqrt{T_{actual}}}{P_{actual}} \qquad \text{eq. 4.2}$$

GT-Power can handle both formats while VE only can use the referred/corrected values. However, it is no problem to calculate referred/corrected values from the reduced by assuming a reference condition which also is input to the software.
Both software require map data along constant speed lines, i.e. mass flow as function of pressure ratio (PR) for a series of constant speeds (and efficiency data for every point). When measuring maps on turbocharger test benches, some manufacturers measure along speed lines while others measure along constant PR-lines and let the speed vary along with the mass flow rate. The maps in this work are of this latter type, but the turbocharger manufacturer has

recalculated the map to constant speed lines, and thus it can be used in the software. This recalculation of the map data was not stated in the map, but was confirmed by the manufacturer. Knowledge about such recalculations is useful since they require some assumptions about the machine that might be of interest for some users of the maps.
An important parameter for the performance of the turbocharger is the turbine inlet temperature, which is dependent on the manifold wall heat transfer. Both software have wall temperature solvers, but the one in VE was not able to give results and GT-Power's needed considerable hands-on adjustment. Parameters available for adjustment were inner and outer wall properties such as surface roughness, heat transfer coefficients, outer wall convection coefficient. The main focus was not to be able to predict the wall temperatures; only the gas temperature, and therefore a simpler solution was selected. To achieve the proper turbine inlet gas temperature the measured wall temperature was imposed in the model. For GT-Power the heat transfer multiplier was then adjusted until the proper gas temperature was achieved. VE did not have this multiplier and thus the imposed wall temperature had to be manually adjusted until the gas temperature was acceptable.

4.3 Simulation results

In this section some results from these simulations are showed. First it must be ensured that the engine is given the proper amount of air, and that the compressor is operating at the proper operation point. Figure 4.1 shows that the fit for air mass flow is within the margin of 5-10% inaccuracy of the measured values.
To determine the compressor operation point, the compressor speed and the outlet temperature are also needed (in the upstream boundary to the model the air pressure and temperature are set to the measured values). Compressor speed and outlet temperature are displayed in figures 4.2 and 4.3. The compressor speed is simulated very well for all speeds except from the highest and lowest. The outlet temperature, indirectly the compressor efficiency, is very well predicted in GT-Power but slightly underpredicted (temperature, i.e. the efficiency is slightly over-predicted) for the higher speeds in VE. For mass flow rate and compressor outlet pressure both software show very similar curves, see figure 4.4 for the compressor outlet pressure trace. A test run with GT-Power where the turbocharger speed were set to a constant value showed the same pressure pulsations as for the free-floating case and from that it was concluded that the pulsations in the compressor outlet emanate from the filling of the cylinders. Thus, the volume between compressor and intake valve is not large enough to entirely damp out the pulsations. Here the volume was 9 litres.

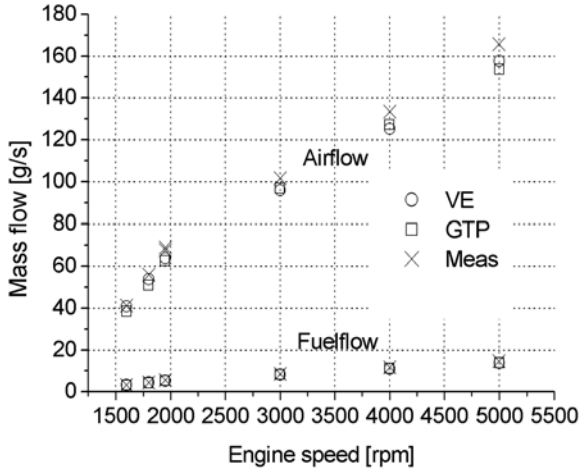

Figure 4.1. Air- and fuel flow rates.

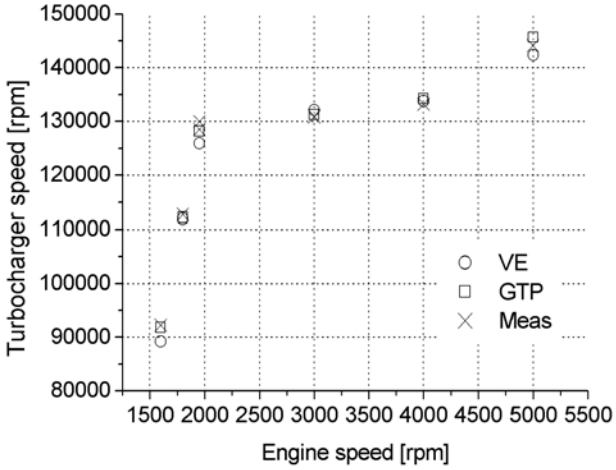

Figure 4.2. Turbocharger speed, WOT operation.

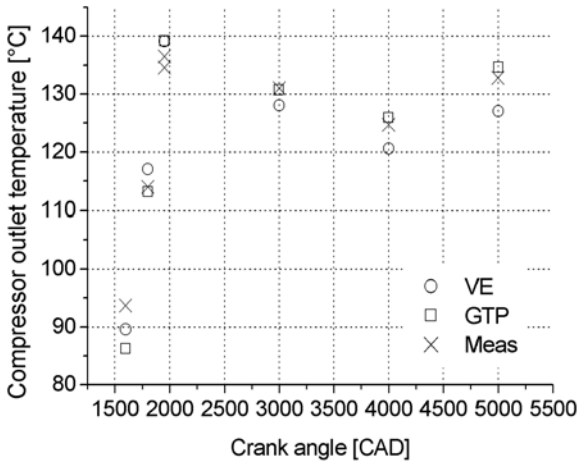

Figure 4.3. Compressor outlet temperature.

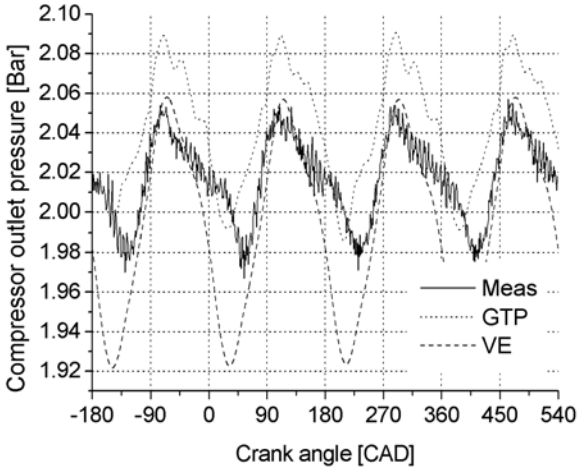

Figure 4.4. Compressor outlet pressure fluctuations.

The difference in fluctuation amplitude might seem large between the three curves in fig. 4.4, but remember that these are a result of resonance's in the pulsation system set up by the inlet plenum and runners, the piping to the

intercooler, the intercooler volume and then possibly also the pipe to the compressor and it's volume. This is a very sensitive system, and thus the fit of the CA-resolved compressor outlet pressure might differ between speeds and due to tolerances in the input volumes in the resonance system.
However, in order to achieve the proper boost pressures, intake air mass flows and turbocharger speeds, the models had to be adjusted. For both software the turbine is the reason for error, but the method of adjustment differs between the two software. The method prescribed for GT-Power is to adjust the turbine efficiency multiplier. In the closed-wastegate region, 1600-1950 rpm, the multiplier must have the value 0.7-0.8 in order for the turbocharger to meet measured speeds. For the open-wastegate region the procedure differs slightly but more on that below. For VE there exists no possibility to adjust the turbocharger efficiencies, aside from manipulating the original map. Instead the wastegate was allowed to open and control the inlet pressure to measured values. For engine speeds above 1950 rpm the wastegate in both software was set to control the inlet plenum pressure equal to measured. As displayed in figure 4.5 the fit between measured and simulated turbocharger speed fluctuation is very good.
It is thus established that the compressor average operation point can be predicted with good accuracy without having to adjust the compressor map. Both compressor speed and pressure ratio fit well to measured values. However the turbine has to be calibrated to achieve the right point of operation. As far as the compressor is concerned, the simulation is predictive.

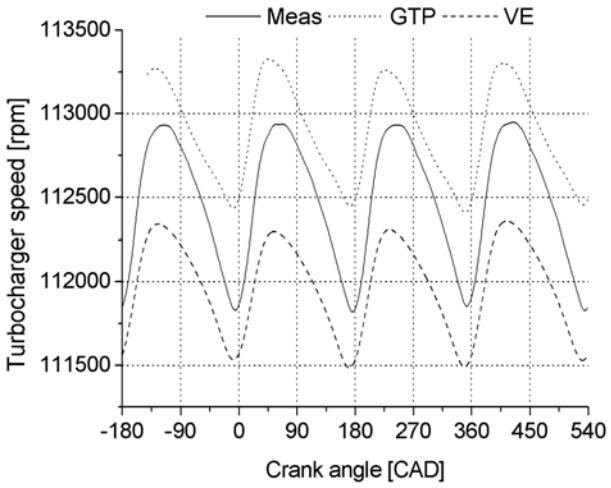

Figure 4.5. The instantaneous turbocharger speed, 1800 rpm WOT.

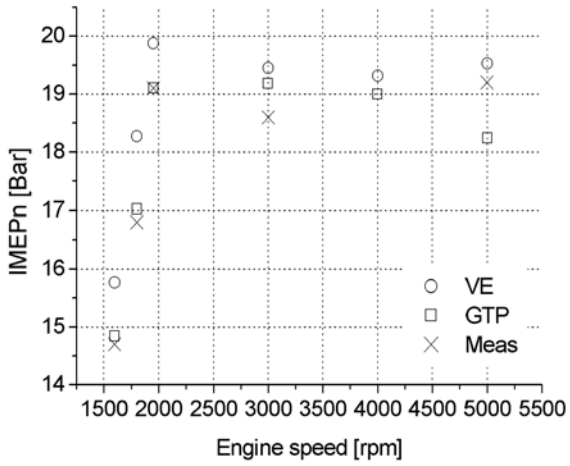

Figure 4.6. Net IMEP.

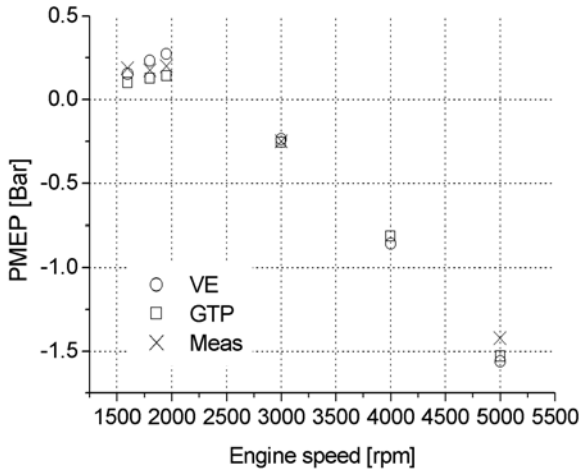

Figure 4.7. Measured and simulated PMEP. GTP 1 is the IMEP-targeted GT-Power simulation and GTP 2 is the turbine inlet pressure targeted (see text).

Figures 4.6 and 4.7 show how well the IMEPn and the PMEP are predicted by the software. Cylinder pressure was only measured at one cylinder in the test cell and the combustion data from this cylinder was imposed on all cylinders in

the simulations. The in-cylinder temperatures and Woschni heat transfer coefficients were used according to the software's manuals.
According to figure 4.8 the fit between measured and simulated cylinder pressure is very good, especially for GT-Power. Here the case is 5000 rpm and full load. The heat release information used to fit the Wiebe function is ensemble average data for 200 consecutive cycles. However, using ensemble average values of heat release might not be the best choice. In figure 4.9 the ensemble average heat release is compared to heat release curves derived from single measured cycles. The combustion evidently differs, which of course is due to the SI-engine's inherent cycle-to-cycle variations [4.4].
If the single cycles' 50% burned points and 10-90% burned duration are plotted along with the 50% burned point and 10-90% burn duration derived from the ensemble averaged heat release curve it is even clearer, see figure 4.10. Thus, deriving the burn characteristics from an ensemble averaged heat release curve might not result in the most typical combustion event. Deriving a Wiebe curve from the average of the single-cycle, non-averaged 50% burned points and 10-90% durations might be more representative for the combustion in question. It must be remembered though that the cycle-to-cycle variations are still not modelled. To be able to do that, stochastic variables must be used.

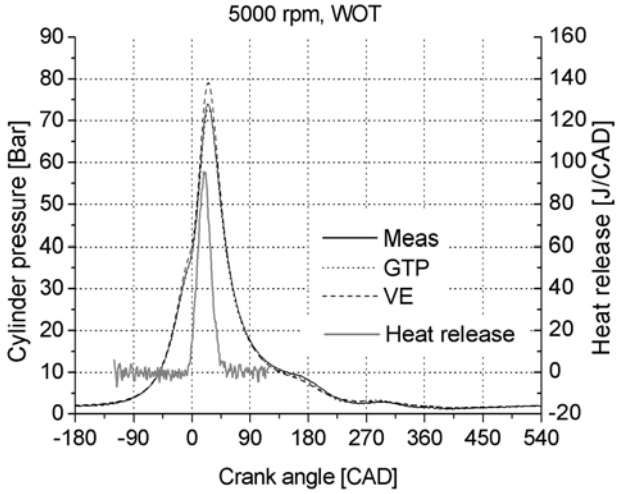

Figure 4.8. Cylinder pressure. The measured heat release is included in the graph to show the combustion phasing.

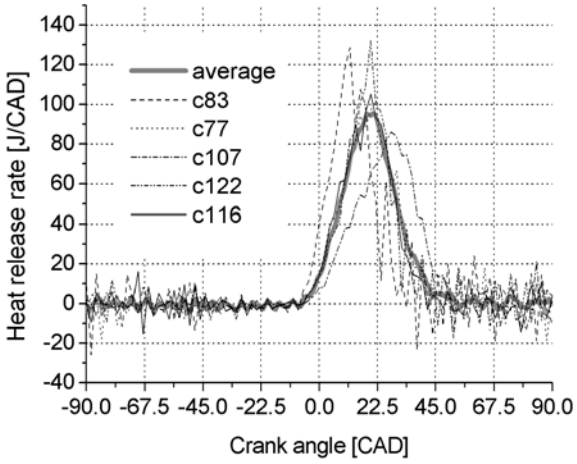

Figure 4.9. Measured heat release indicates that the ensemble average (thick line) might not be representative of the most typical curve. Real cycles can deviate quite much due to cycle-to-cycle variations. This is normally not included in simulations of this kind.

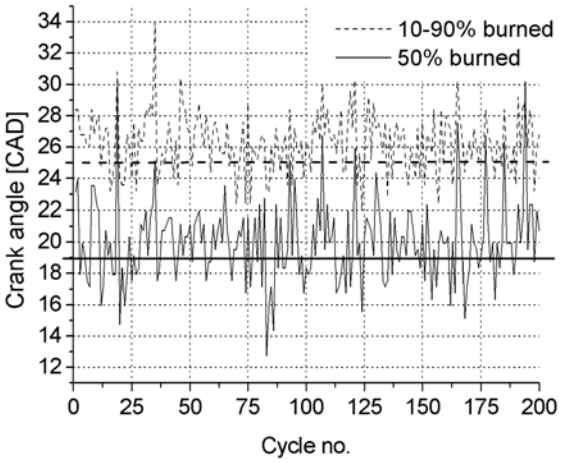

Figure 4.10. Comparing combustion data from an ensemble average with data from single cycles clearly shows that the ensemble average does not have the most typical burn characteristics.

Since turbocharger simulation is the main issue here, the turbine inlet and outlet pressures are very important parameters. Figure 4.11 shows that there are some minor differences in turbine inlet pressure but that the simulations are able to predict the pressure traces very well. For the turbine outlet pressure trace it was very important to model the entire exhaust pipe all the way to the pipe mouth. The engine is equipped with two catalysts in series after the turbine. These are modelled with plenum volumes and an orifice for the pressure loss. Some minor adjustments to these input data had to be done for the good fit for the turbine outlet pressure traces displayed in figure 4.12. Average values of turbine inlet pressure for more than one engine speed are displayed in figure 4.13.
For the non-wastegated cases, the on-engine turbine efficiency seems to differ from the efficiency information in the map. This conclusion is drawn from the necessity of using turbine efficiency multipliers, or opening the wastegate, in regions where the wastegate in reality is closed. In figure 4.14, the predicted turbine efficiency obtained from the maps is compared to measured on-engine turbine efficiency (see chapter 6 for further information on these measurements) [4.5]. The GTP data is the data read from the map multiplied by the turbine efficiency multiplier, in this case equal to 0.758. The VE data is the data read directly from the map, but here the turbine is only fed with 95.4% of the mass flow rate. Equation 4.3 below shows the expression for the maximum extractable power from a turbine (i.e. for 100% isentropic efficiency). This makes it clear that the usable power is linearly dependent on the instantaneous mass flow rate. The turbine efficiency multiplier in the GTP case does not equal the mass flow rate amount through the turbine in the VE simulation since the efficiency multiplier is applied linearly over the cycle while the mass flow bleed over the wastegate is largest when the turbine inlet pressure is highest. Therefore a larger amount of utilizable power is wasted than the amount of mass flow.

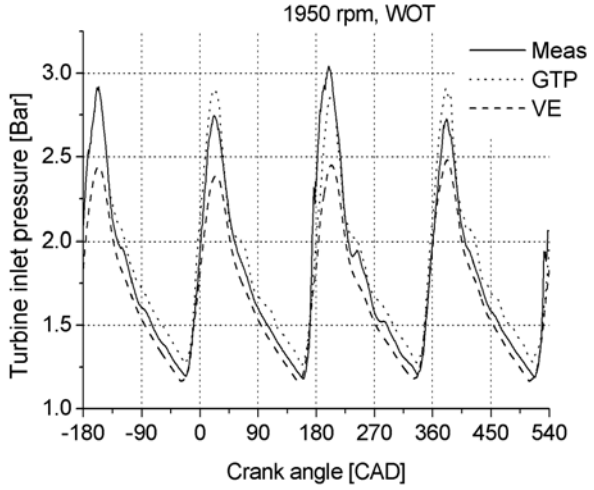

Figure 4.11. Correlation of pressures at turbine inlet. The engine speed was 1950 rpm (closed wastegate) and full load.

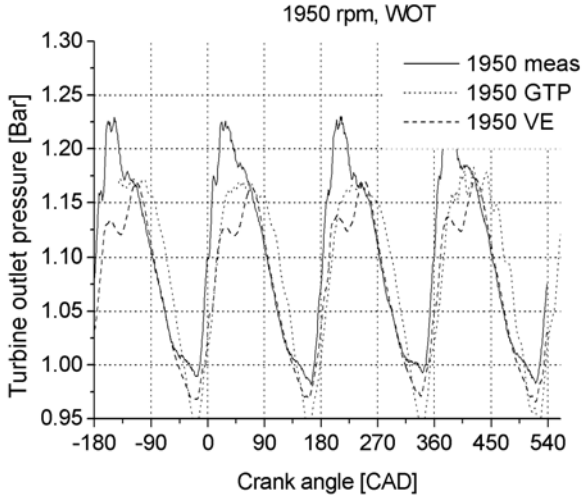

Figure 4.12. Correlation of pressures at turbine outlet. The engine speed was 1950 rpm (closed wastegate) and full load.

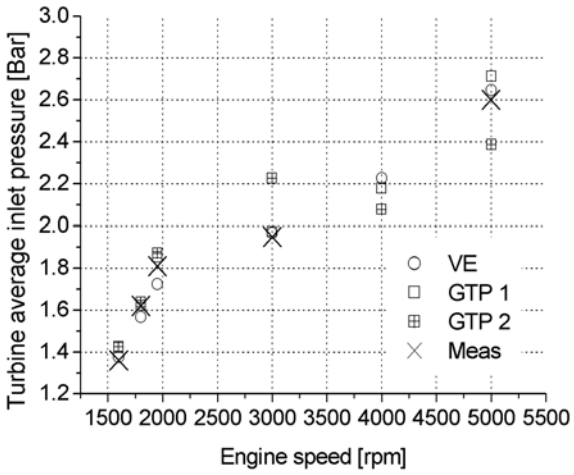

Figure 4.13. Turbine average inlet pressure for the three simulations and measurements. Case GTP 1 is when the turbine efficiency is used to target turbine inlet pressure against measured data, and GTP 2 is when IMEP is targeted against measured.

$$P_{turbine,\max} = \dot{m} c_p T_{stagnation,inlet} \left[1 - \left(\frac{p_{static,outlet}}{p_{stagnation,inlet}} \right)^{\frac{\gamma-1}{\gamma}} \right] \qquad \text{eq. 4.3}$$

In figure 4.14 the simulated turbine mass flow is also included to show when the majority of the power is supplied to the turbine. The mass flow traces did not differ significantly between the two simulations and no measurement data exist.

What about the wastegated cases? Here it is much more difficult to make a direct comparison between measurements and simulations. Since the turbine operates in the boost-controlled regime the turbine efficiency does not noticeably affect the boost pressure, there is always enough power in the total exhaust stream to power the turbine. However, the turbine efficiency can affect other parameters, such as exhaust backpressure and indirectly IMEP. Simulations at 3000 and 5000 rpm with both the same efficiency multiplier as for 1950 rpm as well as multiplier value 1 gave results that differed somewhat from measured values. Since no measured data of the exhaust mass flow exist the actual turbine efficiency on the engine cannot be determined. Therefore, it is difficult to decide which turbine efficiency multiplier to use.

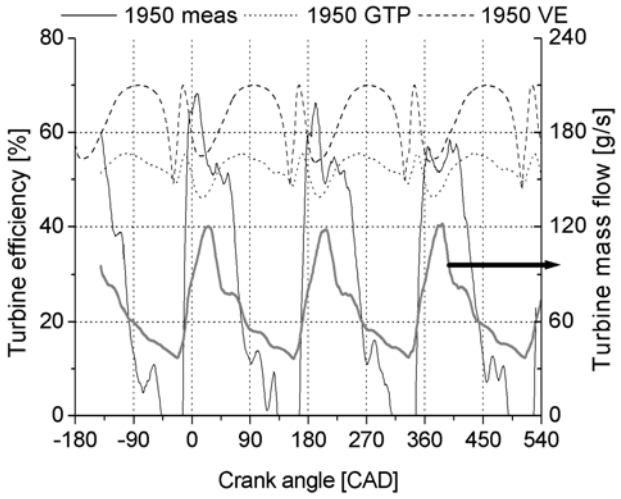

Figure 4.14. Turbine efficiency vs. crank angle for 1950 rpm. The two software's reading of the turbine map seems to be similar, but it is far from measured data. For clarity the simulated mass flow through the turbine is displayed to show when the majority of the power is added to the turbine (thick gray line).

To explore which multiplier to use two simulations were run. In both, the target optimisation function was used to adjust the turbine efficiency multiplier. In the first case the measured average turbine inlet pressure was the target for the optimisation, and in the second case the measured IMEPn.
In figure 4.15 the resultant turbine efficiency multipliers are displayed along with the wastegate exhaust mass flow ratio. The turbine efficiency multiplier calculations were only done in GTP but the VE wastegate mass flow ratio is included for comparison. Thus there exist two GT-Power simulations; GTP 1 where the turbine efficiency multiplier was adjusted so that the turbine average inlet pressure was equal in simulation and measurement, and GTP 2 where the turbine efficiency multiplier was adjusted in order for the measured IMEPn to be met. If the turbine efficiency multiplier is used for IMEP-targeting then the turbine efficiency multiplier shows an unrealistically low value at 3000 rpm. There are no apparent reasons for the turbine to work so well at that particular speed and more normally at adjacent speeds. This indicates that using the turbine efficiency multiplier for targeting IMEP is the more improbable of the two cases. The turbine inlet pressure targeted case shows a more realistic behaviour of the turbine efficiency multiplier.

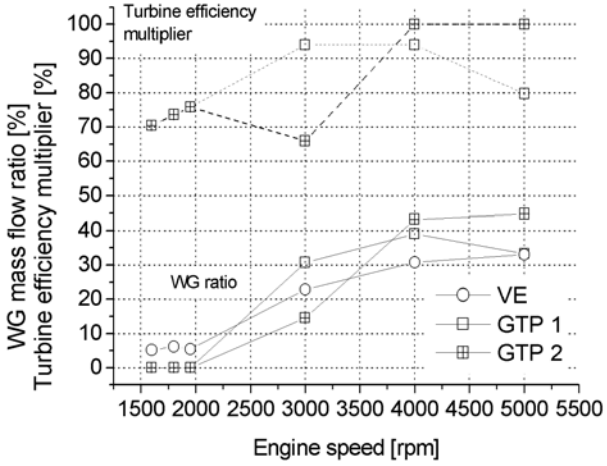

Figure 4.15. Wastegate mass flow ratio for three simulated cases (solid lines) and used turbine efficiency multiplier (dashed line) for two simulated cases. Case GTP 1 is when the turbine efficiency is used to target turbine inlet pressure against measured data, and GTP 2 is when IMEP is targeted against measured.

In figure 4.6 it can be seen that the IMEPn (the values presented are for the turbine inlet pressure-targeted simulation) deviates slightly from that measured at 5000 rpm. However, the difference is only 1 Bar at 19 Bar which equals 5 % which is almost within what can be expected of accuracy limits. It is therefore concluded that it is reasonable to target turbine average inlet pressure with the turbine efficiency multiplier as an adjustment parameter. However, when a measurement technique is available to measure wastegate mass flow rate, or simulation technique is good enough to eliminate use of turbine efficiency multipliers, only then can this assumption be validated.
This assumption is further justified by the turbine inlet pressure, see figure 4.13. The IMEP-targeted case shows very poor agreement with measured turbine inlet pressure. Thus, when the turbine efficiency is targeted for IMEP, the discrepancy between measurement and simulation for turbine inlet pressure is much higher than the reverse.
Both software underpredicted the turbine inlet temperature. The reasons for that can be many apart from weaknesses in the wall heat transfer modelling: wrong input valve lift profile, valve flow modelling at high pressure ratios, slightly wrong cylinder pressure/temperature prediction etc.

Here production data for the camshafts have been used. The cylinder pressure during the blowdown phase have a reasonably good fit, as can be seen in figure 16. A few degrees difference in the blowdown of the pressure can be observed, so the valve lift might be a few degrees off.

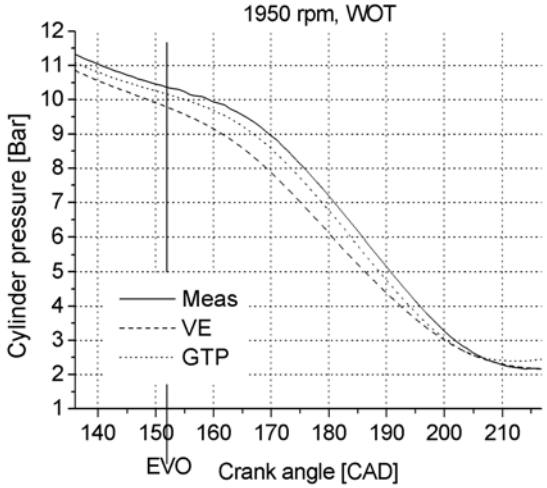

Figure 4.16. The cylinder pressure during the blowdown phase.

The reasons for that can be valve train flex, the chain can stretch, the camshaft can oscillate torsionally and, most important, the hydraulic bucket tappets can be soft. Therefore freedom probably exists for the modeller to shift the valve lift a few degrees and still be within tolerances on the running engine. But then, on the other hand, one needs to be absolutely sure that the cylinder pressure at EVO has a perfect (far less than 1% error) fit to measured and be perfectly sure of an accurately simulated mass flow through the valve in the very unexplored region of high pressure ratios and small lifts. Thus, here we chose not to change anything on the lifts from nominal values. It is also very questionable if a few degrees can make such a large difference to the temperature. Both software have additional software that can calculate dynamic valve lifts from geometric valve train data. However, these dynamic curves have to be imported manually for every single speed. Thus the extra work involved, and the fact that no measured data exists to check the valve train simulations against (which are necessary especially when hydraulic bucket tappets are used [4.6]), were reasons for the choice of not using the possibility of dynamic valve lifts in this work.
To further investigate the turbine inlet temperature, GT-Power's possibility to simulate a thermocouple was used. The thermocouple is simulated as a

spherical bead with both radiative and convective heat transfer [4.7]. The simulated radiative heat transfer was set to zero because a radiation shield was used in the measurements. The simulations showed that the simulated thermocouple temperature was close (i.e. within 1%) to the simulated mass averaged temperature, but even more close to the time-average gas temperature. The latter is in line with the findings of Caton [4.8] who investigated modelling of thermocouples. One of the conclusions was that a thermocouple, modelled as a spherical bead with convective and radiative heat transfer to the surroundings had an equilibrium temperature more close to the time-averaged gas temperature than the mass-averaged. In the simulations Caton had approx. 1-2% difference between simulated thermocouple temperature and time-average gas temperature while the difference between thermocouple temperature and the mass-averaged gas temperature was on the 10% level. This is well in line with the simulations done in this paper. See figure 4.17 where the simulation results for the 5000 rpm case are presented. The difference between time- and mass-average gas temperatures in this work is smaller than those discovered by Caton. This is probably because here the engine is a high-output turbocharged engine with high average pressure in the engine manifold while Caton ran on a low-output naturally aspirated engine where the pressure and temperature is expected to be more intermittent during the cycle.
From figure 4.17 it is clear that the temperature registered by the measured thermocouple is not exactly equal to either simulated time- or mass-average gas temperature or simulated thermocouple temperature. As mentioned above, the exhaust wall temperatures are not solved for in these simulations, instead they are imposed as average values of measurements from three locations. The simulated gas temperatures are therefore dependent on the calibration of the heat transfer model. In the current (GT-Power-) simulations the exhaust manifold heat transfer multiplier was adjusted so that the simulated mass average temperature was equal to measured thermocouple reading individually for 1600, 1800 and 1950 rpm. For speeds above that the multiplier had to be set to 0 both in the manifold and in the port and still the simulation output is lower than the measured thermocouple reading. However, the difference is less than 3% and it is very questionable if the measurement accuracy of this kind of measurements on a real engine under full load operation is better than that. The measurement task is difficult with heat transfer via radiation to the wall, via the thermocouple stem and heavily pulsating flow.

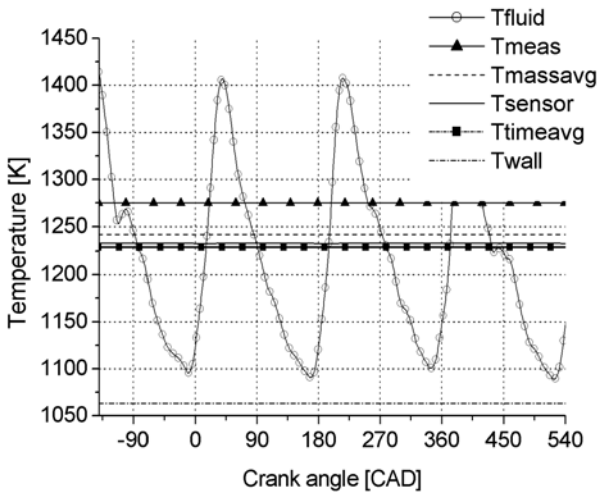

Figure 4.17. The results from the thermocouple simulation. Tfluid is the simulated exhaust gas temperature, Tmeas is the measured gas temperature, Tmassavg the mass average exhaust gas temperature, T sensor the simulated thermocouple temperature and Twall is the imposed wall temperature in the simulation.

4.4 Discussion

It is quite clear that both software require calibration to give results close to measured. Thus there are limits in the predictivity of the simulations. The only part of the models presented here requiring heavy calibration work is the turbine efficiency. When the model is run with a fixed turbocharger speed, equal to measured, all pressures and massflows are close to measured. This indicates that the single most uncertain output from the simulations is the power of the turbine. Mass flow capability, back pressures etc. are modelled with reasonable accuracy without heavy calibration work. Therefore it is, for calibration reasons, unnecessary to simulate and run the engine without a turbocharger. Running with fixed, correct, speed is accurate enough. Thus, predictive simulations can be done for all parts not directly affecting the turbocharger speed. This implies that as long as a (calibrated) turbine is not changed, parameter studies of all other parts could be done with reasonable accuracy.

However, since the turbocharger speed is such a governing property of an engine, the use of running the simulation without knowing in what region the turbocharger speed should be, is limited. Therefore comparative simulation

results with a non-calibrated model is not included here, the results are too far from measured.

4.5 Conclusions

Measured engine data can be predicted very well with 1D software, but certain areas require more manual adjustments than others. Areas that are easy to predict are the flow in pipes, which is a typical 1D phenomenon, and the compressor, which is very well represented by the measured performance map. This chapter mainly deals with use of the turbocharger model. On the turbine side the model needs work on the turbine efficiency modelling to give results close to measured. If these adjustments are acceptable the model can be used for sensitivity studies and redesign predictions, but not for final turbine or manifold selection purposes.
As can be seen in the results presented above, the calculation performance for is quite similar in the two software. The handiwork with the two software is quite equal with similar user interfaces, however they have different strong and weak points. The strong points found with GT-Power are:

- High versatility. The program has very few constraints in terms of engine layouts and design possibilities.
- Input data can be made dependent on most kinds of engine parameters. Thus the program provides the modeller with a great deal of freedom.
- Measured data can be input into he post-processor for easy comparison with simulation results.
- It has PI-controllers that can be utilized to efficiently adjust the model.
- Transient simulations can be performed.

The corresponding points for Virtual Engines are:

- The post-processor has the possibility to animate spatial plots of pressure in an entire pipe system, which is very convenient for the understanding of various resonance phenomena. (This feature was added to later versions of GT-Power)
- The models and resultant data are stored in a database, which makes it very easy to handle a large amount of models and result data.
- When building up the model most input data have some choices of predefined input data, but other values can be input manually if necessary.

4.6 References

4.1 www.gtisoft.com
4.2 www.optimum-power.com
4.3 Japikse D, Baines N C "Introduction to turbomachinery" Concepts ETI & Oxford University Press 1997. ISBN 0-933283-10-5
4.4 Heywood John B "Internal Combustion Engine Fundamentals" McGraw-Hill New York ISBN 0-07-100499-8
4.5 Westin F, Ångström H-E "A method of investigating the on-engine turbine efficiency combining experiments and modeling" ImechE C602/029/2002
4.6 Krieger et al. "Der virtuelle Auslegungsprozess des Grundmotors bei BMW" MTZ no. 12 2000.
4.7 GT-Power v. 5.2 User's manual p. 17
4.8 Caton J.A. "Comparison of Thermocouple, Time-Averaged and Mass-averaged Exhaust Gas Temperatures for a Spark-Ignited Engine" SAE Paper no. 820050

Chapter 5

Engine measurement methods

5.1 Introduction

No simulation can be proved to be more accurate than the measurement data to which it is compared, and comparing against measurement data is unfortunately absolutely necessary in order to check if the simulation results are reasonable. It is therefore of uttermost importance that the modeller has a good understanding of the measurement data and how the data was acquired.
In this chapter the measurement methods used in this work are described.

5.2 Measurement system

The test cell measurement and control system used for this work is Professor Ångström's Cell4 system. For measurements it has different inputs: slow analogue input, fast analogue input and digital input.
The slow analogue input consists of Nudam [5.1] modules reading signals such as thermocouple output, analogue voltages and the dynamometer's load cell output. This system has 1Hz sampling frequency with the exception of the load cell that has a priority and subsequently 10Hz sampling rate.
The fast analogue system consists of a PowerDAQ [5.2] card with a maximum sample rate of 1 MHz divided over maximum 8 channels. The utilized sampling frequency is one sample for every measurement channel at every 0.2 CAD. This system is used for CAD resolved pressure measurements.

The digital input uses PIC-computers for counting pulses and is used for the engine speed (1800 pulses/rev) and turbo speed (1 pulse/rev) measurements.

5.3 Air mass flow

5.3.1 Comparison of methods to determine the inlet air mass flow

The air mass flow was measured in three different ways; direct measurements with two different sensors and calculation from measurements of lambda and fuel mass flow.

The direct measurements were conducted with both the engine management system's hot film air mass meter and an Annubar [5.3] differential pressure probe. The differential pressure over the Annubar was measured with a Setra [5.4] 2500 Pa linear differential pressure transducer. The indirect measurements were made with an AVL Fuel Scale [5.5] and an ETAS [5.6] LA3 broadband lambda sensor. No calibration of this equipment could be done why the only way to investigate the accuracy of the measurement was to compare the different methods against each other. In figure 5.1 the value obtained for every sensor is displayed as a function of engine torque (at 1950 rpm). To increase the confidence, data from two different measurement series is included, one for a mechanically closed wastegate and another with standard wastegate actuation. However, there should be no difference between these two data sets because the speed and load is such that the wastegate is always closed anyway.

As figure 5.1 shows, for mass flows below 0.03 kg/s the Annubar values is much lower than the values measured by the hot film sensor and the value calculated from lambda. But for flows higher than that, no inconsistency in the measured values exists between the measurement principles. However the scatter, especially at the 250 Nm points, indicate that the measurement repeatability is not the very best. This in-repeatability comes from both uncertainty in the measurement probe but also from the fact that the data originate from two test runs, with closed WG and standard WG. For the 250 Nm point the scatter amplitude is about 10% of the measurement signal. Thus it is concluded that the air mass could not be measured with better accuracy than 10%.

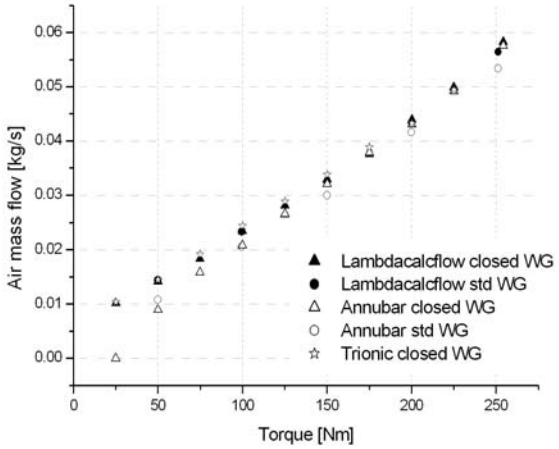

Figure 5.1. Air mass measured in three ways: Lambdacalcflow is the value calculated from lambda and fuel flow and Annubar is the direct measurement. Closed WG means that the WG was shut mechanically. Trionic is the mass flow measured by the engine's standard measurement system Trionic and it's mass flow meter of hot film type.

5.4 Unsteady pressure

For measurements of intake and exhaust pressures two different transducers were used, strain gauge transducers with a steel diaphragm and piezo-resistive transducers. On the intake side only the strain gauge transducers were used.
As regards to the turbine calculations the exhaust pressures are by far the most important. Here data from measurements with piezo-resistive Kistler transducers is used. Plotting the ensemble-averaged signal (averaged over 100 cycles) together with the instantaneous signal shows that the peak cycle-to-cycle variations are small, but the cylinder-to-cylinder variations are bigger. Figure 5.2 shows that an arbitrary chosen curve for an instantaneous cycle show great similarity to the ensemble averaged value, thus the average value seem to be very representative for the process, as long as one keep track of which pulse origins from which cylinder. The exhaust valve of cylinder 1 opens at 146 CAD ATDC so the pulses origin from cylinders 4-2-1-3 when counted left to right. The bumps at the down-slope of the pulses from cylinders 1 and 4 are difficult to explain, but they probably origin from some unsteadiness in the exhaust manifold. The runners from cylinders 1 and 4 are the longest and the ones containing most sharp bends.

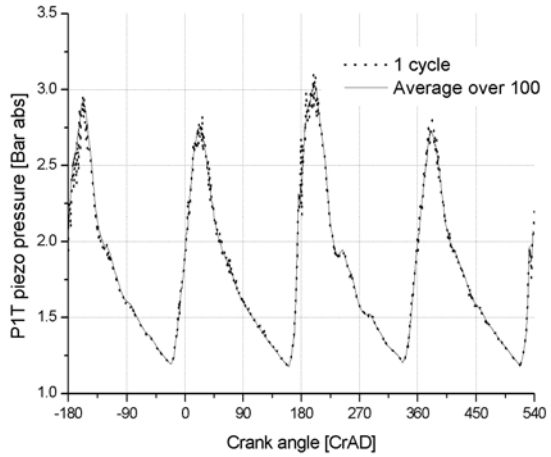

Figure 5.2.Turbine inlet pressure, P1T, measured with a piezo-resistive transducer. Comparison between the ensemble-average (over 100 cycles) and an instantaneous cycle shows very little difference. However, the difference between cylinders in peak pressure and pulse shape is not negligible.

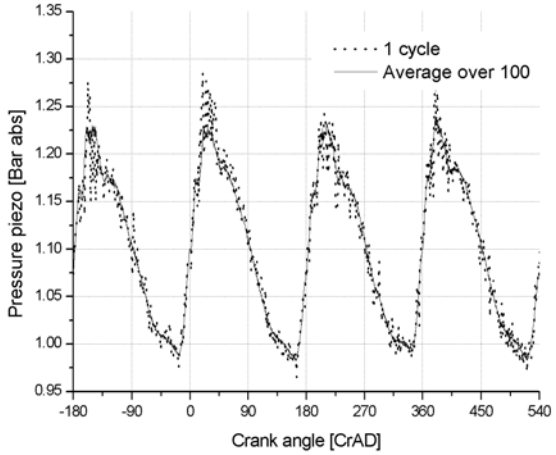

Figure 5.3. Turbine outlet pressure measured with a piezo-resistive transducer. Comparison between the average over 100 cycles and an instantaneous cycle shows very little difference, both in terms on cycles and cylinders.

Figure 5.2 also shows that the peak from cylinder 1 is slightly higher than the rest. The reason for this is that it was not possible to mount the transducer perpendicular to the exhaust flow from that cylinder, therefore the transducer is picking up some dynamic pressure from the cylinder 1 exhaust stream as well.
For turbine outlet, P2T, as well as for compressor inlet and compressor outlet pressure, P1K and P2K respectively, the average value is representative for the process, as figures 5.3 and 5.4 shows.

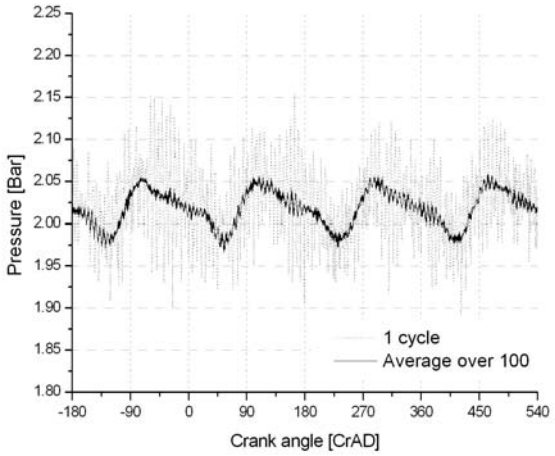

Figure 5.4. Comparison between ensemble-average and a single instantaneous cycle value for compressor outlet pressure P2K.

Another check of the data quality is to see whether the time average value of the cycle averaged pressures gives the same value as the time averaged value measured directly with the slower logging system.
Fast and slow sampling was not absolutely simultaneous, but for one test point they were only 9 seconds apart (first fast sample and then slow) and the engine was running steadily at 1950 rpm WOT.
For the time-average value of the static pressure at the turbine inlet (manifold-volute flange) three values were achieved:

- P1Tslog which is the measured time average with the slow measurement system (instantaneous signal from transducer buffered/averaged with buffer at an unknown rate and read every second by the sampling system, this signal is then averaged over 10 s.)
- P1Tsg which is the ensemble average of the signal from the strain-gauge transducer over 100 cycles of the fast measurement system. The

sample rate is 5 samples/CAD. The signal is then time averaged over the entire cycle giving a value of the time average over 100 cycles.

- P1Tpiezo is similar to P1Tsg but with the piezo-resistive transducer.

The result of these measurements can be viewed in table 5.1. The reasons for the discrepancy between the three different values could be several.

Table 5.1. Comparison of time average turbine inlet pressure acquired in three different ways.

Speed	P1Tslog	P1Tsg ensemble-time averaged	P1Tpiezo ensemble-time averaged	Average
1600	1.2	1.18	1.36	1.25
1800	1.451	1.56	1.62	1.54
1950 11:09:17	1.75	1.9	1.81	1.82
1950 11:15:57	1.92	1.9	1.81	1.88

The difference between the two transducer types but same sampling system can be a consequence of the strain-gauge transducer's recess introducing unsteady phenomena in the recess-pipe which can disturb the measurement signal [5.7]. The piezo-resistive transducer doesn't have this problem because it is almost flush-mounted (recess length approx. 10 mm). Figures 5.5 and 5.6 show comparisons between the two transducer-types at the turbine inlet for a single cycle and for ensemble-average values respectively. The instantaneous signal from the recessed transducer can be off by some 5-10% compared to the flush-mounted piezo-resistive transducer. However, it is not obvious that this holds for other speeds, since unsteady phenomena may arise due to resonance between the pulse frequency and the resonance frequency in the recess pipe. With a measurement signal with significantly lower pulse amplitude, at the turbine outlet for instance, the difference between the two transducer types is much lower, only a few %.

A test was also carried out where a piezo-electric transducer was added to the comparison. No significant differences between the two piezo-types were encountered aside from the slightly larger noise level for the piezo-electric sensor. The piezo-resistive type was chosen for cost reasons, and for user-friendliness due to it's fixed zero level [5.8].

The difference between the two values from the same strain gauge transducer but for different sampling system is more difficult to describe. One reason can be that the measurements are taken with 9 seconds interval between them and that the engine was unstable enough to allow such fluctuations of the signal, this is indicated by the difference between the two slow logs that were made with almost 7 minutes in between, but in this case the speed and load of the

engine was altered in between. Another reason could be that the sampling rate of the measurement buffers in the slow sampling system is unknown. If the sampling rate is too slow and the signal fluctuates heavily, which is the case for turbine inlet pressure, the signal can become skewed. The fact that the two slog-points at 1950 rpm differs so much might justify this. One way of investigating this is to do the same comparison for another signal that is not fluctuating so much. One such signal is compressor outlet pressure, P2K. Table 5.2 shows data from the fast and slow measurement systems for the same strain –gauge transducer. This table shows no big differences between the measurement systems.

Table 5.2. Comparison between two ways of acquiring the average compressor outlet pressure P2K.

Speed [rpm]	P2Kslog [Bar]	P2Ksg [Bar] ensemble_time	Average [Bar]
1600	1.52	1.52	1.52
1800	1.74	1.72	1.73
1950 11:09:17	1.96	2.01	1.99
1950 11:15:57	2.03	2.01	2.02

5.4.1 Unsteady pressure summary

For signals with large fluctuation amplitudes the recessed strain-gauge transducer does not give the same result as the flush mounted piezo-resistive transducer. Instantaneous differences as large as 10% have been observed. However, it seems like it is only the P1T location that shows large enough fluctuations to necessitate the use of flush mounted piezo-transducers.
If using a time average value one should be careful if the measured signal shows large fluctuations. For P1T for instance, it is not very good to use the time average from the slow measurement system, it is better to time average the ensemble average signal from the fast measurement system.

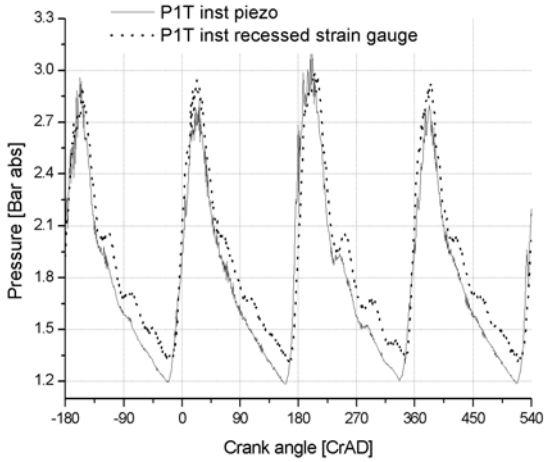

Figure 5.5. Comparison between the two transducer types at turbine inlet, P1T. Values for a single cycle.

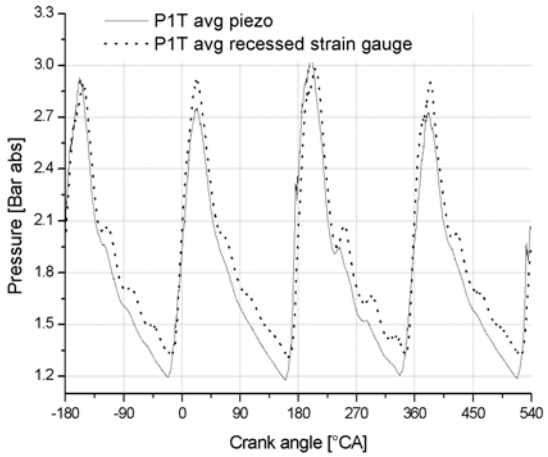

Figure 5.6. Comparison between the two transducer-types at turbine inlet, P1T. Ensemble-average over 100 cycles.

5.5 Turbo speed

The rotational speed of the turbocharger rotor is measured with a commercial system from Micro-Epsilon [5.9]. The transducer is an eddy-current unit fitted in the compressor housing flush with the wall sensing the passage of the blades. The signal is processed in a control unit and the user has different choices of output; voltage or pulses. In the case of pulse output it can be chosen how many pulses per revolution that should be put out. For this work it was decided that one pulse per revolution was enough. This pulse-signal was input to one of the Cell4 digital input channels. For 130000 rpm turbo speed and 1950 rpm engine speed this gives a pulse rate of 5.4 °CA per pulse. The instantaneous speed is then interpolated linearly to give a value for the speed for every crank angle. Figure 5.7 shows a comparison between the ensemble average value over 100 cycles and the instantaneous value for one cycle.

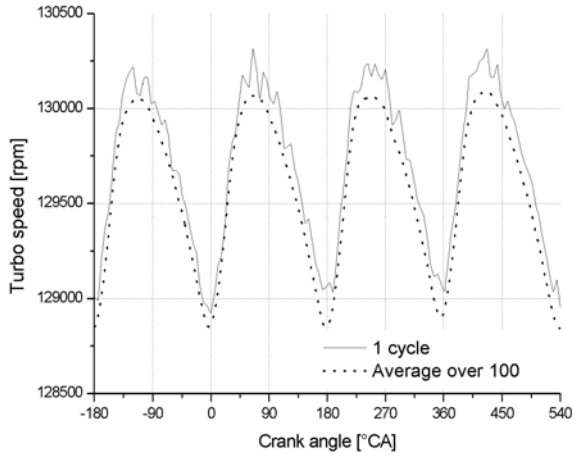

Figure 5.7. Comparison between ensemble-averaged turbospeed and data from a single cycle. The shape of the average signal resembles the instantaneous very well but is shifted slightly downwards. The reason for that is that the average turbospeed fluctuated approximately 200 rpm later on in the measurement. However, 200 rpm fluctuation at 130000 rpm is an error of only 0.15% and thus negligible.

5.6 Turbo rotor moment of inertia

5.6.1 Introduction and scope

When calculating dynamic properties for an engine/turbocharger system, and in particular the boost pressure response during engine transients, the turbo rotor polar moment of inertia - PMOI - is a very important parameter. Values for this

property are supplied by the turbocharger manufacturer, but previously they neglected to present an accuracy of the value provided. The uncertainty of whether the value provided was accurate or not encouraged a simulation test with the PMOI-value different from the one provided, which gave surprisingly good results in terms of transient response. However, since the measurements showed that the initial PMOI information was correct and the simulated altered PMOI was wrong, these results are not included here. Garrett has now presented a publication showing a device for measurement of the PMOI as well as calculations of it from CAD data [5.10]. However, the importance of this value creates a need for acquiring a method to measure this value, to ascertain that the value used in the engine simulations is correct.

5.6.2 Theory

Earlier work at the Department of Internal Combustion Engines at KTH by Agrell et. al.[5.11] has shown that a torsion rod can be used for measuring the moment of inertia of truck-sized turbochargers. Agrell et. al. used strain-gauge displacement sensors bonded onto the torsion rod and the signal from the strain gauge was recorded digitally. However, for the PMOIs as small as for a car-sized turbo a torsion rod would be too thin to be usable. Therefore the trifilar method was chosen.

With the trifilar method the moment of inertia of a rotor can be calculated from measurements of the period time of motion for a rotor hung from three long piano wires. Constraints in the usage of this method are that the rotor must have its center of gravity at the axis of rotation (rotational oscillation) and the piano wires must have a very small mass. Furthermore it is assumed that no friction is present and that the period time is constant throughout the measurement, i.e. that the period time is independent of the oscillation amplitude. The expression for the moment of inertia is (for a detailed derivation see appendix A):

$$J = \left(\frac{T}{2\pi}\right)^2 \frac{mgr^2}{l} \qquad \text{eq. 5.1}$$

Where:

T..... period time for one oscillation
m..... mass of the rotor assembly
r..... distance from rotational axis to thread's attachment to the rotor
l ..... thread length

5.6.3 Experimental setup

The equipment needed for these measurements is very low tech. Aside from very thin piano wires and parts made from machined steel and aluminium the only equipment needed is a chronograph.

The turbo rotor was attached to a turn disc by the M5 left-thread at the compressor end. On the turn disc three 0.5 mm holes were drilled (at the radius 28.5 mm) for attachment of the long piano wires. The upper end of each wire was hung from a screw in order to be able to fine-tune the length of the wires as well as the horizontal alignment of the turn disc. A guidance disc guided the wires through three similar holes at the same radius as on the turn disc, to ensure that the wires were parallel. The setup can be viewed in figure 5.8.

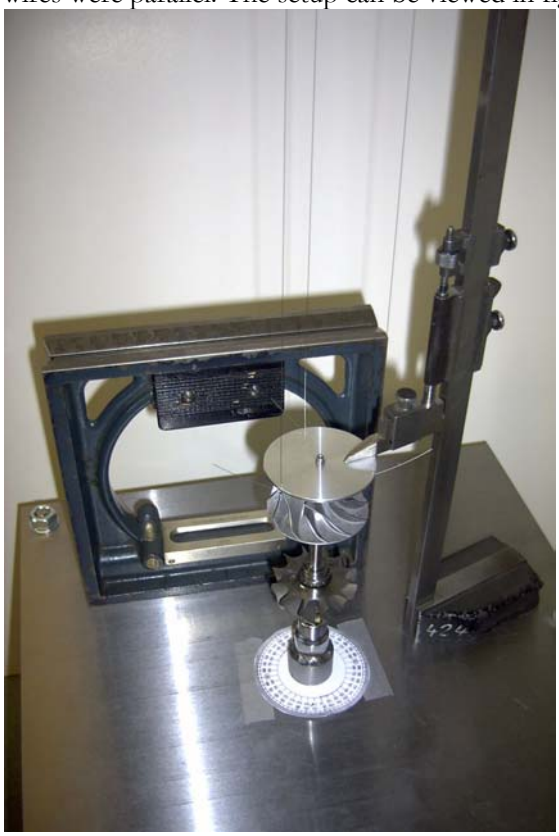

Figure 5.8. The turbo rotor hanging from the three wires via the turn disc. The excitation socket can be seen below. The bubble scale ensured that the base plate was horizontal and measurement of the distance between the base plate and the turn disc enabled adjustment so that the rotor hung vertically.

Below the rotor an excitation device was designed to be able to excite a clean rotating-oscillating motion without precession. It consisted of an ordinary 12 mm wrench socket welded onto a weight and in the end of the weight a steel rod was attached. The steel rod runs through two thoroughly aligned guidance-holes in two base-plates positioned below the rotor, approx. 100 mm apart. The plates were thoroughly aligned horizontally with a high-precision bubble scale, and the two holes were aligned with a weight. To check that the rotor hung vertically the distance between the upper base plate and the turn disc was measured.
The polar moment of inertia for the turn disc was calculated from measured geometry and measured density. The density for this batch of aluminium was 2843 kg/m^3. This proved the necessity of measuring the density for every batch of aluminium, since the tabulated value from the supplier was 2700 kg/m^3.
The period time measurements were conducted manually with a chronograph. The motion was excited and the time measurement was started at one end-point after 3-5 cycles. The time for 100 cycles was measured with half-time measurement at 50 cycles. This measurement was repeated 5 times and the average value of these five measurements was used.
The masses for the various parts were measured with a Sartorius BP4100S scale.

Table 5.3. Data for the parts of the rotor assembly.

Part	PMOI [kgm^2]	Mass [kg]
Turn disc*	7.186730E-06	0.01653
Calibration rotor	2.445252E-05	0.20390
Screw	3.238887E-09	0.00129
Wires (all 3 together)	1.715636E-07	0.00021
* PMOI for wire holes removed		

Except from the measurement objects the setup consists of four parts. Data for these are shown in Table 5.3. PMOI data for these parts are all calculated from geometrical data and formulas for standard geometries.

5.6.4 Calibration

The procedure of acquiring the PMOI data for a rotor to be measured is to attach it to the turn disc and measure the period time of oscillation as described above. From the period time and the total mass of the rotor assembly a total PMOI for the rotor assembly can be calculated with eq. 5.1. To acquire the PMOI for the measurement object the PMOIs for the measurement equipment

has to be subtracted. PMOI values for the measurement equipment are presented in table 5.3.
To test the accuracy of the measurement setup a calibration rotor was manufactured. It had mass and moment of inertia close to the values anticipated for the turbo rotor to be measured. The geometry of the calibration rotor was made as simple as possible in order to enable accurate calculation of the PMOI. Only simple formulas for PMOI of cylinders and cones (bottom of drilled holes) were necessary. For the threaded hole the average diameter was used (4.48 mm for M5). The density for the aluminium used in the calibration rotor was determined by manufacturing a short cylindrical rod from the same piece of aluminium. The density was 2810 kg/m^3 as compared to the standard table value for aluminium, which is 2700 kg/m^3. Note that the calibration rotor was manufactured from a different piece of aluminium than the rest of the rotor assembly. Therefore the density varied.
By applying eq. 5.1 to the measured period time a value for the moment of inertia was achieved that was 8.5% lower than the value calculated from geometry. The reasons for this are discussed in the Discussion of errors below.
By inserting a calibration constant in eq. 5.1 a one-point calibration of the setup can be made from the measurements of the calibration rotor.

$$k = \frac{J_{geometrical}}{J_{measured}} \qquad \text{eq. 5.2}$$

$$J = k \cdot \left(\frac{T}{2\pi} \right)^2 \frac{mgr^2}{l} \qquad \text{eq. 5.3}$$

By applying eq. 5.2 and 5.3 to the results in table 5.4 gives a value for k=1.0934.

5.6.5 Results

The PMOI was measured for four turbo rotors of two kinds, Mitsubishi TD04HL-15T and Garrett GT17. Two units of the same kind were measured to see if there was a large spread between individuals. Every measurement of the period time was repeated five times and the average value of the five measurements was used. The standard deviation achieved with the crude manual time measuring method was surprisingly good. However, the standard deviation grew with the number of measurements conducted in a row. The reason for that was a feeling of dizziness when counting up to 1000 periods in a sequence…

The results of the measurements are shown in Table 5.5 along with the value given by the manufacturer of the turbochargers.

Table 5.4. Measurement results for calibration. T100 is the time for all 100 cycles and T50 is the time after 50 cycles.

Measurement	T50 [s]	T100 [s]
1	57.46	114.66
2	57.43	114.81
3	57.45	114.68
4	57.36	114.56
5	57.49	114.63
Average	57.438	114.668
Std dev[3]	0.04	0.08
Period time	1.14876	1.14668

Table 5.5. Results from measurement of the PMOI. The value provided by Mitsubishi was for the kind of turbocharger, no information was provided for the specific individuals investigated.

Rotor	T [s]	Stddev T	Mass [kg]	J [kgm2]	J_{manuf} [kgm2]
M1	1.2133	0.00139	0.18845	2.58E-05	2.55E-05
M2	1.2100	0.00062	0.18756	2.55E-05	2.55E-05
G1	1.0919	0.00033	0.13777	1.26E-05	
G2	1.0938	0.00050	0.13910	1.29E-05	

5.6.6 Discussion of errors

As could be seen above, without calibration the measurement of the calibration rotor was 8.5% off from the geometrically calculated value. A single reason for this discrepancy is difficult to come up with, however several sources for error are present. Here follows an attempt to quantify them.

Friction

The derivation of eq. 5.1 involves the assumption of negligible friction, which leads to the result that the period time should be constant and not dependent on oscillation amplitude. Since there is always friction present no oscillation can go on forever, however in this case the friction is small since the amplitude of oscillation only decreased from approx. 20° to 5° (half amplitude) in 100

[3] Standard deviation for the time of 50 and 100 oscillations respectively

oscillations. The equation of motion with a speed dependent friction term f is showed in eq. 5.4.

$$\ddot{\varphi} + \frac{f}{J}\dot{\varphi} + \frac{mgr^2}{Jl}\varphi = 0 \qquad \text{eq. 5.4}$$

The solution for this ODE is [5.12]:

$$\varphi(t) = A_1 e^{-(\gamma - q)t} + A_2 e^{-(\gamma + q)t}$$

$$\gamma = \frac{f}{2J} \qquad \text{eq. 5.5}$$

$$q = \sqrt{\frac{f^2}{4J^2} - \frac{mgr^2}{Jl}}$$

where the system is under-damped if q is imaginary. Under-damping clearly is the case having seen the slow damping characteristics of the rotor. Thus:

$$f < \sqrt{\frac{4Jmgr^2}{l}} = 0.00035$$

If this is true, then the frequency of the oscillation is:

$$\omega_d = \sqrt{\frac{mgr^2}{Jl} - \frac{f^2}{4J^2}} = \sqrt{\omega_0^2 - \gamma^2} \qquad \text{eq. 5.6}$$

The solution of eq. 5.5 can be expressed as:

$$\varphi(t) = Ae^{-\gamma T}\cos(\omega_d t + \theta_0) \qquad \text{eq. 5.7}$$

Eq. 5.7 indicates that the max amplitude of two consecutive oscillations differs with a factor $e^{-\gamma T}$ where T is the period time of oscillation. This can be used to estimate γ. In the measurements it could be observed that the max amplitude went from 20° to 5° (approximately) in 100 oscillations. Using eq. 5.7 and this information gives:

$$\frac{\varphi(0)}{\varphi(100T)} = \frac{20}{5} = \frac{e^{-\gamma * 0}\cos(\omega_d t + \theta_0)}{e^{-\gamma * 100T}\cos(\omega_d t + \theta_0)}$$

and thus:

$$\gamma = \frac{-\ln\left(5/20\right)}{100T} = \{T = 1.15\} = 0.012 \qquad \text{eq. 5.8}$$

With $\omega_0 \approx 5$ and T=1.15 it is clear that $\gamma << \omega_0$ and thus $\omega_d \approx \omega_0$. Therefore friction really is negligible.

Small-angle approximation

In order to be able to solve the equation of motion a small-angle approximation was necessary. The target was set not to have any single source of error larger than 1%, but for the small angle approximation 2% error had to be tolerated in order to achieve a reasonable amplitude of oscillation. As can be seen in the derivation of the equation of motion the small angle approximation has an error of max 2% if the max amplitude is less than 19°. Therefore the oscillation was never allowed larger than this value, i.e. the oscillation was excited to this value.

Additional errors

However, in the measurements an increase in period time could be seen as the oscillation was damped. The period time was measured for 100 oscillations and the time for 50 oscillations was also recorded. The period time for the average of the first 50 oscillations was approximately 0.1-0.2% shorter than for the average of all 100 oscillations. This was present in the measurement of all 5 rotors. This shows that the assumption of constant period time is not perfect. The reasons for the non-constant period time can be several, and it is difficult to pinpoint one single reason for it. For instance, it could be friction with other dependencies than just linear with velocity.

Even though a dedicated mechanism was built to excite the motion it was difficult to achieve a perfect rotational oscillation, a certain amount of precession was always present. No effort to take this into consideration in the calculations was made but it was always assumed to be negligible. However, test measurements with exaggerated precession did not result in a period time very much different than for almost no precession.

Another source of error is the attachment of the piano wires to the turn disc. The wires were of 0.15 mm diameter but the holes were 0.5 mm in diameter (for machining reasons). This allows for a certain play, which caused an uncertainty in the radius of attachment of approx. 1.3% as well as slop at the ends points of the oscillation. The error from the slop is very difficult to estimate. All other geometrical units were kept well within 1% error.

One more unknown source of error is how large portion of the piano wires that should be considered as taking part in the oscillations. Using 25% of the wire lengths, as done in these calculations (see table 5.3) results in that the wires make up less than 0.5% of the entire rotor PMOI and less than 0.1% of the mass. Therefore the error from a possible faulty assumption of how large portion of the wires that should be taken into consideration is negligible.

5.7 Exhaust temperature

5.7.1 Gas temperature measurements

Measuring temperatures inside an exhaust pipe introduces some problems if high accuracy is demanded. Standard procedure is to use a thermocouple of some suitable kind; in the KTH engine laboratory the K type is commonly used. The output from the thermocouple is normally assumed to be the time-averaged temperature of the gas. Unfortunately that is not the absolute truth. The sensing tip of the thermocouple is heated by the gas but cooled by the wall through the stem of the probe and through exchange of radiation energy. To avoid this cooling the insertion length of the probe has to be long enough, some say 20 diameters [5.13] and others say 100 diameters [5.14]. If the wall is colder than the gas the probe can also be cooled by radiation. To decrease the influence from radiative cooling the probe can be equipped with a radiation shield. If one radiation shield is used, the shield has a temperature somewhere in between the thermocouple probe temperature and the wall temperature and therefore reduces the exchange of heat via radiation. In theory an infinite number of radiation shields are necessary to completely remove the radiation exchange of heat. However, in this test one shield is considered necessary.

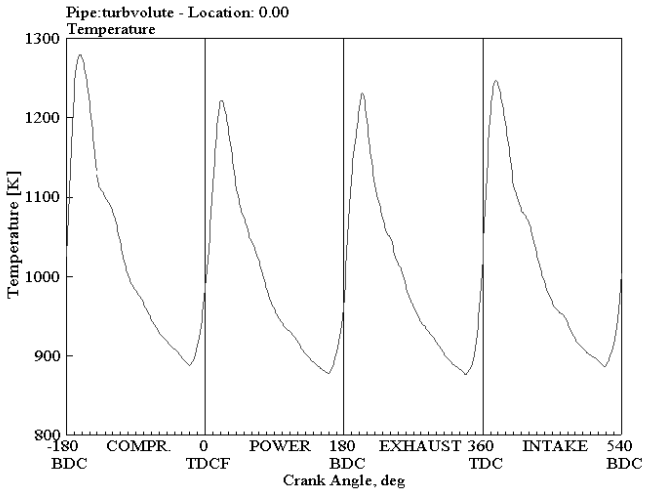

Figure 5.9. Simulation of the temperature at the turbine inlet showing heavy fluctuations. The simulated (energy-) averaged temperature was 1050K. 2000 rpm, full load.

Another issue of more hard-determinable kind is the one of which temperature a thermocouple measures when used in an exhaust manifold. The common assumption is that the probe measures a time average of the temperature.

However, the temperature in the exhaust gas flow pulsates heavily, as well as the density and the flow velocity, which is shown by simulations in figure 5.9 and 5.10 respectively. Therefore, the calculations of what kind of temperature a thermocouple probe measures demand serious heat transfer treatment; an attempt to do this is done with GT-Power below.

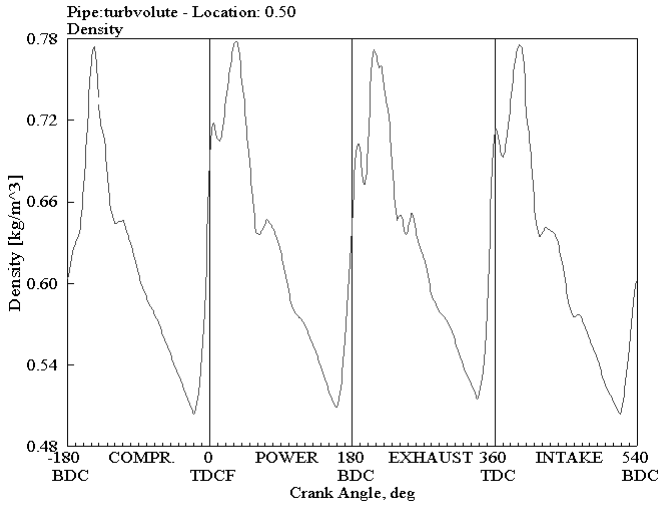

Figure 5.10. Simulated density showed for the same condition and location as figure 5.9.

In order to estimate errors in the exhaust gas temperature measurements, the same temperature was measured with three different probes mounted at the same location simultaneously. The temperature measured was turbine inlet temperature, T1T. The three different probes were (see figure 5.11):

- T1T 3mm. The standard procedure in the KTH SI-engine test cell. A 3 mm diameter probe inserted radially into the manifold pipe in the manifold-turbocharger flange. The length of insertion is thus about half the exhaust pipe diameter, which is approx. 20 mm resulting in an insertion of approx. 7 probe diameters. No radiation shield.
- T1T 6 mm. A 6 mm diameter thermocouple inserted radially into the turbine inlet pipe right below the turbocharger-manifold flange. The length of insertion is half the exhaust pipe diameter, approx. 20 mm resulting in an insertion length of approx. 3 probe diameters. No radiation shield.
- T1Tlong 3 mm. A 3 mm thermocouple inserted in the direction of flow in a 90° bend of the exhaust manifold. The tip was situated at the same location as the other two, i.e. at the manifold-turbocharger flange.

To decrease the exchange of heat between the tip and the wall due to radiation an extra flange was inserted which held a radiation shield, a 10 mm diameter thin-wall stainless steel pipe. The free insertion length was approx. 100 mm, which is approx. equal to 33 probe diameters. In figure 5.12 the arrow points at the tip located concentrically in the radiation shield.

Thus, three different probes were positioned at the same location in order to measure the same temperature.

A test run with continuous recording of temperatures were run, see figure 5.13 for temperature results and 5.14 for speed and load. For every 5 seconds the time average over that period was recorded. During this run the wastegate was closed mechanically why speeds above 2000 rpm could not be run at WOT.

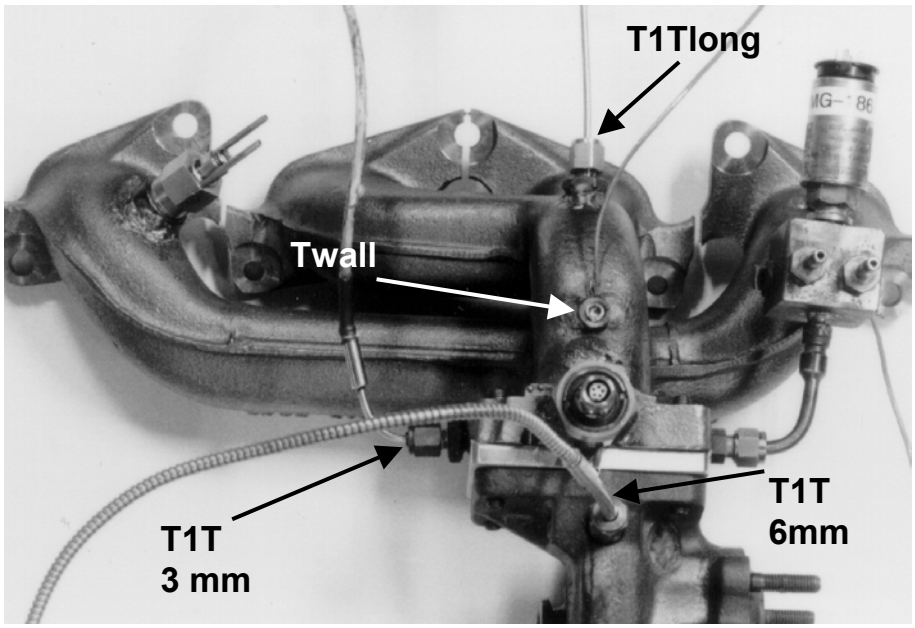

Figure 5.11. The manifold, the heat radiation-shield flange and the turbine housing along with its instrumentation. T1Tlong protrudes from it's mounting point at the arrow to the center of the radiation shield flange between the manifold and the turbine flanges.

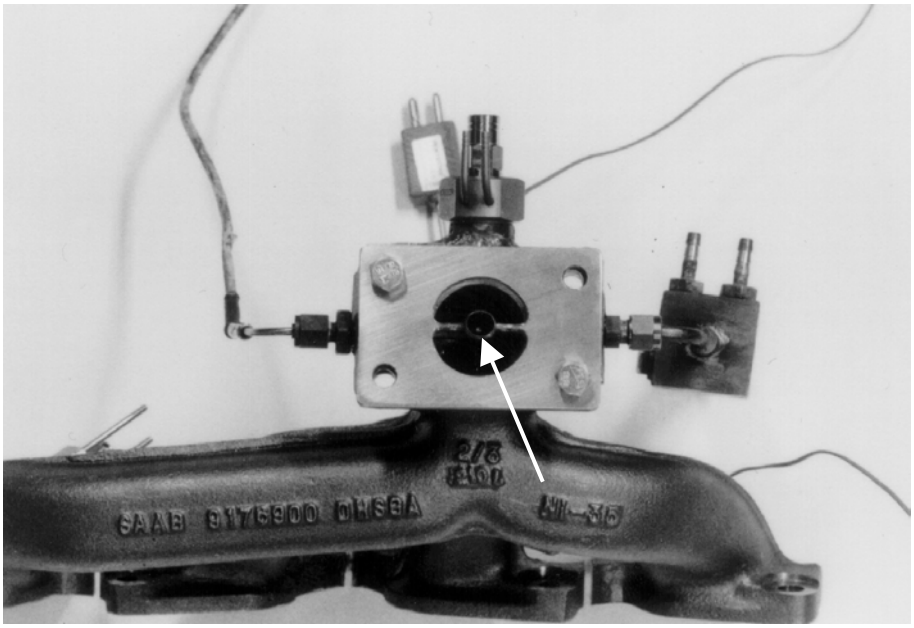

Figure 5.12. The radiation shield flange seen from the turbine side. The T1Tlong thermocouple tip can be seen at the centre of the radiation shield pipe.

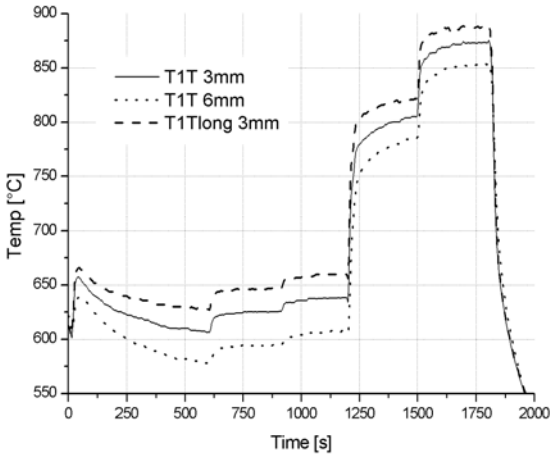

Figure 5.13. The temperature measured with the three different thermocouples.

From figure 5.13 two interesting conclusion can be drawn: first, in order to measure a steady state temperature the engine has to be run at least 3 minutes, more if the load steps are large. Second, the differences in measured temperatures between the three probe types are considerable. At the 1800 rpm 255 Nm load point (at time 1750 s in figure 5.13) the 6 mm probe showed 853°C while the 3mm short insertion length showed 873°C and the long insertion length 888°C. This is a difference of 3% in absolute temperature between the highest and lowest vales. It can be seen in figure 5.17 that the wall temperature at the T1T/Texman2 probe location was 673°C.

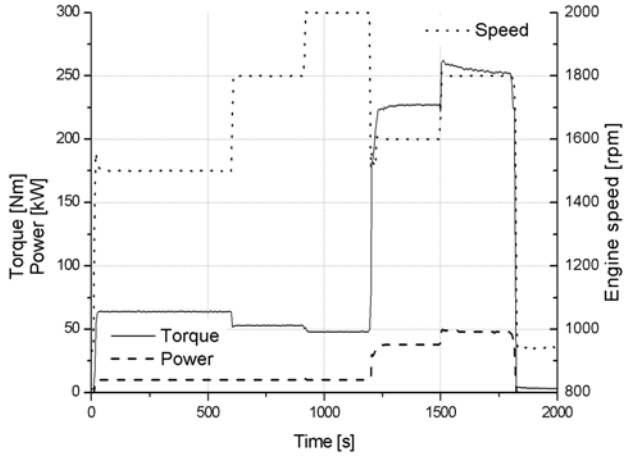

Figure 5.14. The load points run during the temperature convergence test.

Thus, using a long insertion length and a radiation shield results in a higher sensed temperature from the thermocouple. In order to see if 3mm was thin enough a 1.5 mm probe was mounted instead of the 3 mm long insertion thermocouple. This resulted in an insertion length of 67 diameters. Unfortunately there was not test time enough to run exactly the same test cycle all over again. Instead, another test series, now without blades on the turbine and compressor, was run with the 1.5 mm thermocouple. No continuous recording was made; instead one point was measured as a time-averaged value over 10 seconds for every load condition. Every load condition was run for 3 minutes before measurements were taken in order for steady state to be reached. Unfortunately the 1.5 mm thermocouple could not stand the environment very long, it broke after 10-15 min of testing. The result from that measurement is presented in figure 5.15, every data point is marked with a data marker.

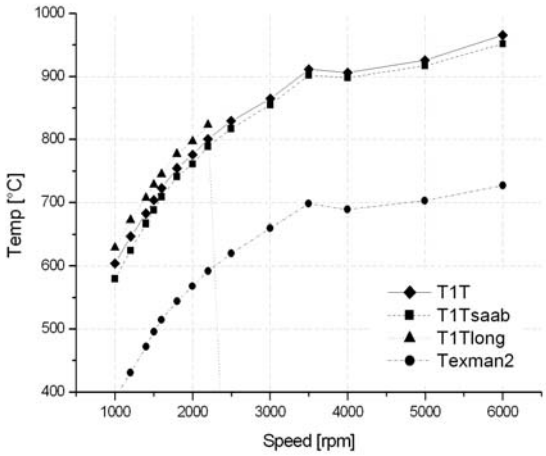

Figure 5.15. Results for the test series with a 1.5 mm probe diameter. T1T is the short 3 mm, T1Tsaab is the short 6 mm. T1Tlong is the 1.5 mm long and Texman2 is the wall temperature at the same location.

It can be seen that the 1.5 mm probe showed 823°C, 3 mm with short insertion length showed 800°C and the 6 mm probe 789°C, the wall temperature at the same location showed 592°C.
It is difficult to compare the two tests (figures 5.13 and 5.15), both because the running condition is not the same and the wall temperatures differ quite much. However, the difference between the highest and lowest (absolute) temperatures were in these two cases 3,1% and 3,2% respectively. Thus the 3 and 1.5 mm with long insertion lengths have equally higher temperatures than the shorter insertion lengths and thus give the same results. Therefore the 3 mm thermocouple with long insertion length had a length/diameter ratio large enough to make the influence from cooling via the stem negligible.

What kind of average is measured with a thermocouple?

The thermocouples used in these measurements were all shielded thermocouples. The shield is made of Inconel 600 and the insulation material is magnesium oxide. The thickness of the shield is 12-15% of the total diameter and the diameter of the thermocouple wires is 20% of the total diameter. The measurement tip is positioned at the end of the shield [5.15].
Normal procedure when correlating a model is to correlate (i.e. adjust some other parameter in the model so that some simulated value equals the corresponding measured value) the simulated mass averaged exhaust gas temperature against the temperature reading from the thermocouple. To be

able to do that one has to assume negligible heat transfer from the measurement tip to the surroundings. The possible heat transfer can be due to conduction in the stem and radiation to the wall. The assumption of negligible heat transfer is justified in this case with the long insertion length and radiation shield.

The heat transfer in the exhaust manifold pipes and exhaust ports is adjusted so that the simulated turbine inlet mass average temperature equals the thermocouple reading. To thoroughly investigate whether this is the right thing to do or not requires serious heat transfer treatment beyond the scope of this work. However, GT-Power offers a simpler way of checking these phenomena through its thermocouple model. It models the measurement tip as a spherical mass and models heat transfer via conduction from gas to thermocouple and radiative heat exchange to the wall. Unfortunately it does not incorporate conduction through the stem to the wall.

Figure 5.16 shows the result from such a model compared to the measured thermocouple signal, along with simulated instantaneous gas temperature and measured/simulated wall temperature. It can be seen that the modelled thermocouple temperature is lower than the measured value (which equals the mass average of the instantaneous gas temperature).

An exact comparison cannot be made since no case exist where the conditions in the model and the real case are the same, the measured case has a radiation shield while the model accounts for full heat exchange through radiation, and the real measured case can possibly have heat transfer to the wall via the stem. However, the difference between measured and simulated thermocouple reading might be explained as difference in radiative heat transfer, which is present in the model but not in the real case due to the heat shield.

It can also be seen that the thermocouple is much too slow to follow the gas temperature fluctuations.

It is here assumed that the temperature measured by the long inserted thermocouple with radiation shield measures a satisfactorily accurate mass averaged temperature.

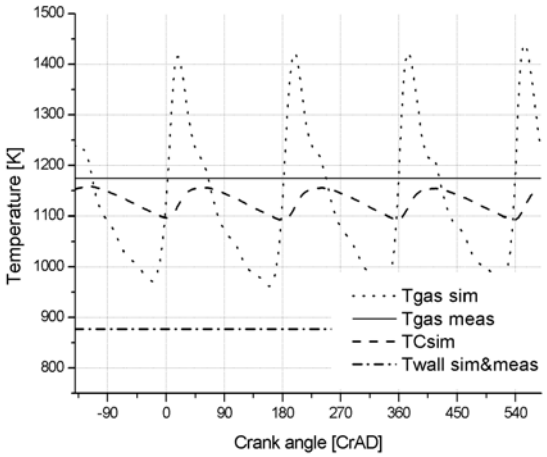

Figure 5.16. Comparison between time-averaged measured thermocouple reading (Tgas meas), simulated instantaneous thermocouple temperature (TCsim) and simulated instantaneous gas temperature (Tgas sim). The wall temperature is measured (time-averaged) and imposed in the model.

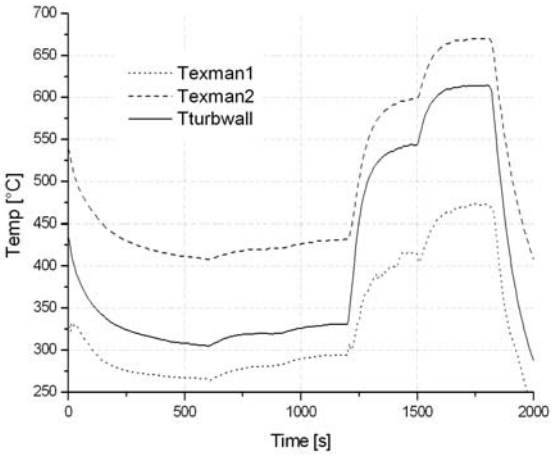

Figure 5.17. Exhaust wall temperatures. Texman1 measured close to the cylinder head for cylinder 4, Texman2 very close to the exhaust manifold-turbocharger flange, Tturbwall was measured on the turbine housing halfway around the circumference. It should be noted that a fan was blowing right at Tturbwall to avoid melting of the cables around the very hot turbine.

5.7.2 Wall temperature measurements

During the same measurement runs an attempt were made to measure the wall temperatures on the manifold and turbine housing. A stainless steel M8 nut was TIG-welded onto the manifold outer wall. Through a slit in the nut a thermocouple wire was inserted and held tight to the wall with a very short screw, see figure 5.11.
The wall temperature measurements showed that the time to reach steady state of the wall temperature was longer than the steady state of the gas temperature, about 4 minutes.
The wall temperature measured in this way cannot be the true wall temperature at the pipe inside. First, heat transfer theory state that there has to exist a temperature gradient across the wall if heat transfer should occur, and heat transfer do occur since the pipe is hot on the outside. Second, the nut holding the thermocouple extrudes farther out in the air than the surrounding pipe wall and therefore acts as a cooler. Therefore the temperature measured is an underestimate of the actual wall temperature.
However, the values are to be used as input to 1D simulations and as such they are much better than just assuming wall temperatures.
Figure 5.17 shows that the error, between waiting 3 and 4 minutes before assuming steady state, is small. Therefore it is concluded that the value reached after 3 minutes gave an inaccuracy smaller than the inaccuracy due to temperature gradient in the wall and cooling through the nut.

5.7.3 Exhaust temperature summary

When measuring temperatures in an exhaust manifold it takes 3 minutes to reach steady state of the thermocouple output for the gas temperature, and for the wall temperature measurements 4 minutes is a minimum for true steady state. The difference, though, in measured temperature between 3 min and 4 min is considered to be smaller than other sources of error such as temperature gradients through the wall and cooling through the mounting equipment for the surface thermocouple.
Of the four tested methods for gas temperature measurements the 3 mm thermocouple with long (100 mm, 33 probe diameters) insertion length was the thermocouple measuring a temperature closest to a true temperature.
The error between using a 6 mm thermocouple with short insertion length and a 3 (or 1.5) mm thermocouple with long insertion length was shown to be approx. 3%.

5.8 Effective mean pressures

The measured pressures interesting in this work are IMEP, BMEP, PMEP and FMEP.
IMEP is calculated from measured cylinder pressure, and with IMEP is here meant the gross IMEP, i.e. calculated for the entire cycle (720 CAD). The cylinder pressure was only measured on cylinder 1 and no information was available of the cylinder balance.

$$IMEP = IMEP(net) = IMEP(gross) - PMEP \qquad \text{eq. 5.9}$$

BMEP is measured with the dynamometer and is a reasonably accurate value for the entire engine. The connection between the engine and the dyno contained rubber elements, which theoretically could dissipate energy, but since the rubber couplings do not get hot it was assumed that the power losses in the rubber was well below 1 kW and therefore negligible.
PMEP is calculated from the low-pressure part of the measured cylinder pressure trace, between 180 and 540 CAD. As in the case of the IMEP cylinder balance could affect the accuracy of this value. As was seen in Chapter 3 the measured PMEP showed inconsistencies, which was assumed to be due to cylinder imbalance. Therefore it could be suspected that pressure measurement is necessary in all cylinders to achieve good values for PMEP. In addition, when measuring the low pressure part of the cycle, when the pressure is around ambient, very little of the transducer's dynamic range is used, which decreases the efficiency.
FMEP is calculated according to eq. 5.10. The values for FMEP acquired in this way have to taken with a pinch of salt. The reason for this is that the IMEP and subsequently PMEP values are only for cylinder one and perhaps not representative for the entire engine, due to cylinder imbalance. Still BMEP is the average value for the entire engine.

$$FMEP = IMEP - BMEP \qquad \text{eq. 5.10}$$

5.9 References

5.1 www.adlinktech.com
5.2 www.ueidaq.com
5.3 www.rosemount.com
5.4 www.setra.com
5.5 www.avl.com
5.6 www.etas.de
5.7 Bergh H. & Tijdeman H. "Theoretical and experimental results for the dynamic response of pressure measuring systems" NLF-TR F.238, Reports and transactions vol. XXXII 1965
5.8 Westin, Elmqvist & Ångström " Correlation between engine simulations and measured data - experiences gained with 1D-simulations of turbocharged SI-engines" SIA International Congress *SIMULATION, as essential tool for risk management in industrial product development* in Poissy, Paris September 17-18 2003
5.9 www.micro-epsilon.de/
5.10 Gjika, LaRue "Dynamic behaviour of rotor-bearing systems involving two oil films in series – application to high speed turbochargers" IMechE Paper C602/021/2002
5.11 Agrell, Alsterfalk "Turboprojektet 1995 - Förbränningsmotortekniks projektkurs" Internal report KTH Dept. of Internal Combustion Engines 1995
5.12 Råde, Westergren "Beta Mathematics Handbook for Science and Engineering" ISBN 91-44-25053-3
5.13 Course material of Cecost course "Measurement Techniques" www.cecost.lth.se
5.14 Ehrlich, "Characterization of unsteady on-engine turbocharger turbine performance" Ph. D. Thesis, Purdue Univ. 1998
5.15 www.pentronic.se

5.10 Appendix

Derivation of the expression for moment of inertia

The turbocharger rotor is hung from a mounting disc hanging from three long wires. The wires are of length l and positioned on the mounting disc on a radius r. The disc displacement angle ϕ and the angle of which the wires are displaced with is θ.

As the disc is displaced an angle ϕ away from the resting position the force in the wires will have one component in the vertical direction and one in the tangential direction. The tangential forces in the three wires will add up to a torque trying to move the disc back to the resting position. This torque can be shown to be:

$$\tau = 3r \cdot F_{\varphi} = -3r\frac{mg}{3}\tan\theta = -mgr\tan\theta \qquad \text{eq. 5.11}$$

With the relationship between θ and ϕ:

$$\theta = \arcsin\left(\frac{2r}{l}\sin\frac{\varphi}{2}\right) \qquad \text{eq. 5.12}$$

the torque thus becomes:

$$\tau = -mgr\tan\left(\arcsin\left[\frac{2r}{l}\sin\frac{\varphi}{2}\right]\right) \qquad \text{eq. 5.13}$$

This torque is driving the acceleration in the pendulum-rotating motion in the ϕ-direction. If zero damping is assumed the equation of motion thus is:

$$J\ddot{\varphi} = -mgr\tan\left(\arcsin\left[\frac{2r}{l}\sin\frac{\varphi}{2}\right]\right) \qquad \text{eq. 5.14}$$

This differential equation is difficult to solve so a small-angle approximation is necessary. Since r<<l both the tan A=A and arcsin B=B will be ok if the sin

C=C is ok. For maximum 1% error in the small angle approximation $\phi<0.33$ ($\phi<19°$). So, for pendulum amplitudes less than 19° the equation of motion is:

$$\ddot{\varphi} + \frac{mgr^2}{Jl}\varphi = 0 \qquad \text{if } \phi<19° \qquad \text{eq. 5.15}$$

Solving this equation gives:

$$J = \left(\frac{T}{2\pi}\right)^2 \frac{mgr^2}{l} \qquad \text{eq. 5.16}$$

where T is the period time of the oscillation.

Chapter 6

Determination of the turbine efficiency when used on the engine (the on-engine turbine efficiency)

6.1 Introduction

As could be seen in previous chapters the turbocharger performance could not be accurately simulated without adjustment of the turbine efficiency and mass flow multipliers. Furthermore, the inability of the simulations, at certain operation points, to predict the measured turbo speed fluctuation amplitude indicates that the efficiency as a function of power delivery, pressure amplitude etc, is not acceptable. This is a non-satisfactory condition and a problem that has to be overcome in order to be able to optimise turbocharged engines. But before a process can be accurately simulated, the real process would preferably be understood, and at least it must be measured. It is thus necessary to be able to measure the turbine's output work and efficiency when used on the engine. The first steps at KTH towards determination of the crank angle resolved turbine efficiency were taken by Roy Ogink [6.1].

6.2 Turbine efficiency definition

The turbine efficiency can be defined in several different ways. Most people have an intuitive understanding of efficiency as the ratio of utilized output work and input energy into a system, which is the case for example the thermal efficiency of an engine, which is defined as the ratio of measured shaft power and input fuel power. For turbomachines however, the isentropic efficiency is the one most commonly used. The isentropic efficiency is the ratio between the actual enthalpy change over the machine and an ideal (i.e. isentropic) enthalpy

change. For a radial turbine this results in an efficiency defined as the ratio of change in actual total enthalpy and the enthalpy change if the pressurized gas stream was expanded isentropically [6.2]:

$$\eta_{TS} = \frac{h_{03} - h_{04}}{h_{03} - h_{4s}} \qquad \text{eq. 6.1}$$

For almost all turbochargers with internal wastegate no diffusion can occur at the turbine outlet, subsequently all kinetic energy at the turbine outlet is dissipated in the exhaust. Therefore the most sensible efficiency to use is the total-to-static efficiency, as shown in eq. 6.1 above.
To obtain the instantaneous efficiency this equation would need to be applied for the conditions in the turbine at every instant. Measuring the actual change in total enthalpy would require measurement of the instantaneous temperature. This was regarded too difficult to attempt within this project. Another problem with the efficiency as defined in eq. 6.1 is that radiative thermal losses would apparently increase efficiency. This since it decreases the enthalpy at the turbine outlet, and thus increases the nominator without changing the denominator, which will result in an apparent higher efficiency. To avoid having to deal with thermal radiation and to avoid having to develop fast responding temperature measurement methods, the actual change in total enthalpy in eq. 6.1 is replaced by the measured utilized power from the turbine [6.3]. Thus the efficiency of the turbine is here calculated as a ratio between a utilized power and an isentropic power. The latter is assumed to be the largest power possible to extract from the turbine. Here these two will be analysed separately.

$$\eta_t = \frac{P_{utilized}}{P_{isentropic}} \qquad \text{eq. 6.2}$$

6.2.1 Isentropic turbine power

The isentropic power is the difference in enthalpy between turbine inlet and outlet. The definition of c_p [6.4] gives that:

$$mc_p = \left.\frac{\partial h}{\partial T}\right|_P \qquad \text{eq. 6.3}$$

$$h = \int_0^h dh = m \int_0^T c_p dT \qquad \text{eq. 6.4}$$

The time-derivative of this is the power:

$$P = \frac{dh}{dt} = \dot{m} \int_0^T c_p dT \qquad \text{eq. 6.5}$$

Thus, the isentropic power is the difference in power flowing into the turbine and out from the turbine:

$$P_{isentropic} = \dot{m}_{in} \int_0^{T_{in}} c_p dT - \dot{m}_{out} \int_0^{T_{out}} c_p dT \qquad \text{eq. 6.6}$$

A polynomial fit of c_p for the valid temperature range concludes the analysis, see Appendix, figure 6.17.
Note, during the calculation of eq. 6.6 it will be convenient to replace a temperature ratio by a pressure ratio according to isentropic conditions. Then there will be a ratio of specific heats, γ, in the exponent. This must be calculated as an average value for the temperature range in the temperature ratio, and thus not directly associated with the c_p elsewhere in the expression.
This expression for the isentropic power is an attempt to treat the problem what happens if the massflow in and out is not equal, i.e. mass accumulation in the turbine, which is discussed among others by Ehrlich [6.5] and King [6.6]. However, there might exist other problems with the expression as well, mainly with the lag in time of the different processes (inflow, power production in the wheel and outflow). What we really would like to have as the isentropic power is the sum of all possible impulses of all gas molecules affecting the blades. But the lack of knowledge about the actual flow and thermodynamic properties inside the rotor, and it's immediate vicinity, force the analysis out towards the boundaries where more information about the state exist. Therefore we define the isentropic power as an enthalpy difference between two boundaries, which is an inheritance from the steady flow theory.
The assumption that the isentropic power is the enthalpy difference between an upstream and a downstream boundary is a sort of a control volume approach. It is assumed that the isentropic power is produced evenly distributed over the volume for every time step. This differs from the real case where the power is

produced at a quite distinct location, in the rotor. Since the rotor volume constitute only a smaller fraction of the entire turbine volume (and thus also the control volume) the control volume approach introduce a phase-problem between inflow, outflow and production of power. A modification to the control volume approach would be to use a massflow that is believed to better reflect that in the rotor. Assuming equal inflow and outflow, and using the arithmetic average of in- and outflow as that equal massflow is one way.
The expression (6.6) is simplified with the assumption that $m_{in}=m_{out}$:

$$P_{isentropic,m} = \dot{m}\left[\int_0^{T_{in}} c_p dT - \int_0^{T_{out}} c_p dT\right] = \dot{m}\int_{T_{out}}^{T_{in}} c_p dT \qquad \text{eq. 6.7}$$

This significantly narrows the range of the integral over c_p, and a common assumption is that c_p is constant over the range, which gives:

$$P_{isentropic,m} = \dot{m}\bar{c}_p\left(T_{in} - T_{out}\right) = \dot{m}\bar{c}_p T_{in}\left(1 - \left(\frac{P_{out}}{P_{in}}\right)^{\frac{\bar{\gamma}-1}{\bar{\gamma}}}\right) \qquad \text{eq. 6.8}$$

Where the massflow is the arithmetic average of in- and outflow at every instant.

6.2.2 Utilized power

The utilized power consists of three terms, the power absorbed by the compressor to compress the intake air, the power used to accelerate and decelerate the rotor along it's speed trace (the rotor is oscillating with an amplitude of approx. 1% of the average speed) and the power loss in the bearings due to friction.

$$P_{utilized} = \left(\frac{2\pi}{60}\right)^2 J_{rotor} N_{rotor} \frac{dN_{rotor}}{dt} + \frac{P_{compression}}{\eta_{mech}} \qquad \text{eq. 6.9}$$

The first term is the power necessary to accelerate and decelerate the rotor (inertial power), the second term is the compressor power together with bearing friction. Simulations show no sign of significant differences in massflow between compressor in- and outlet and the expression for $P_{compression}$ thus is:

$$P_{compression} = \dot{m}_{air} \int_{T_{in}}^{T_{out}} c_p dT \qquad \text{eq. 6.10}$$

Similar to the isentropic power, a polynomial expression for c_p is required. To calculate eq. 6.10 CA-resolved from measured values requires a change from temperatures to pressures, since no CA-resolved temperature measurements could be done. The isentropic relationship cannot be used since the process is not isentropic. Instead the expression for the isentropic efficiency is used and developed into:

$$\frac{T_{out}}{T_{in}} = \left(\frac{P_{out}}{P_{in}} \right)^{\frac{\bar{\gamma}-1}{\bar{\gamma}}} \frac{1}{\eta} - \frac{1-\eta}{\eta} \qquad \text{eq. 6.11}$$

where the bar over γ indicates that γ is the average value for the temperature range.
A linear equation was assumed accurate enough for c_p and the expression was developed from equations 6.10 and 6.11.
A common assumption is that the compressor power is constant, and therefore can be calculated from:

$$\overline{P}_{compressor} = \overline{\dot{m}}_{air} \overline{c}_{p,air} \left(\overline{T}_{0,2K} - \overline{T}_{0,1K} \right) \qquad \text{eq. 6.12}$$

A quick look at the simulation results, as well as the measured data, shows that the fluctuation amplitude of the compressor power is 20-30% and therefore not constant.

6.2.3 Turbine efficiency

The expressions for isentropic and utilized power can be used in several different definitions of the turbine efficiency. The most complex is the fully fluctuating compressor power together with the unequal flow isentropic turbine power, i.e. equations 6.6, 6.9 and 6.10:

$$\eta_{isentropic} = \frac{\left(\frac{2\pi}{60}\right)^2 J_{rotor} N_{rotor} \frac{dN_{rotor}}{dt} + \frac{\dot{m}_{air} \int_{T_{0,C\_in}}^{T_{0,C\_out}} c_p dT}{\eta_{mech}}}{\dot{m}_{t\_in} \int_0^{T_{0,t\_in}} c_p dT - \dot{m}_{t\_out} \int_0^{T_{t\_out}} c_p dT} \qquad \text{eq. A11}^4$$

If the massflow is assumed to be equal in and out from the turbine, equation 6.8 can be used as denominator:

$$\eta_{isentropic} = \frac{\left(\frac{2\pi}{60}\right)^2 J_{rotor} N_{rotor} \frac{dN_{rotor}}{dt} + \frac{\dot{m}_{air} \int_{T_{0,C\_in}}^{T_{0,C\_out}} c_p dT}{\eta_{mech}}}{\dot{m}_t \bar{c}_p T_{0,t\_in} \left(1 - \left(\frac{P_{t\_out}}{P_{0,t\_in}}\right)^{\frac{\bar{\gamma}-1}{\bar{\gamma}}}\right)} \qquad \text{eq. A12}$$

Furthermore, if the compressor power is taken from GT-Power the expression is:

$$\eta_{isentropic} = \frac{\left(\frac{2\pi}{60}\right)^2 J_{rotor} N_{rotor} \frac{dN_{rotor}}{dt} + \frac{P_{C\_GTP}}{\eta_{mech}}}{\dot{m}_t \bar{c}_p T_{0,t\_in} \left(1 - \left(\frac{P_{t\_out}}{P_{0,t\_in}}\right)^{\frac{\bar{\gamma}-1}{\bar{\gamma}}}\right)} \qquad \text{eq. A13}$$

And if the compressor power is assumed to be constant in time, equation 6.12 is used for the compressor power:

[4] Eqs. A11-A14 have different notation than the rest of the eqs. in the chapter in order to be compatible with the notation used in Chapter 8.

$$P_{isentropic} = \frac{\left(\frac{2\pi}{60}\right)^2 J_{rotor} N_{rotor} \frac{dN_{rotor}}{dt} + \frac{\overline{\dot{m}}_{air} \overline{c}_{p,air} \left(\overline{T}_{0,2K} - \overline{T}_{0,1K}\right)}{\eta_{mech}}}{\dot{m}_t \overline{c}_p T_{0,t\_in} \left(1 - \left(\frac{P_{t\_out}}{P_{0,t\_in}}\right)^{\frac{\overline{\gamma}-1}{\overline{\gamma}}}\right)} \qquad \text{eq. A14}$$

Which is the same expression as used in an older publication by Westin & Ångström [6.7] which is presented later in this chapter, as well as Winterbone [6.3].

6.3 Sample results

The question now is which expression for the efficiency is most accurate to use. For the extracted work three alternatives are available. In figure 6.1 an example for T2M3[5] 1500 rpm is displayed. It is obvious that it makes a large difference to account for the fluctuating compression work. This is a case with quite low fluctuation amplitude of the turbocharger speed, for other cases the assumption of constant compressor power is less wrong, but the point is made that it is necessary to account for.

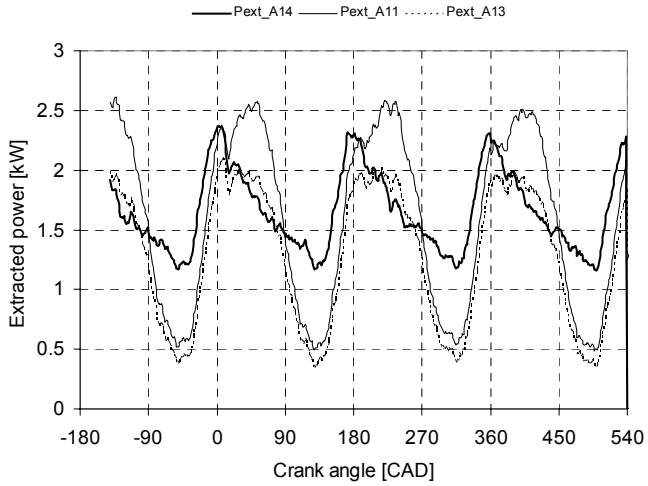

Figure 6.1. The extracted power calculated in the three ways according to equations A11/A12, A13 and A14. For T2M3 1500 rpm.

[5] TiMj denotes turbine number i and manifold number j. Results come from an investigation with 3 turbines and 3 manifolds. More details in Chapter 8.

Furthermore there exist two expressions for the isentropic turbine power. Equation A11 that includes treatment of unequal massflow in- and out and A12 that assumes the same massflow into the turbine as out from it. The massflow could not be measured, therefore only simulated results are used in the calculations. What is interesting is the massflows in and out from the boundaries that have been defined for the efficiency calculations, i.e. the massflows at the locations where the pressures are measured. The volute and turbine outlet chamber are represented by pipe elements in GT-Power, and the massflows used here are the massflows at the inlet to the volute pipe and the outlet from the pipe representing the outlet chamber. Figure 6.2 shows that there are obvious differences in in- and outflow, and the volume of the turbine must act as a buffer.

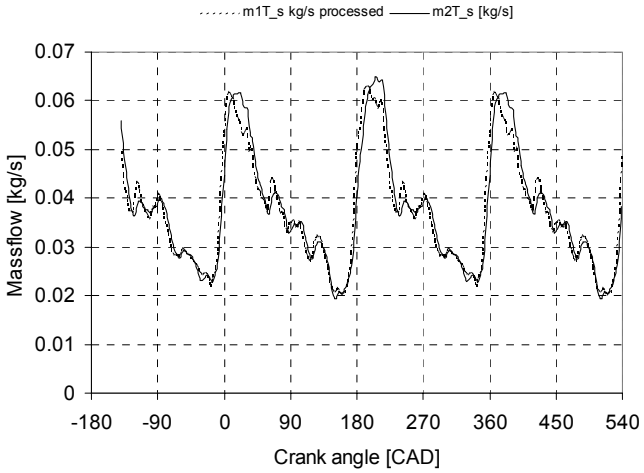

Figure 6.2. Massflow in- and out from the turbine. For T2M2 1500 rpm.

In figure 6.3 examples of results from both versions of the isentropic power are displayed. The example is from T2M2 1500 rpm. The curve from the eq. A11 expression is unrealistically noisy but the two other curves are quite similar to each other indicating that it is not very important where to extract the massflow as long as it is assumed equal throughout the turbine.

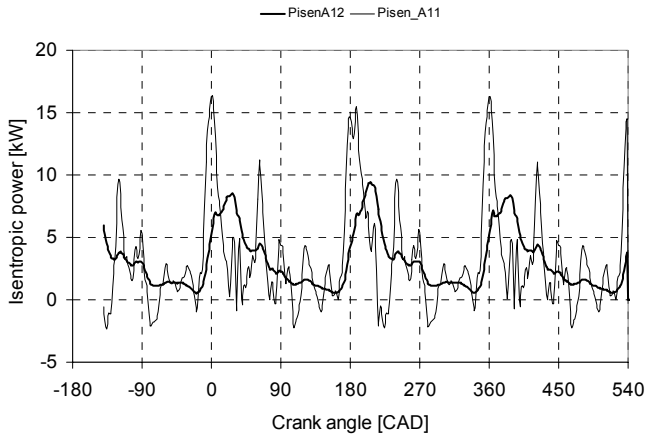

Figure 6.3. The results from the two versions of the isentropic power. For T2M2 1500 rpm.

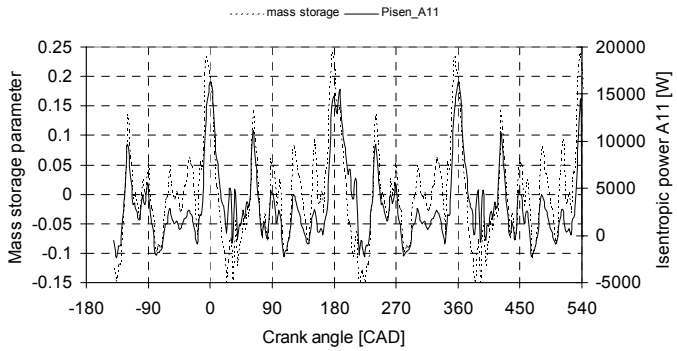

Figure 6.4. A comparison between the A11-isentropic power and the mass storage multiplier. For T2M2 1500 rpm.

The question is why the A11 expression of the isentropic power is so noisy. The answer is in figures 6.2 and 6.4. In figure 6.4 the isentropic power is plotted along with the mass storage parameter, defined by Ehrlich [6.5]:

$$ms = \frac{\dot{m}_{in} - \dot{m}_{out}}{\dot{m}_{in}} \qquad \text{eq. 6.13}$$

It shows the clear correlation between the isentropic power fluctuations and the fluctuation in mass storage. It is obvious that the inlet flow to the volute is changing rapidly and appears to be very noisy. The data is entirely extracted

from GT-Power simulations and it appears from watching animations of pressure and massflow propagation that the noisy inlet massflow is a result of the resonance set up in the manifold between the different pipes and flowsplits. In the figures 6.5-6.7 the A12 and A14 definitions the efficiency are compared for 3 different manifolds that gives three different pulse shapes at the turbine inlet.

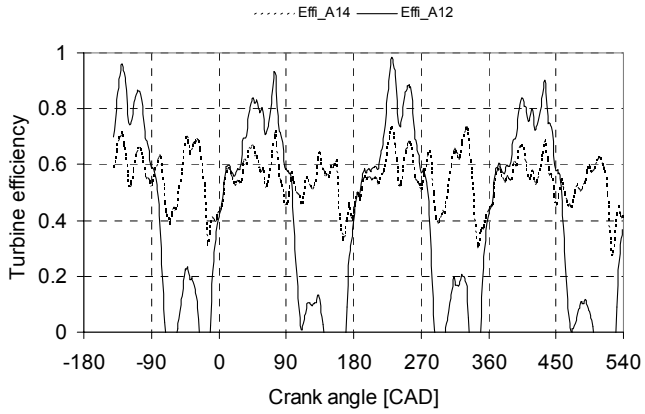

Figure 6.5. Turbine efficiency calculated for method A12 and A14. Turbine 2 and manifold 2 at 1500 rpm.

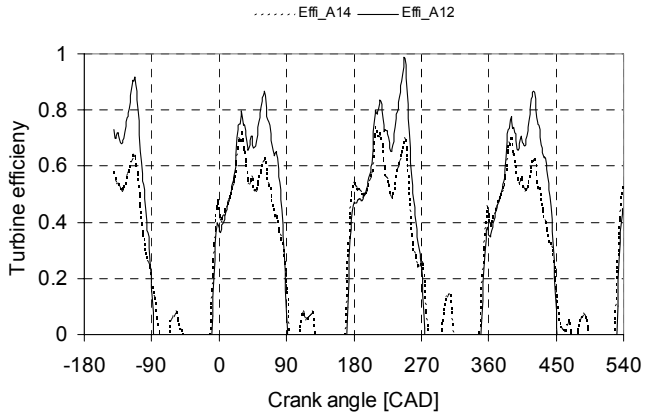

Figure 6.6. Turbine efficiency calculated for method A12 and A14. Turbine 2 and manifold 1 at 1500 rpm.

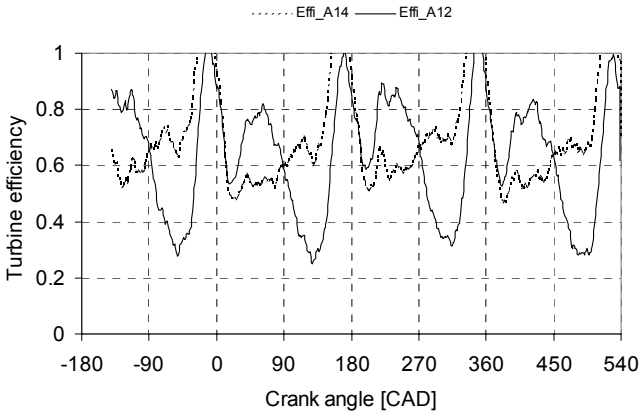

Figure 6.7. Turbine efficiency calculated for method A12 and A14. Turbine 2 and manifold 3 at 1500 rpm.

It is quite obvious that the difference between the methods differ very much between different cases. The calculations based on eq. A14 show quite unrealistical values for both hardware combinations T2M1 and T2M3, which is a consequence of the over-simplified compression work. Furthermore, several of the curves have regions where the efficiency is less than 0. More on that below.

It is concluded here that the most proper instantaneous on-engine turbine efficiency to use is the A12 expression, where the massflow in and out from the turbine is assumed equal, but that the fluctuating compressor power is included. This is in line with the discussion by King. However, note the lack of knowledge about the noisy, fluctuating massflow into the turbine. It would be more confident to have better knowledge about the actual massflow on the engine. The A11 definition is discarded due to the noise levels leading to an unrealistically fluctuating efficiency.

The decision to use the calculated compressor power from measured pressure traces rather than just extracting the power from GT-Power was based on the fact that there existed problems in getting the calculated compressor outlet pressure equal in phase with measured pressure. The reason is that the inlet system between valves and compressor is a sensitive resonance system where sometimes complex geometries such as intercooler, inlet plenum and compressor volute perhaps not always are accurately simulated in all aspects with the 1D simplification.

CA-resolved graphs are good for understanding of phenomena and for detail studies, but when comparing larger amounts of data, several cases, different hardware setups etc. average values are more appropriate. The turbine

efficiency curves in figures 6.5-6.7 could be either time averaged, or the average could be weighted by either the massflow rate or the isentropic power. In addition, an average can be acquired by integrating the nominator and denominator separately and then dividing them. Such a test is displayed in table 6.1.

That the values differ quite much between the averaging techniques is not strange. An efficiency should in essence give a value for how large portion of an inserted amount of work that have been utilized. Thus, calculating an efficiency by dividing the total amount of extracted power by the total amount of inserted power cannot give the wrong value, since it is the core definition of the efficiency.

It is when the average efficiency is calculated otherwise it can get wrong. The difference between the averaged efficiency weighted by isentropic power and the ratio of integral method is that in the first case we take the ratio first and integrate thereafter, and in the latter case the other way around. Since the ratio is a non-linear function, the two expressions will not be the same, i.e. they do not commutate.

Thus, the proper single value for the efficiency of a time-dependent process during a certain time interval must be the ratio of separate time-integrals of the extracted and available powers.

This leads to an alternative way of defining the efficiency; that the efficiency is always the ratio between two time-integrals, one of extracted power and one of ideal (in this case isentropic) power.

Table 6.1. Comparison of different averaging methods for the three definitions of the efficiency.

		Efficiency definition		
		A14	**A12**	A11
T2M1	Time avg	0.19	- 0.08	0.75
	Mass weighted avg	0.28	0.12	0.63
	Isenpow weighted avg	0.43	0.40	0.83
	Ratio of integrals	0.43	**0.40**	0.34
T2M2	Time avg	0.55	0.37	2.20
	Mass weighted avg	0.55	0.45	2.57
	Isenpow weighted avg	0.56	0.55	4.38
	Ratio of integrals	0.56	**0.55**	0.53
T2M3	Time avg	0.73	0.37	0.63
	Mass weighted avg	0.71	0.65	0.64
	Isenpow weighted	0.68	0.66	0.66
	Ratio of integrals	0.68	**0.66**	0.62

$$\eta(t) = \frac{\int_{t_i-\Delta t/2}^{t_i+\Delta t/2} P_{extracted}(t)dt}{\int_{t_i-\Delta t/2}^{t_i+\Delta t/2} P_{ideal}(t)dt} \qquad \text{eq. 6.14}$$

$$P_{ext}(t) = \left(\frac{2\pi}{60}\right)^2 J_{rotor} N_{rotor} \frac{dN_{rotor}}{dt} + \frac{\dot{m}_{air} \int_{T_{0,C\_in}}^{T_{0,C\_out}} c_p dT}{\eta_{mech}}$$

$$P_{ideal}(t) = \dot{m}_t \bar{c}_p T_{0,t\_in} \left(1 - \left(\frac{P_{t\_out}}{P_{0,t\_in}}\right)^{\frac{\bar{\gamma}-1}{\bar{\gamma}}}\right) \qquad \text{eq. 6.15}$$

In these expressions every included property could be a function of time. If Δt is the duration of one engine cycle the result will be the ratio of integrals in table 6.1. With the efficiency definition according to 6.14 there will never exist an instantaneous efficiency, it will always be an integral over a time-interval. But if the interval is 1CAD the result is equal to what above is referred to as instantaneous efficiency (since the resolution of the analysis above is 1CAD). Equation 6.14 also gives a stringent way of analysing the efficiency over certain intervals, for instance during blowdown or for filtering out the efficiency over intervals where the mass flow is over a certain threshold value. In addition, smoothed efficiency curves vs. CAD can be calculated, where the integration limits will be $t-\Delta t/2$ and $t+\Delta t/2$ and one value is calculated for every t (in this case every CAD), i.e. a centred, floating average over the time Δt.
The equation could also explain why there exist problems with phasing of the work inside the control volume. When the interval over which the efficiency should be calculated is not significantly longer than the characteristic time of the phase-lag, the calculation gets very sensitive and the efficiency can take values very far away from $0<\eta<1$ which is to be expected from an efficiency (according to energy conservation). Floating, centred average curves are displayed in figure 6.8. The figure shows three curves for definition A12 with 1, 30 and 90 CAD integration interval and one curve for definition A11 with 90 CAD integration interval.

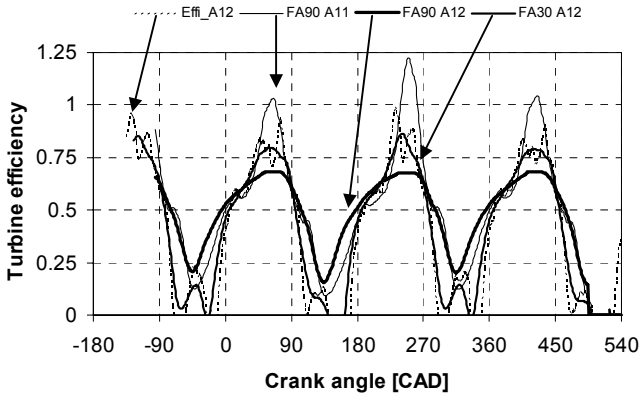

Figure 6.8. The floating average efficiencies for the A11 and A12 definitions for different averaging-intervals. Effi_A12, FA90 A12 and FA30 A12 means definition A12 with 1, 30 and 90 CAD integration interval respectively and FA90 A11means definition A11 with 90CAD integration interval. T2M2 1500 rpm.

Obviously the A11 definition doesn't show good results even though the averaging interval is as long as 90 CAD. To give a picture of how much such large averaging intervals potentially can distort the shape of the curve the A12-efficiency is plotted with 1, 30 and 90 CAD averaging interval. Several other intervals were tested, but it seems like 30 is a proper interval to use for the A12 efficiency.

6.3.1 Negative efficiency

As seen for instance in figures 6.8 and 6.9, the efficiency curve is often negative. That can only happen if either of the utilized or isentropic powers is negative. Of all the operation points analysed in detail here no point is found where the isentropic power has been negative, it is thus the compressor side that causes this negative efficiency. The intervals where the negative efficiency occurs are typically intervals with very small power on both sides of the turbo. Therefore small values of negative power might give very large negative values for the efficiency. The reason for the negative utilized power might well be inaccuracies in the input data, since the negative amplitude is much less than the positive amplitude ($|min| << |max|$). Therefore the negative efficiencies can be neglected and the efficiency at those points be assumed to be 0 since no power is produced.

6.3.2 Efficiency >1

Unfortunately the method is not bulletproof for all operation conditions. For 1000 rpm the efficiency vs. speed curve shows unrealistic values with peaks above 1, see figure 6.9. Efficiencies larger than 1 occurs when the utilized power exceeds the isentropic power. Figure 6.10 shows that that the extracted power (solid line) is larger than isentropic power (grey line) for short periods around –35, 145, 325 and 505 CAD. The problem occurs at the upslope of each peak of isentropic power. The reason for the efficiency larger than one is that the phasing between the inertial power and compression power changes with speed. See figure 6.11 where the inertial power and the power for compression only is plotted for 1000 and 1500 rpm. As can be seen in the figure, the problem is not due to problems with phasing between simulation and measurement, since measured and simulated compressor power are in phase. In addition, the pressure traces of compressor output power matched well within the difference in phase seen in the figure. This indicates that the expression for the compression power might need some more work. For instance the friction has been given a possibly over-simplified treatment. Since the powers for these cases are so low (a few 100 W) it is not impossible that the friction model might be the reason.

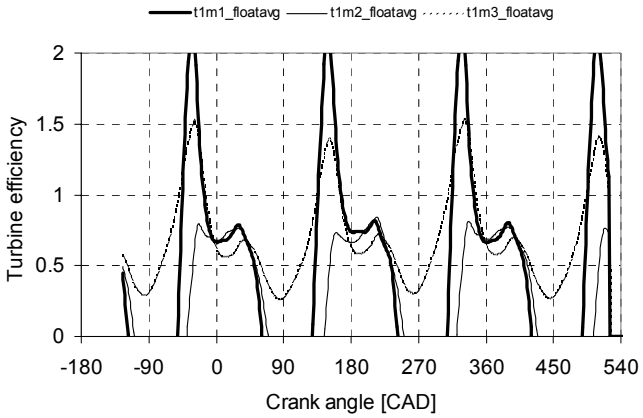

Figure 6.9. The float-average turbine efficiency for 1000 rpm, turbine 1 and all three manifolds. Especially manifolds 1 and 3 show unrealistic high efficiencies.

Table 6.2. Comparison between the calculated turbine efficiency [%] and the mass flow average efficiency calculated by GT-Power.

	Calc	GTP
T2M1	40	47
T2M2	55	51
T2M3	66	50

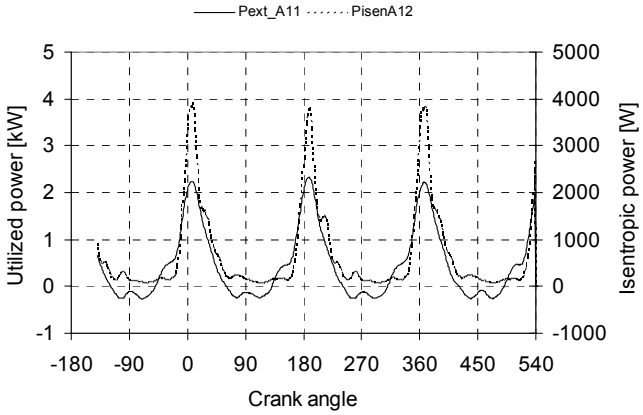

Figure 6.10. The isentropic power and the utilized power for T1M1 1000 rpm. It is obvious that the utilized power is higher than the isentropic at the start of each pulse.

It is also very interesting to compare the calculated values of the efficiency with the values shown in the GT-Power results. In table 6.2 that is done for the three cases shown previously. Unfortunately the efficiency from GT-Power is a mass flow weighted, time-averaged value of the instantaneous (constant during each time step, approx. 1 CAD) efficiency. This might be a part of the reason why the results are not equal.

6.4 Definition discussion

An efficiency definition as the one above is very reasonable in the sense that it relates the actual, measurable extracted power from the turbine to the maximum power possible to extract from the exhaust gas stream. Radiation, heat transfer losses etc. do not need to be treated separately but they will still be enclosed in the determined efficiency. The definition includes one more assumption that has not been mentioned, it assumes negligible heat transfer from turbine to compressor, and negligible heat losses from the compressor.

The assumption is made for simplicity, and the accuracy of that is discussed in chapter 7.

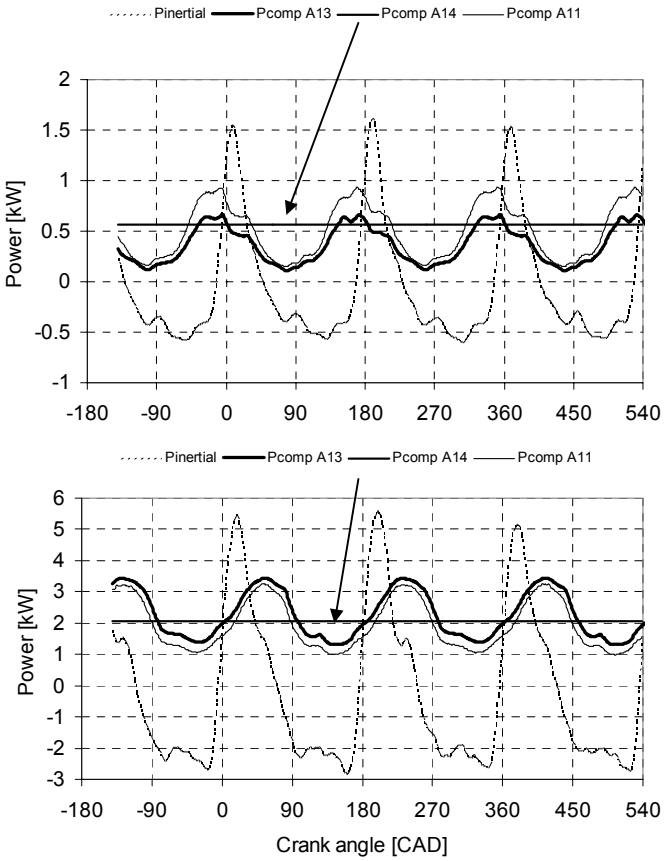

Figure 6.11. The power used for compression (Pcomp) and acceleration of the rotor inertia (Pinertial) at 1000 rpm (upper pic.) for T1M1 and at 1500 rpm (lower pic.) for T2M1. It is clear that the phase between the inertial power and the compression power differs with speed.

6.5 Blade speed ratio U/C_s

Another important parameter commonly used to classify the working conditions of the turbine is the Blade Speed Ratio (BSR or U/C_s), which is the rotor inlet blade tip speed divided by the gas velocity if the gas was expanded isentropically over an ideal nozzle [6.2].

$$U/C_s = \frac{U}{\sqrt{2c_p T_{0,t\_in}\left[1-\left(P_{t\_out}/P_{0,t\_in}\right)^{\frac{\bar{\gamma}-1}{\bar{\gamma}}}\right]}} \qquad \text{eq. 6.16}$$

6.6 Data acquisition

To be able to calculate the CA-resolved turbine efficiency according to equations A11-A14 a large amount of CA-resolved data is needed. The data that was actually measured were static pressures, turbospeed and –acceleration. Other data such as temperatures and mass flows were only measured as time averages. For the rest of the data, gas velocities to calculate total properties, CA-resolved massflow and temperatures, values from the GT-Power simulations were used. For all values taken from simulations the time average values were equal to the measured ones.

For all measured CA-resolved data, ensemble averaging over 100 consecutive measured engine cycles removes noise successfully. c_p is calculated from temperature as described in the appendix below. The mechanical efficiency though cannot be measured with the setup used, therefore the value 0.975 is used since the manufacturer stated the efficiency as somewhere between 0.95-1.00. However, the model might be a proper scope for some further investigation since the results indicate that the utilized power could be calculated better.

Here is a description of the properties used for the calculations in this chapter.

$\dot{m}_{exhaust}$ ..... cannot be measured, only the time average value can be measured indirectly through inlet air and fuel measurements.

$c_{p,exhaust}$ ..... not a measurable quantity but it can be calculated for the gas composition and temperature. Here it is calculated from T_{03} and measured lambda. See Appendix.

T_{o,t_in} ..... The thermocouple used for measuring the turbine inlet temperature is too slow to measure the fluctuating temperature due to the pulsating flow from the cylinders. Only the average value can be measured, therefore instantaneous temperature is taken from the validated GT-Power model.

P_{t_out} ..... Instantaneous static outlet pressure can be measured directly with piezo-resistive transducers.

P_{o,t_in} ..... Instantaneous total inlet pressure cannot be measured due to the high pulsation frequency, only static pressure can be measured. The dynamic pressure contribution is therefore calculated from simulated temperature and gas velocity.

γ ..... Calculated for the average value of time-averaged inlet and outlet temperatures.

Thus, T_3 and $\dot{m}$ are taken from the GT-Power model, where the average values in the model and measurements are similar. In addition, gas velocity for calculation of dynamic properties of T and P, to add to the static for calculation of total properties, is taken from GT-Power.

6.7 Application

Here follows an example of how the equations developed above can be used for analysis of the turbine. These, slightly older, results are based on the A14 definition of the efficiency and were presented at the ImechE 7th International Conference on Turbochargers and Turbocharging in London 2002. More examples of application, including the A12 definition as well, will be presented in Chapter 8.

In figure 6.12 the measured speed trace for the turbo rotor is displayed along with the calculated acceleration torque and the driving pressure at the turbine inlet. The fluctuation amplitude for the speed is slightly below 1% of the average speed, i.e. quite a small fluctuation. The torque curve shows that the acceleration torque is positive only for about 1/3 of the cycle, but has on the other hand larger magnitude on the positive side than on the negative side. The time of maximum torque coincides very well with the time of maximum inlet pressure. Thus, the turbine is propelled by a series of sharp pressure impulses. It is also evident that the pulsation amplitude of the driving pressure is much higher than for the speed, the amplitude is about 80% of the (time-) average absolute pressure (note that the pressure in figure 6.12 is relative pressure).

Previous investigations have shown that the turbine torque shows quite large phase differences with the turbine inlet pressure [6.3, 6.8, 6.9, 6.10]. Hu and Lawless refer to it as mass storage [6.10]. This delay is not seen at all in the present investigation.

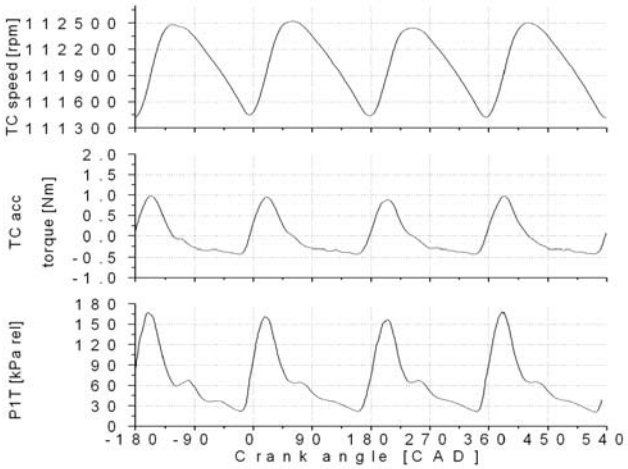

Figure 6.12. Turbocharger speed, turbocharger acceleration torque and turbine inlet pressure as functions of crank angle. No delay between turbine torque and inlet pressure (P1T) can be observed. Data collected at 2000 rpm WOT.

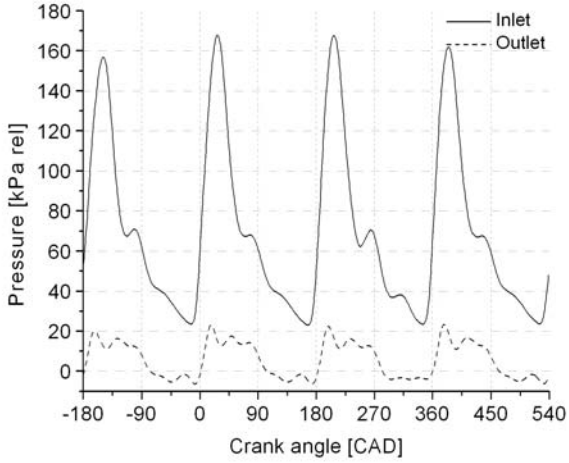

Figure 6.13. Data averaged over 50 cycles showing that the pressure at turbine inlet and outlets are perfectly phased to each other. This was recorded at 2000 rpm, WOT, but the phasing was the same for lower load cases as well as for 1500 and 3000 rpm.

An explanation for the lack of phase difference in the present work as a difference from previous investigations can be that they were all probably measured on larger (truck diesel sized) turbochargers, but then an equivalent phase shift between inlet and outlet pressures as for the inlet pressure and the output torque would be anticipated. Figure 6.13 shows that the measured pressures at turbine inlet and outlet are very close to simultaneous, which also is pointed out by Winterbone et. al. [6.3].
In this measurement the phasing of the turbine torque is very consistent with the modelling results. In the simulation, the pressure and mass flow arrived at the turbine at the same time, and the turbine produced work as the calculated gas flow occurred.
To calculate the on-engine turbine efficiency eq. A14 was applied to data, as described above, for 2000 rpm, full load conditions. The result can be seen in figure 6.14 where the measured turbo acceleration torque, simulated mass flow, calculated isentropic power (the denominator in eq. A14), U/Cs and turbine total-to-static efficiency are displayed individually as functions of crank angle. It can be seen that at the time of peak isentropic power and mass flow through the turbine, the efficiency is close to 50% whereas in between the exhaust flow pulses it is negative. The reason for this negative efficiency is that the utilized power is negative, which is discussed above.
In figure 6.15 the turbine efficiency is plotted vs. the mass flow. It is clear that for the highest massflows the efficiency is 10-15 %-points below peak values during the cycle. To maximize power output the peak efficiency should coincide with peak power delivery, but that is not the case here. The different marker types in the figure show how much isentropic power that is entering the turbine at every instant in the process. For the point of maximum efficiency the power delivery is only 2/3 of maximum, and when peak power occurs, at the same time as peak mass flow it is already pointed out that the efficiency is below peak values.

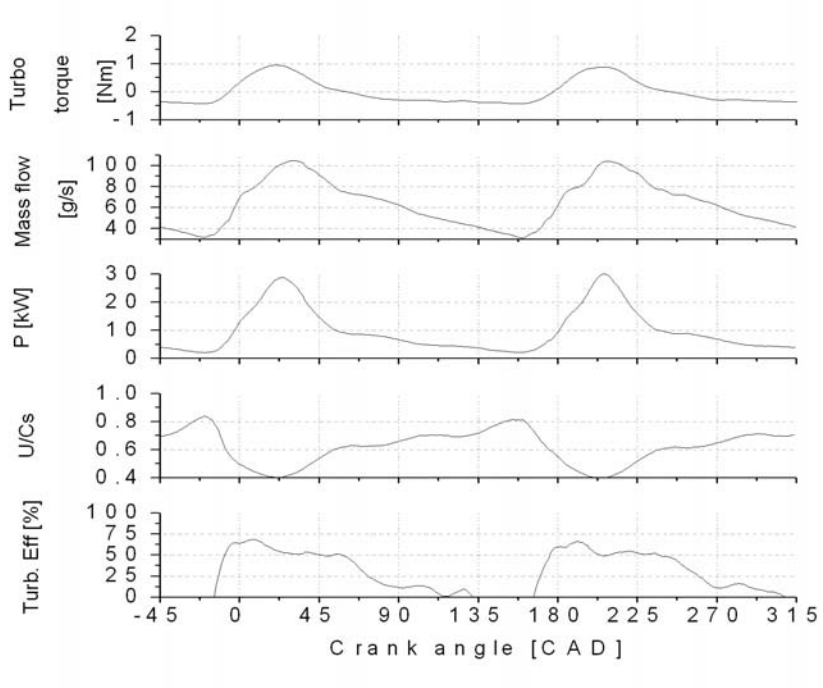

Figure 6.14. Mass flow, turbine isentropic power (P), BSR (U/C_s) and turbine efficiency as a function of crank angle for two exhaust pulses.

In figure 6.16 the efficiency is plotted against blade speed ratio U/C_s for the traverse of one pulse through the turbine. In the ideal steady flow case all measured data would collapse onto a parabola, with a maximum at U/C_s=0,7 ($=2^{-0,5}$) [6.11]. Here that is not the case. The arrows show in which direction the trajectory is traversed. In the beginning of the exhaust valve opening the pressure ratio is low and the U/C_s rather high, then the pulse pressure increases, which result in a decreasing U/C_s. As the pulse propagates through the turbine the pressure ratio again decreases which result in an increasing U/C_s again. Since the rotor speed only fluctuates with about 1%, the speed is effectively constant. Thus the fluctuations in U/C_s only depend on pressure ratio fluctuations.

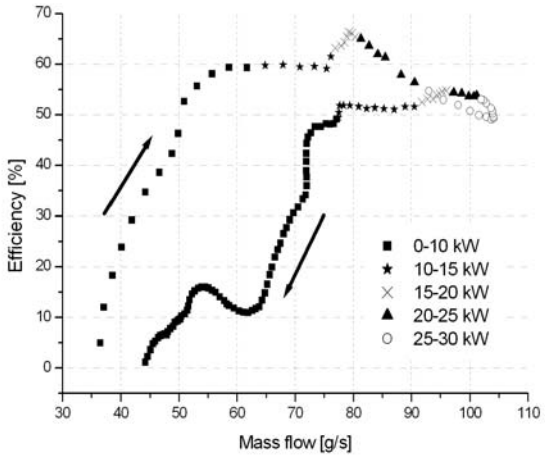

Figure 6.15. Trajectory of efficiency vs. mass flow traversed during one exhaust pulse. The different markers show how much isentropic power that is entering the turbine at every instant.

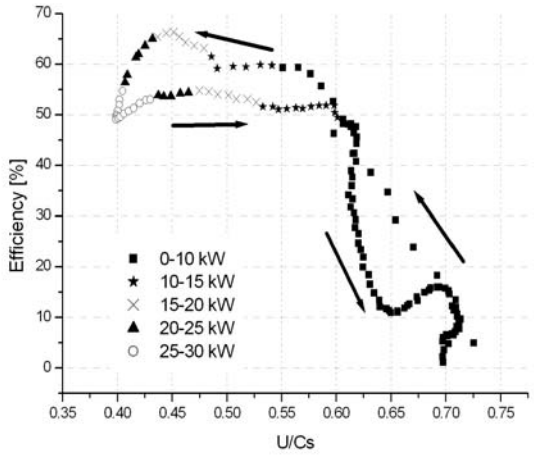

Figure 6.16. The trajectory of efficiency vs. BSR for one pulse differs quite much from the parabola expected for steady flow.

6.8 Discussion on accuracy

There are several uncertainties related to determining the instantaneous efficiency from on-engine measurements. The speed fluctuation of the turbocharger is quite even but the shape of the exhaust pulses differ between the cylinders and from cycle to cycle. The result is that efficiency curves like the one in figure 6.14 can show variations between cylinders and cycles. The cycle-to-cycle variations are avoided from averaging over several cycles. The variations between cylinders are due to different flow paths in the very asymmetric exhaust manifold and cannot be avoided on the engine. The result of this is that the variation of the efficiency with crank angle will be different for different exhaust pulses. However, judging from the efficiency trace for two cycles in figure 6.14, that does not seem to be a big problem in this case.

The data for the efficiency-calculations are averaged over 100 consecutive cycles of a steady state measurement on the engine. Some data is also taken from the simulations. In this way the data contains very little high frequency noise that might deteriorate the calculation results.

Furthermore there is the spatial problem resulting in the possible lag between inlet massflow, power production and outlet massflow, due to the control volume approach discussed above.

Last, the instantaneous massflow and temperature is taken from simulations since they cannot be measured. They are key values and there exist no other way of checking their accuracy than through the time-average values. Furthermore, GT-Power has a damping function included in the compressor model to make it more stable [6.13]. That might make the simulated mass flow to deviate from the map value. This might be an additional source of error.

6.9 Comments on the simulations

For the results presented in figures 6.12-6.16 the values 1.05 and 0.78 were necessary for the mass flow and efficiency multipliers in the simulations, respectively, for the turbine model to fit measurements at full load conditions, 2000 rpm. This means that the turbine on the engine has 5 % higher mass flow, i.e. swallowing capacity, and 22% lower efficiency, than what is measured for steady flow in the turbine map. These values for the multipliers are slightly different from what is presented in chapter 3. The reason for this is that the simulations presented in this chapter is older than the ones in chapter 3 and calibrated against an older measured data set, without measurements of the manifold wall temperature.

The software modeled the flow that is feeding the turbine very accurately. The turbine inlet pressure showed a very good fit throughout the entire simulation

run. For the turbine exit however the fit was quite poor. Poor modelling results of the turbine outlet pressure is of course a source of error, since the turbine output power is proportional to the pressure ratio over the turbine. However, when the largest part of the turbine power is delivered the inlet pressure is much higher than the outlet why the outlet pressure errors result in a limited error in the pressure ratio.

6.10 Conclusions

The efficiency measured during the peaks of exhaust flow was about 50-60%. This is not as bad as suspected, however significantly lower than the approx. 70% stated by the closest point in the TC manufacturer's steady state tests. The measured efficiency is thus about 15-30% lower than the efficiency in the steady flow maps. This corresponds very well to the efficiency multiplier of 0.78 used in the simulations. The on-engine measurement is thus proved to be a useful tool to investigate the turbine performance over the entire working range of the engine.

Furthermore these results show that it is necessary for the turbo manufacturers to provide more extensive maps to avoid having to depend on extrapolation. This is necessary in order to enable the modeller to make reasonably good predictions of engine-turbocharger systems. However, still a discrepancy in efficiency between the unsteady on-engine flow and the steady flow when measuring the maps may exist.

Different methods for CA-resolved analysis of the turbine efficiency were tested. It was shown that using time-averaged data is mathematically incorrect, integration of CA-resolved values is the only correct way of achieving an average value for turbine efficiency. The CA-resolved methods of turbine analysis are not sharp enough to give detailed information on the turbine's on-engine behaviour (with proven confidence). Method development is still needed for:

- compressor power
- bearing friction model
- Additional measured data at turbine inlet, T or $\dot{m}$ or P_{tot}.
- Turbine dynamometer

6.11 References

6.1 Ogink, Roy "Determination of the on-engine turbine efficiency of an automotive turbocharger" M. Sc. Thesis no. MMK 2000:49 MFM52 The Royal Institute of Technology [KTH], Dept. of Machine Design. Stockholm
6.2 Japikse D., Baines N. C. "Introduction to turbomachinery" Oxford 1997.
6.3 Winterbone D.E., Pearson R.J. "Turbocharger turbine performance under unsteady flow – a review of experimental results and proposed models" IMechE paper C554/031/98 1998
6.4 Greiner, Neise & Stöcker "Thermodynamics and statistical mechanics" Springer-Verlag New York 1995, ISBN 0-387-94299-8
6.5 Ehrlich Daniel "Characterization of unsteady on-engine turbocharger turbine performance" Ph.D. Thesis, Purdue Univ. USA 1998
6.6 King Aaron J "A turbocharger unsteady performance model for the GT-Power internal combustion engine simulation" PhD-Thesis Purdue Univ. USA 2002
6.7 Westin F & Ångström H-E "A method of investigating the on-engine turbine efficiency combining experiments and modeling" IMechE paper C602/029/2002
6.8 Winterbone D.E., Nikpour B., Frost H. "A contribution to the understanding of turbocharger turbine performance in pulsating flow" IMechE paper C433/011 1991
6.9 Dale A., Watson N. "Vaneless radial turbocharger turbine performance" IMechE paper C110/86 1986
6.10 Hu X., Lawless P. B. "Predictions of On-Engine Efficiency for the Radial Turbine of a Pulse Turbocharged Engine" SAE Paper 2001-01-1238
6.11 Chen H., Baines N.C. "The Aerodynamic Loading of Radial and Mixed-Flow Turbines" Int. J. Mech. Sci. Vol. 36. No. 1, pp. 63-79, 1994
6.12 Heywood John B. "Internal Combustion Engine Fundamentals" McGraw Hill International Editions ISBN 0-07-100499-8
6.13 GT-Power User's Manual and Tutorial, Version 6.0 March 2003. Gamma Technologies, www.gtisoft.com .

6.12 Appendix

6.12.1. Determination of thermodynamic properties in exhaust gas and air

c_p for the constituents in a gas mixture is each calculated from polynomial fits made in the NASA Equilibrium code referred to in Heywood p. 131 [6.12]

$$\tilde{c}_{p,i} = R_0\left(a_{i1} + a_{i2}T + a_{i3}T^2 + a_{i4}T^3 + a_{i5}T^4\right) \qquad \text{Hey eq. 4.39}$$

where R_0 is the gas constant with value 8.3143 J/(mole*K). The coefficients a_{ij} are taken from table 4.10 in Heywood. Tilde ~ is used to denote molar properties. For exhaust gas there are two temperature ranges for the two temperatures ranges 300≤T≤1000 and 1000≤T≤5000 K.

For a gas mixture the gas c_p is calculated from the individual $\tilde{c}_{p,i}$ and the molar fraction $\tilde{x}_i$:

$$\tilde{c}_p = \sum \tilde{x}_i \tilde{c}_{p,i} \qquad \text{Hey eq. 4.20b}$$

The molar masses are calculated for all constituents (M_i) and the gas mixture molar mass is calculated from:

$$M_{mix} = \sum \tilde{x}_i M_i \qquad \text{eq. 6.17}$$

The c_p is then calculated:

$$c_p = M_{mix}\tilde{c}_p \qquad \text{eq. 6.18}$$

For air this is done with the assumed composition of 21% O_2 and 79% N_2. Results are shown below.

The exhaust gas composition as a function of fuel/air equivalence ratio is taken from figure 4.23 in Heywood. Linear curve fits are made for the major constituents, only the rich side is of interest here. From ϕ between 1.1 and 1.3 the linear assumption has highest accuracy why it is from here the values for the fitting are taken.

Table 6.3.Composition of exhaust gas

Specie	**Conc. at λ= 0.909 [%]**	**Conc. at λ=0.769 [%]**
H_2O	13.93	13.71
CO_2	10.56	7.838
CO	2.559	6.653
H_2	1.077	3.421
O_2	0.5657	0.4579

Which results in:

$$[H_2O] = 1.57 \cdot \lambda + 12.5$$
$$[CO_2] = 19.4 \cdot \lambda - 7.11$$
$$[CO] = -29.2 \cdot \lambda + 29.1$$
$$[H_2] = -16.7 \cdot \lambda + 16.3$$
$$[O_2] = 0.770 \cdot \lambda - 0.134$$
$$[N_2] = 1 - ([O_2] + [H_2] + [CO] + [CO_2] + [H_2O])$$

The $\tilde{c}_p$ for these gases are calculated along with molar masses and c_p is calculated as above.

γ is calculated as:

$$\gamma = \frac{c_p}{c_p - R_0 / M_{mix}} \qquad \text{eq. 6.19}$$

Results

Table 6.4. Air properties.

T [K]	Cp [J/(kg*K)]	gamma
270	1010.1	1.399
280	1010.3	1.399
290	1010.6	1.399
300	1011.0	1.399
310	1011.5	1.398
320	1012.1	1.398
330	1012.8	1.398
340	1013.5	1.397
350	1014.4	1.397
360	1015.3	1.396
370	1016.4	1.396
380	1017.5	1.395
390	1018.7	1.394
400	1020.0	1.394
410	1021.3	1.393
420	1022.7	1.392
430	1024.2	1.391
440	1025.7	1.391
450	1027.4	1.390
460	1029.0	1.389
470	1030.8	1.388
480	1032.6	1.387
490	1034.4	1.386
500	1036.3	1.385

Table 6.5. Exhaust gas properties

Lambda=1.0			Lambda=0.9			Lambda=0.8		
T [K]	**c_p [J/(kg*K)]**	**gamma**	**T [K]**	**c_p [J/(kg*K)]**	**gamma**	**T [K]**	**c_p [J/(kg*K)]**	**gamma**
300	1070.6	1.371	300	1092.6	1.373	300	1115.8	1.376
400	1094.6	1.360	400	1114.6	1.363	400	1135.8	1.367
500	1122.4	1.347	500	1141.1	1.352	500	1160.8	1.356
600	1152.9	1.335	600	1170.6	1.340	600	1189.3	1.345
700	1184.6	1.323	700	1201.8	1.328	700	1219.9	1.333
800	1216.2	1.312	800	1233.1	1.317	800	1251.0	1.322
900	1246.3	1.302	900	1263.2	1.307	900	1281.0	1.313
1000	1273.6	1.294	1000	1290.5	1.299	1000	1308.2	1.304
1000	1273.6	1.294	1000	1290.5	1.299	1000	1308.3	1.304
1100	1297.3	1.287	1100	1314.3	1.292	1100	1332.3	1.297
1200	1318.9	1.281	1200	1336.1	1.286	1200	1354.3	1.291
1300	1338.6	1.276	1300	1356.0	1.280	1300	1374.4	1.285
1400	1356.4	1.271	1400	1374.1	1.276	1400	1392.7	1.280
1500	1372.6	1.267	1500	1390.5	1.272	1500	1409.3	1.276
1600	1387.3	1.264	1600	1405.4	1.268	1600	1424.4	1.272
1700	1400.6	1.260	1700	1418.9	1.265	1700	1438.1	1.269
1800	1412.5	1.258	1800	1431.0	1.262	1800	1450.5	1.266
1900	1423.3	1.255	1900	1442.0	1.259	1900	1461.7	1.264
2000	1433.0	1.253	2000	1451.9	1.257	2000	1471.8	1.261
2100	1441.7	1.251	2100	1460.8	1.255	2100	1481.0	1.259
2200	1449.6	1.249	2200	1468.9	1.253	2200	1489.2	1.258
2300	1456.6	1.248	2300	1476.1	1.252	2300	1496.7	1.256
2400	1463.0	1.247	2400	1482.7	1.251	2400	1503.4	1.255
2500	1468.7	1.245	2500	1488.5	1.249	2500	1509.5	1.253
2600	1473.8	1.244	2600	1493.9	1.248	2600	1515.0	1.252

Data from lambda 0.9 and 0.8 from this table is used and for each temperature linear interpolated to lambda 0.85. For the temperature range $300<T<1500$ a curve fit is done to the data. The result is seen in eq. 6.20 and figure 6.17.

$$c_p(T) = -0.0000001T^3 + 0.0002T^2 + 0.1188T + 1047.3 \qquad \text{eq. 6.20}$$

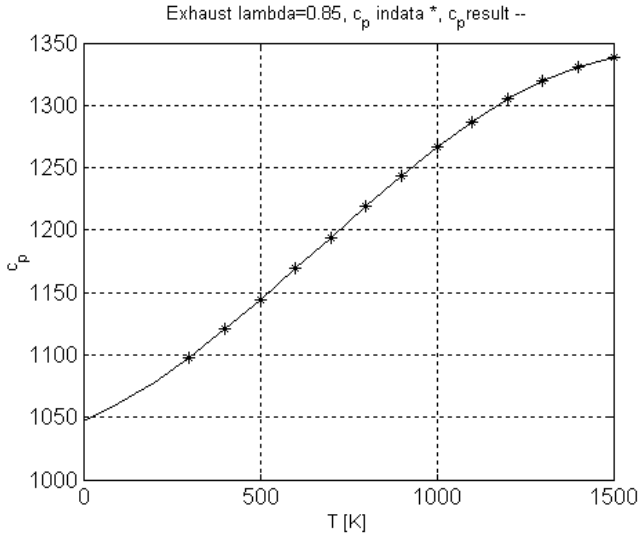

Figure 6.17. The polynomial fit to c_p for the exhaust gas, with the polynomial expression above.

Chapter 7

Heat transfer from the turbine

7.1 Introduction

Traditionally, heat losses from the turbine are neglected in turbomatching calculations as well as in engine simulations [7.1]. Ehrlich [7.2] found that the heat transfer played an important role even at a low output diesel engine. On the SI-engine, with it's high exhaust temperatures, the assumption of negligible heat transfer therefore might lead to errors in the calculations.

This chapter investigates how large portion of the calculation error that can be referred to neglected heat transfer. This is done by investigating the heat transfer situation around the turbocharger.

The engine model used is a well-calibrated GT-Power model [7.3] and the possibility of calculating the wall heat transfer is fully utilized.

7.2 Method

The method used to investigate the heat transfer situation in the exhaust-manifold and turbocharger area is to do measurements of gas and surface temperatures. This data is used to calibrate the simulation model. From the simulation model the various heat fluxes and powers are deduced.

7.2.1 Measurement equipment

The engine is the same as in the rest of this work. It's exhaust manifold is made of sand-cast inconel and is of compact shape. It maintains the cross section area from each individual cylinder runner to the turbine inlet and the total manifold volume is about half the total displacement volume of the engine.
In the test cell a fan is situated right underneath the manifold and turbo. The fan is an ordinary radiator cooling fan from a car. It blows air straight upward in order to circulate the air around the manifold to prevent cables and other sensitive equipment from being damaged by the heat. The turbine is most impacted by the cooling airflow stream. The velocity was measured pointwise with a Prandtl-tube on several locations across the flow path, and the flowfield was found to be non-homogeneous with velocity varying between 6-8 m/s. No effort was put into trying to copy the flow conditions occurring in a vehicle.
All measurements and simulations, in this chapter are conducted at 1600, 1800 and 1950 rpm. The reasons for limiting the investigation to these low speeds are that low-end torque is of main interest, and in order for the results to be comparable to the authors' other work on the subject [7.3, 7.4].
The gas temperature in the manifold was measured with a shielded K-type thermocouple, 3 mm diameter. It has been shown that heat transfer through the stem of the thermocouple can be a significant source of error [7.5]. In order to avoid heat conduction from the measurement tip to the colder manifold wall via the stem the turbine inlet gas temperature thermocouple was positioned with a very long insertion length. It protrudes approx. 33 diameters into the exhaust pipe from the location where it penetrates the manifold wall. The measurement tip is positioned at the location of the manifold-turbocharger flange. At this flange a radiation shield is positioned around the thermocouple tip eliminating heat transfer through radiation from thermocouple tip to manifold wall. This combination of very long insertion length and radiation shield was proven in an earlier chapter to give a measured value right between the time- and mass-averaged gas temperatures, which are only 15K apart [7.3]. Thus a correction of the measured value has not been considered necessary. The turbine outlet gas temperature thermocouple was positioned in the exhaust manifold approx. 150 mm downstream of the turbine wheel outlet.
The surface temperatures were measured with K-type thermocouple wires held against the outer wall surface with welded M8-nuts with very short screws (not protruding out from the nut at all). This surface temperature was double-checked with a hand-held IR (infrared) thermometer. The white arrows in figure 7.1 indicate the locations of the surface temperature measurements. The location close to the turbine is positioned 50 mm from the turbine inlet. The location closest to the cylinder head is indicated by the right arrow, but hidden

behind a pressure transducer in the picture. It is positioned 50 mm from the cylinder head. A schematic picture of the sensor locations can be viewed in figure 7.2.
The IR-thermometer also had a thermocouple for surface temperature measurements. This enabled the measurement of the outer wall surface emissivity. It showed that the emissivity had the value 1 at temperatures well below temperatures where the manifold started to emit visible radiation. For more information about exhaust gas temperature measurements see [7.3, 7.4].

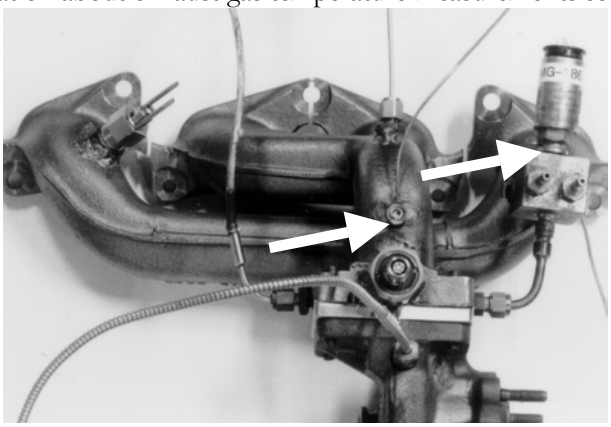

Figure 7.1. The surface temperature measurement locations are indicated by the arrows. The rightmost position hidden behind the pressure transducer.

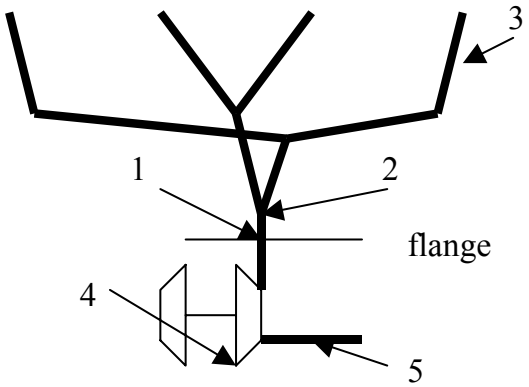

Figure 7.2. Schematic sketch of the temperature measurement locations. 1 is gas temperature at turbine inlet, 2 exhaust manifold wall temperature close to turbine, 3 exhaust manifold wall temperature close to the cylinder head, 4 turbine housing wall temperature, 5 gas temperature at turbine outlet.

Heat loss measurements

The heat losses were assumed to be of 3 kinds: radiative, convective and conductive. The heat transfer to water and oil was measured through flow and temperature measurements. The flow was measured with positive displacement flow meters of oval gear type [7.6]. The output signal from the meter is digital and the sizes were chosen so that the lubrication oil meter gives 1000 pulses per litre and the water meter gives 400 pulses per litre. The inaccuracy is ±1% according to the manufacturer. The temperatures before and after the turbo were measured with Pt100-probes positioned in special made metering blocks positioned on the fluid pipes feeding the turbo. To avoid heat transfer to these pipes, between the measurement position and the entrance to the turbocharger's bearing housing, the pipes were insulated. The measurement equipment can be seen in figure 7.3.

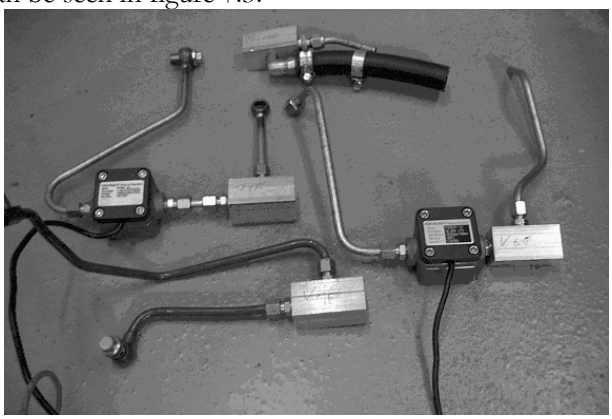

Figure 7.3. The equipment used for measuring the flow rate and temperature rise of the turbocharger's oil and water.

Volumetric flow measurement of oil and water can only be accurate if no gas is dissolved or dispersed in the fluid. Even though the flow meter was positioned upstream of the turbocharger, exhaust gas could possibly slip through the oil seals into the oil and stay dispersed there, thus ruining the volumetric flow measurements. To check that this did not occur, an oil sample was taken from the turbocharger's oil return line during engine operation. An equal oil sample was taken, for comparison, from the oil pan, before the engine had been run that day. The two samples were allowed to stand in bottles without the caps on, and the difference in surface height in the bottles was measured. If exhaust gas had leaked into the turbo return oil, that oil would decrease in volume faster than the sump oil as the exhaust gases were released from the oil to the atmosphere. However, the height of the surfaces only decreased very little over several days, and equally in the two samples. The reason for that was assumed

to be evaporation of light fractions of the oil. The conclusion was drawn that no exhaust gas leaked into the oil in the turbocharger.
The heat lost to the fluids were calculated from:

$$\dot{Q} = \dot{\Phi} \cdot \rho \cdot c_p \cdot \Delta T \qquad \text{eq. 7.1}$$

Where $\dot{\Phi}$ is the volumetric flowrate, ρ is the density, c_p specific heat and ΔT is the temperature increase over the turbo. Radiative heat transfer from the bearing housing was neglected and thus assumed to be emitted from the turbine housing only. It was calculated from Stefan-Boltzmann's law:

$$\dot{Q}_{rad} = \varepsilon \cdot \sigma \cdot A_{turb,surf} \cdot T^4_{turb,surf} \qquad \text{eq. 7.2}$$

Where $\varepsilon=1$, $\sigma=5{,}67 \cdot 10^{-8}$ W/(m²K⁴), $A_{turb,surf}$ the outer surface area of the turbine housing. $A_{turb,surf}$=0,033 m² (estimated from dividing the turbine housing into known geometrical bodies whose area could be calculated from length dimensions. The inaccuracy is estimated to ±10%)
Conductive losses were calculated from Fourier's law:

$$\dot{Q} = \frac{\lambda \cdot A_{cond}}{l} \cdot \Delta T = K_{cond} \cdot \Delta T \qquad \text{eq. 7.3}$$

Where λ is the heat conductivity, l the conduction length and A the conduction area. Conduction occurs from the turbine housing to the manifold and the exhaust pipe as well as to oil and water. Heat losses to oil and water are measured directly, therefore this formula is not needed for that mechanism.
Convective heat losses were calculated from Newton's cooling law:

$$\dot{Q} = \alpha \cdot A_{conv} \cdot \Delta T_{conv} = a \cdot \Delta T \qquad \text{eq. 7.4}$$

Both conductive and convective heat transport equations contain coefficients (heat conductivity λ, heat transfer coefficient α) which are difficult, or impossible, to measure directly. Furthermore, the areas in both equations are difficult to obtain. This applies especially to the convection area since the convective properties will vary significantly depending on the location. For instance, different behaviour on up- or down-side of the pipe is expected. For simplicity another approach is taken here; λ, l & A_{cond} and α & A_{conv} are

lumped together, respectively, and considered as one constant each, according to eq. 7.3 and 7.4.
To determine the convective constant a, a cool-down test was done. The procedure for doing that is to run the engine until steady state temperature occurs. The engine is then shut off and allowed to cool down as the temperature is measured. Heat loss to water and oil can be neglected since no flow occurs when the engine is not running. The heat loss to the exhaust pipe downstream of the turbine is also neglected due to small temperature differences and small heat conduction cross section in the exhaust pipe. Then the heat transport from the turbine housing can be treated with a node-model, see figure 7.4.
Then the heat transport between the three parts can be described with the equation:

$$\underbrace{\frac{(\alpha A)\cdot \Delta T_{env}}{c\cdot m_{turb}}}_{\text{Convection to environment}} + \underbrace{\frac{\left(\frac{\lambda A}{l}\right)_m \cdot \Delta T_m}{c\cdot m_{turb}}}_{\text{Conduction to manifold}} + \underbrace{\frac{\left(\frac{\lambda A}{l}\right)_b \cdot \Delta T_b}{c\cdot m_{turb}}}_{\text{Conduction to bearing hou sin g}} = \left(\frac{dT}{dt}\right)_{turb} \qquad \text{eq. 7.5}$$

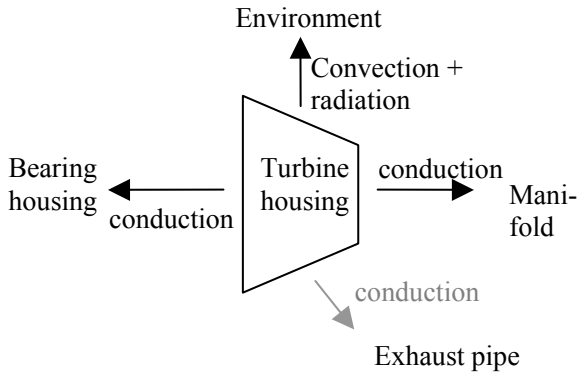

Figure 7.4. The heat transfer described as a node model between the turbine housing, manifold, bearing housing and environment. All parts are described as uniform nodes with constant properties throughout.

For the conduction from turbine housing to manifold eq. 7.3 is used directly. The cross section area for the conduction path is max $3*10^{-3}$ m², the heat conduction coefficient λ=45 W/(m*K) [7.8] and the length of the conduction path is approx. 0.1 m. Thus the lumped conduction coefficient, K_{cond_m}=1.35 [W/K] for the conduction from turbine housing to manifold.

This method may seem rather crude. However, the temperature difference between turbine housing and manifold is quite small during operation and hence this heat transport never will play a major role.
Similarly, the conduction between the turbine housing and bearing housing can be expressed by eq. 7.3. However, in this case a direct measurement of the added heat exists.
The conduction to the bearing housing could be derived from the measured heat loss to oil and water. If it is assumed that heat is added to water and oil through heat conduction from the turbine and through friction in the bearings, the power added to oil and water from conduction can be expressed as:

$$P_{cond\_bearing\_hou\sin g} = P_{meas\_oil\_water} - \frac{1-\eta_{mech}}{\eta_{mech}} P_{compressor} \qquad \text{eq. 7.6}$$

Thus equating eq. 7.3 and 7.6 gives $K_{cond}=P_{cond\_b}/\Delta T$ and is calculated from values measured on the running engine.
Thus, eq. 7.5 reduces to:

$$a \cdot \Delta T_{env} + K_{cond\_b} \cdot \Delta T_b + K_{cond\_m} \cdot \Delta T_m = c \cdot m_{turb} \left(\frac{dT}{dt} \right)_{turb} \qquad \text{eq. 7.7}$$

By using a cool-off test the constant a can be calculated directly from eq. 7.7. If eq. 7.7 is solved for a it is obvious that the derivative of the turbine housing wall temperature is a very central parameter. The measured temperature curve has too much noise to give a stable derivative. Therefore, to achieve a stable value for the derivative, a polynomial of 5th order is least square fitted to the measurement curve and then the derivative of the polynomial is used. The temperatures measured during the cool-off test are displayed in figure 7.5.
This method has a big drawback. Even though the residual of the least square fit is well within measurement accuracy (say 1 K) the derivative can vary significantly depending on the result of the fit. The polynomial resulting from the fit can be different depending on the width of the time interval over which the polynomial is fitted. Thus, this method cannot give a value for a with a particularly high accuracy. Fortunately, even accuracies only slightly better than just the order of magnitude can give valuable information in this case. The results are presented in table 7.1. With this experimentally determined a the convective losses can be calculated with eq. 7.4 and the radiative losses from eq. 7.2, both using outer wall temperature.

Table 7.1. Experimentally determined lumped heat transfer coefficients.

Coefficient	[W/K]
$a = \alpha A$	3.7
K_{cond_m}	1.35
K_{cond_b}	0.22

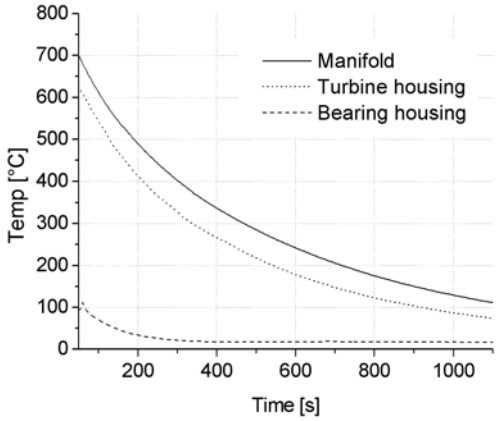

Figure 7.5. The temperatures measured during the cool-off test.

Surface roughness measurement

For more accurate simulations of the heat transfer from the exhaust gas to the manifold wall the surface roughness of the manifold inner wall was measured. The equipment used was a Taylor-Hobson Form Talysurf surface roughness meter [7.7]. The resolution of the instrument was 10 nm and the tip of the measurement point had a radius of 0.002 mm. A manifold, which had been used on an engine, was cut open and three measurements of each 35 mm length were done.

GT-Power requires the surface roughness data as sand surface roughness. The sand roughness is estimated from the surface topology measurements in figure 7.6 to 0.10-0.12 mm. Sensitivity analysis in GT-Power showed that a difference of 0.01 mm in the surface roughness input gives negligible differences in the heat transfer results. Therefore this visual estimate of the sand surface roughness was assumed sufficient.

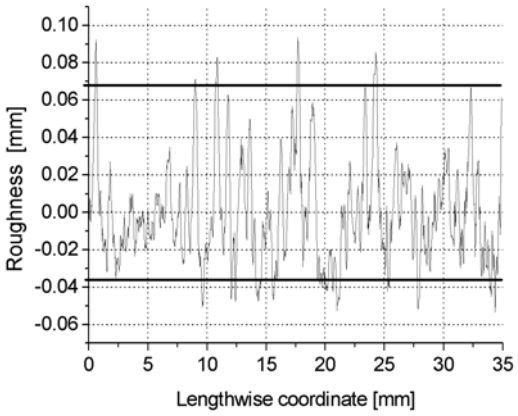

Figure 7.6. Measurement results from one of the measurements of the surface roughness.

7.3 Simulations

7.3.1 Engine simulation model

The engine was simulated in GT-Power v. 6.0. The model has been worked on for a long time and it is well adjusted against measurement data, as described in previous chapters . The engine is modelled with the Wiebe-function adapted to measurement data for the combustion, turbocharger data is from standard turbocharger supplier's maps. For this investigation, exhaust wall temperature modelling was added to the exhaust manifold.

Heat transfer and wall temperature model

The wall temperature model's parameters had to be adjusted in order for the simulation results to equal measured data. Different parameters govern different mechanisms in the process.

In the software the user can adjust the heat transfer from the fluid to the wall through a heat transfer multiplier. Also the wall surface roughness plays a role, and this parameter can also be used as an adjustment factor if it isn't known. The heat transfer from the outer wall to the surroundings is governed by a convection multiplier, the ambient air temperature and the radiation sink temperature. The latter is the temperature of the surrounding objects to which radiative heat transfer occurs, which in this case have little influence on the heat transfer due to the T^4 dependence. Furthermore, heat is conducted from the manifold to the cylinder head through the exhaust manifold flange/gasket. This

heat transfer is modelled as a contact resistance with the unit [K/W], the value 0.5 K/W was used throughout.
Due to the cooling fan installed in the test cell the turbine housing and the rest of the manifold is exposed to very different convective cooling. Therefore different values for the convective coefficient were used for turbine housing and the rest of the manifold.
These model variables had to be adjusted against measured data to give good results. Experience showed that the gas temperature at manifold outlet (turbine inlet) was mainly governed by the heat transfer multiplier at the gas to inner wall surface. Thus this value was adjusted to give gas temperatures within 1-2% of measured results. Then the convection multipliers and the manifold gasket contact resistance were adjusted to give accurate wall temperatures. A small change in gas temperature could give large changes in wall temperatures due to much larger thermal power in the gas flowing through the manifold than the power flowing through the walls as heat conduction.
1D software always divides every pipe into sub-volumes for which the governing equations are solved. In these sub-volumes all parameters such as temperature, pressure, wall temperature etc. are assumed constant. Normally the discretisation length for the exhaust side is approximately half the cylinder bore. However, measurements with the hand-held infrared thermometer during full load operation showed that the lengthwise gradient of the outer wall surface temperature was very large, it could be as large as 50-100 K per 10 mm, therefore 10 mm discretisation length was used for the exhaust manifold.
The simulation model of the wall temperatures can be seen as a node model where power is added from the gases and the heat transfer multiplier is the control valve. Power is then tapped off to the surroundings, where the convective multiplier is the control valve, to the cylinder head, where the contact resistance is the control valve, and then some minor heat flow between manifold and turbine housing. These control valves in the model, 4 in total, must thus be more or less manually adjusted.

Turbine heat loss

In GT-Power the turbine model does not have a volume, therefore the volume of the turbine volute has to be added before the turbine model, as a pipe. Thus in the engine model the actual turbine is modelled with two parts, a pipe part (the volute) and a turbine part, see figure 7.7. The turbine part consists of the maps and is where the work is extracted from the gas. In this paper, the turbine inlet properties are regarded as the properties before the pipe part constituting the volute.
The measured heat losses from the turbine to the surroundings could very easily be input to GT-Power. The calculation of heat transfer from gas to the

inner wall was removed by setting the heat transfer multiplier in the turbine volute to zero. Instead the volute was divided in two sections (lengthwise) and a power addition object was inserted between the two pipes. The power addition object allowed for a negative power addition to be imposed to the gas, thus simulating the measured heat loss. Thus the heat addition will not affect what is here denoted as the turbine inlet temperature, since turbine inlet conditions are upstream of the heat addition object.
Removing all heat losses before the turbine object in GT-Power is justified by the fact that the turbine model in GT-Power is only a power extraction device governed by the map, similar to the wheel in the real turbine. The power losses in the real turbine are mainly conduction from gas to wall of the turbine housing, and possibly some minor heat transfer from gas to the turbine wheel. Almost all power added to the walls is thus taken from the gas before it is entering the wheel.

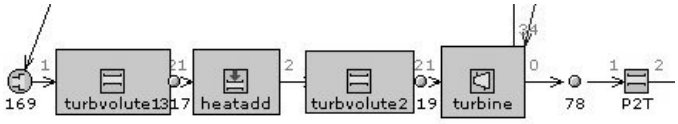

Figure 7.7. The turbine modelled with a turbine object and the volute with heat transfer modelled as two pipes and a heat addition object.

7.4 Results

7.4.1 Simulation of wall and gas temperatures

First the results from the simulations of the wall temperature alone, without incorporation of turbine heat losses, are displayed. All three wall temperatures measured on the engine could be copied in the simulations, with appropriately set heat transfer parameters (described above). In figure 7.8 the wall temperatures for the two locations on the manifold are presented. For the location close to the cylinder head the gradients were so large that the actual location of the temperature measurement, along the direction of flow, is a source of inaccuracy. Measurements with the hand-held IR thermometer indicated gradients approaching 100 K/cm along the direction of flow. Therefore temperature differences of a few 10 K can be due to the uncertainty in the location of temperature reading (measurement or simulation output).

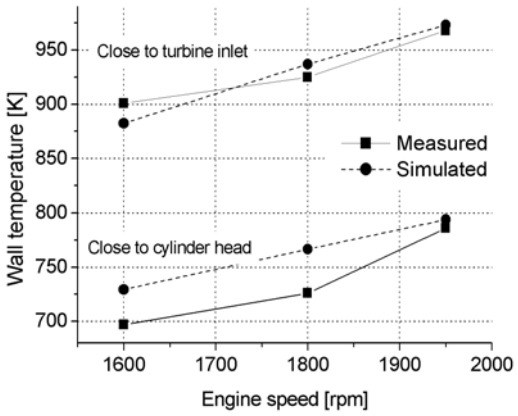

Figure 7.8. Comparison between measured and simulated exhaust manifold wall temperature.

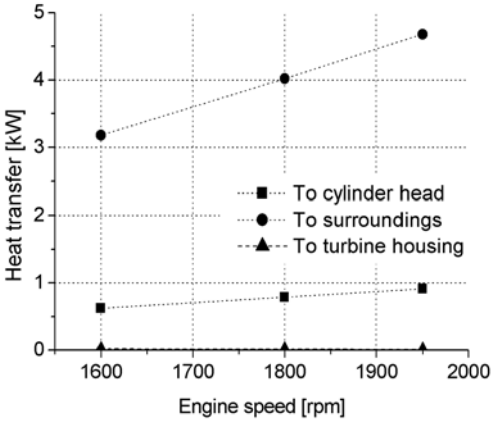

Figure 7.9. Simulated heat transferred from the manifold to it's neighboring components and to the surroundings.

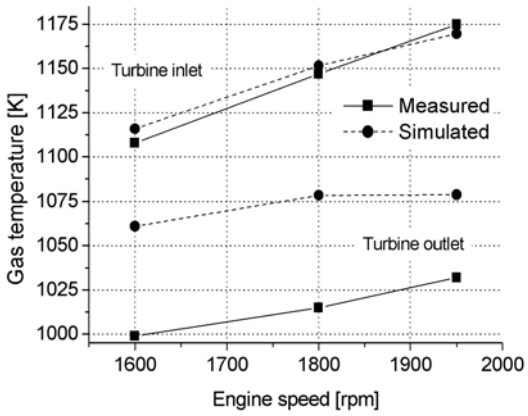

Figure 7.10. Comparison between measured and simulated turbine inlet and outlet gas temperature. Note that heat losses from the turbine are not taken into account here.

In figure 7.9 the heat transferred from the manifold for the various heat transport ways are presented. This data set is purely simulated. The heat transferred to the turbine housing is not absolutely zero, but very low since the temperature difference is low.
For the gas temperatures in the exhaust manifold, only measurements from two locations, before and after the turbine, exist. The turbine inlet temperature could be adjusted to a good fit between simulation and measurement, as figure 7.10 shows. However, at the turbine outlet the temperature is approx. 50 K too high in the simulations. Note that this is when the heat losses from the turbine are not accounted for. Cases with the heat loss included are covered below. Note that the turbine inlet temperature will not be affected by insertion of heat transfer in the model. The turbine inlet temperature is measured before the turbine volute while the heat losses are inserted in the volute.

7.4.2 Turbine heat loss

Measurement data

With the method presented here, the heat transfer to the turbocharger's oil and cooling water could be measured directly. Through surface temperature measurements, the heat transfer to the surrounding air via convection, radiation and conduction to the manifold and the bearing housing could indirectly be measured. In figure 7.11 the total heat loss for the three speeds are presented.

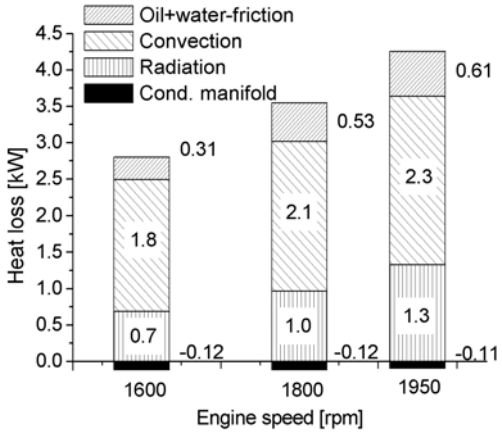

Figure 7.11. Heat losses for every transport path for three speeds.

It is obvious that the conductive heat transfer to oil and water and to the exhaust manifold is negligible. The power loss is totally dominated by the convection and the radiation.
The total heat loss is smaller than the power required to power the compressor, but of the same order of magnitude. However, the heat losses are much smaller than the total thermal power available at the turbine inlet. The thermal power is calculated from eq. 7.8.

$$P_{thermal} = \dot{m} c_p \left(\overline{T}_{turbine-inlet} - T_{env} \right) \qquad \text{eq. 7.8}$$

It might seem crude to calculate the thermal power from average properties. However, a test calculation was made where simulated, instantaneous values were used, and the power was integrated from these values and no significant difference from the average values could be seen.
Figure 7.12 shows the thermal power available at turbine inlet and outlet, compared to the compressor power and the heat losses. The power utilized by the turbine is therefore almost negligible compared to the available thermal power.

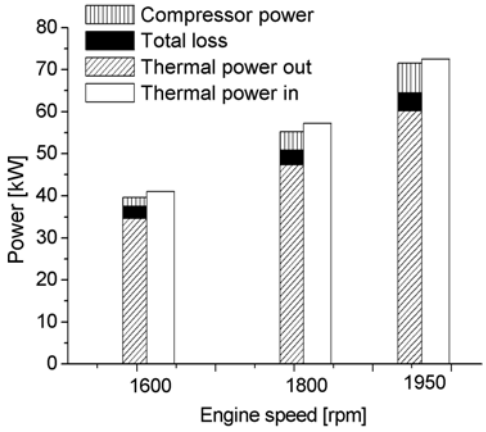

Figure 7.12. The total power fluxes through the turbine for three speeds.

An estimate was also done of how large the heat transfer can be through the shaft of the turbocharger from turbine to the oil and water, or to the compressor. To be able to do this, assumptions regarding the rotor temperature had to be made. The assumptions made were that the turbine temperature was the geometric average of turbine gas inlet and outlet temperature, the compressor wheel temperature was assumed to be equal to the compressor air outlet temperature. The heat transported through the shaft, see figure 7.13, can be developed from Fourier's law (eq. 7.3) to the expression:

$$\dot{Q} = \lambda_{shaft} \frac{T_{TW} - T_{CW}}{\frac{\delta_1}{A_1} + \frac{\delta_2}{A_2}} \qquad \text{eq. 7.9}$$

Where λ_{shaft} =55 [W/(m*K)] [7.8].
The resulting power transmitted is approx. 30W for the three engine speeds covered in this paper. With a specific heat capacity for air of 1.00 kJ/(kg*K) and a mass flow rate of about 0.050 kg/s, the power required to heat the air in the flow 1 K is 50 W. The measured power of 30 W is therefore negligible compared to the power required to drive the compressor and should not affect the compressor efficiency noticeably (1 K of compressor outlet temperature makes less than 1 %-point in compressor efficiency). In figure 7.14, the measured compressor efficiency is compared to the efficiency used by the simulation software from the map when simulating the same cases. The

software seems to over-predict the compressor efficiency for 1600 rpm and under predict for 1950 rpm. A reason for this can be heat transfer. The results indicate that for 1600 rpm, heat is added to the compressor, probably due to conduction from the bearing housing, but also from radiation from the turbine housing. Measurement with the hand-held infrared thermometer during full load operation gave much higher temperatures on the compressor housing surface facing the turbine than the surface facing the opposite direction. This indicates that the radiative thermal loading is high. For 1950 rpm on the other hand the measured efficiency is higher. This indicates that heat is transported from the compressor to the surrounding, probably only through convection. The compressor outlet temperature is also higher for higher speed, which enhances heat transfer to the surroundings from the compressor. The curves measured and simulated compressor outlet temperature and efficiency should cross each other at the same speed, but in figure 7.14 that is not the case. The reason for that is a combination of things: The method of averaging the efficiency is different between measurement and simulation. In the simulation the efficiency is mass averaged instantaneous efficiency, from instantaneous values of temperature and pressures. The measured efficiency however, is a calculated figure from measured time-average of pressure and temperature measured with a thermocouple, which is somewhere in between time- and mass averaged.
The measurement inaccuracy of the inlet and outlet temperature is estimated to app 1-2K, and that will affect the efficiency calculated from measured values by 1-2%-points.

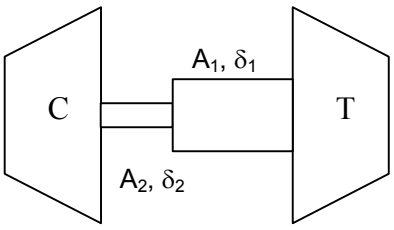

Figure 7.13. The geometry over which heat is conducted from turbine wheel to compressor wheel.

This influence on the compressor efficiency from heat transfer from and to the surroundings have also been detected by Baar & Lücking [7.9] who investigated the influence from free and forced convection on the turbocharger, and Pucher & Nickel [7.10] who investigated the compressor and turbine efficiency as functions of turbine gas inlet temperature.
An equal calculation as for the conduction from turbine wheel to the compressor wheel is made with assumed heat transfer from turbine wheel through the shaft to the oil in the bearing housing. The assumed shaft temperature is equal to outlet oil temperature. The result from such a calculation is approx. 70 W for all three speeds.

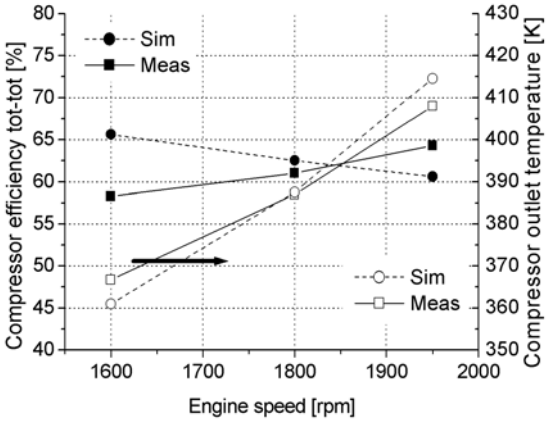

Figure 7.14. Comparison between measured compressor efficiency and value read from the map as well as comparison between measured and simulated compressor outlet temperature.

In figure 7.15 the measured heat added to the oil in the bearing housing is compared to the friction power in the bearings (which is assumed to be totally absorbed by the oil) and the estimated heat conduction from turbine wheel to the oil via the shaft. It is clear that the sum of the friction and shaft-conduction power is equal to the measured power added to the oil. This indicates that all heat added to the oil comes from the shaft and friction; no conduction via housing reaches the oil. All power conducted to the bearing housing must then be absorbed by the water.

Simulation results

The measured heat losses presented above are inserted as heat losses from the turbine in the simulation model. When the turbine map was measured heat would have been lost to the surroundings via radiation and free convection, and that heat loss is incorporated in the efficiency values in the turbine map.

However, when the turbine is used on the engine the temperatures are much (at least 50%) higher, and forced convection is present. Therefore it is assumed here that the heat transfer present when the maps were measured is negligible compared to the heat losses on the engine. It would be preferable if heat loss information would be enclosed with the map. That would enable incorporation of only the difference in heat loss between on-engine condition and map-measurement conditions.
One way of comparing the simulation results with and without heat losses taken into account is to look at the turbine outlet temperature. For all simulations done without the turbine heat losses taken into account, the turbine outlet temperature has been around 50K too high, as could be seen in figure 7.10. This indicates that there is a heat loss in the real case that is not included in the simulation. In figure 7.16 the measured and simulated turbine outlet temperatures are displayed, now also with heat losses included. When the measured heat losses are incorporated in the simulation, the turbine outlet temperature approaches the measured value, but is still not low enough. The simulated heat losses were then further increased until the measured and simulated turbine outlet temperatures equalled. The heat losses imposed on the turbine in the simulations in this case were 35%, 29% and 8% higher than the values measured for 1600, 1800 and 1950 rpm respectively.

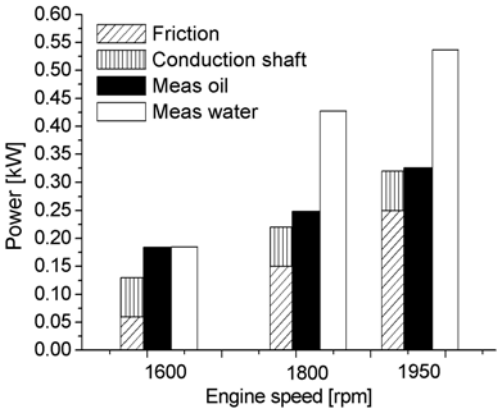

Figure 7.15. The measured heat added to the oil and water is compared to the estimated heat addition to the oil from bearing friction and conduction from turbine wheel to oil via the shaft.

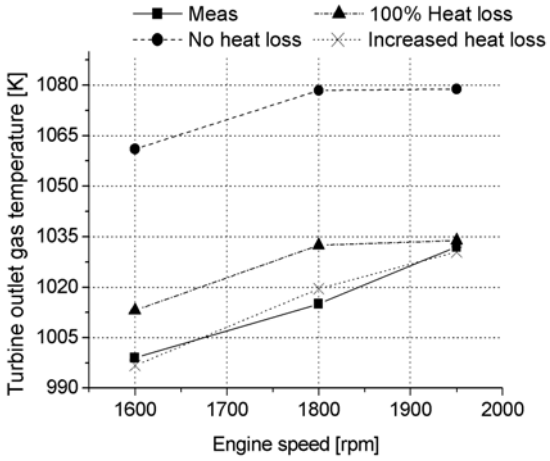

Figure 7.16. Measured and simulated turbine outlet temperature for three simulated and one measured case. 100% heat loss is where heat loss is equal to measured and increased heat loss is when heat loss is adjusted so that turbine outlet temperature is equal in simulation and measurement.

Inserting a heat loss in the turbine volute will affect the turbine wheel inlet temperature, but not the turbine inlet temperature, according to the explanation above. Different turbine wheel inlet temperature will affect the turbine power, and thus the turbocharger speed. To compare the results achieved with heat transfer taken into account with the results achieved when the heat transfer is neglected, both simulation cases were setup so that the turbine efficiency was adjusted until measured turbine speed was achieved. Then the difference in the simulated mass-flow averaged turbine efficiency is a measure of how much the model's predictability is improved when taking heat transfer into account. The software reads the instantaneous operation point in the map for every time step in the simulation, calculates a mass flow and from that calculates a mass-averaged turbine efficiency.
In figure 7.17 below the used average turbine efficiencies are displayed for the three speeds. For comparison the average value read directly from the turbine map is displayed (the value used if the turbine efficiency multiplier would have been 1).

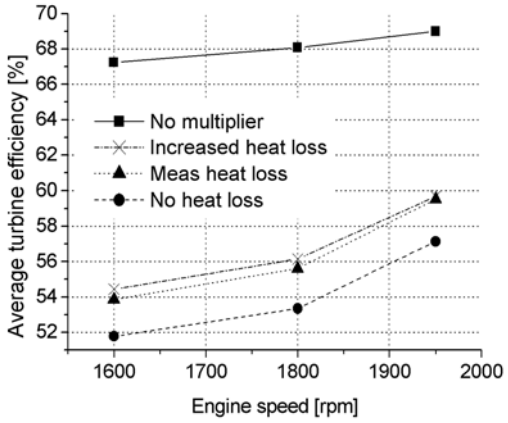

Figure 7.17. The average turbine efficiency necessary to meet measured turbine speed for the three different cases. For comparison, the turbine efficiency that should have resulted if the correction factor would have been 1, is included (no multiplier).

Here a comment on turbine efficiencies is needed. The efficiency the software reads from the map is values that are extra- and interpolated from the (quite few) map points the turbocharger manufacturer has measured. Thus it is absolutely not necessarily the correct efficiency, for reasons described in Chapter 2.
The aim of this investigation was to see if the heat losses could be attributed for a major part of the calculation error in turbine power. The conclusion is that that is not the case.

7.5 Conclusion

This combined measurement and simulation work shows that the turbine outlet temperature cannot be accurately simulated without taking the heat transfer from the turbine to the surroundings into account. The investigation shows that several kW can be lost in the turbine and the simulated outlet temperature thus differ by around 50 K from measured if the losses are not accounted for.

Heat transfer from the turbine to the compressor can deteriorate the compressor efficiency. At least for cases where the compressor outlet gas temperatures are moderate, that is for cases when maximum boost pressure is not developed. However, for cases with high compressor outlet temperature the compressor efficiency might be better than in the map. This indicates that heat is lost from the compressed air in the compressor to the surroundings through the compressor casing, and in a larger extent in these measurements than when the maps were measured. Forced convection is probably the reason for the difference.

The main transport mechanisms for the turbine heat losses are convection and radiation. The conduction to bearing housing (and manifold) is significantly smaller.

The heat added to the oil is equal to the sum of the power dissipated in the bearings and the estimated heat transferred trough the shaft from turbine wheel to the oil. Thus the oil seems to be heated by these mechanisms alone. Therefore the heat conducted from the turbine housing to the bearing housing can only be absorbed by the water or conducted to the compressor.

Including the heat losses from the turbine in the simulations reduces the magnitude of the correction factor for turbine efficiency necessary in order to give turbine speed equal to measured. However, only a fraction of the gap between the turbine efficiency necessary in the simulations and the efficiency stated by the map is reduced with the heat losses included. Thus, the main reason for the discrepancy in turbine power is something else than heat transfer.

7.6 Abbreviations

a lumped radiation parameter
A_{cond} cross section area over which heat is conducted [m²]
A_{conv} area over which convection occurs [m²]
A_i shaft cross section area i [m²]
$A_{turb,surf}$ outer surface area of the turbine housing [m²].
c heat capacity of the turbine housing [J/(kg*K)]
c_p heat capacity (at constant pressure) [J/(kg*K)]
K_{cond_b} lumped conduction parameter, to bearing housing
K_{cond_m} lumped conduction parameter, to manifold
l distance between the two points between which conduction occurs [m]
$\dot{m}$ average mass flow rate [kg/s]
m_{turb} mass of the turbine housing [kg].
P power [W]
$\dot{Q}$ heat flux [W]
T_{CW} compressor wheel temperature [K]
T_{env} environment temperature [K]
T_{TW} turbine wheel temperature [K]
$\overline{T}_{turbine-inlet}$ measured average temperature at turbine inlet and outlet respectively [K]
$T_{turb,surf}$ surface temperature of the turbine housing [K]
α convective heat transfer coefficient [W/(m²*K)]
δ_i length of the turboshaft section i [m]
ΔT_b temperature difference between bearing housing and turbine housing wall temperatures [K]
ΔT_{env} temperature difference between environment air and turbine housing wall temperatures [K]
ΔT_m temperature difference between manifold and turbine housing wall temperatures [K]
ε emissivity [-]
$\dot{\Phi}$ volumetric flow rate [m³/s]
λ heat conductivity [W/(m*K)]
η_{mech} turbocharger mechanical efficiency [-]
ρ density [kg/m³]
σ Stefan-Boltzmann's constant [W/(m²K⁴)]

7.7 References

7.1 Watson N, Janota M S "Turbocharging the Internal Combustion Engine" MacMillan Press 1982 ISBN 0 333 24290 4.
7.2 Ehrlich, Daniel "Characterization of unsteady on-engine turbocharger turbine performance" Ph.D. Thesis, Purdue Univ. USA 1998
7.3 Westin F, Ångström H-E "Simulation of a turbocharged SI-engine with two software and comparison with measured data" SAE Paper no. 2003-01-3124.
7.4 Westin F "Accuracy of turbocharged SI-engine simulations" Licentiate Thesis KTH Machine Design Trita-MMK 2002:18, ISSN 1400-1179
7.5 Odendall B "Fehlerbetrachtung bei der Messung von Gastemperaturen" MTZ no. 3 2003, pp. 196-199
7.6 http://www.macnaught.com.au/m_series.htm
7.7 http://www.taylor-hobson.com/talysurfpgi.htm
7.8 Tefyma - Handbook for technology, physics and mathematics, available in Swedish only ISBN 91-87234-13-0
7.9 Baar R & Lücking M "Anforderungen an zukünftige PKW-Aufladesysteme auf Basis der Energiebilanz eines Turboladers" 8. Aufladetechnische Konferenz, 1-2 2002 October at TU-Dresden
7.10 Pucher H & Nickel J "Vermessung erweiterter Kennfeldbereiche von Fahrzeugmotoren-Turboladern" 8. Aufladetechnische Konferenz, 1-2 October 2002 at TU-Dresden
7.11 Winterbone D.E., Pearson R.J. "Turbocharger turbine under unsteady flow – a review of experimental results and proposed models" ImechE paper C554/031/98 1998
7.12 Winterbone D.E., Pearson R.J. "Theory of Engine Manifold Design" ISBN 1-86058-209-5

Chapter 8

Calculation accuracy of pulsating flow through the turbine of SI-engine turbochargers

8.1 Introduction and scope

Turbocharging can both increase the power density of an engine as well as decrease the fuel consumption of a vehicle. However, to fully explore the potential, some problems must be overcome during the development of the engines. For low engine speeds, turbocharged engines often have less torque than N/A-engines with comparable peak torque and speed. For the highest speeds, the maximum power of the engine is limited by turbine inlet temperatures. In addition, especially for low engine speeds, the turbocharged engine has slower transient response than a naturally aspirated engine. All of these issues are related to the gas exchange process of the engine and selection of turbocharger components. To optimise this process, virtually all engine manufacturers use 1-D engine simulation codes. Unfortunately these simulation codes, for certain engine modes, have problems in accurately predicting the performance of the engine.

For the mid-speed region, where the wastegate is open, the codes have reasonable prediction accuracy. The simulation controls the wastegate to the set boost-pressure, just as the real controller on the engine, thus compensating for possible inaccuracies in the prediction of efficiency. This was observed very

early on by Hong and Watson [8.1]. Very seldom do correlation data between measurements and simulations of the wastegate massflow fraction exist. However, for the low speed region, where the wastegate is closed, the simulation is much more sensitive to error in predicted turbine power. The reason is that there is no control mechanism to adjust the turbine power. Therefore this region, up to where the wastegate is opened on the engine, normally cannot be simulated accurately without calibrating the simulation model against measurement data for the particular engine in question. The same also holds for transients, since the wastegate is closed up to when the desired boost pressure is reached. Figure 8.1 shows, for low engine speed with closed wastegate, an example of poorly predicted turbospeed due to poorly predicted turbine power.

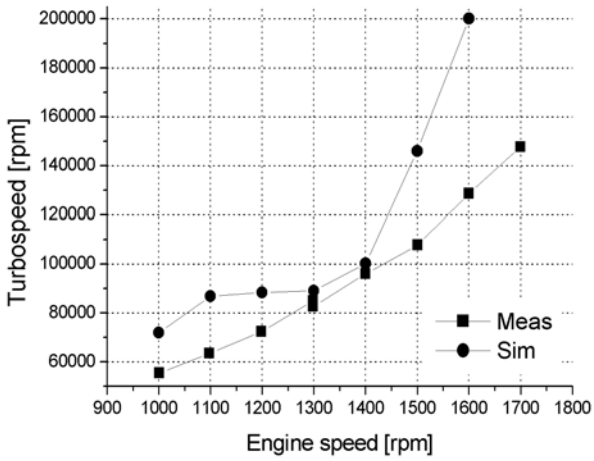

Figure 8.1. Measured and simulated (without calibration) turbocharger speed vs engine speed. With calibration the curves can be put on top of each other. The simulated turbospeed was limited to max 200000 rpm.

Thus, the most useful tool for removing two of the turbocharged engine's largest drawbacks has drawbacks in itself exactly where it can be of largest use. The primary scope here is to investigate if the accuracy of the simulation, or the size of the adjustments needed, is a function of pulse shape and turbine design. An attempt is also made to characterize how different turbines perform in unsteady flow with different pulse shapes. The investigation includes: measurements on engine in the test cell, 1D engine simulations, zero-dimensional turbine calculations as well as turbine measurements in a turbocharger test bench.

This is done for three turbines with different characteristics. The characteristic in this case is degree of reaction, but otherwise similar flow capacity. Simultaneously, the shape of the pulsating flow is altered by using three different manifolds. This gives nine different setups, which are tested on a 2-liter, 4-cyl turbocharged SI-engine.

8.2 Turbine analysis and selection

8.2.1 Theory

The turbine is a device that extracts energy from a gas stream and converts it into shaft power. The turbine consists of two parts, a stator and a rotor. Kinetic energy in the gas is transferred to kinetic energy of the wheel. The task of the stator is to act as a nozzle and to give the wheel inlet the right flow-properties.
Turbines for use with gas as the fluid are expanders, thus they expand the gas from a high pressure to a lower pressure. When expanding the gas, the volume increases and thus also the flow velocity. This kinetic energy is then converted to shaft power by the wheel. The isentropic power of a turbine can (with the assumption of equal massflow throughout the turbine) be written as:

$$\dot{W} = \dot{m}\Delta h = \dot{m}c_p\Delta T = \left(\frac{P\dot{V}}{R}\right)_{inlet} c_p\left(1-\left(\frac{P_{out}}{P_{in}}\right)^{\frac{\gamma-1}{\gamma}}\right) \qquad \text{eq. 8.1}$$

where Δh and ΔT are enthalpy and temperature drops over the entire turbine.

Reaction

The expansion in the turbine can either occur entirely before the wheel, entirely in the wheel or at a certain balance between them. This balance in expansion between the stator and the wheel is called reaction, and is defined as the ratio between the change in static enthalpy over the wheel and the change in total enthalpy over the entire turbine [8.2]:

$$\Lambda = \frac{\Delta h_{wheel}}{\Delta h_{0,turbine}} = \left\{\Delta h = c_p\Delta T\right\} = \frac{T_{w,in}-T_{w,out}}{T_{0,in}-T_{0,out}} = \frac{T_{0,in}\left(\frac{P_{w,in}}{P_{0,in}}\right)^{\frac{\gamma-1}{\gamma}} - T_{0,out}\left(\frac{P_{w,out}}{P_{0,out}}\right)^{\frac{\gamma-1}{\gamma}}}{T_{0,in}-T_{0,out}} \qquad \text{eq. 8.2}$$

This assumes that c_p is constant over the temperature interval used. A turbine with all the expansion in the stator thus has a low reaction and a turbine with all expansion in the wheel has a very high reaction.

Blade Speed Ratio, BSR or U/C_s

The ability of the wheel to extract power from the gas is affected by the difference in velocity of the gas entering the wheel and the velocity of the wheel itself. However, the velocity at the wheel inlet is very difficult to measure, and is also dependent on the design of the housing, the stator exit state etc. To be able to compare different turbines against each other it is convenient to have a property that only takes into account inlet and exit conditions of the turbine and the wheel inlet tip speed. Thus the blade speed ratio, BSR or U/C_s, is defined as the ratio between the blade tip speed U and the gas velocity achieved if the gas is expanded isentropically from inlet pressure to outlet pressure. Thus,

$$U / C_s = \frac{U}{\sqrt{2 c_p T_{0,in}\left[1 - \left(P_{out} / P_{0,in}\right)^{\frac{\gamma-1}{\gamma}}\right]}} \qquad \text{eq. 8.3}$$

Flow angles

For analysis of the internal flow of a turbine the blade speed ratio is too crude. Calculated flow angles are usually convenient aids to explain certain behaviour. U is used to denote wheel tip velocities at inlet and outlet, C absolute flow velocities at various locations and W relative flow velocities between flow and blade. Angles α (alpha) and β (beta) are defined according to Figure 8.2.

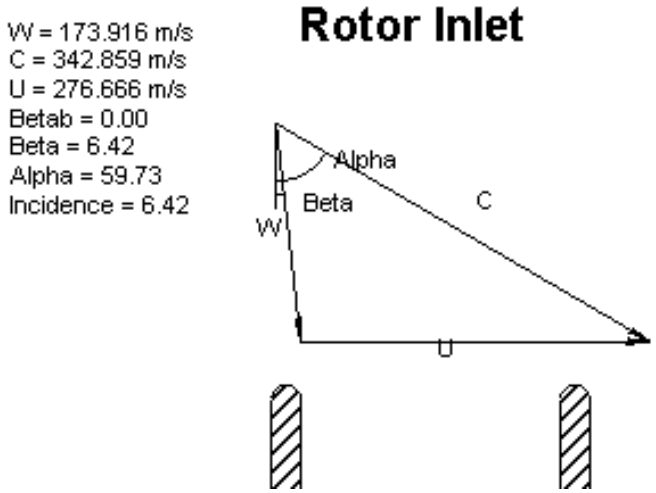

Figure 8.2. Definition of velocities and flow angles. U is the wheel tip velocity, C and W gas absolute and relative velocities, respectively. Figure from Rital [8.3].

Efficiency

When discussing how a turbine performs on an engine the turbine efficiency is a commonly used term. Usually, efficiencies are defined as the ratio between extracted work and available energy. However, for turbines the efficiency is defined as the ratio of extracted work and maximum utilizable power. That is the power gained by expanding the gas isentropically from inlet state to outlet state. Baines and Japikse [8.2] define the total-static efficiency as:

$$\eta_{ts} = \frac{h_{0,in} - h_{0,out}}{h_{0,in} - h_{0,out,isentropic}} = \frac{1 - T_{0,out} / T_{0,in}}{1 - \left(P_{out} / P_{0,in}\right)^{(\gamma-1)/\gamma}} \qquad \text{eq. 8.4}$$

As described in Chapter 5, CA-resolved temperature measurements are very difficult to achieve. So if a CA-resolved efficiency is desired, a more direct measurement of the output power of the turbine is necessary. Such a definition was developed in Chapter 6.

However, such efficiency definitions have a certain expansion ratio (P_{out}/P_{in}) built in. When a turbine cannot deliver satisfactory power for low engine speeds, it is often referred to as the turbine having too low efficiency at that point. But according to the efficiency definition that is not necessarily true. The efficiency might be good, but the power is low because the expansion ratio is too low. The turbine is a restriction in the exhaust stream that builds up it's own expansion ratio to extract power from. That expansion ratio depends on the actual inlet throat size of the turbine. Think of it as a nozzle, then different sizes correspond to different turbine sizes. For non-VGT turbines the engine has to cope with the flow characteristics inherent in the fixed-nozzle turbine, which is very different from the linear flow vs. speed characteristics of the piston engine.

8.2.2 Turbine selection

The three turbines in this investigation must have the same swallowing capacity, but different reaction and blade speed ratio. This is accomplished by using different A/R[6] and trim[7], but equal wheel inlet diameter, blade design and number. Turbines were available with trims 67 and 72 and A/R of 0.27, 0.31, 0.35, 0.40, 0.46 and 0.50. The combination A/R 0.46 and trim 67 was used on a production engine of 2 litre displacement and was thus assumed to be proper for the test engine and chosen to be the baseline for the investigation.

---

[6] A/R - ratio between volute inlet throat area and the radius from the centroid of that area to the rotational axis of the turbine.

[7] Trim defined as $(d_{exit}/d_{entry})^2*100$, d is wheel diameter.

Meanline calculations

The selection of the turbines was done with meanline calculations in the turbine simulation software Rital [8.3]. Rital is a zero-dimensional, semi-empirical turbine-modelling software. It calculates the expansion process, velocities and flow directions throughout the turbine for any specified geometry and boundary condition [8.2]. Rital has no time dependence, but if quasi-steadiness is assumed and several calculations done, one for each time step, a pulsating event can be calculated.

The software requires turbine geometry data such as A/R, throat area, wheel inlet diameter, inlet and exit blade angles and exit diameter. Furthermore it utilizes loss coefficients for a range of possible flow mechanisms internally. The software also uses backpressure, pressure ratio, rotational speed and inlet temperature as input.

The Rital model was calibrated for the baseline turbine with data from the manufacturer's performance map. Various model parameters were adjusted to give the best possible fit to the map data. The calibration was limited to actual speed of 115000 and 96000 rpm. The fit for blade speed ratio at 115000 rpm can be viewed in Figure 8.3. Note that this is based on data from the steady slow performance maps supplied by the manufacturer.

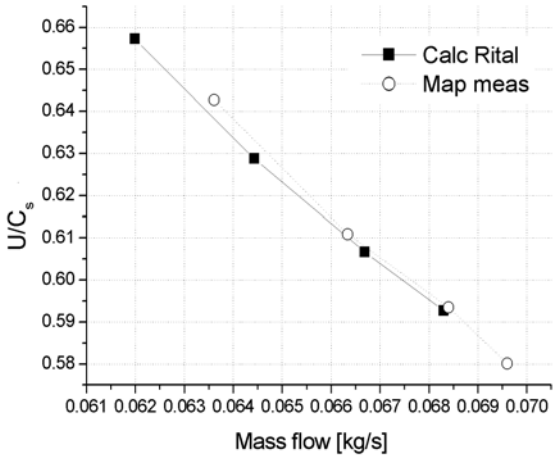

Figure 8.3. U/C_s calculated in Rital compared to data from map measurement. The difference in U/C_s was literally negligible.

Table 8.1. A/R and trim for the three selected turbines.

Turbine no.	**1**	**2**	**3**
A/R	0.4	0.46	0.50
Trim	72	67	67
Throat area [mm^2]	431	513	599
Rotor outlet diameter [mm]	39.9	38.5	38.5
No. of blades	12	12	12
Rotor inlet dia. [mm]	47	47	47

It was assumed that a proper combination of an increase in A/R (which increases swallowing capacity [8.2]) and a decrease in trim (which decreases swallowing capacity [8.2]) would result in a swallowing capacity that is equal to the baseline turbine, but with altered rotor inlet conditions. Unfortunately, A/R could not be decreased and trim increased due to the availability in trims, therefore the same trim as the baseline was chosen together with one A/R step larger than baseline. The selected turbines are displayed in table 8.1.

8.2.3 Meanline calculation of a real case

With the model for the baseline turbine as a base, models for the other two turbines were created with maintained loss coefficients. To explore the possibilities of the method, an exhaust pulse was taken from previous measurements and 1D engine simulations of the same engine, but with another, but similar, turbine. For eight locations on this pulse the necessary data were picked from engine measurements and engine simulations. The reason for using data from both measurements and simulations is that some of the data could not be measured, for reasons mentioned in Chapter 5. Figure 8.4 shows the chosen points. The data were (all instantaneous, CA-resolved):

- exit pressure (measured)
- pressure ratio (measured)
- speed (measured)
- inlet temperature (simulated, since only mass averaged values could be measured)
- mass flow rate (simulated, since only time averaged values into the engine could be measured)

Table 8.2. Data for the selected points on an exhaust pulse. Data from 1800 rpm, WOT.

CAD [°]	PR [-]	N_{tc} [rpm]	T1T [K]	m [kg/s]	V [m^3/s]
-20	1.16	111974	954	0.034	0.081
0	1.70	111860	1261	0.073	0.144
15	2.06	112181	1358	0.102	0.167
25	2.02	112506	1270	0.100	0.152
35	1.81	112750	1248	0.071	0.118
50	1.56	112909	1184	0.061	0.115
90	1.33	112813	1047	0.045	0.096
130	1.21	112404	975	0.039	0.089

This data was fed to the meanline models of the three turbines to enable calculation of internal flow properties. First it was important to ensure that the three turbines had the same flow capacity, which is displayed in Figure 8.5. The massflow indicates that the pulse is rather sharp, with a narrow regime with very high flow rate. However, eq. 8.1 states that the turbine can be viewed as a volumetric flow sensing device. If the volumetric flow for the pulse is calculated the peak is more flat, and wider, see Figure 8.6.
Once it is established that the swallowing capacity is equal for all three turbines, it is interesting to look at how the internal flow differs between the turbines. A central parameter is the degree of reaction. The reactions for the three turbines for the points on the pulse are displayed in Figure 8.7. It is clear that the reaction varies very much during one exhaust pulse. The difference in reaction during the pulse is of the same magnitude as the difference in reaction between the turbines. It also appears that the trim is the property with largest impact on the reaction, since T2 and T3 with equal trim has very similar reaction. The simulations show that the reaction for some points actually exceeds 1. Since the enthalpy at the rotor outlet equals the enthalpy at the turbine outlet (the same station); eq. 8.2 and the definition of total enthalpy gives:

$$\Lambda = \frac{\Delta h_{wheel}}{\Delta h_{0,turbine}} = \left\{ h_0 = h + \frac{1}{2}C^2 \_ and \_ h_{w,out} = h_{out} \right\} = \frac{h_{w,in} - h_{out}}{h_{in} + \frac{1}{2}\left(C_{in}^2 - C_{out}^2\right) - h_{out}} \qquad \text{eq. 8.5}$$

Thus, since the static enthalpy at the inlet of the turbine is larger than the static enthalpy at the wheel inlet, C_{out} has to be significantly larger than C_{in}. This

results in a large amount of kinetic energy wasted at the turbine outlet, with a subsequently low efficiency, which also can be seen in Figure 8.10.
With different reactions for the different turbines the relative inlet velocity and hence the flow angle will differ between the cases. Figure 8.8 shows the rotor inlet relative velocity. In Figure 8.9 the relative angle between flow and blades is displayed (radial blades are used here as almost always on radial turbines). This change in flow angles and velocity affects the efficiency of the turbine. Rital calculates efficiency as well as the power. These properties are shown in Figures 8.10 and 8.11.
The power does not have a maximum at the same massflow as the efficiency. It is quite natural that the power depends more on the massflow rate than on efficiency, since the massflow rate varies much more than the efficiency over the pulse. It is obvious that the peak of massflow forces the turbine to operate in a sub-optimal operation point, where the massflow is too large. Since the flow pulsates so heavily, the operation points vary very much, even at a steady operation point in terms of the engine. Understanding this pulsating phenomenon and learning how to put the peak efficiency and the shape of the massflow at optimal levels is the key issue for the design of turbocharged engines.

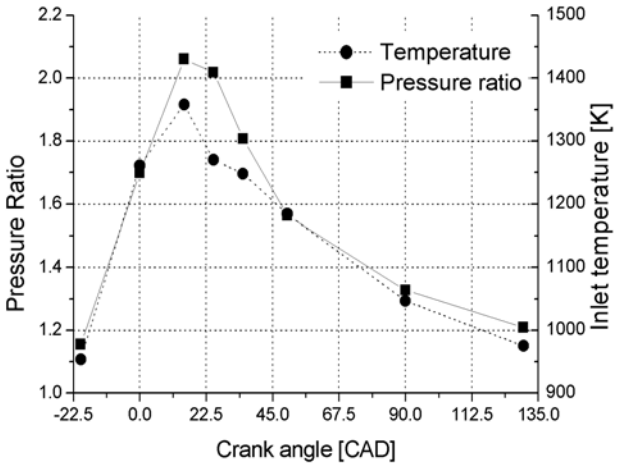

Figure 8.4. Points chosen for pointwise meanline calculations of turbine performance.

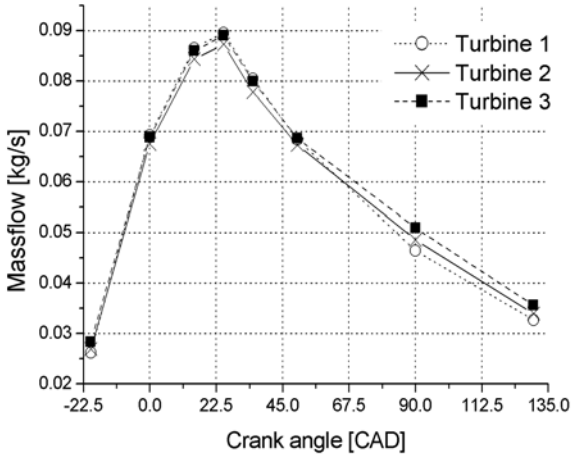

*Figure 8.5. All three turbines lie within 10 % of massflow, but often within a narrower range. Dotted line is turbine 1 (A/*R *0.40, trim 72), solid line is turbine 2 (Baseline, A/*R *0.46, trim 67) and dashed line is turbine 3 (A/*R *0.50 and trim 67).*

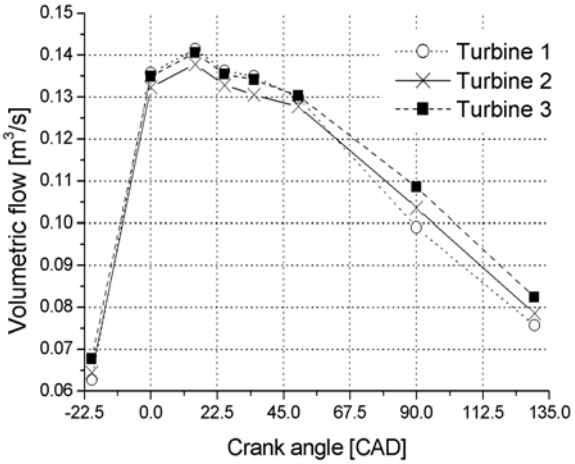

Figure 8.6. The volumetric flow has a flatter shape of the curve than the mass flow rate.

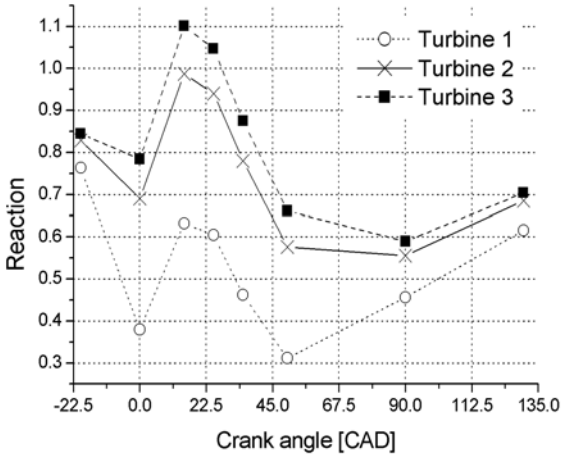

Figure 8.7. Calculated reaction for the points on the pulse.

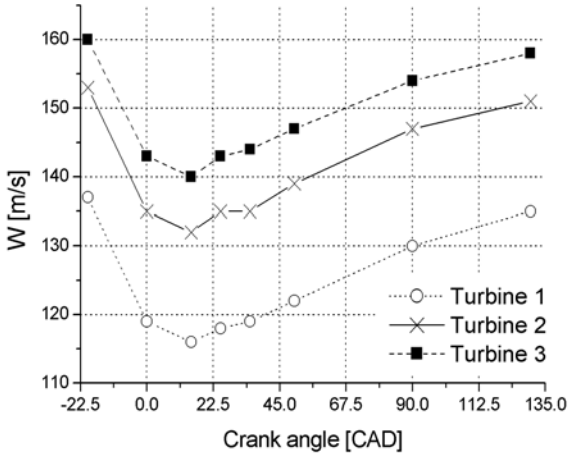

Figure 8.8. Calculated rotor inlet relative velocity for the points on the pulse.

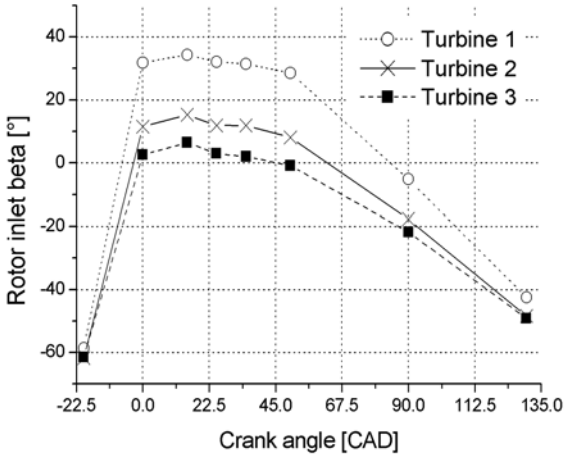

Figure 8.9. Rotor inlet relative flow angle for the three turbines on the exhaust pulse.

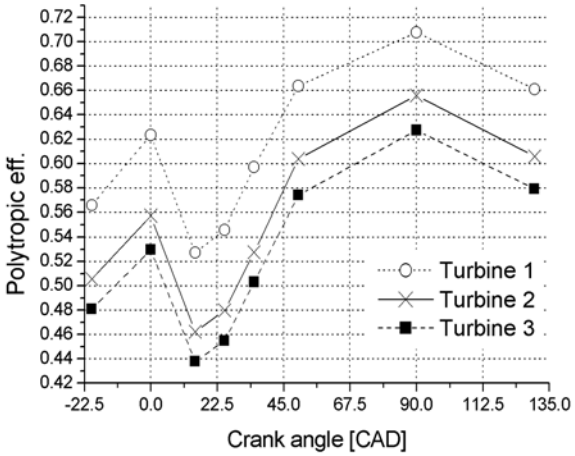

Figure 8.10. Polytropic TS-efficiency for the three turbine vs massflow on the exhaust pulse

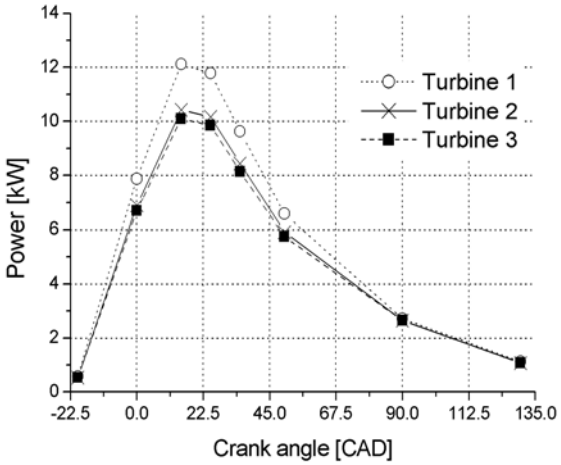

Figure 8.11. The power output from the turbine as function of crank angle, on the specified pulse.

This presentation of the data is more to present the method than to actually analyse these turbines for this pulse. However, a few interesting observations can be made. Judging from the different curve shapes of the mass and volumetric flows one can see which properties mostly depend on each of them. It is obvious that the rotor inlet beta (relative angle between flow and turbine blade) shows larger similarity to volumetric than mass flow. It also appears as if the strong peak of the mass flow affects the reaction heavily. Consequently this affects the efficiency of the turbine.

8.3 Manifold flow and function

The exhaust manifold can be utilized for more than just transporting the exhaust gases from the outlet of the cylinder head to the turbine inlet. By altering the geometry of the manifold the time-dependency of the flow, i.e. the pulse shapes, can be shaped according to some design target. To investigate which parameters influence massflow and pressure amplitudes most, some 20 manifolds were tested in simulations. Three types of manifolds were tested, 4-1, 4-2-1 and log type manifolds, see Figure 8.12. For the 4-1 type the volume was changed both by changing the diameter and length. For the log type manifold the volume was changed by changing the log diameter. For the 4-2-1 manifold the volume was changed by changing the length of the 2-1 part. The reason for these limitations is simplicity. It was seen from the 4-1 manifolds that when the diameter was changed it quite quickly resulted in diameters that would be very

difficult to fit on the engine. Therefore the pipe length was much more convenient to alter. A drawback is of course that the pulse propagation is affected when changing the tuning-lengths.
Figure 8.13 shows simulation results of how the pressure fluctuation amplitude (fluctuation divided by the average level) of the flow varies for manifolds of these three types with several different volumes, at one engine speed. For the pressure amplitude one can approximately say that the amplitude is inversely proportional to the volume. For the 4-1 manifold the diameter was 37.2 mm except for the two x-marked results where the length was maintained at 180 mm and diameter changed to 54.5 and 82.5 mm respectively in order to change the volume.
However, the inverse proportionality is not true if one looks into detail. For the 4-2-1 manifold the volume does not seem to affect the amplitude as much as for the other two manifold types. A reason for that is that the pipe diameter was maintained for all 4-2-1 manifolds and that the amplitude does not seem to fall as rapidly with volume if the pipe cross section can be maintained throughout the manifold. For the pulse amplitude to decrease, the gas entering the manifold needs a certain volume to expand into. The results in figure 8.13 indicate that the expansion volume is not entirely the complete manifold volume but a combination of the local volume (the pipe branch which the pulse is propagating through) and the entire manifold.
The maintained high amplitude of the 4-2-1 manifold was also a reason for not altering the pipe diameter of the 4-2-1 manifold. The purpose of this manifold was to achieve long tuned runners but with maintained pulse amplitude. With such a manifold the low speed performance can be maintained thanks to the pulse amplitude, at the same time high-speed performance can be high thanks to long propagation-paths for the cross-talk pulses that normally worsens scavenging of 4-cylinder engines.
For the log-type manifold only the diameter was used as a volume-changing parameter, due to simplicity. The loss of kinetic energy, which is impossible to avoid when a high velocity gas stream enters a larger volume, will be affected by the log volume. However, achieving a low amplitude by just altering the log length would result in unrealistically long pipes, and the pulse amplitude might not drop if the pipe diameter is not altered significantly, for the same reasons as for the 4-2-1 manifold.

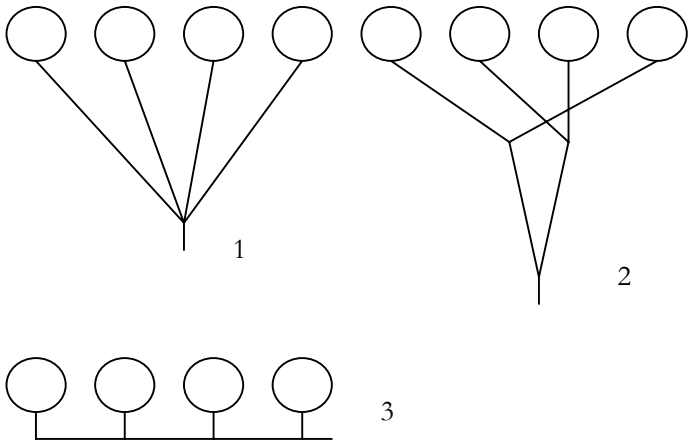

Figure 8.12. The layout of the three different tested manifolds. 1 is the 4-1 type, 2 is 4-2-1 and 3 the log type manifold.

For the engine experiments three manifolds were designed/selected. One of the manifolds was considered as baseline. This was an as-compact-as-possible 4-2-1 manifold. The second manifold was designed to give similar pulse shape as the first one, but also to aid the gas exchange on the engine, and the third was designed to give much lower amplitude of the exhaust pulsations. The three manifolds are shown in Figure 8.17.

The baseline manifold was built up from 37.2 mm ID pipes. Cylinders 1-4 and cylinders 2-3 were connected to each other. To minimize the total volume of the manifold the lengths of the two manifold halves could not be equal. The distance between cylinder head flange and turbine flange was 385 mm for cylinders 1-4 and 283 mm for cylinders 2-3. This manifold was chosen since it is very similar to the engine's standard manifold and a very common design for 4-cylinder engines. The volume of it is 0.95 litre. The second manifold is similar to the baseline, but with 300 mm longer 2-1 pipes resulting in a volume of 1.5 litre. The third manifold was designed to have low pulsation amplitudes. To have both low pressure and massflow amplitudes, as well as being easy to realize on the engine, the 5-liter log type manifold was selected (the measured volume was 5.3 litre for the manifold).

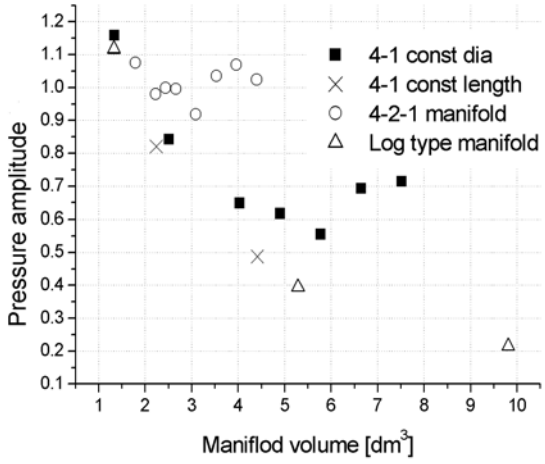

Figure 8.13. Amplitude of pressure pulsations vs volume for 20 manifolds, at 1800 rpm and equal average massflow.

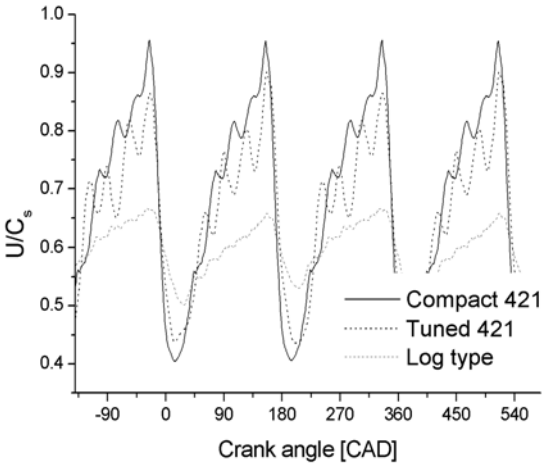

Figure 8.14. U/Cs as a function of CA for one engine cycle for the three selected manifolds. The manifold volumes were 0.95 dm³ for the compact 4-2-1, 1.5 dm³ for the turned 4-2-1 and 5 dm³ for the log type.

Table 8.3. Data for the three manifolds. No. 1 is most similar to production manifolds. The tuned length for 1 and 2 are different for runners 2/3 and 1/4, therefore two values are shown.

Manifold no.	**1**	**2**	**3**
Volume [dm³]	0.95	1.5	5.1
Tuned length [mm]	280/380	580/680	105
Runner diameter [mm]	37.2	37.2	37.2
Configuration	4-2-1 compact	4-2-1	log

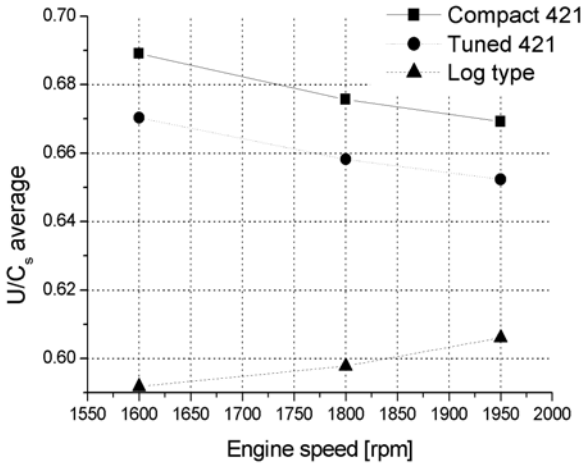

Figure 8.15. How the time average of U/Cs changed with manifold and engine speed. The manifolds are the same as in Figure 8.14.

Both U/C_s and the reaction have been shown to depend on the exhaust pulsations. The fluctuation amplitude of the turbocharger speed on the other hand is only about 1% of the average value and therefore, in practice, constant. Therefore U/C_s will depend on the manifold geometry due to the different pulsation shapes in the manifolds. The choice of manifold will be a means of altering the operation point of the turbine, which can be used as an alternative to redesign of the turbine. In the Figures 8.14 and 8.15 U/C_s (simulated results from GT-Power) is displayed both as instantaneous and time averaged values for the three different manifolds that were tested. It is clear that the relative variation of U/C_s is much larger as a function of crank angle than as function of engine speed, further stressing the necessity of using CA-resolved data for analysis of these kinds of phenomena.

8.3.1 Total heat loss to surroundings

The heat loss from the exhaust gas to the surroundings is heavily dependent on exhaust manifold wall area and temperature. The latter depends on convection and radiation to surroundings as well as heat conduction to the cylinder head. The heat flux situation in the production manifold of the engine used here is investigated and modelled in chapter 7. Here the manifold wall temperature is calculated the same way, using GT-Power's wall temperature solver with the same heat transfer environment. For the three selected manifolds the total heat loss vs. engine speed is displayed in Figure 8.16. The manifold having the largest heat transfer is the tuned 4-2-1 manifold. That manifold has the longest propagation lengths and therefore most time for the gas to exchange heat with the wall. It seems like the ratio of propagation length and outer wall area is an important parameter.

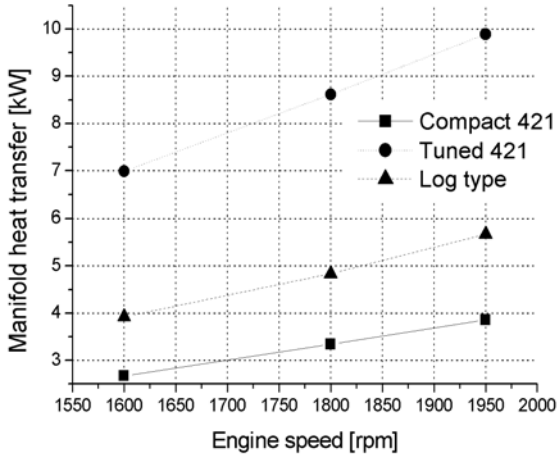

Figure 8.16. Simulation prediction of how the heat losses from the different manifolds varied with engine speed.

Figure 8.17. Manifolds 1, 2 and 3 counted from the top. Manifold 1 is a compact 4-2-1 design, 2 is a tuned 4-2-1 and 3 is a damping volume of 5 litres.

8.4 Engine measurement

The engine tests were performed on an in-line 4-cyl., 2-liter, 4-valve per cylinder, gasoline PFI engine. The turbochargers were from the same family with data as in Table 8.1. The compressors were equal on all three turbochargers. The turbines had internal wastegate, but these were welded shut to ensure tightness. The turbine wheels had 12 blades. The trim is defined as the ratio of squares of exit and inlet diameters multiplied by 100. The data for the manifolds is presented in Table 8.3.

The engine had cylinder pressure measurement on cylinder one and turbine in- and outlet pressures were measured with almost flush-mounted, piezo-resistive sensors positioned in water-cooled sockets. The turbo speed was measured with an eddy-current probe positioned in the compressor shroud. Other pressures were measured with strain-gauge, steel-diaphragm sensors and temperatures were measured with K-type thermocouples. Exhaust manifold surface temperature was measured by squeezing thermocouple wire to the manifold wall with screws in welded nuts on the manifolds, as in Chapter 7. Three measurement positions were used, close to the cylinder head, close to the turbine and midway between these two.

The test cell had a fast and a slow measurement system. The fast system gave one measurement point for every 0.2 CAD and the slow system had a frequency of 1 Hz. The cylinder pressure, exhaust pressures before and after the turbine, pressures before and after the compressor and in the intake manifold were connected to the fast system. An additional digital I/O system measured the turbocharger speed by measuring and logging the time when the blade passes the eddy-current sensor. The system used one pulse for every revolution of the turbocharger rotor.

8.5 Engine simulation

The engine simulation model was built up in GT-Power [8.4]. The combustion was modelled by GT-Power's own calculation of burn-rate from measured cylinder pressure (an ensemble average of 100 cycles was used). The setup in the test cell was copied geometrically accurately from the engine's standard air-mass meter to the mouth of the exhaust pipe. It proved necessary to model the entire exhaust system in order to achieve proper pulse shape of the turbine outlet pressure. For the intake side and internally in the cylinders, wall temperatures were set to fixed, assumed values. For the exhaust manifolds, the wall temperature was calculated using the wall temperature solver in GT-Power. The wall temperature solver has three important input parameters aside from geometrical and material data, that is the heat transfer multiplier for heat

transfer from gas to inner wall, and the External Convection Coefficient and radiation sink temperature governing the heat transfer on the outer wall. The radiation sink temperature was set to 310K but the other two coefficients needed calibration. Although the wall temperature of the manifolds was measured for three locations, the same coefficient values were used for the entire manifold. But different coefficients were necessary for different manifolds and different load points.
As in Chapter 7, the heat loss to the surroundings from the turbine housing was modelled by a heat sink at the turbine entry. The amount of heat to be dissipated here is a matter of calibration. The necessity of including heat transfer in the turbine analysis was found by Ehrlich [8.5] and Pucher et. al. [8.6].

8.5.1 Calibration

A set of input parameters to the simulation model proved to need calibration in order to achieve correct results from the simulations. The most important was the turbine efficiency multiplier. Calibration of this was achieved by setting a PID-controller on the efficiency multiplier, and having it control the turbine speed to measured results.
It was found that the time-average turbine inlet pressure could deviate approx. 5% from measured, and therefore another PID-controller was added to the turbine mass multiplier. It controlled the time average turbine inlet temperature against measured values.
Similarly the two heat-transfer multipliers and external convection coefficient were controlled by PID-controllers controlling to measured turbine inlet temperature and wall temperature respectively (the measurement position midway from cylinder head to turbine inlet was used here).
Another PID-controller was set to control the heat sink at turbine entry against measured turbine exit temperature.
By using PID-controllers to adjust certain parameters against measured data, an enormous amount of time and effort is saved. The settling time of the controllers is of the same order as the time for convergence of the turbocharger speed (if non-controlled) and therefore the run time of one simulation is barely increased at all. The alternative would have been to use the iterative optimisation algorithm in GT-Power once for every parameter and hardware setup. With the controllers the coefficients are calibrated all at the same time as the model is run. The number of simulation runs has thus been reduced by approximately a factor of 50.
The simulation results were carefully checked against measured data, both time average values as well as CA-resolved pressures.

8.6 Turbine measurement

For two reasons new turbine maps were measured for this work: first to give more data than standard maps and second to give map data for the actual individual turbines that were tested (to test if the spread between different turbines of the same type is large).
The turbine maps were measured in a steady-flow gas stand. The turbine inlet temperature was fixed at 620°C and the speed was controlled by throttling the compressor, which acted as a dynamometer.

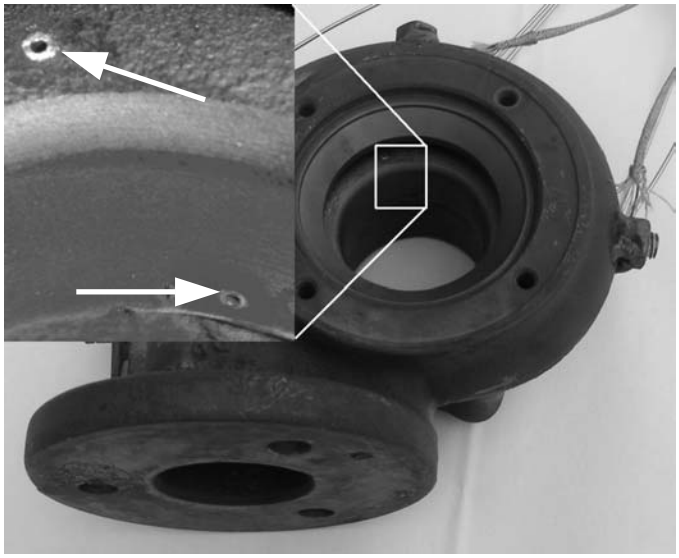

Figure 8.18. The brazed-in pressure taps, here showing at wheel inlet (upper hole) and wheel exit (lower hole). Turbine housing photographed from where the bearing housing normally is located.

The measurements taken were first standard map measurement data such as mass flow rate, inlet temperature and static pressure. In addition static pressure taps were fitted to the internals of the turbines. The pressure taps were 1.5 mm OD, 1 mm ID stainless steel pipes which were brazed into holes drilled through the turbine housing. Pressure taps were fitted at: the throat, at the nozzle at wheel inlet (2 taps) and at wheel exit (2 taps), see figure 8.18. The taps at wheel inlet and exit were mounted in pairs with the same circumferential position. The reason for having more than one tap at these positions was to see if there were any circumferential variations of the flow properties.
A sample of the measured data is displayed in figure 8.19. The single data points at inlet and at the nozzle is displayed, as well as the double measurement points at nozzle and at the wheel outlet. The difference between the double

measurement points indicates that the distribution around the circumference is far from perfect. This data is the higher speedlines for turbine no. 3.

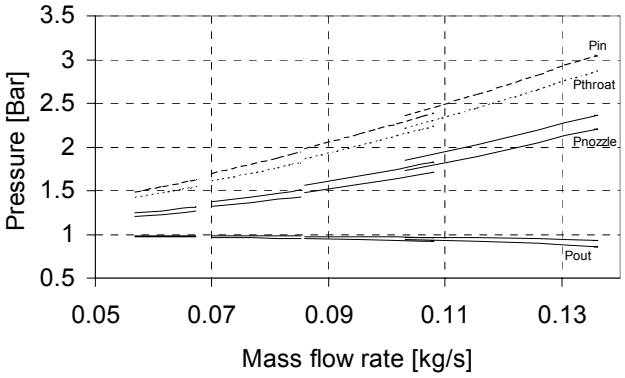

Figure 8.19. Sample of the data measured in the turbine gas stand. Note the difference in pressure for the two measurement points in nozzle and at the outlet, this indicates a quite un-even distribution around the circumference..

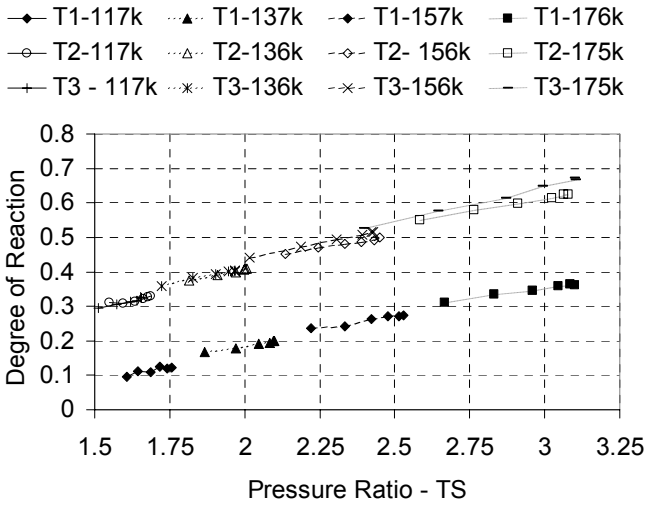

Figure 8.20. The degree of reaction vs. pressure ratio for all 3 turbines (T1, T2 and T3) for the 4 highest speed lines measured (117, 136, 156 and 175 krpm). Obviously only T1 and T2 has significant differences, T3 is too close to T2 to be of important with regards to reaction.

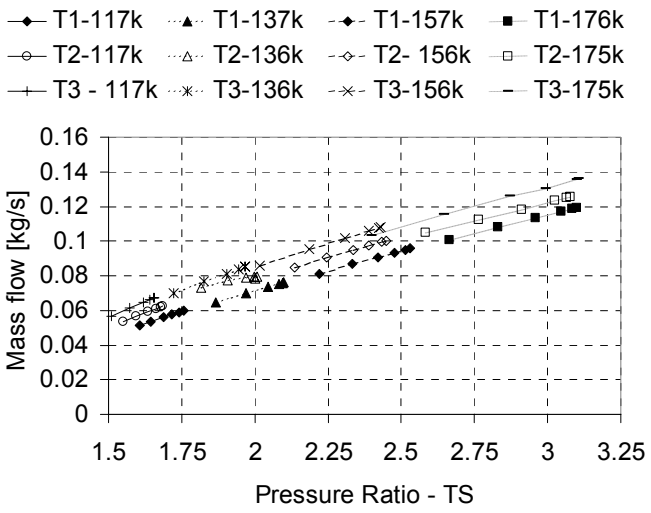

Figure 8.21. The mass flow vs. pressure ratio for all 3 turbines (T1, T2 and T3) for the 4 highest speed lines measured (117, 136, 156 and 175 krpm).

The reaction was calculated from the measured map data. The results are shown in figures 8.20 and 8.21. Between T1 and T2 there is a significant difference in reaction, but for T2 and T3 the difference is too small to be of practical importance. For the massflow rate the difference is small (5-10%), but still exist. Therefore it seems like it will only be between T1 and T2 the question is valid whether the reaction will have an important influence on the turbine behaviour or not.

8.7 Turbine calculation

The Rital-model of the baseline turbine was recalibrated with the new set of measured map data. Rital offers 3 solver possibilities as well as 4 loss models. Here the RTP-solver was the only applicable and the NASA loss model was used. The Rital models for the three turbines were calibrated/checked with data from the turbine measurements. The coefficients required by the model, which were adjusted during the calibration, were (values for T2 in brackets):

- Volute inlet blockage (0.0)
- Swirl coefficient (1)
- Loss coefficient (0.1)
- Rotor inlet optimum incidence (-20)
- Rotor inlet blockage (0.0)

- Rotor exit deviation (30)
- Trailing edge loss multiplier (1.0)
- Incidence loss multiplier (1.0)
- Passage loss multiplier (0.6)
- Axial clearance loss multiplier (1.0)
- Radial clearance loss multiplier (1.0)
- Exit diffuser pressure recovery factor (0.6)

The properties for which the coefficients in the Rital model were calibrated were:

- Massflow rate
- Pressure at the throat
- Pressure at the nozzle (volute exit / rotor inlet)
- Pressure at the rotor exit
- Degree of reaction
- TS-Efficiency

These properties were chosen since they were available from the gas stand map measurements. The calibration was assumed successful when all properties were within normal engineering accuracy (10%). The coefficients did not need to be changed between operating conditions, but different turbines required different coefficients. Since the calculations only would be used for high load operation points, the models were only calibrated for the 4 highest speedlines from the measurements.
Between T2 and T3 it was required to only change the swirl coefficient in the volute, but between T1 and T2 several other parameters had to be altered. The most important of these was that the inlet blade height had to be decreased from 6.5 to 5 mm in order to emulate a nozzle blockage.

8.8 Results

8.8.1 Engine tests

The engine was only run with wide-open throttle on the test bed. The ignition timing was set to be a function of speed only, and equal for all setups. Lambda was maintained at 0.85 throughout all tests. Figure 8.22 shows the torque for all 9 setups. As expected the smallest manifold and turbine gave highest torque at low speed due to higher ability to build up boost pressure. In the figure, curves with the same line style are for the same manifold and curves with same marker are for the same turbine. It is clear that with few exceptions the torque is much more dependent on the manifold than on the choice of turbine. The curves

group up in three vaguely overlapping groups, one for each manifold. In each of these groups the turbine 1 produces most torque, turbine 2 second most and turbine 3 least.
The reason for the exhaust manifolds' influence on boost pressure is found if the inlet pressure is plotted vs. (time-) average exhaust manifold pressure as in figure 8.23. The relationship is very close to linear. Thus, the available inlet (or boost-) pressure is heavily dependent on the manifold and turbine's ability to convert the cylinder pressure at EVO into usable pressure at turbine inlet. The manifold with smallest volume is the one producing highest torque for each speed (with a few exceptions for the highest speeds tested).
However, figure 8.23 does not show when on the powerband the boost pressure starts to build up, thus not showing the ability of low-end torque.
Torque is not dependent on inlet pressure alone, different pulse shapes at the exhaust port will affect gas exchange quality via residual gas content as well as pumping losses through the pressure level and shape. Figure 8.24 shows the engine torque vs. P1T. It is clear that manifold no. 3 gives the lowest torque per exhaust pressure, which indicate that the PMEP increases with the flatter pulse-shapes. Also this figure shows that the manifold gives a larger impact on torque than the choice of turbine, the smallest manifold M1 is the top performer in this graph for all three turbines.

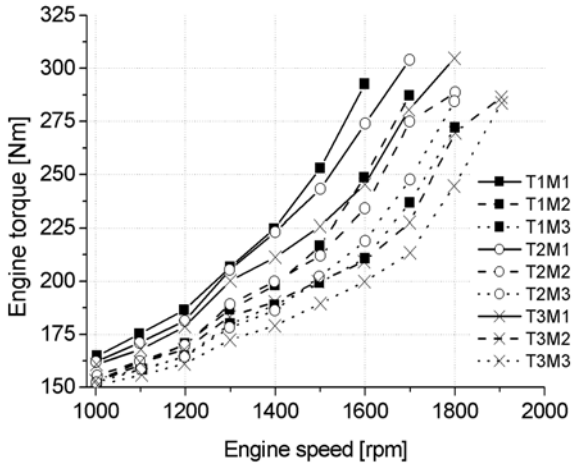

Figure 8.22. How the torque varies with speed for all nine setups.

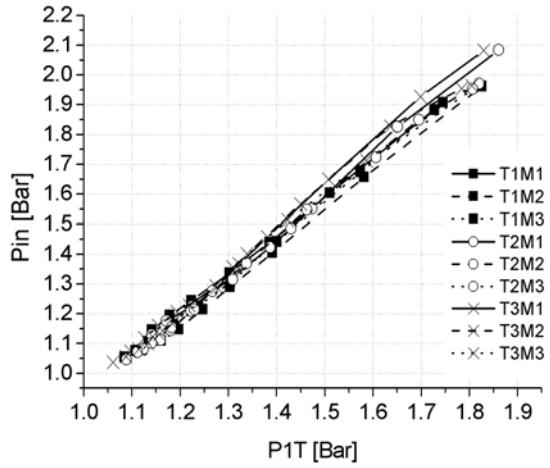

Figure 8.23. Inlet pressure vs. turbine inlet pressure for all measured cases.

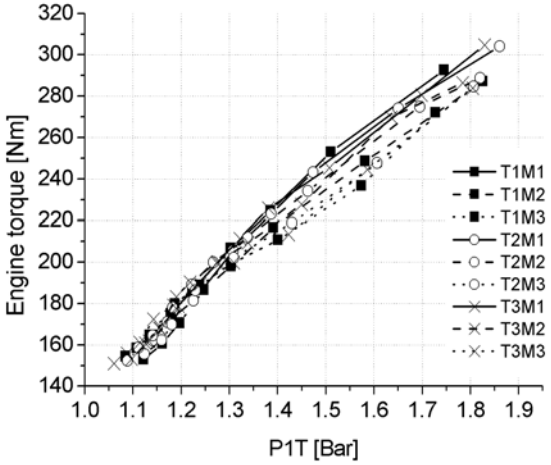

Figure 8.24. Engine torque for all speeds and setups.

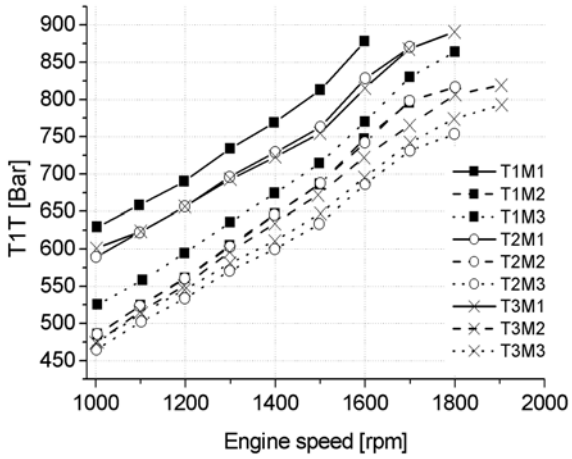

Figure 8.25. Turbine inlet temperature vs. engine speed for all nine setups

Different manifolds give different efficiency in the delivery of the exhaust energy from the cylinder to the turbine inlet. The most basic measure of that, is the temperature at the turbine inlet, see Figure 8.25. As expected, the smallest manifold causes least losses of thermal energy in the gas. For the two larger manifolds the trend is not as clear.

Thus, low-end torque is much more dependent on the manifolds' ability to maintain the pressure from the cylinder to the turbine inlet, than the turbine's efficiency. This is the reason why all manufacturers of turbocharged engines have converged toward ultra-compact manifolds.

Let's thus concentrate on manifold 1 and compare the various turbines against each other. In Figure 8.26 the torque and turbine inlet pressures are plotted vs. engine speed. It appears that the production of torque depends on the different ability to maintain turbine inlet pressure. Since turbine 1 has the highest turbine inlet pressure and 3 the lowest, it seems like the turbine inlet pressure (and indirectly torque) is inversely proportional to A/R and through that also to throat area. Thus, the attempt to achieve equal mass flow capability does not seem to have succeeded, which also the map measurements indicated.

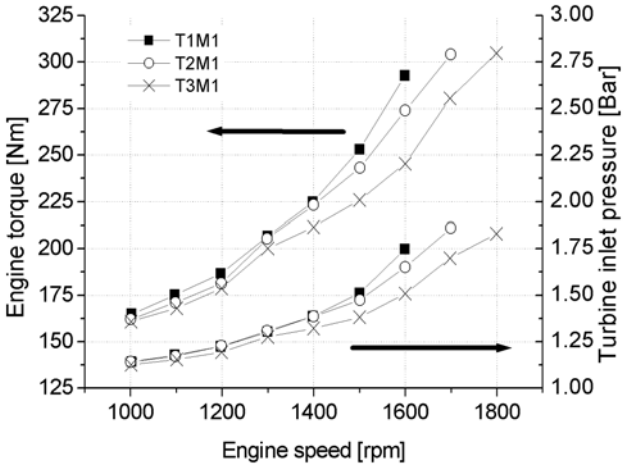

Figure 8.26. Engine torque and turbine inlet pressure for manifold 1 and all turbines.

Since the turbine efficiency cannot be measured directly, some other measure must be found to determine the quality of the turbine's behaviour on the engine. One such is the relative pressure balance of the engine, defined as:

$$PB_{rel} = \frac{P_{in} - P_{1T}}{P_{in}} \qquad \text{eq. 8.6}$$

That value is plotted vs. engine speed in figure 8.27. According to that measure T1 seem to be significantly better than the other two turbines for speeds up to 1400 rpm, but above that the three turbines seem to be similar. On the other hand, T1 did not produce significantly more torque for 1000-1400 rpm (why it does not seem to exist any advantages there).
Thus, there do not seem to be any influencing factors on the turbines' performance on the engine other than those related to differences in swallowing capacity. Calculation of the turbine efficiency might shed more light on this; more on that below. The most interesting speeds are 1500 rpm and above.

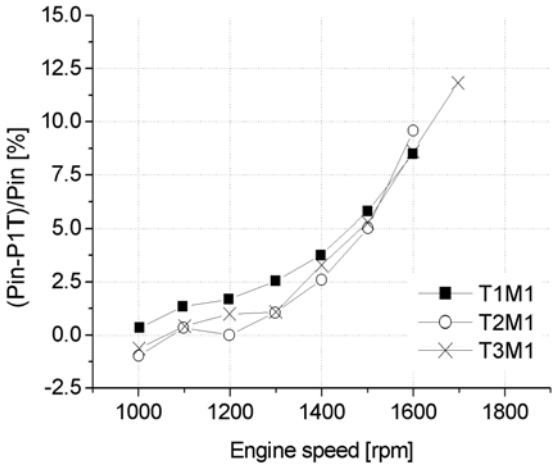

Figure 8.27. The relative pressure balance over the engine for manifold 1 and all turbines.

8.8.2 Engine simulation

All models were thoroughly calibrated and checked against measured data, both time average and CA-resolved properties. As a sample the exhaust manifold pressure is displayed in figure 8.28. Note that such results only could be achieved after the calibration procedure outlined above.

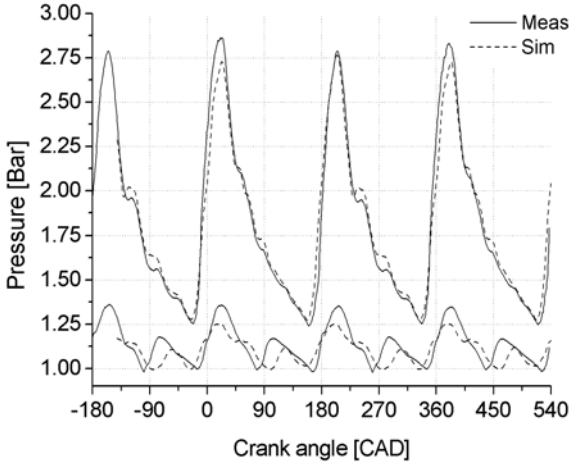

Figure 8.28. Correlation between measured (solid) and simulated (dashed) pressures before and after the turbine. This sample is from turbine 3 and manifold 1 at 1800 rpm.

As the main cause of this paper is to investigate the simulation accuracy, and how it depends on the hardware, the output from the adjustment/calibration of the simulation model is of utmost interest. As written above, PID-controllers were used to adjust various adjustment coefficients in the model towards the measured results. Thus the output from these PID-controllers is very interesting. The most important is the value for the turbine efficiency multiplier for every simulated case. The value of that multiplier is plotted vs. engine speed for every hardware setup in figures 8.29- 8.34. The data are divided in six figures, 8.29- 8.31 show the multiplier for all three turbines, one graph for each manifold, 8.32- 8.34 show the multiplier for all turbines, one manifold for each figure.

Several interesting things can be said about these results. It is perfectly clear that the predicted turbine power is approximately accurate for the lowest speeds and then gradually worsens to 1300-1500 rpm where the error is at largest. Therefore the controller must compensate for that by applying a multiplier significantly smaller than 1. For higher speeds the turbine power gets more and more accurately simulated and the efficiency multiplier approaches 1. That holds for all 9 setups.

From the six figures it is also obvious that the multipliers seem to be more dependent on the manifold than on the turbine. For figures 8.29-8.31 there is a clear and similar trend for all turbines for each manifold, but the same is not as clear in figures 8.32- 8.34 with results for all manifolds for each turbine.

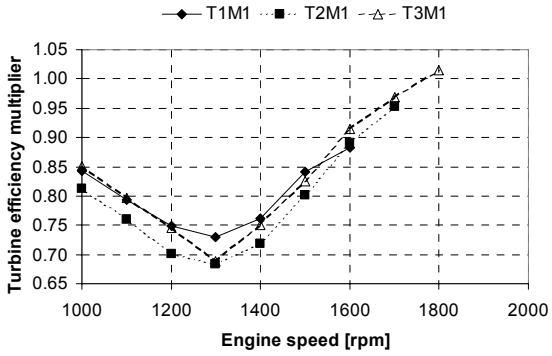

Figure 8.29. The turbine efficiency multiplier for manifold 1 and all three turbines.

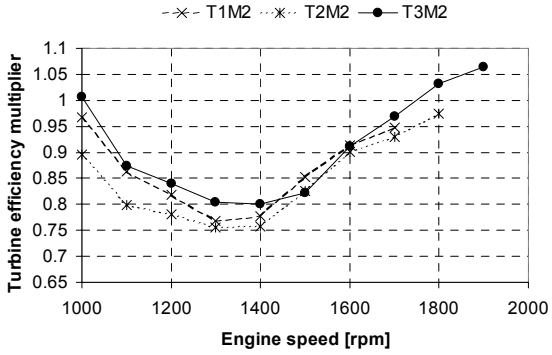

Figure 8.30. The turbine efficiency multiplier for manifold 2 and all three turbines.

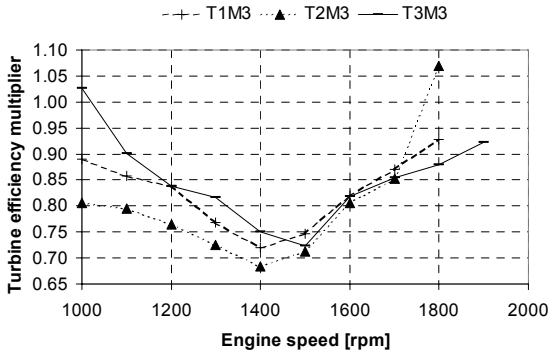

Figure 8.31. The turbine efficiency multiplier for manifold 3 and all three turbines.

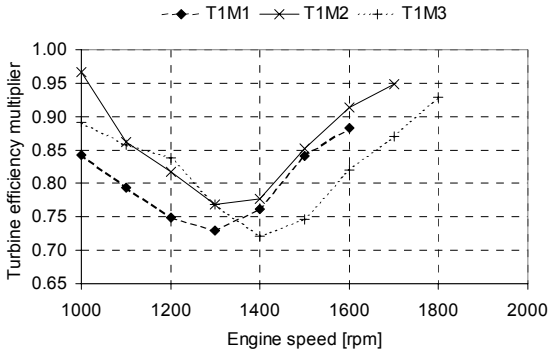

Figure 8.32. The turbine efficiency multiplier for turbine 1 and all three manifolds.

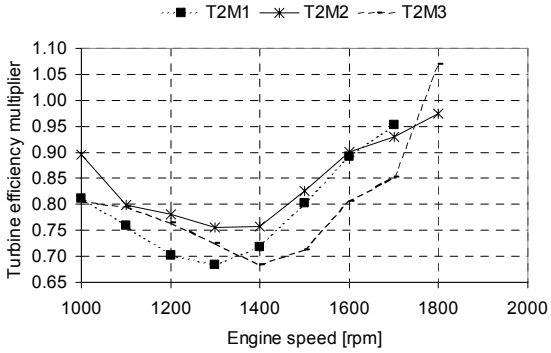

Figure 8.33. The turbine efficiency multiplier for turbine 2 and all three manifolds.

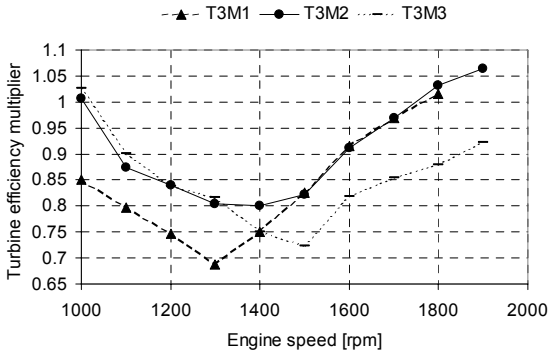

Figure 8.34. The turbine efficiency multiplier for turbine 3 and all three manifolds.

It is interesting to note that the magnitude of the efficiency multiplier needed (magnitude here denotes absolute value of deviation from one of the multiplier) is not significantly lower for manifold number 3. It was expected that the turbine model would perform better for low pulsation amplitudes at the turbine inlet. Manifold 3 was designed and tested for the sole purpose of providing the turbine with a low amplitude inlet flow. In spite of this the largest multiplier magnitude was similar for manifold 3 as for manifold 1 (which had highest fluctuation amplitude of the flow at the turbine inlet). In figure 8.35 the turbine efficiency multiplier is plotted vs. measured relative turbine inlet pressure amplitude for all cases. Relative turbine inlet pressure fluctuation is defined as:

$$P1T_{amp,rel} = \frac{P1T_{\max} - P1T_{\min}}{P1T_{avg}} \qquad \text{eq. 8.7}$$

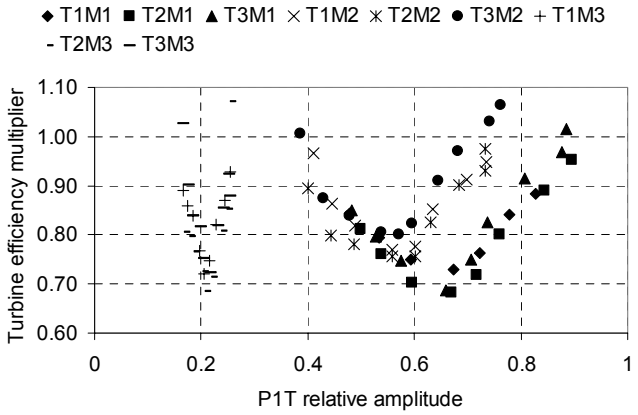

Figure 8.35. The turbine efficiency multiplier plotted vs. the relative amplitude of turbine inlet pressure.

Plotting the efficiency multiplier against mass flow rate shows a uniform trend for all setups, but still with a spread of 0.1-0.15 in multiplier for each mass flow rate, see Figure 8.36.

In order to achieve equal average pressure in the manifold, between measurements and simulation, the turbine mass multiplier had to be adjusted. The values for the mass flow multiplier are displayed in figure 8.37. For all individual setups the massflow multiplier is very well approximated by a linear function. In addition, it varies less between setups than the efficiency multiplier. Aside from two setups (T2M1 and T3M1) the mass multiplier lies within a band of 10 % for each speed, and for each manifold T1 had the largest multiplier and T3 the lowest, but the differences were very small.

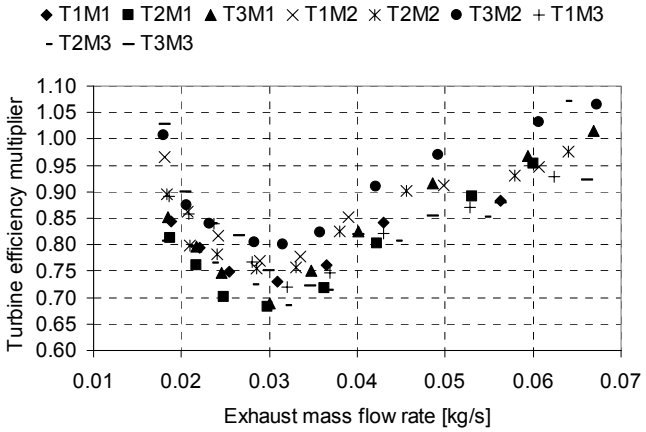

Figure 8.36. The turbine efficiency multiplier vs. exhaust massflow rate show a similar trend as well as phasing vs. massflow for all cases. But still a spread exist.

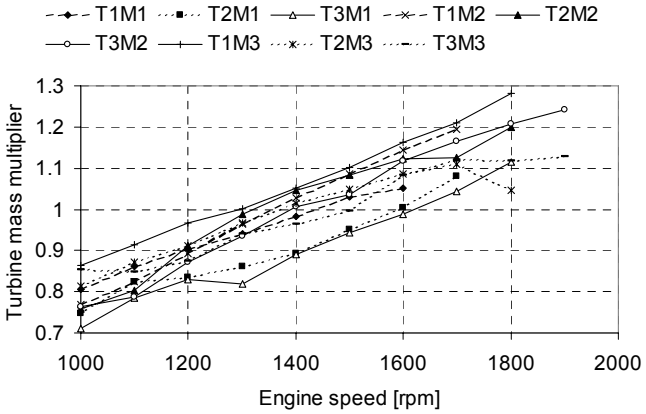

Figure 8.37. The turbine mass multiplier necessary for the average inlet pressure to equal the measured.

The efficiency multiplier deviated most from the value 1 at 1300-1500 rpm for all setups (a minimum around massflow 0.03 kg/s for all setups), a speed region where the massflow multiplier was closest to the value 1 for most speeds. This region is thus very interesting to look closer at. Since manifold 1 is the most commonly used due to it's ability to maintain isentropic power, it is the one most interesting to examine closer. In addition, since the trends for the efficiency and mass multipliers are similar for all setups it is of most interest to investigate the multiplier's dependence on speed/massflow than the variations between setups.

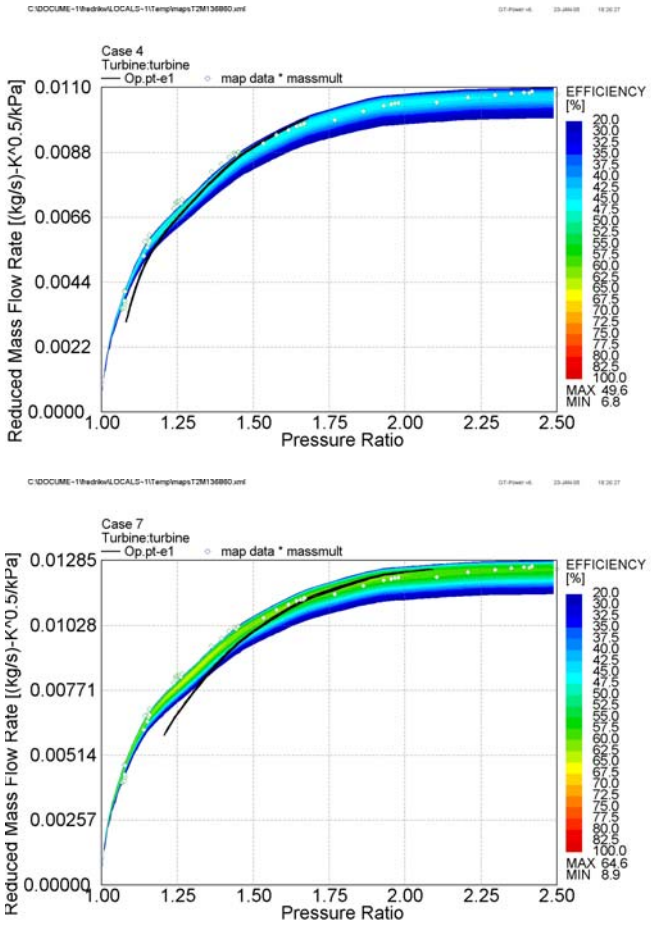

Figure 8.38. GT-Power turbine maps for 1300 rpm (upper) and 1600 rpm (lower). The solid line is the instantaneous operation line, the white markers are the original map points and the field is GT-Power's extra- and interpolated map. The difference in efficiency in the maps is due to different efficiency multiplier.

One issue is whether there exist any significant differences between the maps and their operation points between the cases with efficiency multiplier values close to 1 and those with values far from 1. In figure 8.38 GT-Power's inter- and extrapolated efficiency maps are plotted together with original map data and operation line for one engine cycle, the plotted cases are T2M1 1300 and 1600 rpm. Note that the GT-Power maps have had both massflow and efficiency multipliers applied, that is why the maps look slightly different for

each speed. Unfortunately no significant differences are present. It appears as if the instantaneous operational lines are approximately equally close to real map points in both cases. Thus it appears that the reason for differing efficiency multipliers should be searched elsewhere.
The same check was done for other turbines and for all speeds as well. For T1 the fit of the inter- and extrapolation to the measured map values were worse than for T2 and T3. This could possibly be a source of error, but since T1 does not differ from the other turbines in terms of multiplier values (as was seen in figures 8.29- 8.34) it is assumed non-significant.

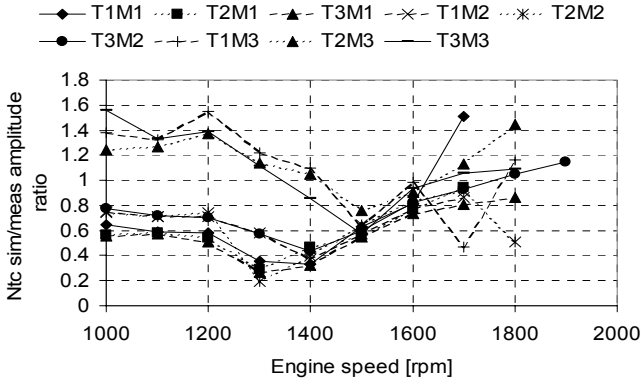

Figure 8.39. The ratio of simulated and measured fluctuation amplitudes for turbocharger speed, plotted vs. engine speed.

In the GT-Power simulations, the fluctuations of the simulated turbocharger speed did not fit very well. The phase was well matched but the fluctuation amplitude differed. As a measure for the simulation error of turbocharger speed, the ratio between simulated amplitude and measured amplitude is used. In figure 8.39 the amplitude error is plotted vs. engine speed. The speed-dependence shows resemblance to the turbine efficiency multiplier, and in 8.40 the efficiency multiplier is plotted vs. the amplitude ratio, one plot for each manifold. It is clear that there is a close relationship, at least for manifolds 1 and 2. For manifold 3 there is no correlation. For that manifold the turbospeed fluctuation is much smaller, due to the larger manifold volume that dampen the exhaust flow pulsations, which decrease the fluctuation in the map as well as the speed fluctuations. The typical fluctuation amplitude divided by time average of turbine power is 2.5 for M1 and M2 while for M3 it is 1.

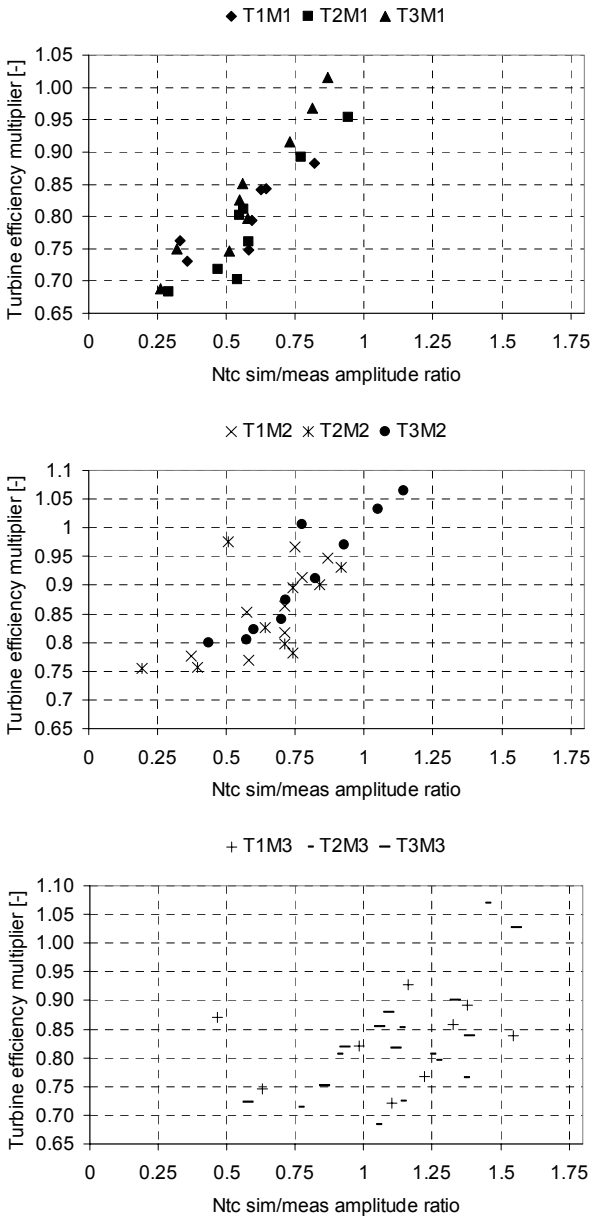

Figure 8.40.The efficiency multipliers plotted vs. the amplitude ratio between simulated and measured turbospeed fluctuation amplitude.

From this, one can assume that either the simulation error is due to efficiency fluctuations over the operation range of the turbine that is not covered very well within the map, or that the power consumption, for instance the constant friction model in the turbocharger, is not very good. Investigating the friction model of the rotor is outside the scope of this investigation, but certainly worth looking into. Investigating the instantaneous behaviour of the turbine operation is covered in the next two sections.

8.8.3 Turbine calculation

From measured data, with some simulated properties that could not be measured, the on- engine turbine efficiency was calculated as in Chapter 6.

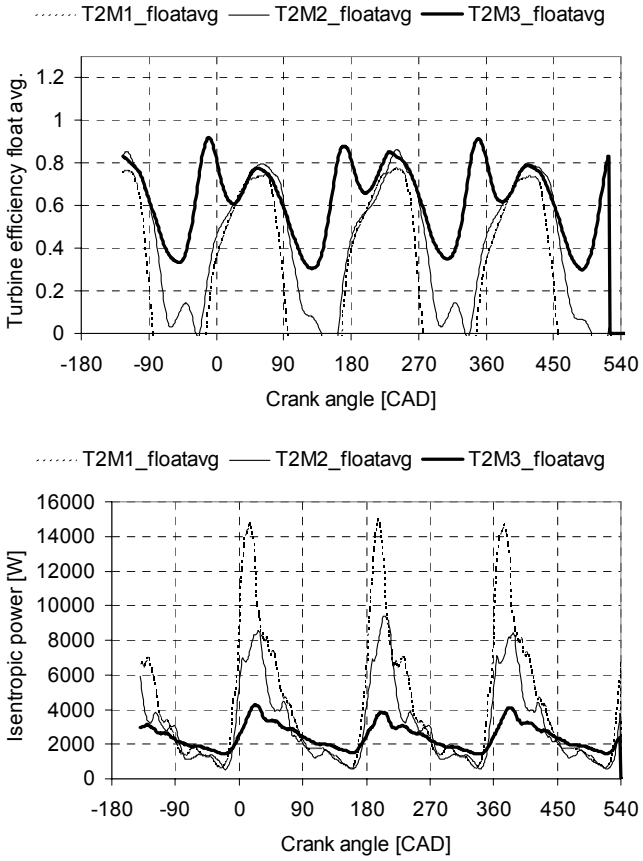

Figure 8.41 a & b. The efficiency calculated according to method A12 for the three manifolds but the same turbine (T2), 1500 rpm. In the lower square, b, the isentropic power according to the A12 definition is included.

In figure 8.41 the efficiency (from A12 definition, float averaged over 30 CAD for all results in this section) for all three cases are compared. It is clear that the turbine behaves very similarly between the two 4-2-1 manifolds, which is to be expected since the shapes of the pulses are similar. For the manifold no.3 (log type) the process seems to be completely different. Here the turbine has it's peak efficiency at the blowdown whereas the other two manifolds are characterized by a rising, but very low, efficiency at blowdown. For none of the manifolds is the efficiency at it's peak when the isentropic power peaks (see b). The same holds for 1700 rpm, as displayed in Figure 8.42 (this example is for turbine 3). It appears that the inflow to the turbine is too large for it to absorb the power effectively.

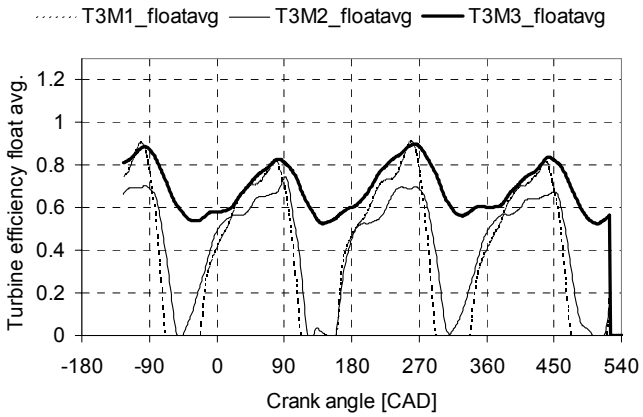

Figure 8.42. The efficiency calculated according to method A12 for the three manifolds but the same turbine (T3), 1700 rpm.

As was established earlier in the paper the difference in isentropic power between the different manifolds was much larger than the variation in efficiency. Therefore it is more interesting to investigate differences between the turbines for the same manifold, no. 1. In figure 8.43 the efficiency and isentropic power for all three turbines and manifold 1 is presented for 1500 rpm. Turbine 3 has highest efficiency, T1 second and T2 lowest. However, since the turbines captured different amounts of isentropic power, due to different flow capacity the result was that T1 gave the engine most torque due to most boost pressure and T3 least, as was seen in figure 8.26. Generally, the difference in isentropic power due to different flow capacity was larger than the differences in efficiency. Therefore the setup with highest isentropic power was always the best in terms of engine output, regardless of speed, manifold etc.

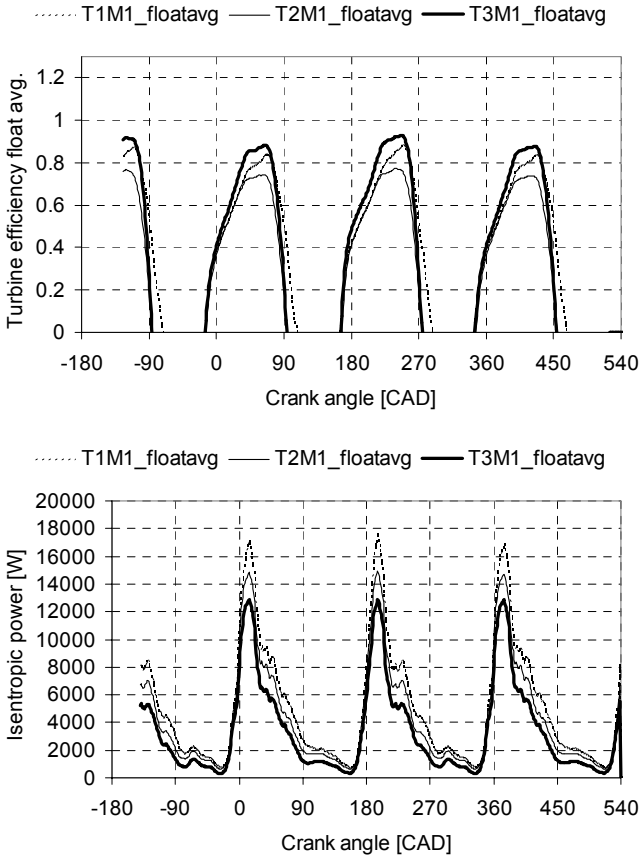

Figure 8.43 a & b. The efficiency calculated according to method A12 for the three turbines but the same manifold (M1), 1500 rpm. In the lower square, b, the isentropic power according to the A12 definition is included.

The peak efficiency is very high. Higher than normally seen in steady flow for this kind of turbine. The reason might be the width of the floating average or from (unknown) inaccuracies in the expression for turbine efficiency. It is however assumed that the relative difference is of significance, as well as the shape.

8.8.4 Different sources for the on-engine efficiency

As seen above, there is a need to study the instantaneous operation point of the turbine. No direct measurement of this (pressure, massflow etc.) was possible to perform. How do the three methods of acquiring the instantaneous

efficiency compare? I.e. the calculated/measured instantaneous on-engine efficiency, GT-Power results and Rital simulations. As mentioned, Rital is a steady flow program, but points from the unsteady conditions were extracted and inserted into Rital one at the time, thus a quasi-steady condition is assumed. In figure 8.44 these three are compared, together with the isentropic power.
It is obvious that the measured efficiency is different from the Rital and GT-Power predictions. It appears that the turbine needs some time before the efficiency has risen to acceptable levels. The Rital and GT-Power results are similar since they both are based on the same theory, i.e. that the efficiency varies with U/Cs along a parabola. That the levels are not equal is due to the fact that the GT-Power results are with the efficiency multiplier applied. In addition, the Rital efficiency must be calibrated by the user according to the procedure outlined above. From the similarity between GT-Power and Rital it can be assumed that the results predicted by Rital can be used to describe the operation condition assumed by GT-Power. Whether that is the condition that prevailed during actual engine testing, can neither be proved nor rejected.

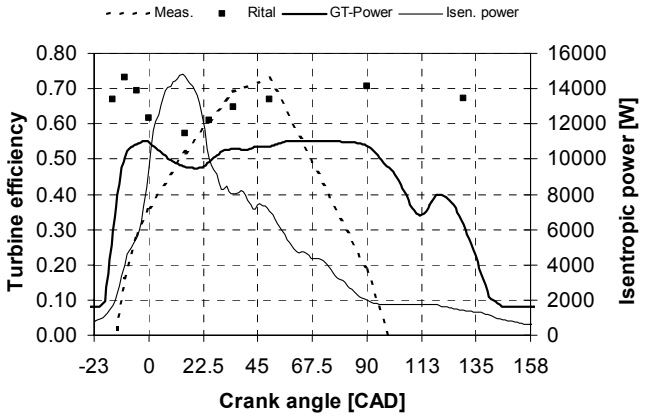

Figure 8.44. Turbine efficiency from calculation / measurements, Rital and GT-Power. The isentropic power according to definition A12 is included to show where on the cycle largest amount of power is entering the turbine. This example is for T2M1 1500 rpm.

So, what are the differences in internal flow between the three different turbines at manifold 1 at 1500 rpm? The results below are calculated in Rital. One aim of the investigation was to see if the reaction had an important influence on the efficiency. As was seen, for 1500 rpm the turbine 3 had highest efficiency, followed by 2 and 1. In figure 8.45 the reaction is plotted vs. CAD for one pulse. It is clear that the relative difference in reaction follows the map measurements, T2 and T3 are very similar while T1 has a lower value. Since there is an equal difference in efficiency (from figure 8.43) between T1 and T2

as between T2 and T3, while the same does not hold for reaction, it can be concluded that the reaction has little influence on the efficiency. In the same figure as reaction, the U/Cs for the three turbines are plotted vs. CAD. Due to the similarity in pulsation shape, since the engine practically is operated at the same point, the U/Cs does not change much.

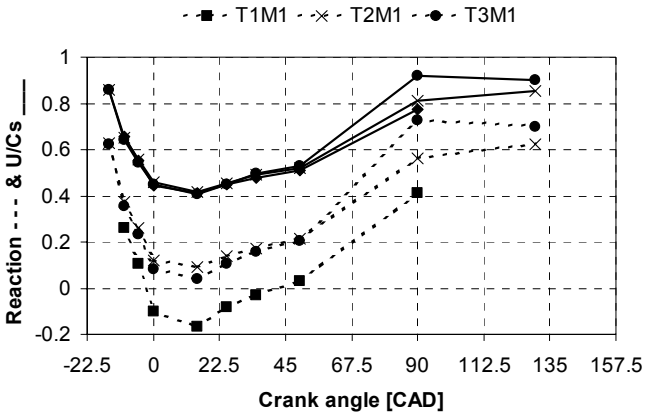

Figure 8.45. Reaction and U/Cs for the three turbines and M1. Solid line for U/Cs and dotted line for reaction.

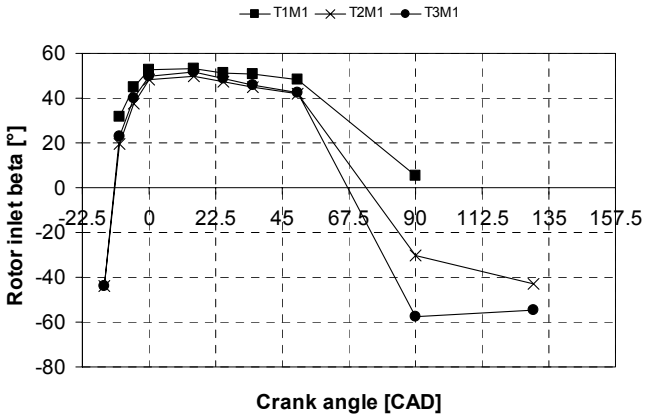

Figure 8.46. Relative inlet angle at rotor inlet. Remember that positive flow angle means that the relative flow vector points toward the pressure side of the blades (see Figure 8.2).

In Figure 8.46 the relative angle between blade and flow is displayed for the three cases. In spite of the differences in volute for the three cases the angle

varies very little. Remember that positive flow angle means that the relative flow vector points toward the pressure side of the blades, see figure 8.2.
Thus the radial turbine shows little sensitivity to reaction, compared to the importance of throat area other design parameters are of minor importance.

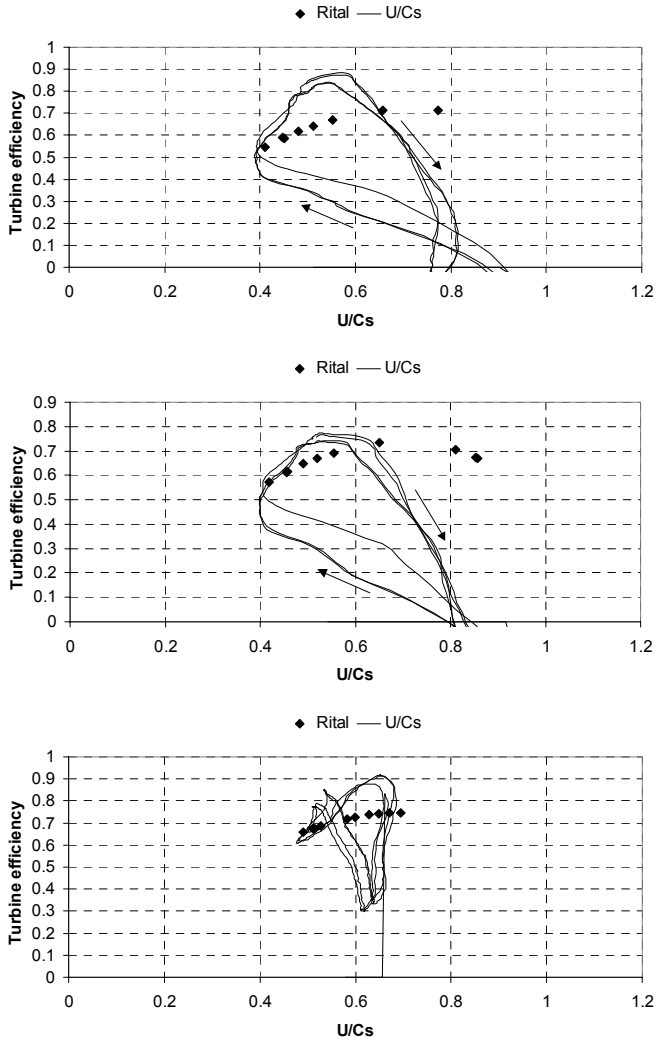

Figure 8.47. Turbine efficiency vs. U/Cs at 1500 rpm for T1M1, T2M1 and T2M3 from top to bottom.

Finally, commonly it is assumed that the efficiency vs. U/Cs varies along a parabolic line [8.4 8.2]. From the data presented above it is possible to present these data both calculated from Rital and from the CA-resolved efficiency calculation. In figure 8.47 some samples are shown, all at 1500 rpm but with different manifolds and turbines. It is clear that for one part of the cycle the turbine works along the parabola assumed in Rital, but it seems as if the turbine works with significant hysteresis, since the up- and down-slope of efficiency does not follow the same operation line. Similar results have been shown before in special-built test rigs, among others Watson whose results were shown in figure 2.1.

8.9 Discussion

It has been shown that governing properties such as the blade speed ratio, reaction, flow velocities and directions vary significantly as the flow propagates in a pulsating manner through the turbine. By varying the trim and A/R of the turbine these variations from flow pulsations will be affected even though the turbine's swallowing capacity, and thereby it's ability to build up an inlet pressure, is maintained. In addition, since the manifold geometry affects the shape of the pulsations, the governing properties mentioned above are dependent on the manifold.

Three different turbines were selected through meanline calculations to give different reaction and blade speed ratio, but equal swallowing capacity. Three different manifolds were also designed to give different pulse shapes into the turbines.

The scope is more to shed light on the phenomenon than to make an attempt to directly increase the accuracy of engine simulations. Thus, note that this method does not test the accuracy of the quasi-steady assumption. Instead, it is a method that can be used to produce more information about the results acquired using the quasi-steady assumption. Then, in the long run, this data can be used to draw conclusions about the accuracy of that method.

The results show that the peaks of power and massflow do not coincide with the efficiency. The peak of massflow forces the turbine to operate in a sub-optimal operation point, where the massflow is too large. Since the flow pulsates so heavily the operation points vary very much even at steady operation points in terms of the engine. Understanding this pulsating phenomenon and learning how to put the peak efficiency and the shape of the massflow at optimal levels is the key issue for design of turbocharged engines.

Many assumptions had to be made in order to calculate the data presented in this chapter. First it is assumed that the GT-Power model, once calibrated as done here, is a proper image of the real case. This enables the use of CA-

resolved properties such as massflow and temperatures for which only time-average data was possible to measure. Of course this is a weakness and must be remembered when drawing conclusions from the calculation results.
Second, it can never be guaranteed that the modelling is done in the absolutely accurate way. Thus, is the turbine efficiency multiplier needed due to some flaw in the modelling? The calibration procedure has tried to avoid this, but of course there exist details that still can be perfected. Correlations such as figure 8.28 are examples of very good correlation, but there exist points where the correlation is not that good. Especially in terms of CA-resolved turbospeed where the error in fluctuation amplitude has been as large as 50% as well as the phase of the compressor outlet pressure that could differ 25 CAD between measurement and simulation.
Third, Rital is a steady flow software. It uses the same, semi-empirical theory as used in GT-Power for the inter- and extrapolation of the maps. Here Rital is used to make step-to-step calculation trying to represent a pulsating phenomenon. Thus, quasi-steadiness is assumed, but the quasi-steady assumption cannot be proved. Therefore there is no guarantee that the results presented here are accurate. Instead, the results should be regarded as an image of how the turbine operates if GT-Power's and Rital's assumption of quasi-steadiness and efficiency vs. U/C_s dependencies are accurate. Data matching these results strengthens the assumptions while data in opposition raises questions.
The engine tests show that it was not possible, with the selected turbines, to change the sizes on rotors and housings simultaneously so that the massflow capability was kept constant. Therefore the boost pressure ability is mostly dependent on housing size (A/R or throat area). Thus it would be interesting to perform a similar study, but only change the trim of the wheel. However, the differences between the turbines will be very small and very accurate methods are required. The CA-resolved calculations here must be upgraded to give that accuracy, as well as the assumptions made with Rital must be proven more strongly to be of significant accuracy.

8.10 Conclusions

The results from the calibration of the GT-Power model show that the turbine efficiency multiplier does not depend on pulsation amplitude, but in this case rather on massflow. However, the reason for that massflow dependence could not be found.

The turbines and manifolds showed insensitivity to small design variations in such a way that differences in isentropic power always gave larger influence on turbine power than differences in efficiency.

No accuracy could be gained by using maps for the actual individual turbines, instead of just a similar turbine of same type.

Rital and GT-Power gave equal turbine efficiency vs. CAD as well as vs. U/Cs dependence due to same theoretical base. The measured / calculated curves had equal shape for a part of the operation line, but showed a hysteresis not present in GT-Power and Rital.

According to measured/calculated turbine efficiency the turbines seem to be poor at absorbing the first and most powerful part of the exhaust pulse.

Finally, the point must be made that the difference in available isentropic power is larger than the difference in efficiency, therefore the tradeoff (toward minimal manifolds) that have been made by the engine manufacturers is accurate.

8.11 References

8.1 Hong C W & Watson N "Turbocharged S.I. Engine Simulation under Steady and Transient Conditions" SAE Paper 880122
8.2 Baines & Japikse "Introduction to turbomachinery" Concepts ETI Inc. ISBN 0-933283-10-5
8.3 http://www.conceptsnrec.com/products/agile.htm 2005-02-13
8.4 http://www.gtisoft.com/broch_gtpower.html 2005-02-13
8.5 Ehrlich, Daniel "Characterization of unsteady on-engine turbocharger turbine performance" Ph.D. Thesis, Purdue Univ. USA 1998
8.6 Pucher, H. et. al.:"Erweiterte Darstellung und Extrapolation von Turbolader-Kennfeldern als Rand-bedingung der Motorprozesssimulation" Abschluss-bericht, FVV-Heft R 517 (2002), Frankfurt am Main, 2002

Chapter 9

Optimisation of Turbocharged Engines' Transient Response with Application on a Formula SAE / Student engine

9.1 Introduction

A turbocharged engine is superior to an NA-engine in terms of potential for power density. It has potential for a wider power band as well as higher efficiency through the retrieval of exhaust energy. However, this potential cannot be utilized if the engine is not properly designed, and the right compromises are made.

The transient response, i.e. the delay in time from demand of power to delivery of power, is one of the most important design criteria for turbocharged engines. Ever since turbocharged cars started to show up on racetracks during the nineteen fifties [9.1] their largest drawback has been the ability to control the delivery of torque. This inherent weakness of turbocharged engines is also called turbo-lag. The reason is that when the engine power is low, the turbocharger spins slowly and must speed up before it can raise the pressure above atmospheric. Decreasing the response time, i.e. increasing the transient response, is the primary development target for turbocharged SI-engines.

Usual rules of thumb for minimization of turbo lag are small volume exhaust manifolds, low moment of inertia of the turbo rotor and small volume from compressor outlet to intake valves. These factors might deteriorate steady state

performance, so the question is how to balance gain in transient response against loss in steady state performance.
In order to aid this development, the present investigation aims to sort out which engine design parameters that are most important for improvement of the transient response, and how these parameters interact. This is done by using sequential fractional factorial designs with 1D engine simulation. The method is developed on a standard production 2-liter, 4-cylinder passenger car engine and then applied to the optimisation of a Formula SAE / Formula Student engine.

9.2 Hardware

9.2.1 Engine outline

The regulations for the Formula SAE / Formula Student competition [9.2] stipulates that the engine must be a 4-stroke, reciprocating piston engine, have a displacement below 610 cm^3, breathe through a 20 mm restrictor, run on gasoline[8] and the only allowed sequence is throttle – restrictor – compressor – engine. Otherwise it is up to designer to decide whether the engine should be force-inducted or naturally aspirated.
On a restricted engine the restrictor sets a maximum value of the inlet air massflow. The turbocharger can draw maximum possible airflow through the restrictor over a wide range of engine speed. This results in a very wide powerband of the engine. That will make the driver's task easier, allowing him to concentrate more on the handling of the car. It also maximizes the integral of the power for the used speed-range of the engine, which in turn will minimize acceleration time. Therefore the choice to turbocharge was obvious.
A study of competitors' engines showed that very few had produced more than 100 hp (claimed). A calculation of the theoretical maximum mass flow that is possible to draw through the restrictor showed that 75 g/s is the limit. 100 hp on 75 g/s of air gives a thermal efficiency of 33% if stoichiometric mixture is assumed. This seems to be quite difficult to achieve, especially when considering that the pressure loss over the restrictor could not be reduced below 0.2-0.3 Bar. The engine is thus forced to run as if it were slightly throttled. For more details on these calculations see Appendix A.
With this information at hand the targets for the engine were set to (in order of importance):

[8] In the American competition, FSAE, E85-fuel is an option, but then the restrictor diameter must be 19 mm.

- No engine failures during development
- Negligible turbo lag
- Widest possible power band
- 100 hp peak power

The very tight time schedule (4 months from start of project to running car) and the small budget for acquisition of engine parts necessitated the first point.

9.2.2 Laboratory equipment

In the KTH Combustion Engine laboratory a computer-controlled hydraulic dynamometer was used, measuring the power at the gearbox output sprocket. The measurement system consisted of a slow and a fast part. The slow system measured time-averaged pressures, temperatures and turbocharger speed at a measurement frequency of 1Hz. The fast measurement system measures at 1MHz divided over 8 channels measuring crank angle resolved pressures, cylinder pressure and crankshaft position. In addition, a flow bench was available for measurement of restrictor performance.
The simulation tool GT-Power was used for design of the engine's piping and manifolds, compression ratio selection and turbocharger selection.
The engine chosen for the task was a Yamaha YZF600R. It was chosen because it had it's cylinders screwed onto the crank case. Thus the compression ratio could be decreased by inserting a distance plate between the cylinder base and the crankcase, a region where sealing is no problem due to low pressures (only crankcase pressure). The turbocharger was selected and an intercooler of appropriate size was, for cost reasons, taken from a production car with high production volume.
For fuel and spark management an MBE970 system was chosen, see MBE's web page for specifications on it's predecessor 941 which is very similar [9.3]. All sensors were taken from Saab's production range except from the ignition coils, which were the standard items of the engine. The system usually reads the engine load from the throttle position sensor and a boost pressure sensor. However, a completely MAP-based system was assumed to be easier to work with. This is because the flow properties for the throttle and the rest of the intake system do not need to be known in order to calculate the airflow through the engine. Therefore a second pressure transducer was connected to the throttle position sensor input of the management system. This second sensor measured the sub-atmospheric pressure in the intake plenum while the boost pressure sensor measured the pressure above atmospheric. The system also has the possibility of boost pressure control, but that proved to be unnecessary, more on that below. In addition, the system had a logging

function which was utilized to check properties such as: intercooler effectiveness in the car, that the proper gearchange speeds were used, that the coolant temperature was below limits and that the transient response was good enough.

9.3 Engine design by simulation

The race engine was designed entirely using 1D simulation in the software GT-Power [9.4]. The model was built up from geometrical data measured on a dismantled engine. The valve flow coefficients were taken from a correlated model of another high-performance SI-engine [9.5] and the combustion was modelled with a Wiebe-function. Combustion duration and position of 50% burned (CA50) was assumed to be 30 CAD and 8 CAD ATDC respectively. For the boosted regime the timing was retarded to always result in a cylinder pressure below 90 Bar. The valve lifts were measured using an incremental rotary encoder at the crankshaft in combination with a linear incremental encoder for the valve lift. The accuracy of that measurement is far higher than the 1 CAD and 0.1 mm necessary for these simulations. To validate the simulation model the engine was first simulated as naturally aspirated, with it's standard intake and exhaust system. This enabled calibration, however approximate, of the valve flow coefficients and FMEP.

Since the turbocharger doesn't have linear mass flow vs. pressure characteristics, while the engine has, there will always be a speed range of the engine where the turbocharger practically doesn't contribute to the power of the engine. When measured at steady state, the turbocharger boost pressure is increasing quite rapidly as engine speed approaches the lowest speed of desired boost pressure (LSDBP). For engines without restrictor the turbocharger will need some kind of control device above this speed to prevent over-boosting. This device is normally a wastegate or a variable geometry turbine. On this engine, the restrictor limits the amount of air entering the system, therefore the need for control is reduced. The simulations showed that the turbocharger was working with approximately equal speed for the used speed range. It is only the pressures that change as a function of engine speed, due to the changing volume flow capacity of the engine. Therefore wastegate control was assumed to be unnecessary. Furthermore, since the turbocharger speed was approximately constant, the transient problem during gear change was eliminated if the time for gear change could be short enough.

If the intake and exhaust manifolds were optimised for maximum volumetric efficiency at LSDBP, largest possible power band could be combined with negligible transient response time. This engine has a maximum speed at approximately 12000 rpm, therefore 5000 rpm was chosen as LSDBP.

Subsequently the intake runner length was optimised for this speed. Actually, intake runner length should be optimised for a speed slightly below LSDBP, but since LSDBP is quite uncertainly determined in the simulations [9.9], the intake runners are optimised for LSDBP. This resulted in a runner length of 600 mm from valve head to plenum.

Many aspects influence the selection of exhaust manifold: steady state performance, transient performance, car packaging, manufacturability, heat loss etc. It was desired from packaging reasons to position the turbocharger at the side of the engine, in the car's right side pod. For steady state performance the resonance length of the pulse propagation inside the manifolds need to be optimised [9.6] and for transient performance the volume has to be minimized. Therefore a 4-2-1 layout was chosen with smallest possible pipe diameters. The 4-2-1 was chosen since it gave negligibly reduced steady state performance compared to a 4-1 system, but with less volume. The simulations showed that a pipe inner diameter of 22 mm was sufficient.

The restrictor is of course a very central part on an engine like this since it governs the maximum amount of airflow that the engine can inhale. It also controls the pressure at the compressor intake. At start it was assumed that hard work was needed to minimize the restrictor volume, in order to avoid slow throttle response. However, that was not necessary. The inlet diameter of the compressor was so small, and the minimum throttle diameter without pressure loss was very similar. Therefore the restrictors' diameter ratio between inlet and narrowest section was very close to 2. Thus the restrictor could have very generous flow angles. This optimises the performance of it, without contributing to a significant amount of the total intake system volume (from the throttle via the compressor, intercooler and intake manifold to the engine).

Since the gas undergo expansion from restrictor inlet to narrowest section [9.7] it can be showed that:

$$a = \sqrt{\gamma RT}$$

$$\rho = P/RT$$

$$\dot{m} = a\rho A_{narrow\,section} = PA_{narrow\,section}\sqrt{\frac{\gamma}{RT}} \qquad \text{eq. 9.1}$$

where a is the speed of sound, γ is the ratio of specific heats, R the gas constant, A area and T temperature. Since the temperature decreases it is lower in the narrowest section than ambient.

It is quite surprising that the temperature at the narrow section calculated from Eq. 9.1 is as low as 240K. Therefore insulation of the restrictor is important to

avoid that the airflow is heated due to heat transfer from the surroundings. This would decrease density and thus massflow. However, no problem with icing of the inside of the restrictor was ever detected. The restrictor was fabricated from carbon fibre to reduce heat transfer from the air to the surroundings.

9.4 Transient optimisation

As stated above the transient performance is of central importance for turbocharged engines. Therefore this should be given a major portion of the development effort. Unfortunately there was no time available to adapt the dynamometer to transient operation, therefore this development had to be done with simulations.

All development efforts must be given a limited amount of time. Every transient simulation takes about 1-1.5 hours to run, and further 5-15 min to setup and analyse. Therefore there is development time to gain if the work is done more efficiently than to simply run one setup, analyse, come up with new ideas, setup and run again. Thus, finding a way to automate, or semi-automate, will enable more simulation runs per spent workday.

A first step is to change all parameters that are included in the optimisation one at the time. If the system is linear, the results for each of the parameters can be linearly interpolated. However, here the transient response is suspected to have non-linear response to several of the parameters included. In addition, this method does not tell if there are any interactions between the various parameters. To find interactions, several parameters must be changed at the same time. A commonly used systematic approach to do this is design of experiment (DOE) and factorial designs. With this method all parameters are varied at two levels, one high and one low. By means of factorial design, it is possible to calculate an average value as well as the effect of increasing the factors from low level to high level. It is also possible to calculate how two or more factors interact. This is in contrast to experiments where only one factor is varied at the time. For a detailed description about factorials, see Box, Hunter & Hunter [9.8]. Note that to detect non-linearity, more than two levels in the factorial design are needed. However, in this optimisation the scope is to find if there are any interactions that are more important than every single parameter, one at the time. Here this is done by first choosing two levels for every parameter and run a one-parameter at the time test to see the isolated importance of every single parameter and check that the levels are properly chosen. Then two level factorials are run to determine the interactions.

Here the application of this method is showed on two different engines. The first engine is a standard passenger car engine of 2 litre displacement, 4-cylinders, a speed range of 800-6500 rpm, no restrictor and a maximum inlet

pressure of 1.8 Bar. The second engine is the Formula SAE / Formula Student engine. The reason for using two engines is that the method was initially developed on the standard car engine for which transient measurements were available to validate the simulations.
For the standard engine, 11 variables were tested. Doing a complete 2-level factorial (that measures all interactions between two and more parameters) would require 2048 tests. That would result in 85 full days and nights of computer time. Therefore the number of simulation runs has to be reduced. Thus, the number of tests was reduced from 2048 to 72 tests, divided over three fractional factorials.
The way to do this is to neglect the three-factor interactions and higher, i.e. assume that only main effects and two factor interactions influence the transient response.

9.4.1 Engine 1: Standard passenger car engine

Selection of transient type/setup

When driving a car, the transients that the engine undergo are rather complex. If running at steady speed and then open the throttle, the engine will build-up torque and boost-pressure while the car starts to accelerate. This is gear dependant and complex to specify and therefore it is beneficial to simplify the transient.
There are several choices, for instance running constant acceleration ramps, recorded speed ramps or with simulated car rolling resistance. However, a far more easily controlled transient is a constant speed transient. In such a transient the dynamometer is set to maintain the same speed throughout the transient even though the torque is increasing rapidly as the throttle is opened and the turbocharger speeds up. For this engine the dynamometer was an eddy-current Schenck W260 with in-house built control system that managed to maintain constant speed during the transient.

Transient simulations correlated to measurements

The transient event used is a load step from 45 Nm at 2000 rpm to maximum open throttle at the same speed. During the transient the ignition angle changed on the engine as a result of the ECU (engine control unit) responding to changing inlet pressure. From experiments the points of 50% burned and 10-90% burn duration were calculated for every measured cycle during the transient and inserted in the model as functions of cycle number in the transient event. This enables the simulation results to show very realistic cycle-to-cycle variations. However they are not really predicted, the procedure is more like recording and playback. Figure 9.1 shows the agreement between measured and simulated net IMEP, which indicates that the air consumption is

modelled very accurately. Note that adjustment of the turbine efficiency model was necessary to achieve these results. For more information about this simulation and measurement, see [9.9]. This transient model was used for the transient optimisation of the standard passenger car engine.

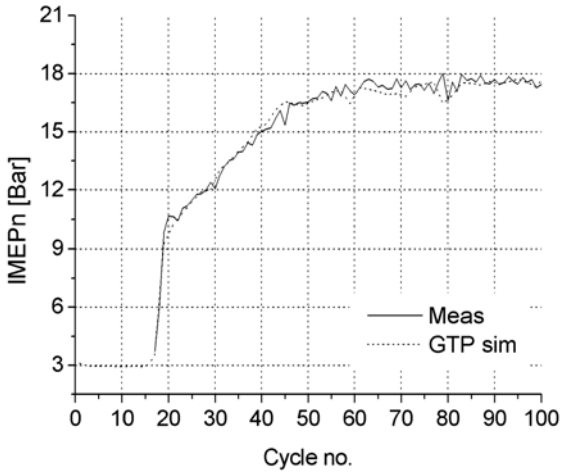

Figure 9.1. The steady speed transient measured and simulated on the standard engine. This simulation model is used as a base for the transient optimisation of the standard engine.

The engine and the simulation model

The engine model has been built up and calibrated over a long time [9.9, 9.10] for steady state and for transient conditions. From the calibrated transient simulation (calibrated to give the same response characteristics as the real engine) a parameter study is made.

The engine is a 4-cylinder, 2-liter, 4-valve per cylinder, pent-roof shaped cylinder head unit and the turbocharger has one single inlet and a wastegate. The transient was measured as a constant speed transient. Thus the engine was run on constant low load of 10 kW and 1950 rpm (which is LSDBP for this engine). The throttle was opened and the power increased while the dynamometer maintained the engine speed. Unchanged, the engine is able to deliver 55 kW and 45 kW was chosen as the threshold value at which the transient response time is measured.

In the simulation model a PI-controller was connected to the throttle to control the power of the engine to 10kW during the low power part of the run. After the engine had stabilized, the controller input-value was changed to a very large value, causing the controller to instantaneously (i.e. in the same simulation time-step) open the throttle to wide open position. The turbocharger speed at

the time of throttle opening will be an influencing factor on the response. Of course the start speed of the turbocharger will be influenced by several of the other parameters. In order to isolate these other parameters' influence on transient response in other ways than just through the start speed, the start speed must be kept constant at the two levels selected. This was achieved by applying a very high value to the turbocharger polar moment of inertia during the low power part of the transient and the start speed was set to a value equal to measured at that load. At the same instant as throttle opening, the polar moment of inertia was reset to the correct value. No wastegate was used in the simulation, as the wastegate normally does not open before 2000 rpm.

Parameters

11 parameters were selected for the factorial. These are displayed in Table 9.1. Two levels had to be chosen for each parameter, one low and one high. For every parameter the engine's standard value was chosen as one level. As the other level a parameter value was chosen that would require a reasonable and approximately equal amount of engineering to realize. Every individual level is discussed more in detail below.

Table 9.1. The parameters used for optimization of the standard engine.

	Level values	
Parameter	**-**	**+**
ERPM Engine speed [rpm]	1950	2500
TWALL Exhaust manifold wall temp [°C]	300	618
PMOI Turbo polar moment of inertia [kg*m^2]	1.25E-05	2.50E-05
TRPM Start speed of turbocharger [rpm]	24900	50000
VEX Exhaust manifold volume [dm^3]	std	100% larger
VIN Intake plenum volume [dm^3]	std	add 22%
EVO Exhaust valve opening [CAD]	std	10CAD earlier
TEFF Turbine efficiency [-]	std	add 10%
TMEFF Turbo mechanical efficiency [-]	std	add 100%
EFLOW Exhaust port flow capability [-]	std	add 10%
CEFF Compressor efficiency [-]	std	add 10%

When the throttle opens, the pressure in the intake manifold increases very rapidly to atmospheric. The amount of exhaust energy, and subsequently the turbine power, increases. The turbocharger speed gradually increases, which further enhances the airflow through the engine. The increased airflow from the compressor will increase the pressure on the intake side and more air will be pressed into the cylinders. Many parameters influence how fast the transient

will be, the efficiency of the turbocharger, polar moment of inertia, buffer volumes etc. The 11 selected parameters are explained here.

Engine speed (ERPM)
This parameter is no design parameter but it is still of interest. The response time is mainly governed by the flow capacity of the turbine. The higher the speed is for the given power, the more the engine has to be throttled. Then the step in mass flow, from throttled to wide open throttle, when opening the throttle will increase for higher engine speed. That is for subatmospheric to atmospheric inlet pressure, before the turbo has reached operation speed. A common design target for passenger car engines is to try to achieve high boost pressure and good transient response at very low engine speeds. Engine speed is included in this investigation to give a perspective of how much transient response could be improved if the engine speed is allowed to increase a few 100 rpm. This is interesting at least for cars with automatic transmission, since for these the engine speed is a parameter that could be controlled by simultaneous control of engine and gearbox.

Manifold wall temperature (TWALL)
For different exhaust manifold wall temperatures the heat transfer from gas to wall will be different, thus the heat losses from the gas will be different as well as the turbine inlet gas temperature. With different temperatures the available energy will be different and thus the turbocharger might spin up differently. This is interesting because it might tell if the double-skinned sheet-metal manifolds will give faster response. In this case the high level is 618°C, which is equal to the measured temperature at steady state 1950 rpm WOT. As low level 300°C is chosen, which is assumed to be a realistic value for low load operation of the engine.

Turbo polar moment of inertia (PMOI)
High turbo polar moment of inertia requires more turbine power for a given acceleration, therefore lowest possible polar moment of inertia is requested.
The high level is $2.5*10^{-5}$ kgm^2, which equals standard for this engine, and the low level $1.25*10^{-5}$ kgm^2, which is similar to the polar moment of inertia of the turbocharger used on the lower power versions of this engine. The power of the two engines is 205 hp and 185 hp. Thus the difference in PMOI can be large for small differences in flow capacity. Therefore the two levels are chosen although the difference between them seems large.

Start speed of the turbocharger (TRPM)
Since the turbocharger cannot give boost pressure until a certain operation speed is reached, the start speed is an important parameter. Ideally the turbocharger should be able to idle just below operation speed all the time, but it would require much larger ability to control the turbines, and it would consume more energy with higher idle speed.
The low level is 24900 rpm, which equals the measured turbo speed at the start of the transient. The high level is 50000 rpm, which would be possible to reach with a variable turbine (either through variable flow area or variable diffuser guide vanes).

Exhaust volume (VEX)
The volume of interest here is the total volume between exhaust valves and turbine wheel. This volume affects the transient in two major ways: Smaller volumes give higher pressure peaks which keeps the energy in the gas high. Larger volumes also give longer response times because the manifold has to be filled with gas before the turbine can start to produce more power, i.e. the manifold volume acts as a buffer.
The low value is the standard volume for this engine, which is 1.03 dm^3. The high value is achieved by extending the four runners from 180 mm length to 450 mm length and the volume thus is 2.15 dm^3. The exhaust runners' influence on pulse tuning is neglected here.

Intake volume (VIN)
The volume of interest here is the volume between compressor wheel and intake valves. It might act as a buffer volume, which have to be filled with high-pressure air before the engine can start producing more power.
The low value is the standard value for this engine, which is 9.3 dm^3. The high value is chosen to 11.3 dm^3, which could be squeezed under the hood of a car. The volume increase is 22 %.

Exhaust valve opening (EVO)
Earlier EVO will release more energy to the manifold and subsequently to the turbine. Low value in this test is the standard value for this engine, which is 150 CAD ATDC. High value is 10 CAD earlier, which is easily achieved with a cam phaser mechanism.

Turbine efficiency (TEFF)
Higher turbine efficiency will give faster response time. Often the turbine efficiency and PMOI are in opposition to each other; therefore it is very interesting to know the relative importance between these two parameters.

The low value in this investigation is the efficiency used directly from the map and calibrated for the unchanged engine model to have the same transient response as in the measurement. For the higher value the efficiency is increased by 10%.

Turbo mechanical efficiency (TMEFF)
The mechanical efficiency represents the friction of the bearings. A common motivation for the use of ball-bearing turbochargers on engines where cost is of less importance is the superior transient properties. The value for the mechanical efficiency is supplied by the turbocharger manufacturer as being between 95-100% and independent of operation point. The low value used in this investigation is 97.5% and the high value is 100%.
Ball bearing turbos might have another benefit by having higher efficiency due to smaller clearance between housing and rotor (which on normal turbos is governed by the bearing clearance), but that is neglected here.

Exhaust port flow capability (EFLOW)
Would better flow through the exhaust ports enhance mass flow through the engine enough to give better transient response? The low value used here is standard C_d-values for the engine and the high values are 10% higher, which could be achieved by redesign of the ports.

Compressor efficiency (CEFF)
How much could the compressor efficiency affect the transient response? The low value is the standard compressor efficiency read directly from the map, and the high value is 10% higher.

Results: 1 variable at the time

In order to see the relative importance between the eleven parameters as well as to ensure that the levels are properly chosen, a one-factor at the time test was run, i.e. 11 runs. The results are displayed in Figure 9.2. In the figure it is obvious that the by far easiest way to increase the transient response of the engine is to increase the engine speed. It seems very difficult to achieve the same improvement by changing any single one of the other properties. However, slight redesign of two other parameters might give the same effect on transient response as increasing engine speed. But a 1-at-the-time test does not test interaction between two factors. To test all two-factor interactions one at the time would require 54 more runs. There exist more efficient methods than one-at-the-time tests, factorial designs and fractional factorial designs are such more efficient methods.

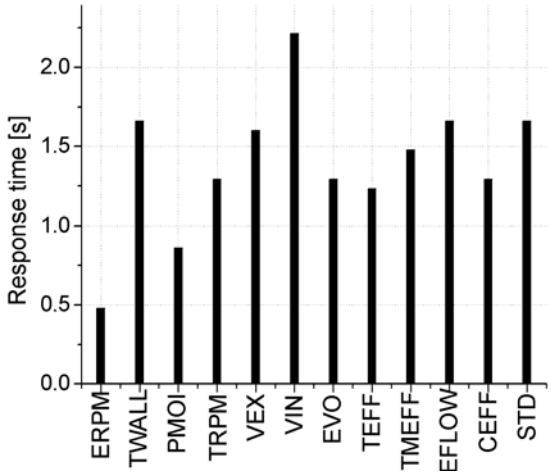

Figure 9.2. Response time achieved when changing one factor at the time. STD means unchanged from standard or equal to measurement.

First fractional factorial design

To see if there are any significant interactions a factorial design was run. The first experiment was designed as a sequential fractional factorial with 11 parameters on two levels. A full factorial design would require 2^{11}=2048 experiments, which is too much to perform. Therefore a fractional design was necessary.

The idea was to run a fractional factorial design with as small test matrix as possible. The output from the change of every parameter in the factorials are called effects and should be seen as average improvement in transient response as a result of the chosen parameter change from low level to high.

Running a smaller amount of experiments than necessary for a full factorial means that the results are being mixed up. Thus some additional work is necessary to resolve the mixed effects. The strongest first-order effects are used to select which second order effects that should be resolved. This resolution of the second order effects is through successive fractional factorial designs. Once the levels were set a 2_{IV}^{11-6} fractional factorial was run [9.8]. This means that 2^{11-6}=32 transient simulations were run. In the results the first-order (single-factor) effects and two-factor effects are mixed with three-factor effects, two-factor effects are mixed with each other, but one- and two-factor effects are not mixed with each other and one-factor effects are not mixed with each other. However, the amplitude of the effects is expected to decrease as the number of

factors is increased. Therefore it is here assumed that all three-factor effects are negligible.

Results from first factorial design

The resultant output of each single test run is the time in seconds from 10 kW to 45 kW of engine power. The effects of each variable were calculated in a spreadsheet. The effect was calculated as the average (over many experiments where several parameters are changed) change in result when changing the parameter from low to high level. In the results the absolute value of the effect is displayed since it is the magnitude of the change that is of interest.

Table 9.2. The results from the first factorial.

Parameter name	**Effect abs [s]**
ERPM	0.84
PMOI	0.35
(ERPM+PMOI)=(TWALL+VIN)=(TRPM+TMEFF)	0.24
(TEFF+EFLOW)	0.24
VIN+(ERPM+TWALL+PMOI)	0.20
TWALL	0.18
(ERPM+TWALL)=(PMOI+VIN)	0.16
(EVO+TMEFF)	0.16
(EFLOW+CEFF)	0.16
TEFF	0.16
(ERPM+VIN)=(TWALL+PMOI)=(TRPM+EVO)	0.16
(TEFF+CEFF)	0.16
TRPM	0.15
(ERPM+TEFF)	0.12
(PMOI+EFLOW)	0.12
(VEX+TMEFF)	0.12
(VIN+CEFF)	0.12

The results are displayed in Table 9.2. A note about notation is in place, effects in brackets with "+"-signs in between means interaction effects, 2 for two-factor interactions, 3 for three-factor etc. Effects, of any order, with "="-sign between them means that the results are mixed, due to the limited number of tests. It is quite obvious that the engine speed has the largest effect on transient response. Second largest effect was from the turbo polar moment of inertia, but the effect is less than the half of the effect of engine speed. Third on the list are three mixed two-factor interactions (ERPM+PMOI)=(TWALL+VIN)= (TRPM+TMEFF). Of the single parameters from which these two-factor

interactions are built up only one factor, TMEFF, is not on the list of assumed significant effects (above 0.1). It is also important to note that the magnitude of an effect is dependent on the magnitude in step between high and low level.
The two factor interactions, and the possibly large effect from three-factor interaction (ERPM+TWALL+PMOI) which is confounded with VIN, need to be sorted out.

Second factorial design (full 2^3)

The results in Table 9.2 above contain an anomaly. It is the interaction between (EVO+TMEFF) that is quite high on the list even though both first order effects of these two parameters are completely negligible. To test this anomaly a full 2^3 factorial was run between these two and PMOI for comparison. This required 8 runs. In this factorial the three variables are:

PMOI	Turbo polar moment of inertia
EVO	Exhaust valve opening
TMEFF	Turbocharger mechanical efficiency

The results from this factorial are displayed in Table 9.3 below. It is obvious that the effects of EVO and mechanical efficiency are negligible compared to PMOI. It is also clear that all interaction effects are negligible. Therefore the strong effect from the interaction between EVO and TMEFF in the previous factorial is probably due to mixing with some other strong two-factor interaction.

Table 9.3. The effects from the second factorial design.

Variable	**Effect abs [s]**
PMOI	0.57
EVO	0.14
TMEFF	0.077
(PMOI+EVO)	0.015
(PMOI+EVO+TMEFF)	0.015
(EVO+TMEFF)	0.015
(PMOI+TMEFF)	0.015

Third factorial design

To sort out the mixed effects a second fractional factorial is run. A 2_{IV}^{7-2} run with:

PMOI	Turbo polar moment of inertia
VIN	Intake plenum volume
TRPM	Start speed of turbocharger

TWALL	Exhaust manifold wall temperature
TEFF	Turbine efficiency
CEFF	Compressor efficiency
EFLOW	Exhaust port flow capability

The reason for leaving out engine speed in this factorial is that it is well established from the first factorial that the engine speed is the parameter that has the absolutely dominant effect on transient response.
In this test CEFF and EFLOW are mixed with one four-factor interaction each, and two-factor interactions are mixed with three-factor interactions, but no two-factor interactions are mixed with each other. Still the three-factor interactions and higher are assumed to be negligible.

Table 9.4. The effects from the third factorial design.

Variable	**Effect abs [s]**
VIN	0.75
TEFF	0.63
PMOI	0.58
CEFF	0.53
(VIN+TEFF)	0.29
(VIN+CEFF)	0.25
TRPM	0.25
TWALL	0.24
(TRPM+EFLOW)	0.23
(TEFF+CEFF)	0.23
EFLOW	0.15
(TRPM+TWALL)	0.15
(PMOI+TRPM)	0.13

The results from this test are displayed in Table 9.4. Effects smaller than 0.1 seconds are still assumed negligible and thus not included in the table. It is obvious that VIN, TEFF, PMOI and CEFF are the most important factors, having more than twice as large effect as the next one-factor effect in the table, TRPM.

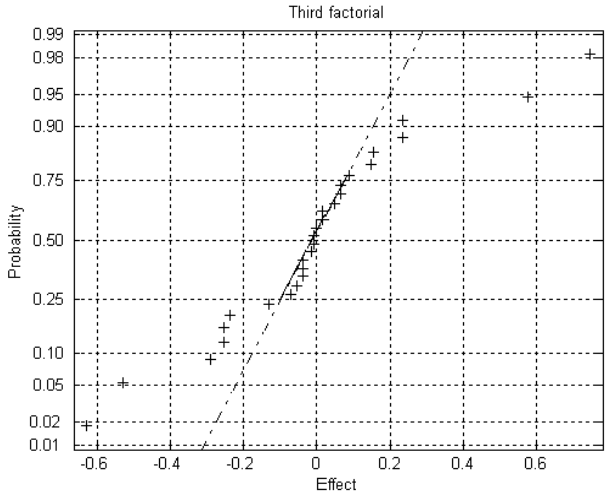

Figure 9.3. Normal probability plot of the results in factorial 3.

How accurate is the assumption that effects below 0.1 s are negligible? Plotting the effects in a normal probability plot can check that assumption, see Figure 9.3. The theory behind the normal probability plot is that if all tests were assumed to be independent and equal tests of the transient response (i.e. no parameter change is assumed to have influence), then they all should be normally distributed. That is, all differences in the effect are assumed to be white noise until otherwise is proved. Thus, only effects that are outside the normal distribution should be significant, since they cannot be white noise. In the normal probability plot the probability that a certain effect is below it's value is plotted versus the effect itself. Thus, if some effect's probability deviates from the straight line through Effect=0.5 and Probability=0.5 in the plot it does not belong to the normal distribution and is therefore significant. Plotting the current results in a normal probability plot, Figure 9.3, reveals that effects up to somewhere between 0.1-0.2 are normal distributed. From the plot it seems like effects less than 0.2 s are negligible.

9.4.2 Engine 2: Formula Student/SAE engine

The second engine in this investigation is significantly different from the first one. It has a only a third of the first engine's swept volume, it operates at 2-3 times higher speeds, it has a restrictor and the throttle is positioned upstream of the compressor.

In contrast to the passenger car engine it was not possible to make any transient tests with the Formula engine in the test cell. Therefore the type of simulated

transient could be chosen more freely. Ideally an entire vehicle model should have been built up in GT-Suite [9.4], including all friction and drag forces. However, a less time consuming method that still measures the impact on acceleration over the entire speed range is to run constant-acceleration speed ramps and simply measure the torque produced vs. time.

Study of engine design parameter's impact on transient performance

Nine parameters, subject to redesign on the engine (compared to it's specifications as run on the motorcycle), were chosen for the transient optimisation. They are displayed in Table 9.5. All values denoted std in the Table were the values chosen from steady state performance considerations. Running a full 2^9 factorial would require 512 runs, which was not possible to perform. 64 runs were considered feasible and thus a fractional factorial of 2_{IV}^{9-3} was chosen. That gives no mixing between first and second order effects, but with third order effects and higher.

Simulation setup

The transient response is more important on the racetrack than the maximum power of the engine. The simulation is thus aimed at emulating a real acceleration of the racecar. The engine must, in this application, perform well in a drag race of 75 m with standing start as well as on a twisty circuit. From recorded track data, see Figure 9.4 provided by Honda Research and Development UK, the average duration for all maximum throttle actuations on the circuit is estimated to 1-2 seconds. In the drag race the car will need three gears and the total acceleration time is aimed at below 4 seconds. From that information 1.5 seconds is selected as the duration for the transient.

Table 9.5. The parameters used to optimise the race engine.

	Level	
Parameter	**-**	**+**
ERPM Engine start speed [rpm]	5000	6000
TWALL Exhaust manifold wall temp [°C]	300	500
IRUN Intake runner length [mm]	minimal	std
VEX Exhaust manifold volume [dm^3]	std	minimal
VIN Intake system volume [dm^3]	-20%	std
TC Turbocharger	small	large
IVO Inlet valve opening timing [CAD]	20 CAD later	std
EVO Exhaust valve opening timing [CAD]	std	20 CAD earlier
CR Compression ratio [-]	8	9

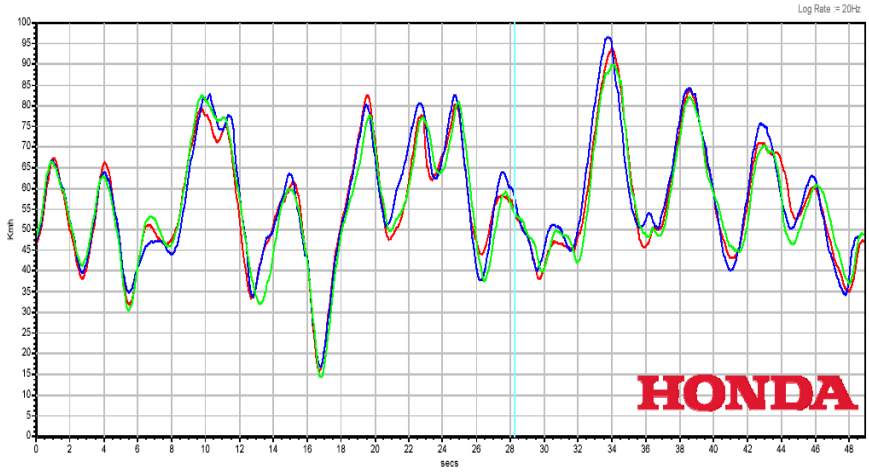

Figure 9.4. Measured speed versus time for the twisty circuit, scales ranging from 0-100 km/h and 0-45 s. Figure provided by Honda Research and Development UK.

The car can be geared to run either from 5000-10000 rpm on each gear or from 6000-12000. For the first gearing the low-speed boost pressure is the main problem area whereas for the second gearing the high-speed friction losses are. The simulation is run as a linear speed ramp. The measure of transient response is the time-integral of the power produced from the start speed to twice the start speed, all transients are of equal length in time of 1.5 seconds. Before the throttle actuation the throttle was controlled to 0.8 Bar abs with a PI-controller in GT-Power.

Results from the factorial design for the race engine

The results from the factorial design are presented in Table 9.6. The largest effect was obtained by altering the inlet runners. The effect is positive, verifying the choice of the long tuned intake runners. Note that these were chosen to optimise the volumetric efficiency between 5000-6000 rpm to enhance the engine's breathing at the critical speed range where the turbo is first delivering desired boost pressure. Second and third effects are virtually equal, which was engine speed and compression ratio. The effect of engine speed is also positive; therefore the 6000-12000 rpm speed range should be preferred to 5000-10000 rpm. For compression ratio, not surprisingly, higher value gives better acceleration. However, the selection of CR=8 is due to safety issues, to avoid knock and engine failures, which could not be tolerated. Effect number 4 is IVO and it is the engine's standard value that is better than 20 CAD later. Fifth in the list is EVO and it is the std value that is preferred to 20 CAD earlier.

Then follows a range of combination effects of these 5 first order effects and then terms with effects assumed low enough to be negligible (approx. 1.5 kWs).

Table 9.6. Results from the factorial used for race engine optimisation.

Variable	**Abs. effects [kWs]**
IRUN	7.8
CR	5.0
ERPM	4.8
IVO	4.3
EVO	3.8
(ERPM+IRUN)	2.3
(IRUN+IVO)	1.9
(ERPM+IVO)	1.8
(ERPM+TC)	1.6
(TC+IVO)	1.4
(TWALL+VEX)	1.2
(ERPM+TWALL)	1.2
(ERPM+VEX)	1.0
(EVO+CR)	1.0
TWALL	0.99
VEX	0.92
VIN	0.76
(TWALL+IVO)	0.75
(TC+EVO)	0.71
(ERPM+CR)	0.61
(VEX+EVO)	0.61
(IVO+CR)	0.60
(TWALL+TC)	0.54
TC	0.50

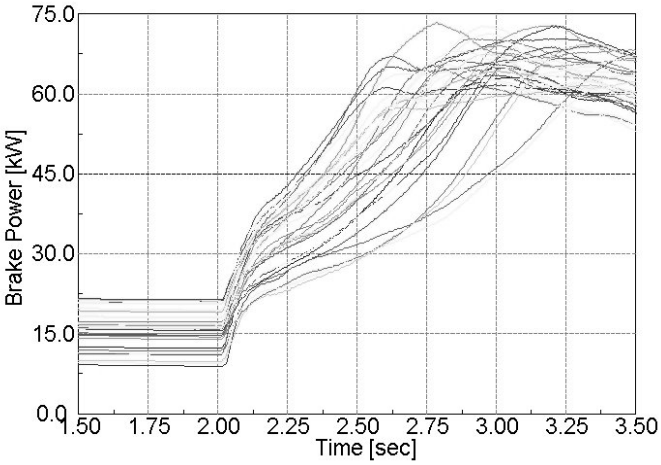

Figure 9.5. 32 of the 64 simulated transients. Up until t=2.0 sec the simulation stabilizes at the part load condition and then the throttle is opened and the turbocharger is speeding up, increasing the engine power. There is a very large spread in transient response as the parameters are changed.

Regarding the turbocharger the choice was between the larger turbo, which was selected from a steady-state point of view, and a smaller one. With the smaller turbo the engine would possibly sacrifice maximum power for a gain in transient response through lower polar moment of inertia. It is interesting to note that the turbo choice had negligible effect. Therefore there is nothing to win by using the smaller turbo, in this case. Overall it can be concluded that the initial choices made for steady-state power was also correct for transient power.

Comparison between the results for the two engines

The results from the optimisation of the two engines are not equal. This is due to the fact that a different mix of design parameters was used for the optimisation and that the differences between the levels were different. For the standard engine the parameters could be chosen very freely since it was only of theoretical interest. For the race engine on the other hand the parameters were chosen so that they could be changed on the actual engine.

The most important parameter for the race engine, the intake runner length, i.e. intake tuning, was not considered on the standard engine. On the other hand different intake runner lengths affect the intake volume, which was of a large importance for the standard engine. But the intake tuning was more important than minimization of intake volume. This is an important result since it indicates that turbocharged engines have much to gain from intake tuning at critical speeds. The reason is that the tuned runners increase the massflow

through the engine regardless to the operation point of the turbo, and increased massflow increases the turbine power, which improves transient response.
For both engines the change in manifold volume gave very little effect. For the standard engine the change was made from the standard compact manifold with very short runners to a longer manifold that possibly could be used for tuning. For the race engine the change was made for the steady state optimised, tuned manifold to a very compact manifold. The conclusion to be drawn from this is that using long manifold runners with large volumes to gain steady state performance doesn't decrease transient performance significantly.
Compression ratio was not used in the standard engine optimisation, but it would probably be of equal importance in that case.
The engine speed at the start of the transient was very important for both engines. The reason is that the step in massflow from sub-atmospheric inlet pressure to atmospheric increases with increasing speed, and this will serve the turbo with more flow earlier in the transient thus further increasing the massflow.
Valve timing gave only small effects for both engines. Start speed of the turbo and manifold wall temperature both gave almost negligible effect.

9.5 Race Engine performance

9.5.1 Dynamometer results

The engine design produced with GT-Power was built, then calibrated and finally tested on the dynamometer. Initially a very simple ignition map was programmed and the fuel map was calculated from simulated air-consumption of the engine. With these initial maps the engine could be started and run, however it was running roughly. The fuel map was calibrated to give approximately lambda=0.8 along the full load line and 0.9-1.0 at part load. These slightly rich values were selected to give a safety margin against lean running and subsequent engine failures. The ignition maps was successively advanced for selected points and then interpolated for the entire map. It was regarded very important during the calibration to minimize the running time on the dynamometer to minimize the risk of blowing the engine. Therefore no on-line calibration was used, all changes in the maps were done with the engine shut down, or at idle. The measurement capabilities were utilized during short test runs and the data was analysed with the engine shut down and, if necessary, further changes to the maps were done.
The targets for the engine were 100 hp and as-constant-as-possible power throughout the speed range to be used, 6000-12000 rpm. This targets could not be met, however, the power predicted from simulations during the design of

the engine could be met within less than 10%. Figure 9.6 shows the simulated power curve vs. the curve that could be realized on the engine. Maximum power is reached at 6000 rpm and is then constant up to 8000 rpm. For increasing speed the power is then reduced, mainly due to increased friction.

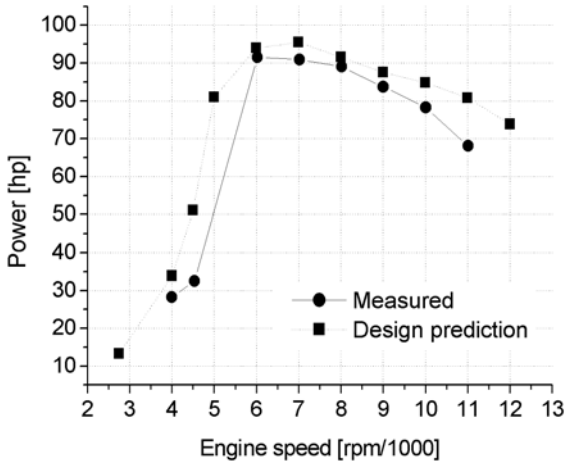

Figure 9.6. The measured power curve compared to the design prediction.

For 5000 rpm the measured data is missing due to problems with the dynamometer control. Unfortunately this is the lowest speed with target boost pressure, one of the most interesting points on a turbocharged engine's full load curve. It governs how low in speed one can allow the engine to drop during driving and it is for many reasons [9.9, 9.10] the most uncertain point in the simulations.

The turbocharger was expected to work at approximately constant speed over the used engine speed range. That proved to be true within 10 % for almost the entire used engine speed range. However, for 4500 rpm the measured turbospeed and power was much more than 10% less than simulated. The reason for this was that the wastegate needed to be set slightly open. It showed that with closed wastegate, above 6000 rpm, the compressor inlet pressure was very low (<0.5 Bar), the compressor outlet temperature very high (>200°C), the turbocharger speed above 250000 rpm and the exhaust temperature very high. The reason for this was excessive amounts of turbine power delivered to the compressor. The only way the compressor could dispose of that power was to increase pressure ratio. With the mass flow restricted it could not do that by increasing the compressor outlet pressure. Instead the compressor inlet pressure dropped dramatically, which resulted in very low compressor

efficiency and higher temperatures throughout the system. The solution was to open the wastegate, but just very slightly. The opening was approximately a 0.5 mm slit around the valve circumference. This solved the temperature problem but resulted in a slight increase of the lowest speed for target boost pressure. In Figure 9.7 the measured and simulated turbospeeds are compared, note that the simulations are run with completely closed wastegate.

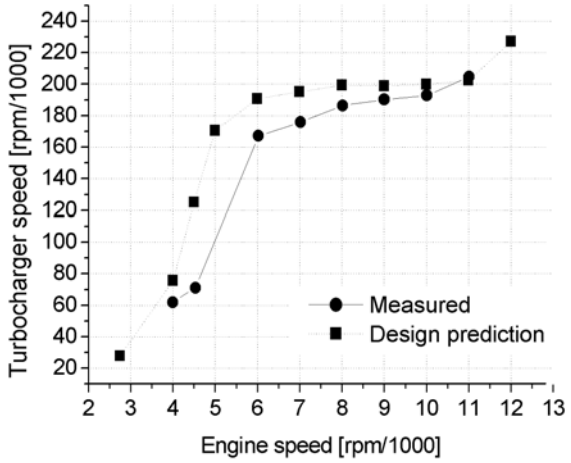

Figure 9.7. Comparison between measured and simulated turbocharger speed.

Figure 9.8 shows the compressor inlet and outlet pressures as well as turbine inlet pressure for both simulation and measurement. It is obvious that the results differ more than 10%. The reason for this is probably that the restrictor performed better than what was anticipated. Therefore the pressure at the compressor inlet was higher on the real engine. This resulted in a lower pressure ratio over the compressor and thus less power was necessary. Therefore the turbine inlet pressure was also less on the real engine than in the simulations. The discrepancy between simulated and measured pressure around 4000-5000 rpm is due to the same reason as for the turbocharger speed.

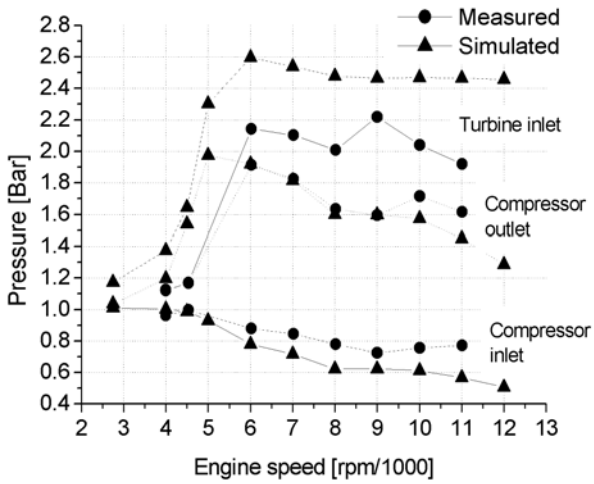

Figure 9.8. The time average pressures at compressor inlet and outlet as well as turbine inlet for measurement (circles) and simulation (triangles).

The time-average pressures do not reveal everything about the scavenging process. CA-resolved pressures are necessary to tell how the engine actually breathes. Both intake and exhaust manifolds were optimised for 5000-6000 rpm and therefore it is most interesting to see the CA-resolved pressures at those speeds, here 6000 rpm is chosen. Figure 9.9 shows the measured pressures in the cylinder, turbine inlet (P1T), compressor outlet (P2K) and compressor inlet (P1K). However, most interesting pressures for the cylinder gas exchange process are the pressures at the inlet and exhaust ports. These pressures could not be measured since the water-cooled pressure transducers used (especially on the exhaust side) were too bulky. Therefore only simulated data is available, see Figure 9.10. In this Figure the measured turbine inlet pressure is displayed along with the same simulated value. These differ some in the amplitude due to lack of tuning[9] of the simulations after the engine had been run. They match in phase, which is most important here. In addition the port pressures on both intake and exhaust sides are displayed. The most interesting thing, and most important for the engine performance is that the intake port pressure is higher than the exhaust port pressure for almost the entire overlap period, i.e. the engine has a positive scavenge pressure. This despite that the time average

[9] Tuning of restrictor pressure loss, intercooler effectiveness, turbine efficiency etc.

pressure measurements show 0.2 Bar higher exhaust back pressure than boost pressure.

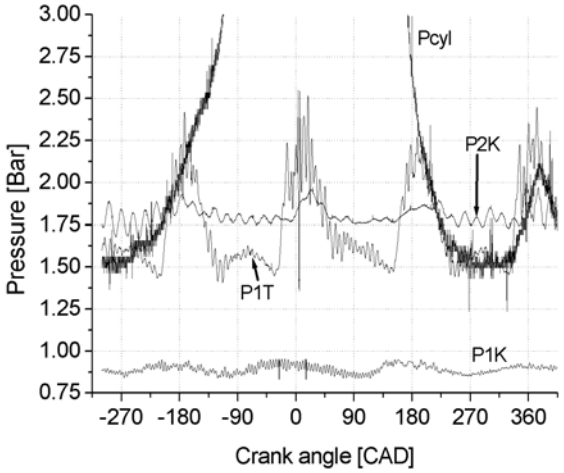

Figure 9.9. Measured pressures at cylinder, turbine inlet (P1T), compressor outlet (P2K) and inlet (P1K).

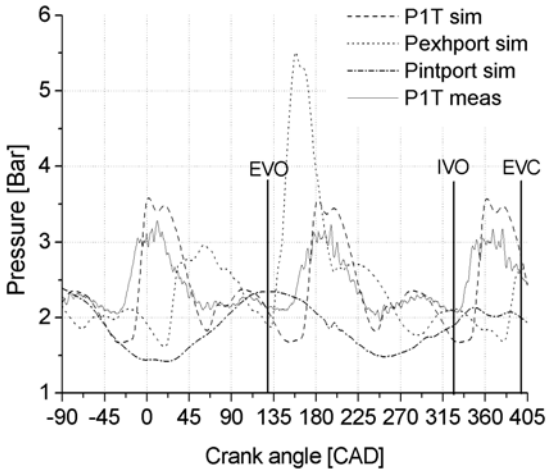

Figure 9.10. The measured turbine inlet pressure (P1T meas) displayed together with simulated turbine inlet pressure (P1T sim), and port pressures.

Having a positive scavenge pressure enables effective scavenging, which results in low residual gas fraction as well as good charging efficiency. This is a well-known fact for naturally aspirated engines, but here the same is utilized for a turbocharged engine.
The exhaust temperature was always below 900°C and the temperature after the IC was maximum 45°C with the engine in the car during track testing on a sunny day with 20°C ambient temperature. The intercooler effectiveness [9.11] cannot be calculated from measured data alone, since no temperature measurement existed at compressor outlet. But if the simulated temperature is used (150°C) the effectiveness was 80%.

9.5.2 Results on track

The engine can perform ever so well in the test cell, but it is the performance in the car that matters if races are to be won. To ensure that the engine performs as good in the car as in the test cell, the engine management system's logging function was utilized. The most important value is the intake manifold pressure (MAP). In Figure 9.11 the engine speed and manifold pressure during an acceleration run is displayed versus time. It shows the event from start of staging at idle (3250 rpm). At t=192 the driver increases the speed to start speed (around 8000-9000 rpm), at t=194.5 he releases the clutch and the speed drops and the boost pressure starts to build up, at t=196.9 he shifts to second and the boost pressure falls somewhat, at t=199 he shifts to third. It is clear that the turbocharger does not respond instantaneously, it takes almost a second from start until maximum boost pressure is reached. An anti-lag function could therefore be utilized to increase engine power during start. However, the drivetrain with the motorcycle's original gearbox and the driveshafts would not cope with such a treatment.
Figure 9.12 is another plot of the manifold pressure vs. time along with engine speed. The difference from Figure 9.11 is that the subatmospheric part of the intake pressure is shown and that the data were recorded on a circuit instead of a drag race track. Also here it is clear that the turbo-lag could not be completely eliminated. The response is however fast enough, no driver said that they had difficulties in controlling the engine as he wanted with the accelerator.
Finally the KTH01 engine is compared to other engines with sporty profile. In Figure 9.13 the BMEP is calculated for a wide variety of engines, all input data is collected from the Internet, and therefore the accuracy cannot be guaranteed. Still, the KTH01 engine is at the top notch along with other super-car engines and the best of competition engines. The only engine being really superior is the WRC rally car, where high boost pressure at very low speeds clearly has been an optimisation target.

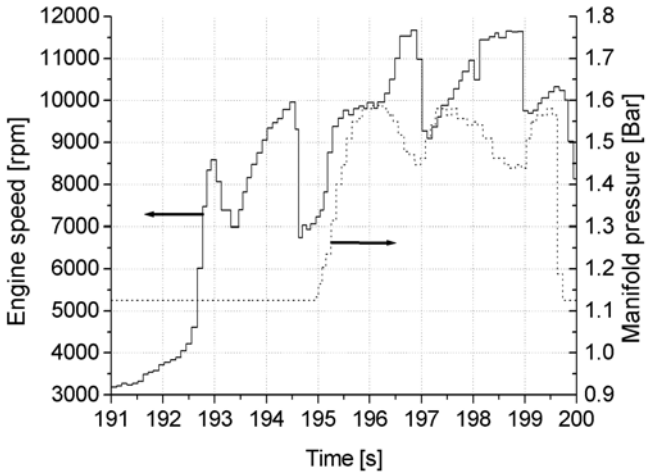

Figure 9.11. This Figure shows the engine speed and manifold pressure during an acceleration event. Note that the manifold pressure is measured with the boost pressure sensor, which only give signal when the pressure is above 1.1 Bar.

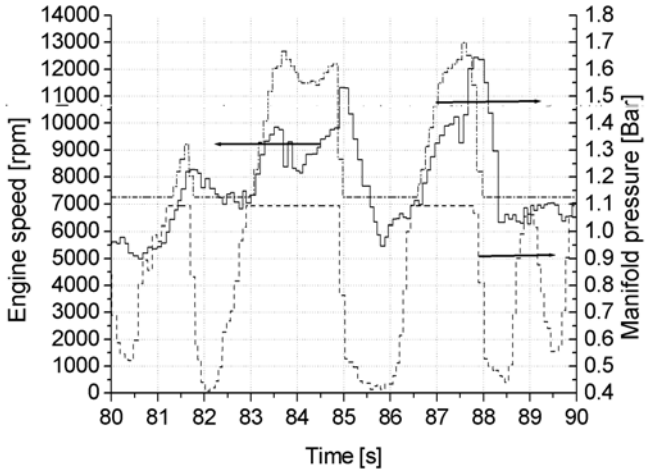

Figure 9.12. The engine speed is plotted vs. time along with intake manifold pressure. There are two pressure curves because he ECU uses two sensors, one for boost pressure and another sub-atmospheric sensor instead of a throttle potentiometer.

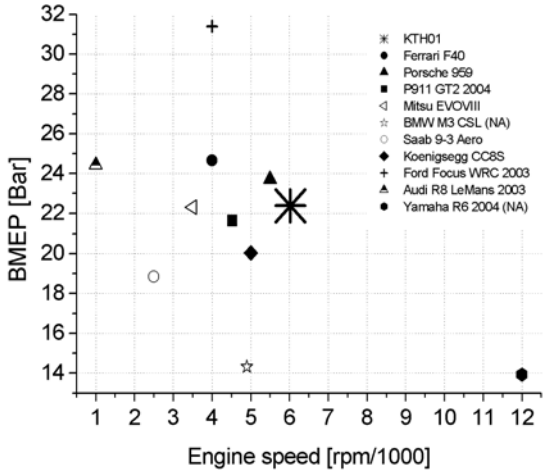

Figure 9.13. Comparison of BMEP for several sportscar and racecar engines.

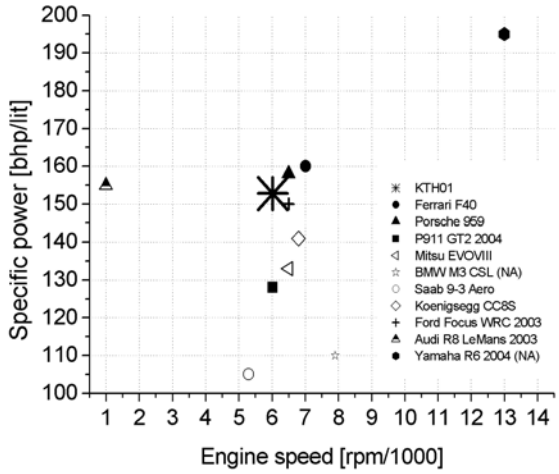

Figure 9.14. Comparison of specific power for several sportscar and racecar engines.

In Figure 9.14 the same engines are compared but now in terms of specific power. Here the KTH01 engine is at the same level as the best of super- and competition cars. However, when compared with the best of production motorcycles it falls short. Note here that all engines except the KTH01, the Audi R8 and the Focus WRC engines are non-restricted.

9.6 Conclusions

With fractional factorial design of experiments the first- and second-order effects on transient turbo response for a standard engine from 11 design variables has been determined. The fractional factorials reduced the number of tests from 2048 to 72, thus reducing the simulation time from 3000 to 100 hours.

Engine speed was the by far most important factor, followed by intake system volume, turbine efficiency, turbocharger polar moment of inertia and compressor efficiency.

The methodology developed was then applied to a Formula SAE / Student race engine. The performance targets for the race engine (see Appendix B) were achieved through successful optimisation of the trade-off between steady state and transient performance. The method enabled efficient utilization of computer and user time for the task. By using fractional factorials the computer could be utilized 24 hours a day with a minimum of user effort for setup and analysis.

The most important conclusion to be drawn from the race engine optimisation is that using long, optimised intake manifold runners with large volumes to gain steady state performance doesn't decrease transient performance significantly. Thus the transient response gains more from good volumetric efficiency than a small buffer volume.

The targets for the engine were:

- No engine failures during development
- Negligible turbo lag
- Widest possible power band
- 100 hp peak power

The first target was fulfilled since the development program could be carried out using the same engine without repair whatsoever.

If measurement data alone is considered, the second target could not be met. But if one listens to the driver's comments it is fulfilled.

Target number three is fulfilled with a wide margin, the engine having peak power over the 6000-8000 rpm speed range and more than 75% of peak power over the entire operation range (5000-12000 rpm).

The peak power target could not be fulfilled; the engine was 8% short from target.

9.7 References

9.1 Taylor, Rich "INDY – Seventy-five years of racing's greatest spectacle" St. Martin's Press, NY 1991. ISBN 0-312-05447-5
9.2 http://students.sae.org/competitions/formulaseries/rules/ 2005-02-05
9.3 www.mbesystems.com/941_040200.PDF 2005-02-05
9.4 http://www.gtisoft.com/img/broch/broch_gtpower.pdf 2005-02-05
9.5 Private communication with Fredrik Agrell, KTH Dept. of Internal Combustion Engines, Fredrik@md.kth.se 2003-12-11.
9.6 Blair.Gordon P "Design and simulation of four-stroke engines" SAE Warrendale Pa 1999 R-186 ISBN 0-7680-0440-3
9.7 Andersson J D "Modern compressible flow" McGraw Hill1990 ISBN 0-07-100665-6
9.8 Box, Hunter & Hunter "Statistics for experimenters" Wiley & Sons 1978 ISBN 0-471-09315-7
9.9 Westin & Ångström "Simulation of a turbocharged SI-engine with two software and comparison with measured data" SAE 2003-01-3124
9.10 Westin "Accuracy of turbocharged SI-engine simulations" Licentiate Thesis TRITA-MMK 2002:18.
9.11 Watson & Janota "Turbocharging the internal combustion engine" MacMillian Press Ltd 1982 ISBN 0-333-24290-4

9.8 Abbreviations

ABS ..... Absolute
ATDC ..... After Top Dead Center
BMEP ..... Brake Mean Effective Pressure
CA50 ..... Timing of 50% burned point
CAD ..... Crank Angle Degrees
CEFF ..... Compressor efficiency
CR..... Compression Ratio
DOE ..... Design Of Experiments
ECU ..... Engine Control Unit
EFLOW..... Exhaust port flow capability
ERPM ..... Engine speed or engine start speed
EVO..... Exhaust Valve Opening
FMEP..... Friction Mean Effective Pressure
FSAE..... Formula SAE
LSDBP..... Lowest Speed for Desired Boost Pressure
IMEPn ..... net Indicated Mean Effective Pressure
IRUN ..... Inlet runner length
IVO ..... Inlet valve opening
MAP ..... Manifold Air Pressure
NA ..... Naturally Aspirated
PMOI..... Polar Moment Of Inertia
SI..... Spark Ignited
TC..... Turbocharger
TEFF..... Turbine efficiency
TMEFF..... Turbo mechanical efficiency
TRPM ..... Start speed of turbocharger
TWALL ..... Exhaust manifold wall temp °C
VEX ..... Exhaust manifold volume
VIN ..... Intake plenum volume
WOT ..... Wide Open Throttle

9.9 Appendix

Restrictor airflow and engine efficiency

The calculations shown here are completely derived from Anderson [9.7].
When the ratio of static pressure at the narrow section of the restrictor, and the total inlet pressure is 0.528 and below, sonic speed will be reached at the narrow section. Depending on the recovery of the dynamic pressure in the diffuser that means a pressure ratio over the entire restrictor of approximately 0.7. Once sonic speed is reached, decreasing the restrictor exit pressure will not increase the mass flow rate further.
From the area at the narrowest section, and the velocity of sound, the volumetric flow could be calculated. The state at critical flow in the narrow section is denoted by an asterisk *.

$$V = A \cdot \sqrt{\gamma R T^*} \qquad \text{eq. 9.2}$$

Where V is volumetric flow [m^3/s], A is the area at the narrowest section, R is the gas constant and T is the temperature. The temperature at the narrowest section can be calculated from the fact that the pressure at the narrow section P* is $P^*=0.528P_{inlet}$. With $P_{inlet}=1$ and the gas law:

$$T^* = \frac{P^*}{\rho^* R} = 240 \text{ [K]} \qquad \text{eq. 9.3}$$

The density is calculated from:

$$\rho^* = \frac{\rho_{inlet}}{\left(\frac{\gamma+1}{2}\right)^{\left(1/\gamma-1\right)}} \qquad \text{eq. 9.4}$$

The massflow is obtained by multiplying the volumetric flow with the density. The result is 74.6 g/s.